SLIMP: a mitochondrial protein involved in cell cycle regulation

Alba Pons Pons

SLIMP: A MITOCHONDRIAL PROTEIN INVOLVED IN CELL CYCLE REGULATION

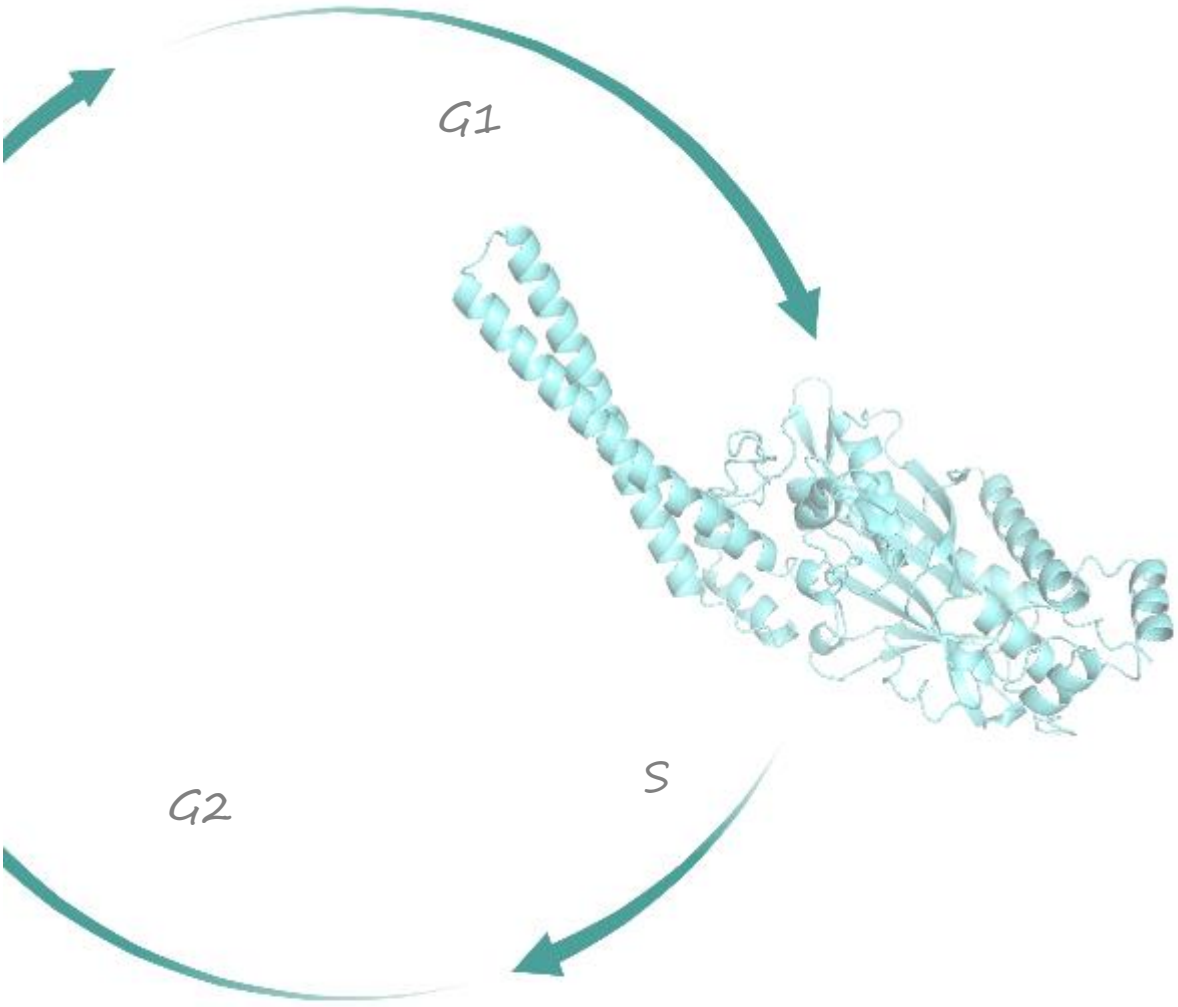

Alba Pons Pons

Doctoral thesis

UNIVERSITAT DE BARCELONA

INSTITUTE FOR RESEARCH IN BIOMEDICINE
IRB BARCELONA

UNIVERSITAT DE BARCELONA
FACULTAT DE BIOLOGIA

Programa de Doctorat en Biomedicina

Institut de Recerca Biomèdica de Barcelona

SLIMP: A MITOCHONDRIAL PROTEIN INVOLVED IN CELL CYCLE REGULATION

Memòria presentada per **Alba Pons Pons** per optar al grau de Doctora en Biomedicina per la Universitat de Barcelona

Lluís Ribas de Pouplana	Alba Pons Pons	Montserrat Corominas
Thesis director	PhD Candidate	Tutor

Alba Pons Pons
2021

TABLE OF CONTENTS

ABBREVIATIONS

A - Ala	Alanine
aa	Amino acid
AAA+	LON ATP-binding domain
aaRS	Aminoacyl-tRNA synthetase
Ab	Antibody
ABCP1	ATP-binding cassette protein 1
ADK1	Adenylate kinase 1
ADP	Adenosine diphosphate
AlaRS - AARS	Alanyl-tRNA synthetase
AMP	Adenosine monophosphate
APC/C	Anaphase promoting complex/cyclosome
APN1	Apurinic/apyrimidinic endonuclease 1
ArgRS - RARS	Arginyl-tRNA synthetase
AsnRS - NARS	Asparaginyl-tRNA synthetase
AspRS - DARS	Aspartyl-tRNA synthetase
ATFS-1	Stress activated transcription factor 1
ATM	Ataxia-telangiectasia protein
ATP	Adenosine triphosphate
ATR	Ataxia-telangiectasia-related protein
BrdU	Bromodeoxyuridine
C - Cys	Cysteine
CAK	CDK-activating kinase
CBT	Cabut
CC	Coiled-coil domain
CDK	Cyclin-dependent kinase
CDK1-P	Cyclin dependent kinase 1 phosphorylated
cDNA	Complementary DNA
CKI	CDK-inhibitor
CNC	Cap-n-collar
CPC	Chromosome passenger complex
CRISPR	Clustered regularly interspaced short palindromic repeat
CuSO4	Copper sulfate
CXCR1	C-X-C Motif Chemokine Receptor 1
CXCR2	C-X-C Motif Chemokine Receptor 2
CYC	Cyclin
CYP2E1	Cytochrome P450 Family 2 Subfamily E Member 1
CysRS - CARS	Cysteinyl-tRNA synthetase
D - Asp	Aspartic Acid
DAP	Dacapo
DAPI	4′,6-diamidino-2-phenylindole

dDP	*Drosophila* dimerization partner
DDR	DNA damage response
DMT	Dalmatian
DNA	Deoxyribonucleic acid
dNTP	Deoxyribonucleoside triphosphate
DP	Donor plasmid
DREF	DNA replication-related element binding factor
Drp1	Dynamin-related protein 1
DUP	Double-Parked
E - Glu	Glutamic Acid
ECL	Enhanced chemiluminescent
ECM	Extracellular matrix
eEF	Eukaryotic elongation factor
eIF	Eukaryotic initiation factor
EMAPII	Endothelial Monocyte-Activating protein II
eRF	Eukaryotic release factor
ETC	Electro transport chain
EWG	Erect wing
F - Phe	Phenylalanine
FAD	Flavin adenine dinucleotide
FBS	Fetal bovine serum
Fis1	Fission protein 1
FSC	Forward scater
FW	Forward primer
FZR	Fizzy-related protein
FZY	Fizzy
G - Gly	Glycine
GD	Globular domain
GDP	Guanosine diphosphate
GFP	Green fluorescent protein
GINS	Go-Ichi-Ni-San
GlnRS - QARS	Glutaminyl-tRNA synthetase
GluRS - EARS	Glutamyl-tRNA synthetase
GlyRS - GARS	Glycyl-tRNA synthetase
GO	Gene ontology
GST	Glutathione-S transferase
GTP	Guanosine triphosphate
H - His	Histidine
H2Av	Histone H2A variant
HA	Homology arm
Hint-1	Histidine triad nucleotide-binding protein 1
HisRS - HARS	Histidyl-tRNA synthetase
HR	Homologous recombination

HSP	Heavy strand promoter
HU	Hydroxyurea
I - Ile	Isoleucine
IF	Immunofluorescence
IleRS - IARS	Isoleucyl-tRNA synthetase
IMM	Inner mitochondrial membrane
IMS	Mitochondrial intermembrane space
INF-g	Interferon gamma
K - Lys	Lysine
KLF	Krüppel-like factor
L - Leu	Leucine
LeuRS - LARS	Leucyl-tRNA synthetase
LSP	Light strand promoter
LysRS - KARS	Lysyl-tRNA synthetase
M - Met	Methionine
MAPK	Mitogen-activated protein kinase
MCM	Minichromosomal maintenance
MDP	Mitochondria-derived peptides
mEF-G1	Mitochondrial elongation factor G1
mEF-Tu	Mitochondrial elongation factor Tu
MetRS - MARS	Methionyl-tRNA synthetase
MFN1	Mitofusin 1
MFN2	Mitofusin 2
mIF2	Mitochondrial initiation factor 2
MITF	Microphthalmia-associated transcription factor
MPF	Mitosis promoting factor
mRNA	Messenger RNA
MSC	Multi-synthetase complex
MSP	Mitochondrial signal pepdite
mtDNA	Mitochondrial DNA
MTFB1	Mitochondrial transcription factor B1
MTFB2	Mitochondrial transcription factor B2
mTORC1	Mammalian target of rapamycin complex 1
MTP18	Myotubulin-related protein 18
mtSSB	Mt-DNA single-stranded binding protein
mTTF	Mitochondrial termination factor
mtUPR	Mitochondrial-unfolded protein response
N - Asn	Asparagine
NAC	Nascent Associating Complex
NAD	Nicotinamide adenine dinucleotide
NCR	Non-coding region
NES	Nuclear export signal
NHEJ	Non-homologous end joining

NLS	Nuclear localization signal
NRF1	Nuclear respiratory factor 1
NRF2	Nuclear respiratory factor 2
ns	No significant
OD	Optic density
OMM	Outer mitochondrial membrane
OPA1	Optic atrophy protein 1
ORC	Origin of recognition complex
OXPHOS	Oxidative phosphorylation
P - Pro	Proline
PAM	Protospacer adjacent motif
PARP-1	Poly (ADP-ribose) polymerase 1
PBS	Phosphate buffered saline
PCNA	Proliferating cell nuclear antigen
PCR	Polymerase chain reaction
PD	LON proteolytic domain
PDC	Pyruvate dehydrogenase complex
PGC-1a	Peroxisome proliferator-activated receptor gamma coactivator 1-alpha
PheRS - FARS	Phenylalanyl-tRNA synthetase
PI	Propidium iodide
Pi	Monophosphate
PKA	Protein kinase A
PLB	Protein loading buffer
PP2A	Protein phosphates 2A
PPAR-g	Peroxisome proliferator-activated receptor gamma
PreIC	Pre-initiation complex
PreRC	Pre-replication complex
ProRS - PARS	Prolyl-tRNA synthetase
PTC	Peptidyl-transferase complex
PVDF	Polyvinylidene difluoride
Q - Gln	Glutamine
R - Arg	Arginine
RBF1/2	Retinoblastoma factor 1/2
RNA	Ribonucleic acid
RNAi	RNA interference
ROS	Reactive oxygen species
RPA	Replication protein A
rRNA	Ribosomal RNA
RT qPCR	Real time quantitative polymerase chain reaction
RTG	Retrograde regulation protein
RV	Reverse primer
S - Ser	Serine
S2	Schneider 2 *Drosophila* cells

SBD	LON Substrate-binding domain
SCF	Skp1-Cullin-Fbox
SDS-PAGE	Sodium dodecyl sulfate–polyacrylamide gel electrophoresis
SerRS	Seryl-tRNA synthetase
SerRS2	*Drosophila* mitochondrial Seryl-tRNA synthetase
SGO1	Shugoshin 1
SLIMP	Seryl-tRNA synthetase-like insect mitochondrial protein
SSC	Side scatter
STG	String
T - Thr	Threonine
TCA	Tricarboxylic acid
TFAM	Mitochondrial transcription factor A
ThrRS - TRAS	Threonyl-tRNA synthetase
TIM	Translocase at the inner membrane
TOM	Translocase at the outer membrane
tRNA	Transfer RNA
TrpRS - WARS	Tryptophanyl-tRNA synthetase
TSS	Transcription start side
TyrRS - YARS	Tyrosyl-tRNA synthetase
USF2	Upstream transcription factor 2
V - Val	Valine
ValRS - VARS	Valyl-tRNA synthetase
VDAC	Voltage dependent anion channel
W - Trp	Tryptophan
WB	Western blot
WT	Wild type
Y - Tyr	Tyrosine

ABSTRACT

SLIMP (Seryl-tRNA Synthetase-Like Insect Mitochondrial Protein) was identified during the generation of a mitochondrial human disease fly model. SLIMP was described as a previously uncharacterized paralog of the *Drosophila* mitochondrial seryl-tRNA synthetase (SerRS2), which became an essential protein, universally distributed in insects, echinoderms, and molluscs. Notably, SLIMP constitutes an aaRS-like protein that can bind to tRNAs, but it has lost the aminoacylation activity (Guitart, Bernardo, Sagalés, et al., 2010). Interestingly, we recently reported that SLIMP plays an essential role in the mitochondria by simultaneously regulating the mitochondrial protein synthesis and mtDNA copy number through interacting with SerRS2 and LON, respectively (Picchioni, Antolin-Fontes, et al., 2019).

On the other hand, two reported studies pointed to SLIMP as an essential cell cycle regulator (Ambrus et al., 2009; Liang et al., 2014). Previous experiments in our group showed a G_2 accumulation phenotype in SLIMP-KD cells, which can be rescued by overexpressing SLIMP without the mitochondria-targeting signal. Additionally, transcriptional upregulation of a core set of E2F1-target genes was detected upon SLIMP depletion. All these data point to a cell cycle-related role of SLIMP, potentially carried out from outside the organelle.

Interestingly, here we first experimentally characterized the SLIMP MSP and proved that it is essential for driving the protein into the organelle. Moreover, we discovered an extra-mitochondrial population of SLIMP potentially shuttling between the cytosol and the nucleus, presumably in charge of the cell cycle role of SLIMP. Furthermore, our results suggest a role of SLIMP repressing the transition from the G_1 to S phase during the cell cycle progression in an E2F1-independent pathway. Finally, interestingly, we demonstrate that the CDK1-P levels are increased upon SLIMP depletion, suggesting an activation of the G_2/M checkpoint.

In balance, the data presented in this thesis reinforces the idea of SLIMP playing a non-canonical function outside the mitochondria regulating the cell cycle progression near the R point. Thus, SLIMP would represent a single molecule at the crossroad between the mitochondrial homeostasis and cell cycle regulation.

RESUM

SLIMP (Seryl-tRNA Synthetase-Like Insect Mitochondrial Protein) es va identificar com un paraleg prèviament desconegut de la seril-tRNA sintetasa mitocondrial de *Drosòfila* (SerRS2), durant la generació d'un model de malaltia mitocondrial humana. Segurament SLIMP és fruit d'una duplicació gènica a la base dels animals i s'ha convertit en una proteïna essencial i universalment distribuïda en artròpodes, mol·luscs i equinoderms. A més, SLIMP ha perdut l'activitat aminoaciladora, tot i que encara conserva la capacitat d'unir-se a ARNs de transferència (Guitart, Bernardo, Sagalés, et al., 2010). El nostre laboratori ha demostrat recentment que SLIMP desenvolupa una funció clau a la mitocòndria, regulant simultàniament la traducció gènica a l'orgànul i el número de copies de ADN mitocondrial, a traves de la interacció amb SerRS2 i LON respectivament (Picchioni, Antolin-Fontes, et al., 2019).

D'altre banda, dos estudis publicats en els últims anys vinculen SLIMP amb la regulació del cicle cel·lular (Ambrus et al., 2009; Liang et al., 2014). En aquest sentit, experiments prèviament realitzats al grup demostren que quan els nivells d'SLIMP baixen, les cèl·lules s'acumulen en la fase G2 del cicle. Curiosament, aquest fenotip es pot revertir sobre-expressant un forma truncada d'SLIIMP que no pot entrar a la mitocòndria. A més, en aquestes condicions, també s'observa una pujada a nivell transcripcional d'alguns gens regulats per E2F1. Conjuntament aquestes dades apunten a una possible funció d'SLIMP relacionada amb la regulació del cicle cel·lular potencialment portada a terme des de fora de la mitocòndria.

En aquesta tesi, nosaltres, primer determinem la seqüència del pèptid senyal mitocondrial d'SLIMP experimentalment, i demostrem que es essencial i suficient per dirigir la proteïna cap a l'orgànul. A més, detectem una petita població d'SLIMP fora de la mitocòndria, present tant en el nucli com en el citoplasma. És important remarcar, que varis experiments presentats en aquesta tesi suggereixen que SLIMP estaria reprimint la progressió del cicle cel·lular a nivell de la transició G1-S, mitjançant un mecanisme alternatiu a E2F1. Finalment, demostrem que els nivells de CDK1-P son mes elevats en les cèl·lules que els hi manca SLIMP, cosa que indica una activació del punt de control de G2/M i que podria explicar la acumulació en G_2 observada en aquestes cèl·lules.

En conjunt les dades presentades en aquesta tesi, reforcen la idea que SLIMP desenvolupa una funció no canònica des de fora de la mitocòndria, reprimint l'entrada en la fase S del cicle cel·lular. Per tant, SLIMP representaria una molècula que vincula directament la homeòstasi mitocondrial i la regulació del cicle cel·lular.

INTRODUCTION

1. INTRODUCTION

1.1. EUKARYOTIC TRANSLATION

Gene translation is a central reaction in all the domains of life. The process by which the information contained in the cell genome (DNA) is transferred into an RNA molecule is known as transcription, and the sequential conversion of the messenger RNA (mRNA) into a protein is called translation. During protein synthesis, the mRNA is loaded onto the ribosome and decoded by triplets, termed codons, based on the standard rules of the genetic code (Figure 1). The genetic code establishes that each codon corresponds to a particular amino acid (aa) and is considered universal as it is conserved among eukaryotes, prokaryotes, and archaea, with very few exceptions. Interestingly, there are only 20 natural amino acids while 64 different codons can be created by combining the four bases (A, G, C, U), resulting in a degenerated genetic code in which similar but still different codons encode for the same aa (Crick, 1963) (Figure 1). It is thought that the genetic code has evolved to confer efficiency to the translation process and minimize the error rate since a point mutation or base misreading would not necessarily lead to an aberrant protein product (Volkenstein, 1966; Woese, 1965).

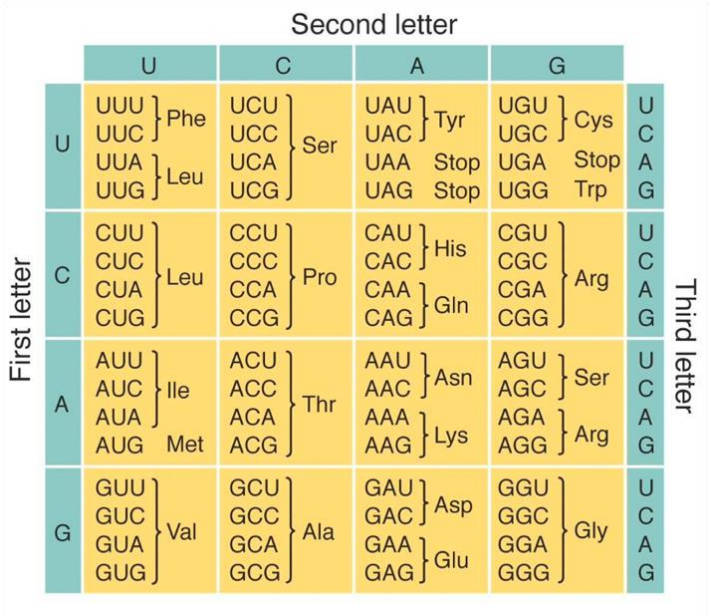

Figure 1 | Standard genetic code. Correspondence between codons (DNA triplets) and the 20 natural amino acids plus the three stop codons (UAA, UAG, and UGA) (B. Alberts, 2015).

Protein synthesis is the most expensive mechanism of the cell in terms of energy; around 30% of ATP is invested in the protein-generating factory. Several proteins and RNA molecules are responsible for orchestrating protein synthesis, ensuring its efficiency and accuracy. Transfer RNAs (tRNAs) are leading players in the translation process and a key link between the mRNA and the growing polypeptide chain. Transfer RNAs show a very well conserved secondary structure compost of four double-strand stems/arms and four single-strand loops. The tRNA structure (Figure 2) consists of a D-arm and D-loop, a T-arm and T-loop, a variable loop and the two principal elements: the anticodon loop holding a nucleotide triplet called anticodon, that matches the mRNA codon, and the acceptor stem, where they carry the specific amino acid that the codon encodes for. Thus, tRNAs act as adaptor molecules transforming nucleotide language into amino acids (Holley et al., 1965). Importantly, tRNAs undergo a maturation process after transcription, where they are highly modified. The process called tRNA editing is essential for cell survival and provide them specificity and complexity (A.G. Torres and L. Ribas de Pouplana, 2016; Nangle et al., 2006).

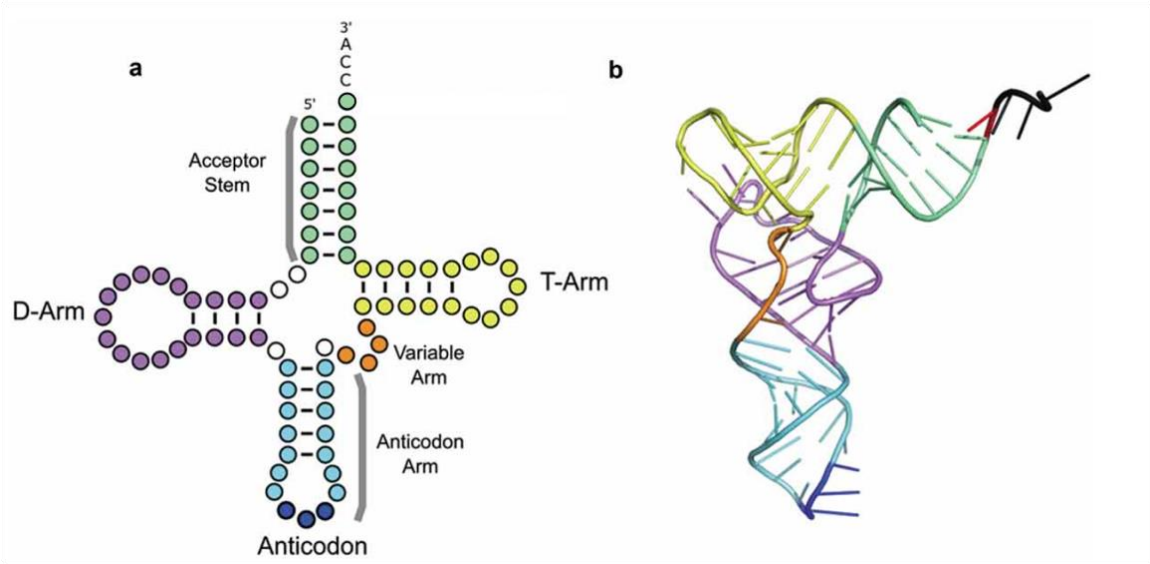

Figure 2 | Transfer RNA secondary structure. (A) Schema representing the cloverleaf-shaped tRNA structure. The main structural elements mentioned before are indicated in the figure. (B) Schema representing the 3D structure of a tRNA. Adapted from (Berg et al., 2019).

Moreover, ribosomes also represent crucial elements in protein synthesis. Ribosomes are large structures consisting of two subunits (the 40s and 60s, respectively, in

eukaryotes) which are 70% RNA and 30% protein. In the protein-generating factory, the ribosome works as a docking station for the tRNA charged with the cognate amino acid that will be incorporated as part of the growing polypeptide chain which will eventually become a protein. Notably, the ribosome structure holds three essential spaces for the translation process designed as A-site (binds to the aminoacyl-tRNA), P-site (binds the peptidyl-tRNA) and exit or E-site (binds the free tRNAs) (Alberts. B., 2015; Steitz, 2008).

Importantly, gene translation is a two-step process (Figure 3): first, the tRNAs need to be charged with its cognate amino acid, a reaction catalyzed by specific enzymes termed aminoacyl-tRNA synthetases (see section 1.2). The second step is the ribosomal translation itself, which can be broken into four phases: initiation, elongation, termination, and ribosome recycling.

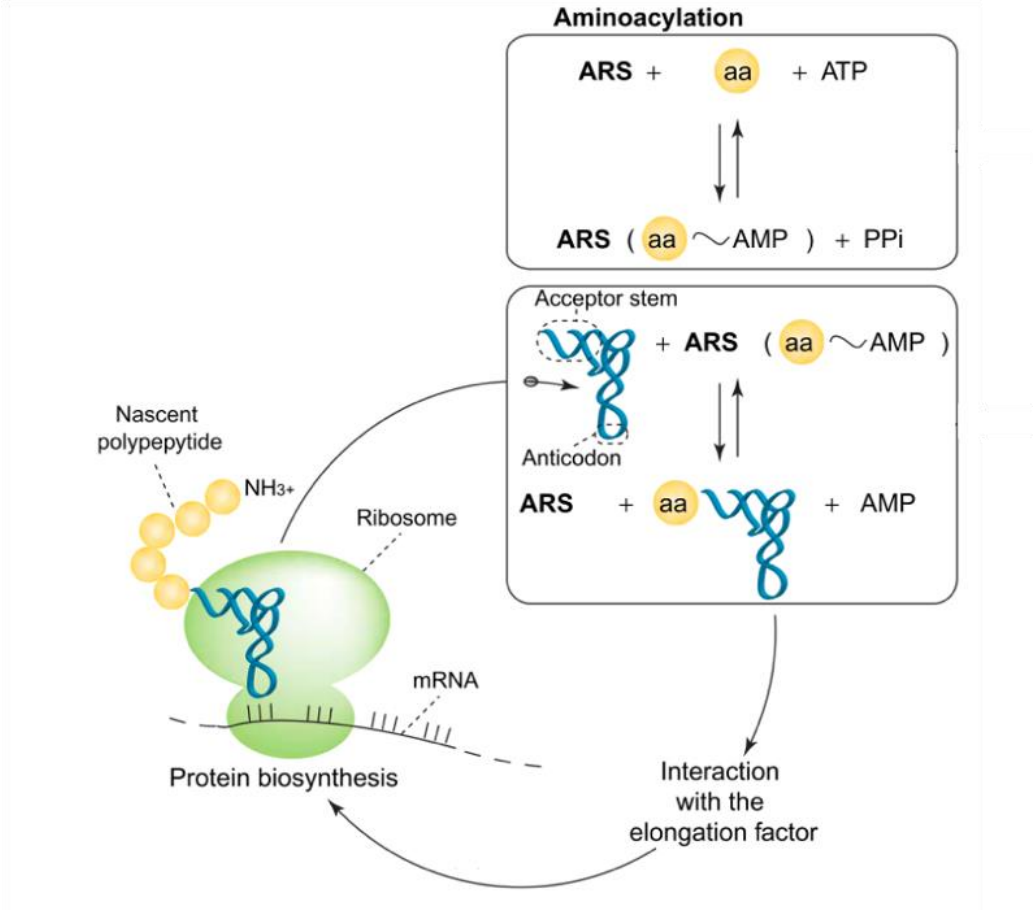

Figure 3 | Eukaryotic translation. The schema illustrates the two main phases of gene translation: tRNA aminoacylation (it will be further discussed in the next section) and ribosomal translation. Adapted from (Geslain & De Pouplana, 2004)

In eukaryotic cytosolic translation, the first codon to be translated is always AUG and corresponds to methionine (MET). The initiation step begins when the tRNA-MET, termed the initiator tRNA, binds to the P-site of the smaller ribosome subunit (the 40s) together with the eukaryotic initiator factor 2 (eIF2) in a GTP consuming manner. Then, the eukaryotic initiator factor 4G (eIF4G) recognizes the mRNA poly-A tail, the eukaryotic initiator factor 4E (eIF4E) binds to the 5'-end, and together with other translation initiator factors, they load the mRNA molecule into the ribosome 40s subunit. This mechanism avoids the translation of defective or partially unprocessed mRNAs. Afterwards, the eIF2 and the hydrolyzed GDP are released, and the large ribosome subunit (the 60s) joins the complex (Hernández et al., 2010; Jackson et al., 2010).

Once the translation initiator complex is assembled, the second tRNA charged with its cognate aa enters the ribosomal A-site bound to the elongation factor 1 (eEF1). At this point, the elongation step starts. During this phase, the peptide-bond between the growing polypeptide-chain, placed at the P-site and the new aa, residing at the A-site, is catalyzed by the peptidyl-transferase complex (PTC). Interestingly, the PTC as part of the ribosome consists of a ribonucleoprotein complex and its enzymatic activity is provided by the rRNA instead of protein (Rodnina et al., 2006). As soon as the reaction occurs, the elongation factor 2 (eEF2) promotes the movement of the 60s ribosome subunit three nucleotides toward the mRNA 3'-end, leaving the free tRNA at the E-site. Finally, the small ribosome subunit moves through the mRNA, leaving the A-site free and ready for uptaking the next aminoacyl-tRNA. Finally, the empty tRNA is released from the exit site.

The translation process terminates when one of the STOP codons (UGA, UAG, UAA) enters the A-site of the ribosome, and none of the charged tRNA's anticodons can pair efficiently enough with that codon (Jackson et al., 2012). At this point, the eukaryotic release factor (eRF) joins the A-site of the ribosome and promotes the complex disassemble.

Ribosome recycling is the last step of protein translation. Firstly, the ATP-binding cassette protein 1 (ABCP1) release the 60s ribosome subunit from the complex, and then

the eIF1 is responsible for disassembling the other components. The resulting polypeptide and the deacetylate-tRNA are released, and the ribosome subunits are recycled and ready to undergo further translation rounds (Dever & Green, 2012; Hellen, 2018). The translation process is illustrated in Figure 4.

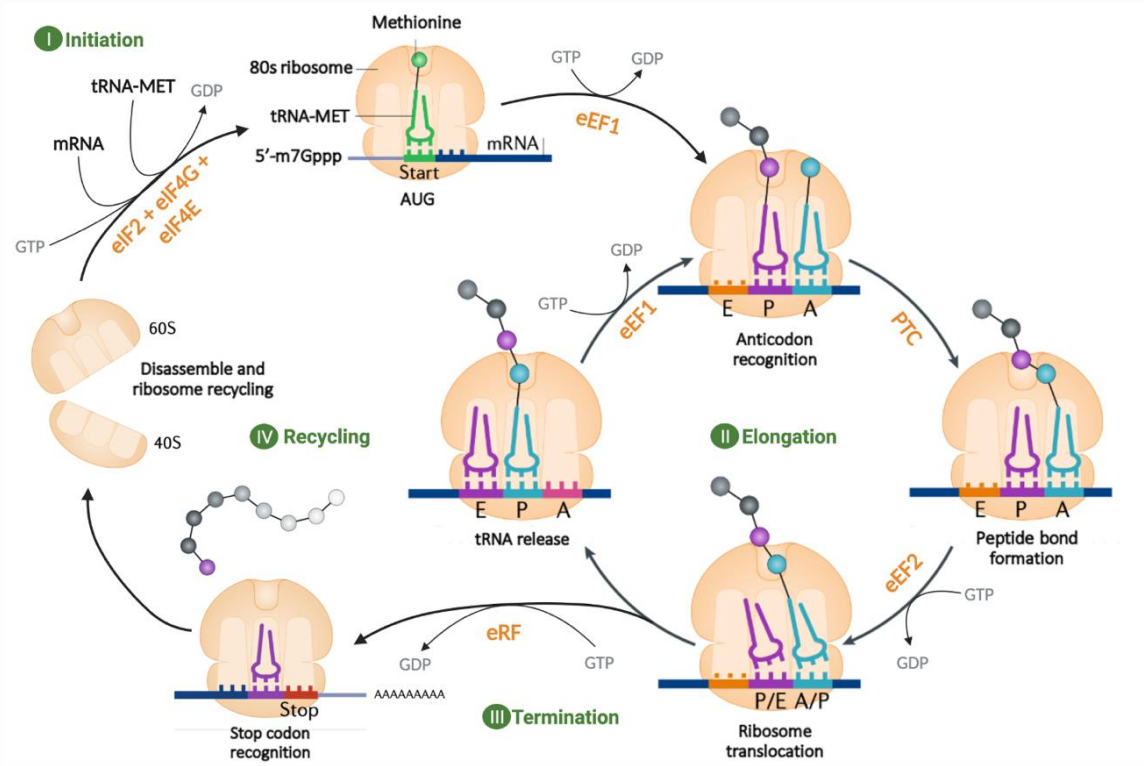

Figure 4 | Ribosomal gene translation. The schema shows the four phases of cytosolic gene translation: initiation, elongation, termination, and ribosome recycling. Adapted from (Schuller & Green, 2018)

1.2. AMINOACYL-tRNA SYNTHETASES (aaRS)

1.2.1. Aminoacyl-tRNA synthetases overview

Aminoacyl-tRNA synthetases (aaRS) comprise an ancient family of enzymes involved in the first step of protein synthesis, the aminoacylation reaction, consisting of charging each tRNA with its cognate amino acid. Interestingly, the requirement of an element mediating the genetic code translation was already pointed in the late fifties by F. Crick (Crick F. H., 1958).

The aminoacylation reaction is catalyzed in two steps. Firstly, the tRNA synthetase adenylates the corresponding amino acid by hydrolyzing an ATP molecule. The adenyl-aa works then as an intermediate molecule to attach the amino acid to the corresponding tRNA, specifically recognized by the enzyme. As a result, the AMP molecule is released, and the aminoacylated tRNA is delivered to the ribosome contributing to the nascent polypeptide chain (B. Alberts, 2015). Figure 5 illustrates the aminoacylation reaction.

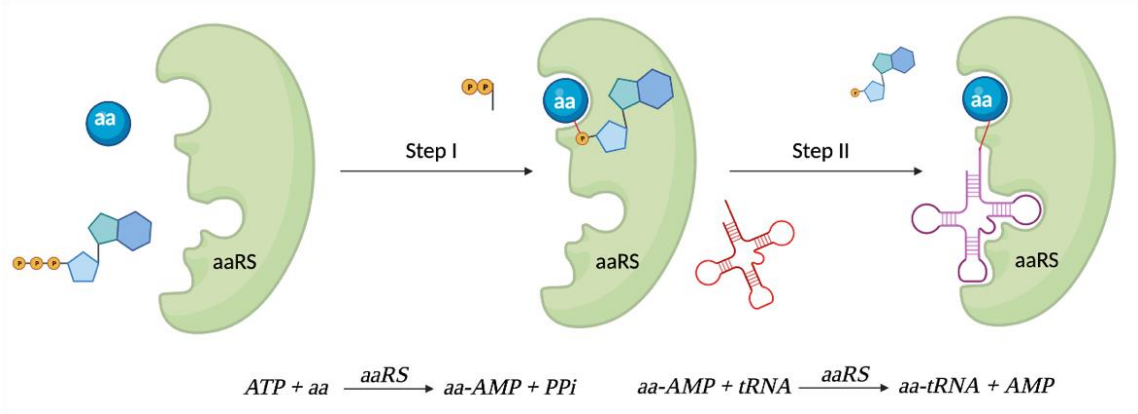

Figure 5 | Aminoacylation reaction. The figure shows the two steps conforming the aminoacylation reaction: Firstly, the amino acid is activated and then it is loaded into its cognate tRNA.

As mention before, there are 20 natural amino acids in the standard genetic code, and eukaryotes are expected to bear at least one aaRS per amino acid. Each of them might precisely aminoacylate all the tRNAs isoacceptors by recognizing not only the anticodon sequence but also specific structural tRNA features. Thus, aaRS confer the first level of fidelity and specificity to protein synthesis and constitute fundamental elements of gene translation, universally distributed across the tree of life (Giegé et al., 1998; M. Ibba & Soll, 2000). Notably, the vast majority of aaRS characterized to date are autonomous and self-sufficient enzymes that do not require the help of other proteins or cofactors to perform the aminoacylation reaction.

The aminoacyl-tRNA synthetase family present a well conserved structure, composed of a catalytic domain, where both steps of aminoacylation reaction occur, and a nucleic acid-binding domain involved in the tRNA recognition. Besides that, aaRS have been traditionally categorized into two classes based on the architecture of the catalytic domain, consensus sequences and chemical properties, which in turn are divided into subclasses. Class I aaRS present a typical Rossman ATP-binding domain in the catalytic core and they usually work as monomers. Alternatively, class II aaRS frequently form oligomers and hold a core structure based on seven antiparallel β-strands flanked by α-helixes very rarely found in other enzyme families (Carter, 2017; Ribas de Pouplana & Schimmel, 2001). Moreover, according to the subcellular compartment where they act, aaRS may be classified as cytosolic, mitochondrial or dual-localized, which act on both compartments (cytosolic and mitochondrial).

In *Drosophila melanogaster,* 34 genes have been identified to date encoding for tRNA-synthetases: 15 cytosolic, 15 mitochondrial and 4 dual-localized aaRS (Lu et al., 2015). The cytosolic glutamyl-prolyl-tRNA synthetase (GluProRS or EPRS) constitute a bi-functional enzyme that aminoacylates both tRNA pools ($tRNA^{GLU}$ and $tRNA^{PRO}$). Moreover, no mitochondrial glutaminyl-tRNA synthetase (GlnRS) has been identified so far in *Drosophila*. This is consistent with publish data showing that, in other organisms, the mitochondrial $tRNA^{GLN}$ is originated from the $tRNA^{GLU}$ as a result of the Glutamyl-$tRNA^{GLN}$ amidotransferase-catalyzed reaction (Echevarría et al., 2014; Nagao et al., 2009).

1.2.2. Non-canonical functions of aaRS

The aaRS family is considered one of the most ancient families of proteins. Throughout their long evolutionary history, they have adapted to acquire alternative activities that go far beyond the aminoacylation function. These non-canonical roles impact on a wide range of other cellular processes, including transcription and translation regulation, immunologic response or mitochondrial RNA splicing, among others (Levi et al., 2020; Martinis et al., 1999; Pang et al., 2014; Paul & Schimmel, 2013; Smirnova et al., 2012; Yao et al., 2014).

The non-canonical functions of aaRS benefit from their existing binding sites for RNA, ATP and amino acids. However, aaRS are also considered remarkable scaffold platforms to incorporate new protein domains that allow them to acquire new aminoacylation-independent functionalities (M. Guo, Schimmel, et al., 2010; M. Guo, Yang, et al., 2010). Some of the typical domains that aaRS incorporated through evolution are the Endothelial Monocyte-Activating protein II (EMPAII) domain, the Glutathione S-Transferase (GST or GST-like) domain, or the helix-loop-helix WHEP domain, which appeared in the base of animals, and it has been evolutionary conserved to humans (Shiba. K., 2002). Importantly, it is well known that another mechanism through which aaRS achieved non-canonical roles is by generating aaRS splicing variants or proteolytic-derived fragments, which lack specific structural domains allowing them to gain new functions.

On the one hand, some members of the aaRS family have been suggested to regulate gene expression at both transcription and translational levels through its ability to bind nucleic acids. For instance, the *E. coli* alanyl-tRNA synthetase (AlaRS) can negatively regulate its gene expression by joining and blocking its transcription start site (TSS) at the specific position of the DNA strand (Putney & Schimmel, 1981). Similarly, the methionyl-tRNA synthetase (MetRS) in prokaryotes and the glycyl-tRNA synthase (GlyRS) in yeast can self-regulate their mRNA levels by binding to the 3'-UTR of the nascent mRNA molecule, which undergoes premature transcription termination (Dardel et al., 1990; Johanson et al., 2003).

On the other hand, the threonyl-tRNA synthetase (ThrRS) in *E. coli* regulates its own gene translation when it binds to the 5'-CAP region of the mRNA and generates a competition with the smaller subunit of the ribosome (Springer et al., 1988). A comparable mechanism is carried out by the aspartyl-tRNA synthetase (AspRS) in *S. cerevisiae*, which regulates its translational rate depending on the cellular $tRNA^{ASP}$ (Frugier & Giegé, 2003). Interestingly, a recent study performed in yeast suggested that the vast majority of aaRS may show a self-regulation mechanism at the translational level mediated by mRNA-binding and stabilization (Levi & Arava, 2019).

Moreover, aaRS can modulate transcription and translation processes in general trends beyond autonomous regulation. For instance, the mammalian Seryl-tRNA synthetase (SerRS) has been reported to modulate global protein synthesis thanks to the EF-1α-homologous motif hold in its sequence (Miseta et al., 1991). In addition, the human glycyl-tRNA synthetase (GlyRS) participates in the ribosome biogenesis by modulating the rRNA transcription in proliferative cells (Ko et al., 2000). Besides, the *E. coli* lysyl-tRNA synthetase (LysRS) can promote DNA replication when attaches to the upstream region of the replication start site and stabilizes the single DNA strand (Mirande, 1991). Remarkably, some studies associated the mitochondrial tyrosyl-tRNA synthetase, and leucyl-tRNA synthetase (mtTyrRS, mtLeuRS) with the Group I intron self-splicing in yeast (Caprara et al., 1996; Rho et al., 2002).

In the field, the interest for the aaRS non-canonical functions is constantly increasing and it has been shown that besides the gene expression-related roles, aaRS can perform regulatory roles in many other cellular scenarios. For example, it is consistent in yeast and mammals that the leucyl-tRNA synthetase (LeuRS) acts as an intracellular leucine sensor for the mTORC1 pathway activation. When the leucine levels increase, the LeuRS binds and activates the Rag GTPase protein in a leucine-depending manner, which stimulates mTORC1 and ultimately regulates protein synthesis, cell size, and autophagy (Han et al., 2012; S. Kim et al., 2021). Similarly, upon elevated glutamine levels, the human glutaminyl-tRNA synthetase (GlnRS) antagonizes the proapoptotic kinase ASK1 in a glutamine-dependent manner (Ko et al., 2001).

Interestingly. under certain conditions, a fragment or the full-length aaRS can translocate into another cellular compartment and carry out an aminoacylation-independent function. For instance, under stress conditions, both the LysRS and the GlyRS can translocate into the nucleus and generate a large amount of AP4A. This molecule has downstream effects on several pathways such as immune response, DNA replication or cellular growth (Carmi-Levy et al., 2008). Particularly, the LysRS inhibits Hint-1 (transcriptional repressor), allowing MITF and USF2 to release and induce the transcription of its target genes (R. T. Guo et al., 2009; Y.-N. Lee & Razin, 2005).

Intriguingly, some aaRS have evolved to acquire multiple roles beyond the aminoacylation activity, which eventually antagonize each other. This is the case of the TrpRS and TyrRS, which upon INF-γ stimulation undergo contrary downstream effects. The TrpRS translocates to the extracellular matrix where the N-terminal WHEP domain is cleaved. The derived fragment binds then to the VE-cadherin of epithelial cells and inhibits vessel formation (anti-angiogenic effect) (Tzima & Schimmel, 2006). Moreover, it was shown that a full-length form of the protein presents a DNA damage-protective role through translocating to the nucleus and promoting a PARP-mediated DNA-PK activation, which ultimately stimulates the activation of p53 (Jin, 2019; Sajish et al., 2012). Regarding the TyrRS, under stress conditions, its N-terminal domain (Mini-TyrRS) moves to the extracellular matrix where it interacts with the CXCR1 and CXCR2 receptors to promote immune cells migration and angiogenesis (Wakasugi et al., 2002). Following the same trend, its C-terminal EMAPII-like domain also works as a pro-inflammatory and pro-angiogenic cytokine in the extracellular matrix. On top of that, recent studies proposed a role of TyrRS full-length in DNA damage response. Apparently, upon stress conditions, the enzyme would translocate to the nucleus, where interacts with TRIM28 to activate the transcription factor E2F1 (Cao et al., 2017; N. Wei et al., 2014).

Remarkably, in eukaryotes, eight aaRS (IleRS, LeuRS, ArgRS, AspRS, GlnRS, EPRS, LysRS and MetRS) and three non-aaRS proteins (AIMP1/p43, AIMP2/p38 and AIMP3/p18) build the multi-synthetase complex (MSC). It was postulated that it serves as a scaffold platform for tRNA channeling to the ribosome and other factors involved in protein synthesis (Kyriacou & Deutscher, 2008). Some elements can release the complex under

certain conditions to perform alternative functions. For instance, the p43 acts very similar to the TyrRS (explained above) since it holds an EMAP II-homology domain in its sequence. As a second example, upon INF-γ stimulation, EPRS shows an angiostatic effect (similar to the TrpRS fragment explained above). It is phosphorylated and released from the MSC to join the GAIT complex, which negatively regulates the VEGF-A translation (Arif et al., 2011; Sampath et al., 2004). The p18, in contrast, is released in response to DNA damage; it translocates to the nucleus, where it activates ATM and ATR kinases to promote p53 phosphorylation (Park et al., 2005).

1.2.3. aaRS-like proteins

Interestingly, throughout their long evolutional history, numerous aaRS genes have experienced partial or complete gene duplications. This fact originated aaRS-like proteins or paralogs of aaRS, which have adopted new functions. Together with the non-canonical roles acquisition mentioned above, aaRS-like proteins emerged as drivers of organism evolution, providing increased complexity (Schimmel & Ribas De Pouplana, 2000).

Frequently, aaRS-like proteins are not considered members of the aaRS family so far since they have usually lost the aminoacylation activity. However, from a structural point of view, they tend to share a relatively high degree of identity with their aaRS paralogs. We find examples of aaRS paralogs spread throughout the three life kingdoms, and they are involved in a wide range of cellular functions (Figure 6). However, the molecular role of several aaRS-like proteins has not been deciphered yet.

In prokaryotes, a subset of aaRS-like proteins has been related to tRNA modification, translation fidelity or amino acid biosynthesis, among other cellular processes. For instance, the GluRS paralog, YadB, can activate glutamate. Interestingly, the amino acid does not attach to the catalytic core but to the anticodon region of the $tRNA^{ASP}$ instead, conferring a substantial tRNA modification at the position 34 (Blaise et al., 2005; Campanacci et al., 2004). Moreover, HisZ (HisRS paralog) and AsnA (AsnRS paralog) are

involved in the histidine and asparagine biogenesis, respectively (Nakatsu et al., 1998; Sissler et al., 1999). Alternatively, a group of aaRS-like proteins guarantees translation fidelity by unloading tRNAs that have been charged wrongly. Two examples are the AlaRS paralog, AlaX, and the ProRS-like protein, ProX (Ahel et al., 2003).

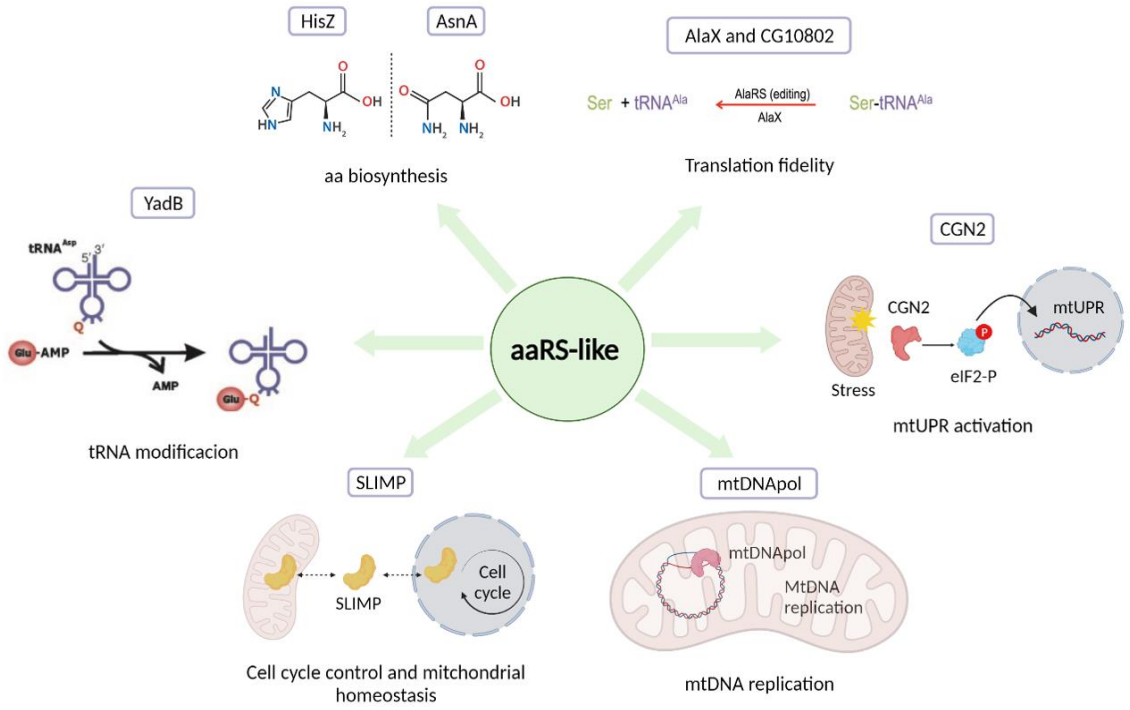

Figure 6 | Cellular implications of aaRS-like proteins. The schema collects some examples of aaRS-like proteins that evolved to acquire a wide range of cellular functions, such as, translation fidelity, mtDNA replication, tRNA modification, mtUPR activation or amino acid biosynthesis. SLIMP is the object of study of the present thesis and is also included in the figure because it is a SerRS-like protein with an essential role in mitochondria homeostasis and cell cycle regulation (see section 1.5). Adapted from (Michael Ibba & Francklyn, 2004; Novoa et al., 2015).

Interestingly, in yeast, the GCN2 protein kinase carboxyl-end is homologous to the entire sequence of HisRS. This protein is involved in the eIF2 phosphorylation during gene translation (Wek et al., 1989). Intriguingly, the *S. cerevisiae* Arc1p, paralog of the mammalian p43, is considered an aaRS-like protein involved in RNA binding and RNA nuclear transport (Deinert et al., 2001).

Furthermore, the mammalian mitochondrial DNA polymerase gamma (mtDNA-polγ) contains a domain homologous to the GlyRS (Fan et al., 1999). This enzyme is responsible for enhancing mitochondrial DNA (mtDNA) replication. Another example of aaRS-like protein in higher eukaryotes has been recently described: a paralog of the ThrRS called TARSL2. Notably, its protein structure contains an N-terminal extension partially homologous to the ArgRS and has been reported to interact with p43 as a former of the MSC (Zhou et al., 2019).

Remarkably, in *D. melanogaster*, employed as a model organism in the present work, few proteins have been identified as aaRS-like proteins. Some examples are the AlaRS paralog, *CG10802*, predicted to have a role in translation fidelity by recognizing and hydrolyzing Ser-tRNA^{ALA}; or the *CG8097* (paralog of ArgRS), which has ATP-binding activity, although its cellular role remains unknown (Lu et al., 2015; Zhou et al., 2019).

Finally, SLIMP (Seryl-tRNA synthetase insect mitochondrial protein) was identified as a paralog of the mitochondrial SerRS (SerRS2), which became an essential protein in *Drosophila* although it lacks the aminoacylation activity (Guitart, et al., 2010). It was recently published that SLIMP is a crucial component for the mitochondrial homeostasis (Picchioni, et al., 2019), and this project is focused on studying the cell cycle-related role of SLIMP.

1.3. MITOCHONDRIA

1.3.1. Mitochondrial origin and physiology

Mitochondria is broadly known as the "powerhouse" of the cell since it is responsible for most of the chemical energy produced in the cell. As the primary role, the organelle generates adenosine triphosphate (ATP) through oxidative phosphorylation (OXPHOS), but additionally, it has been linked to many other cellular processes and constitutes a key regulator for cellular physiology and homeostasis.

It is generally accepted that mitochondria (and plastids) are of bacterial ancestry. According to the endosymbiotic theory, mitochondria originated from a free-living form of bacteria which was eventually phagocyted by a host cell around 1500-2200 million years ago. It seems clear that the primitive mitochondria belonging to the bacterial phylum of alpha-proteobacteria would metabolize oxygen, while the host cell would be anaerobic until that moment. Thus, the symbiotic phenomenon entailed a significant evolutional advantage for both organisms, offering protection to the bacteria and the capability to increase energetic currency (ATP) through oxidative phosphorylation to the host cell. Intriguingly, the theory was already suggested in the late XIX century and postulated for the first time in 1927 by Ivan Williams (Wallin, 1927). However, it did not become popular and universally accepted until Lynn Margulis published it thirty years later (Margulis, 1967). The mitochondrial evolution became a hot topic and has been extendedly reviewed during the last half-century. However, there are still some issues under debate, for instance, the nature of the host cell (Davidov & Jurkevitch, 2009; Gray, 2012; Gray et al., 1999).

Throughout evolution, mitochondria transferred the bulk of their genome to the host cell. However, mitochondria still conserve a small DNA molecule (mtDNA), which is replicated and expressed within the organelle matrix. Mitochondrial genome only encodes for thirteen proteins, including seven subunits of Complex I (NADH ubiquinone oxidoreductase), one subunit from complex III (cytochrome c oxidoreductase), three

subunits from complex IV (cytochrome c oxidase) and 2 subunits of complex V (ATP synthase).

Whereas the other 99% of the mitochondrial proteome, including the whole Complex II (Succinate dehydrogenase), comes from the nuclear genome. Thus, in eukaryotes, nuclear and mitochondrial gene expression must be coordinated to guarantees mitochondrial physiological function and homeostasis.

Interestingly, the endosymbiotic theory places the mitochondria in the base of eukaryotic organisms and as the origin of compartmentalization, one of the main features acquired by eukaryotes during evolution. Unlike prokaryotes, eukaryotic cells are structured based on a membrane-bound organelle system that separates the essential cellular functions in different spaces within the cell. This system confers several evolutional advantages to eukaryotic cells, including the nucleus appearance that isolates and protects the DNA within the cell (Mcbride, 2018).

Regarding mitochondrial structure, the organelle is surrounded by two membranes that divide it into two aqueous compartments: the matrix and the intermembrane space (IMS). The outer mitochondrial membrane (OMM), a phospholipid bilayer, enclose and separate it from the rest of the cellular compartments by reducing the passage only to small molecules. The inner mitochondrial membrane (IMM) is a tight diffusion barrier for ions and molecules that need specific channels or transport proteins to pass through. The IMM holds the complexes of the respiratory chain involved in ATP production. It forms several invaginations called *cristae*, which increase the organelle's internal surface and enhance oxidative phosphorylation (OXPHOS) (Figure 7).

Adenosine triphosphate production happens when complexes I-IV anchored in the IMM generate an electron transport chain (ECT) by oxidizing the electron carriers (NADH and FADH) resulting from pyruvate and fatty acid oxidation in the mitochondrial matrix. Electrons will be pushed out into the IMS, generating an electrochemical gradient that ultimately leads to the ATP molecule formation through the F_1F_0-ATP synthase (Complex V) (B. Alberts, et al. 2015) (Figure 7). Moreover, the IMM electrochemical gradient state

is utilized by the cell as a sensor of mitochondrial physiology to trigger signal transduction upon unfavorable conditions. Additionally, it has been described the membrane potential to be essential for protein import (Neupert & Herrmann, 2007; Nunnari & Suomalainen, 2012)

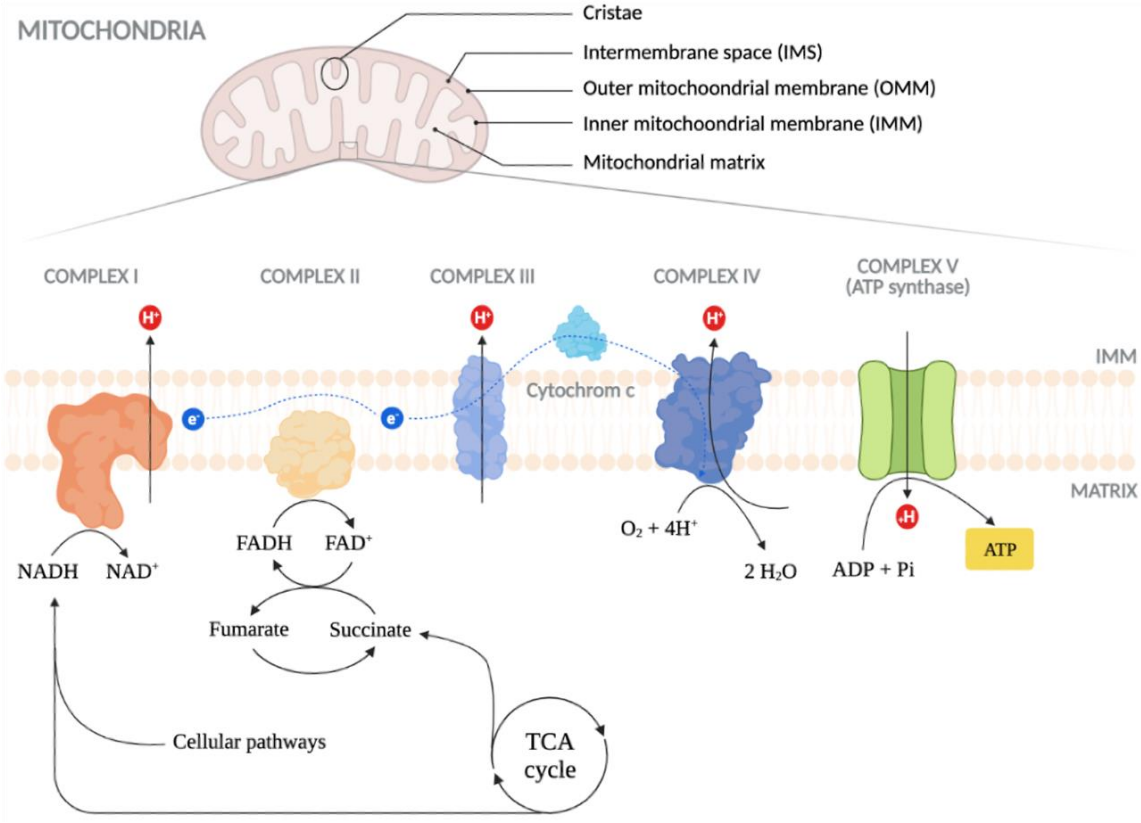

Figure 7 | Mitochondrial structure. The schema represents the mitochondrial structure and organization in different organelle compartments (upper part). Moreover, the respiratory chain elements are represented in the lower part of the figure, together with a simplified representation of OXPHOS for the ATP production. Electrochemical gradient is generated by the free electrons (blue) coming from NADH and FADH oxidation and the proton (red) transport through the different complexes. Finally, the ATP synthase uses the membrane potential resulting from the electrochemical gradient to generate ATP highlighted in yellow.

Furthermore, mitochondria have evolved to accomplish several cellular processes beyond ATP production, including the urea cycle, signal transduction, lipid metabolism, calcium storage or pyrimidine biosynthesis. Additionally, mitochondria have been described to be at the crossroad between nutrient availability and cellular growth, and

it is a fundamental regulator of autophagy and apoptosis within the cell (Chandel, 2015; Galluzzi et al., 2012).

1.3.2. Mitochondrial biogenesis and dynamics

Mitochondria are very plastic and dynamic structures that constantly undergo fission and fusion. Fusion occurs when two mitochondria become one, sharing their content (proteins and metabolites). It is essential for mtDNA repair. In mammals, Mitofusin 1 and 2 (MSN1 and MSN2) are responsible for mitochondrial outer membrane fusion, while OPA1 participates in inner membrane fusion. On the other hand, mitochondrial fission, carried out by Drp1, Fis1 and MTP18, refers to splitting a pre-existing organelle into two new mitochondria. Fission is essential to ensure equal mitochondrial segregation during cell division and allows the isolation of damaged mitochondrial pieces promoting autophagy. Overexpression of fusion-related proteins or down-regulation of fission-related proteins promotes the appearance of long mitochondrial filaments. Conversely, overexpression of fission-related proteins or fusion-related proteins depletion results in mitochondrial fragmentation (Chan, 2012) (Figure 8).

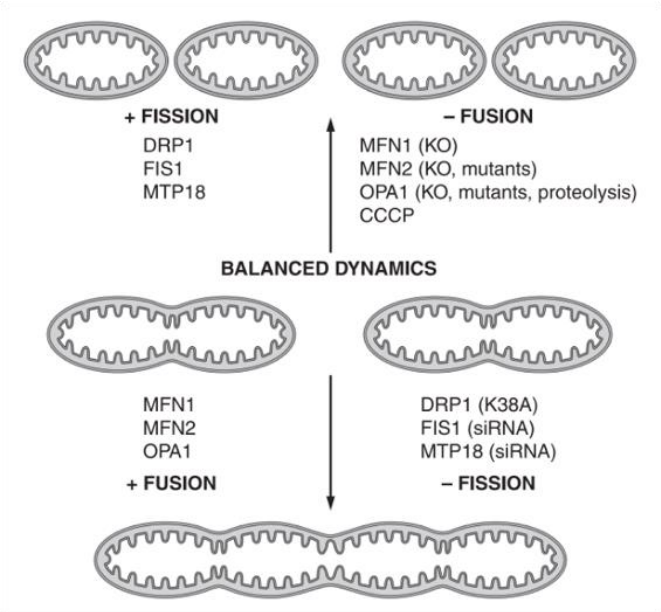

Figure 8 | Mitochondrial dynamics. Representation of mitochondrial fusion and Fission processes. Mitofusin 1 (MFN1), mitofusin 2 (MFN2) and OPA1 are implicated in fusion process,

while DRP1, FIS1 and MTP18 are crucial elements for the fission process. As it was mentioned a downregulation of any of these proteins can cause a decompensation in mitochondrial dynamics, resulting in mitochondrial fragmentation or mitochondrial filaments. Adopted from (Liesa et al., 2009).

Mitochondrial biogenesis is known as the growth and division process of pre-existing organelles. Importantly, the mitochondrial network is responsible for supplying the energetic requirement of every cell. Because of that, the mitochondrial number, size, and shape vary a lot depending on the tissue or cellular physiology. Good coordination between mitochondrial biogenesis, fusion/fission balance and mtDNA replication is essential to guarantee the proper mitochondrial mass and energy supply.

In the nucleus, the transcription factor PGC-1α is the master regulator of mitochondrial biogenesis. PGC-1α upstream modulates PPAR-γ, EWG and CNC (*Drosophila* homologous of the mammalian NRF1 and NRF2, respectively). These elements, together with the mitochondrial transcription factors A, B1 and B2 (TFAM, MTFB1 and MTFB2), are responsible for expressing mitochondrial-essential proteins, encoded in the nuclear and mitochondrial genomes. Interestingly, it has been reported that exercise-dependent AMP kinase (AMPK) and MAPK p38 stimulation can enhance PGC-1α activity (Akimoto et al., 2005). In contrast, the acetyltransferase GCN5 has been demonstrated to reduce PGC-1α activity and mitochondrial biogenesis (Fernandez-Marcos & Auwerx, 2011; Popov, 2020).

1.3.2.1. MtDNA replication

The mitochondrial genome consists of a circular double-stranded DNA molecule encoding for 13 polypeptide-coding genes, 22 tRNA genes and two rRNA genes, in both *Drosophila* and mammals. Moreover, the mtDNA contains a non-coding region (NCR) enriched on deoxyadenosine and thymidine (A + T), also known as the control region. The NCR condensates all the regulatory elements, including the replication origins and promoters needed for transcription. Intriguingly, the mitochondrial genome presents some general features, such as a highly compact organization and the lack of introns.

Each organelle holds several copies of the mtDNA molecule (G. L. Ciesielski et al., 2016; R. Garesse, 1988).

Three fundamental elements orchestrate the mtDNA replication: the DNA-helicase (TWINKLE, in mammals), the mitochondrial single-stranded DNA binding protein (mtSSB) and the mtDNA polymerase γ (DNApolγ). Because the polymerase can only bind single-stranded DNA, the helicase unwinds the DNA strand, and the mtSSB stabilizes it just before the polymerase catalyzes the replication reaction.

The mitochondrial DNA strand richer in guanosine is known as the heavy strand, while the complementary strand, richer in thymidine, is called the light strand. In mammals, each strand has an origin of replication differentially distributed in the mtDNA molecule. The heavy strand replication origin (O_H) is placed at the NCR, while the O_L (light strand replication origin) is located at two-thirds of the mtDNA molecule downstream from the O_H. MtDNA replication begins at the O_H when TWINKLE starts unwinding the DNA and allowing the DNApolγ catalyze the heavy strand's replication reaction. This asymmetry between the strands generates a displacement-loop (D-loop), a single-strand loop stabilized by the mtSSB. The light-strand replication starts as soon as the replication machinery arrives at the O_L. This replication model is called asymmetric or unidirectional (Rafael Garesse & Kaguni, 2005).

Much less is known about mtDNA replication in *Drosophila*. However, another system for mtDNA replication called the strand-synchronous model has been postulated in insects. In this model, the replication of both strands would start simultaneously at the single origin of replication (O_R) placed at the NCR. The replication process happens synchronously and bidirectional as in a regular replication fork. Nevertheless, both systems seem to coexist in insects, and there are many issues still under debate (Jõers & Jacobs, 2013; Saito et al., 2005). The *Drosophila* mtDNA is illustrated in Figure 9.

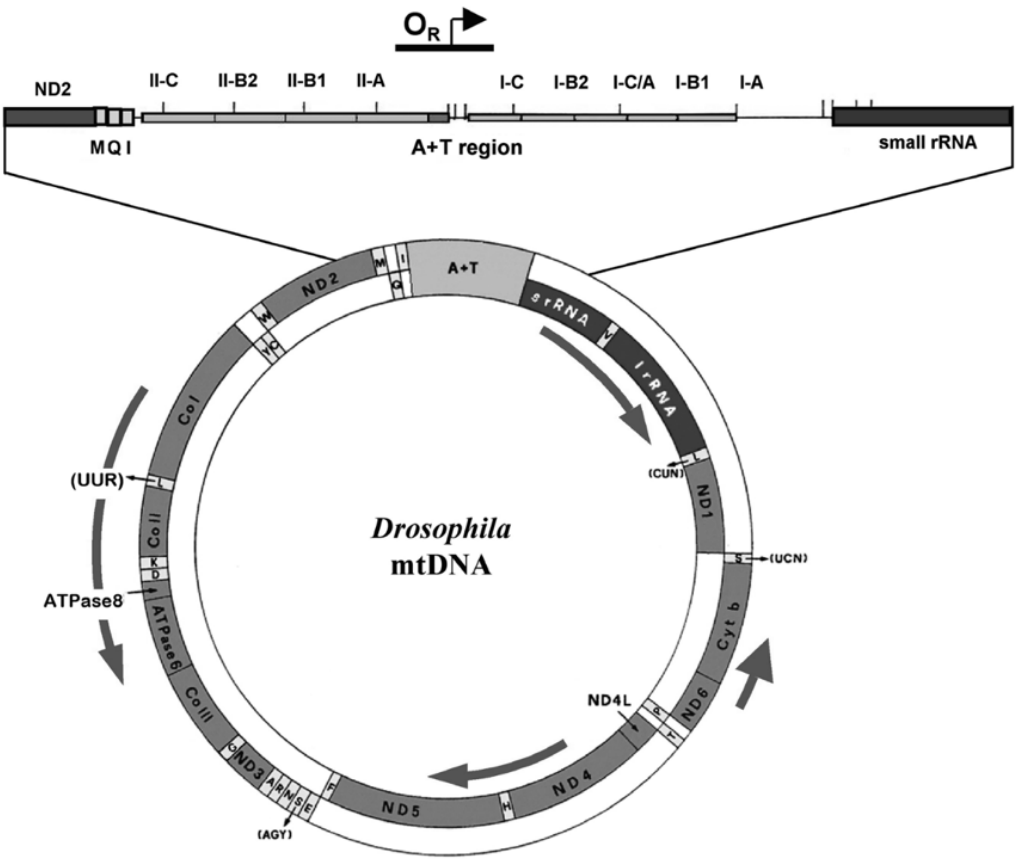

Figure 9 | *Drosophila* mtDNA organization. The content of the mitochondrial DNA in *Drosophila* is the same than in vertebrates, but the distribution of the genes through the two strands differ. The mtDNA encode for 13 protein-encoding genes: 2 subunits of the ATP synthase (ATPase), three subunits of the cytochrome c oxidase (CO), the cytochrome b (CytB) and seven subunits of the NADH dehydrogenase (ND). Moreover, mtDNA encode for the large and the small ribosomal RNAs (lrRNA and sRNA respectively), and 22 tRNAs which are indicated by the letter of its cognate amino acid. It can be observed the regulatory region (NCR) holding the putative origin of replication (O_R) with an arrow indicating the replication direction of the leading strand. Adapted from (Rafael Garesse & Kaguni, 2005).

1.3.2.2. Mitochondrial transcription

The mtDNA is transcribed as a polycistronic RNA molecules, which will be cleaved, and processed afterwards. In *Drosophila* five different transcription start sides have been described, while in mammals only two polycistronic structures has been identified so far, one per strand (Berthier et al., 1986). After transcription the tRNA molecules fold

into a cloverleaf secondary structure generating boundaries between the mRNA and rRNA transcripts that will guide ribonucleases to cleave and release the individual transcripts. The ribonuclease P (RNase P) cleaves the 5'-end, whereas the ribonuclease Z (RNase Z or ELAC2) processes the 3'-end of each tRNA molecule (Dubrovsky et al., 2004; Hartmann et al., 2009). Finally, the mRNAs will be adenylated at the 3'-end while the CCA addition to the 3'-end of the tRNAs will conclude the tRNA maturation. This system is called "tRNA punctuation model" and is illustrated in the Figure 10 (Ojala et al., 1981).

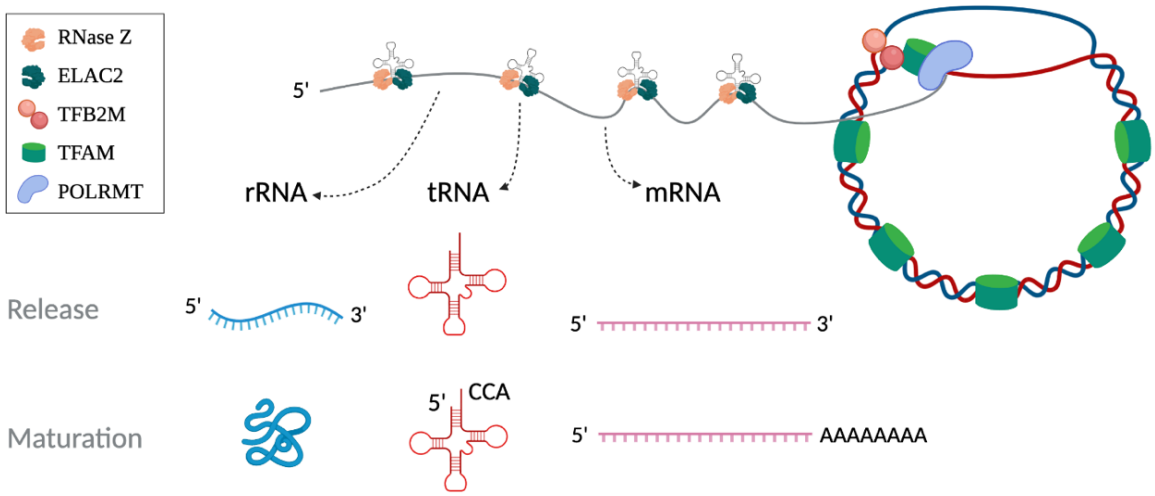

Figure 10 | Mitochondrial gene expression and maturation. The scheme illustrates the punctuation method. The mtDNA is transcribed as a long polycistronic RNA where the tRNA acquire a secondary structure working as a guide for the ribonucleases (RNase Z and ELAC2) to cut between the transcripts. Afterwards each RNA molecule will be processed and get mature: mRNA will be adenylated, tRNAs will be modified (CCA incorporation) and the rRNA processed and folded.

MtDNA expression requires the catalytic activity of the mitochondrial RNA polymerase (POLRMT) along with mitochondrial transcription factors, such as transcription factor A, B1 and B2 (TFAM, MTFB1 and MTFB2) and some termination factors like the *Drosophila* mTTF.

TFAM is the main mitochondrial transcription factor. It binds non-specifically to the mtDNA through two high mobility groups (HMG) and plays an important role, not only as transcription factor enhancing mtDNA expression, but also confers structural features to the mtDNA architecture by binding and stabilizing it. TFAM directly interacts and stimulates both promoters at the heavy strand (HSP) and light strand (LSP) (Matsushima et al., 2010; Yonghong Shi et al., 2012). It creates a U-turn structure that may be needed to enhance the interaction with TFB2M to increase the transcription initiation rate at the LSP (Rubio-Cosials et al., 2011). While the TFB2M also interacts with mtDNA and TFAM and is essential for mtDNA transcription, particularly in *Drosophila*, the MTFB1 has been described to not be involved in mtDNA transcription or mtDNA copy number, but it seems to play an important role in mitochondrial translation instead (Matsushima et al., 2004, 2005).

The mitochondrial termination factor mTTF is responsible for the mtDNA transcription termination. It binds to two mtDNA sequence elements located at the boundary of clusters of genes transcribed in opposite direction, named the boundary ND3/ND5 and Cytb/ND1, respectively (Roberti et al., 2006). It has been shown that when mTTF is attached to the mtDNA, the transcription process ceases, so it is though that it could mediate replication/transcription conflicts in the organelle (Jõers et al., 2013).

Interestingly, the mtDNA together with the replication and transcription machinery are packed in a compact structure called the mitochondrial nucleoid, within the mitochondrial matrix (Bogenhagen et al., 2008; Rebelo et al., 2011). Another important component localized in the nucleoid is the LON protease which belongs to the ATP-dependent proteases family. It consists of a homo-oligomeric ring-shaped structure organized in three domains: The ATP-binding domain (AAA^+), the substrate-binding domain (SBD) and the proteolytic domain (PD) (S.C. Park et al., 2006; Stahlberg et al., 1999). LON constitutes the main mitochondrial protease and has several target proteins. However, it is involved in several roles within the organelle, such as chaperon activity or DNA-binding protein, beyond the protease canonical function (Pinti et al., 2016). In *Drosophila*, it has been demonstrated that LON specifically degrades TFAM, directly regulating the TFAM:mtDNA ratio. Since it has been reported that lower levels of TFAM

correlate with a decrease in the mtDNA copy number, LON has a direct impact on the regulation of the mtDNA copy number and replication rate (Matsushima et al., 2010).

1.3.2.3. Mitochondrial translation

The mitochondrial protein synthesis machinery is distinct from its nuclear/cytosolic counterparts and has also diverged markedly from its bacterial ancestor. For instance, the mitochondrial ribosomes (mitoribosomes) contain a small subunit (28S) and a large subunit (39S) comprising only one rRNA per subunit (Faye & Sor, 1977). As in bacteria, the first codon to be translated (AUG) encodes for formyl-methionine instead of methionine (Clark & Marcker, 1966). Moreover, the genetic code in mitochondria and prokaryotes diverges a little bit from the universal genetic code. For instance. in *Drosophila*, the mitochondrial AGG codon is absent, the cytosolic isoleucine codon AUA is decoded as methionine in the organelle, and the cytosolic stop codon UGA is decoded in the mitochondria as a tryptophan (Jukes & Osawa, 1993). Finally, the initiation, elongation, and termination factors that participate in the process are organelle-specific (Gaur et al., 2008; Pietromonaco et al., 1991).

The mitochondrial translation starts when the small subunit of the mitoribosome (SSU) binds to the mitochondrial initiation factor 3 (mIF3) and together they join the initiation factor 2 (mIF2), the mRNA and the tRNA loaded with formyl-methionine (tRNA-FM) (Spencer & Spremulli, 2004). Once the initiation complex is assembled, the large subunit of the mitoribosome (LSU) joins the complex, and both initiation factors are released in a GTP-consuming manner. Then, the next tRNA charged with its cognate aa enters the A-site of the mitoribosome, with the mitochondrial elongation factor Tu (mEF-Tu), which participates in the codon-anticodon recognition. Base-pairing is an energy-consuming step. The ribosome is responsible for catalyzing the peptide bond formation at the A site, and the mitochondrial elongation factor G1 (mEF-G1) promotes the translocation of the tRNA with the growing polypeptide chain from the A to the P-site within the ribosome. Finally, when a stop codon enters the A-site of the ribosome, it is recognized by an uncharged tRNA, and a termination factor promotes the dissemblance of the

complex, releasing the polypeptide product (Chrzanowska-Lightowlers et al., 2011; Hällberg & Larsson, 2014).

1.3.3. Mitochondrial protein import

Most of the proteins essential for mitochondrial biogenesis and homeostasis are encoded in the nuclear DNA, synthesized in the cytosol, and imported into the organelle afterwards. Several cytosolic soluble elements, called chaperones, are responsible of stabilizing and protecting the nascent polypeptide chain as soon as it releases the ribosome to avoid misfolding or protein aggregation. On the other hand, membrane receptors on the mitochondrial surface participate in recognizing sequences or secondary structures that promote the protein internalization into the organelle.

In general, the import process is carried out through the TIM/TOM system, consisting of two transmembrane channels in the outer membrane (TOM) and inner membrane (TIM). Nevertheless, mitochondrial-imported proteins comprise different chemical features depending on the mitochondrial sub-compartment they are directed to, and specific receptors and proteins have been identified to be involved in each type of protein internalization. Proteins targeted to the mitochondrial matrix tend to have a mitochondrial signal peptide (MSP) at the N-terminus, enriched in hydrophobic residues and cleaved once the protein reaches its natural location. Proteins placed in the inner membrane present an additional hydrophobic signal peptide inside the sequence that is not cleaved and anchors the peptide to the IMM. Very similarly, proteins directed to the intermembrane space have two signals, being both hydrophilic and cleaved after reaching the IMS. Finally, proteins located in the OMM present a long hydrophobic signal peptide at the N-terminus that is not cleaved and anchors the protein to the outer membrane (Avendaño-Monsalve et al., 2020; Dudek et al., 2013; Wiedemann & Pfanner, 2017).

The post-transcriptional mitochondrial import (explained above) has been extendedly studied and has been accepted for many matrix proteins known to date (Avendaño-

Monsalve et al., 2020; Chacinska et al., 2009). However, evidences of co-translational import are constantly increasing. It was recently demonstrated the presence of cytosolic ribosomes together with some mRNA molecules near the OMM receptors, suggesting the simultaneously translation and import of these nuclear-encoded mitochondrial proteins (Ahmed & Fisher, 2009; Gold et al., 2017; Lesnik et al., 2014, 2015; Williams et al., 2014). Nevertheless, the specific features that determine which type of import will follow each protein remains still unclear.

In recent years, it has been demonstrated that some proteins can localize at more than one compartment within the cell where at least one of them might be an organelle. It is called dual-localization, and several mechanisms have been proposed to underly this phenomenon. The targeted sequence accessibility is one of the major forces driving dual-localization. It may happen that due to a protein interaction, post-translational modification or folding conditions, the targeting sequence becomes inaccessible or otherwise, more accessible, changing the protein localization under certain conditions (Kalderon & Pines, 2014; Karniely & Pines, 2005).

The yeast adenylate kinase (ADK1) is an example of dual-localized protein due to the folding speed force. ADK1 present a mitochondrial signal peptide (MSP) within its sequence. However, when it is very rapidly folded after translation, the MSP gets hided. Therefore, if the nascent polypeptide reaches the OMM receptors before getting fold, the protein localizes at the organelle matrix, but if instead, it folds in the cytosol, the protein will never reach the mitochondria (Strobel et al., 2002). Something similar occurs with Fumarase in yeast which also contains an MSP. In this case, all molecules would be translocated into the mitochondria and get the MSP cleaved, but it is known that a subpopulation of the protein can then be retro-translocated back to the cytoplasm, generating a MSP-lacking isoform outside the organelle (Sass et al., 2001, 2003; Yogev et al., 2010).

As mentioned before, the signal peptide accessibility can also be affected by a post-translational modification or protein interaction which eventually conceals the targeting sequence. For instance, the apurinic/apyrimidinic endonuclease 1 (APN1) bears a

nuclear localization signal (NLS) and a MSP within the sequence. Whenever APN1 interacts with the cytosolic protein Pir1, it masks the NLS, and the protein is mainly imported into the mitochondria. Conversely, when they do not interact, APN1 is more efficiently imported into the nucleus. APN1 display similar roles in both compartments related to DNA damage response (Vongsamphanh et al., 2001). On the other hand, the cytochrome 450 family member CYP2E1 is regularly imported into the endoplasmic reticulum (ER). However, the PKA-mediated phosphorylation unmasks the previously cryptic MSP and promotes its import into the mitochondria (Avadhani et al., 2011).

Furthermore, mitochondrial membrane breakage or vesicles-mediated export have been proposed as mechanisms to explain the presence of mitochondrial proteins in the cytosol. For instance, Parkin is a mitochondrial protein demonstrated to be exported from the organelle through vesicle-derived traffic to regulate mitochondrial quality control (McLelland et al., 2014; Sugiura et al., 2014).

Finally, a set of mitochondrial proteins has been described to localize in other cellular compartments in response to stress or dysfunction. The organelle uses the dual-targeting system to communicate with the rest of the cell. This scenario will be explained in depth in the next section. Figure 11 represents some of the driving forces for dual-localization proteins explained above.

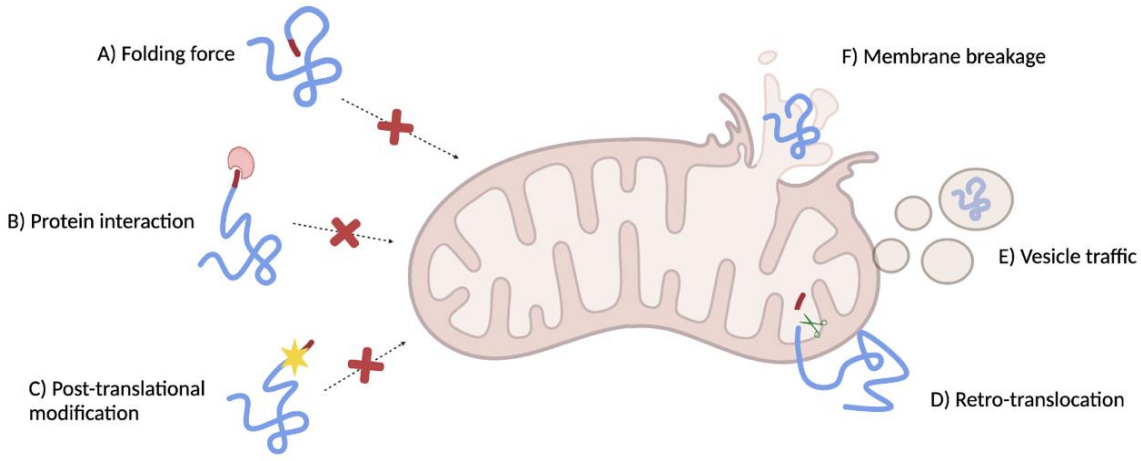

Figure 11 | Molecular mechanisms for dual-localized proteins. The schema represents some of the more common molecular mechanisms underlying the dual-localization of a single protein product. (A) Folding force, (B) Protein interacting with the targeting sequence, (C) A post-translational modification interfering with the MSP recognition,

(D) Retro-translocation of the protein after MSP cleavage, (E) Vesicle-derived traffic and (F) Mitochondrial membrane breakage due to damaging conditions.

1.3.4. Mitochondria-nucleus communication

As mentioned before, mitochondria are not only at the heart of cellular energy harvesting, but they also regulate many aspects of cellular physiology. Consequently, mitochondria are constantly in tight communication with the rest of the cell, especially with the nucleus. Mitochondrial activity is under nuclear control through the so-called anterograde signaling, mainly consisting in mitochondrial nuclear-encoded proteins expression and import. These signals can modulate mtDNA expression, mitochondrial biogenesis, dynamics and activity depending on the cellular needs. On the other hand, the organelle can send retrograde signals to the nucleus to alter the expression of nuclear genes in response to mitochondrial stress or damage, activating a set of pathways, such as mitochondrial unfolded protein response (mtUPR), mitochondrial biogenesis, mitochondrial protein import or cellular proliferation (English et al., 2020; Quirós et al., 2016).

Different types of mitochondrial-derived molecules have been described to work as retrograde signals, including peptides, nucleic acids, metabolites, and proteins. For instance, the mitochondrial-derived peptides (MDP) known as MOTS-c are small peptides generated in the organelle, which under exercise-related stress, travel to the nucleus and stimulate the gene expression of certain transcription factors. It promotes a signaling cascade that ends up stimulating mitochondrial biogenesis (C. Lee et al., 2015; Reynolds et al., 2021).

In addition, mitochondrial-derived small molecules also affect gene expression in the nucleus. For instance, NAD^+ is a cofactor of several enzymes, including PARP-1, hence changes in extra-mitochondrial NAD^+ levels can ultimately modulate chromatin organization or DNA damage response (M. Y. Kim et al., 2005; Koch-Nolte et al., 2011). On the other hand, metabolite-mediated signaling through methyl and acetyl groups

from mitochondrial signaling to the nucleus is crucial for epigenetic regulation (Kaelin & McKnight, 2013; Shaughnessy et al., 2015). Moreover, the mtDNA-derived fragments exported to the nucleus have been described to be involved in enhancing immunologic response. Finally, mtROS (mitochondrial reactive oxygen species) and calcium (Ca^{2+}) seems to play crucial roles outside the organelle in response to oxidative stress (Chandel, 2015; Fetterman & Ballinger, 2019).

Furthermore, as mentioned in the previous section, several studies revealed that mitochondrial proteins could dual-localize in other compartments under stress conditions. A set of mitochondrial proteins have emerged as nuclear regulators and constitute an essential part of the retrograde signals (Monaghan & Whitmarsh, 2015). Thus, they work as powerful signals which inform the nucleus about the organelle physiological state and enhance a particular cellular response. Examples of this regulatory mechanism have been found in all the eukaryotic kingdom, from yeast to humans. In *C. elegans*, for instance, ATFS-1 is usually imported into the organelle to get degraded there. However, under mitochondrial stress conditions, the mitochondrial import is reduced and ATFS-1, which also contains an NLS signal, accumulates within the cytosol and translocates to the nucleus, where activates the mitochondrial unfolded protein response (mtUPR) (Nargund et al., 2012, 2015). Similar mechanisms occur with the yeast transcription factors RTG1, RTG2 and RTG3, which leave the organelle to localize to the nucleus and modulate gene expression depending on the ATP requirement and availability (Torelli et al., 2015).

Similarly, the pyruvate dehydrogenase complex (PDC) in mammals was reported to travel from the mitochondrial matrix to the nucleus to coordinate metabolism status and cell growth upon growth stimuli or oxidative phosphorylation impairment. Although the role is clear, the transport of the whole complex from one organelle to the other is still under research. Non-degradative vesicle traffic has been recently proposed as a protein retro-translocation method which could be underlying this mechanism. Intriguingly, it has been shown that the retro-translocation of a protein fragment outside the mitochondria is enough to send a retrograde signal. For instance, recently, it was described that upon stress conditions, DELE1 gets cleaved by the mitochondrial protease

OMA1 (in mammals) and translocate into the cytosol, where it activates mtUPR by inducing ATF4 translation and promoting eiF4α phosphorylation (Fessler et al., 2020; X. Guo et al., 2020)

Finally, it is fundamental for cellular and organism viability that the cell cycle regulators may be aware of cellular physiology to fix any trouble before the cell getting divided. In that sense, retrograde signals are crucial to keep the nucleus informed about the organelles physiology and guarantee the quality of the progeny. For instance, it was described in *Drosophila* that upon complex I dysfunction, the increased mtROS levels are enough to signal a set of transcription factors outside the organelle, such as FOXO and ASK-1, and impair the G1 to S transition of the cell cycle through its downstream effector Dacappo (p27 *Drosophila* homolog). This mechanism is known to be conserved in mammals (Owusu-ansah et al., 2008).

1.4. CELL CYCLE

Organisms, tissues and ultimately organs need to be of specific size and shape. At the cellular level, these features depend on a tightly regulated equilibrium between cell mass (cellular growth), cell survival, and, more importantly, cell division (proliferation). The molecular mechanism underlying the coordination of these three events is known as cell cycle or cell division cycle. It is defined as the process by which a cell grows and is divided, resulting in two daughter cells identical between them and to the progenitor in terms of mass and genetic information.

Proliferation is a central process in cellular biology, and it depends directly on cell cycle regulation. It is well-known that any slight alteration of the cell cycle can drive the organism to severe viability problems. For instance, in humans, a decrease in the division rate can lead easily to developmental defects, and conversely, a non-controlled increase in cell proliferation often head to tumor formation. For this reason, a complex on-off biochemical switch-based system regulates the cell cycle progression. Numerous cellular pathways, frequently redundant, orchestrate a robust and reliable system that senses intracellular and extracellular signals and adapts the cell cycle progression to different physiological situations, including starvation, stress, or DNA damage (B. Alberts, A. et al, 2015).

The classical eukaryotic cell cycle comprises four phases: G_1, S, G_2, and M. Chromosome duplication occurs in the Synthesis phase (S-phase) and chromosome segregation in the Mitotic phase (M-phase). Intriguingly, most cells require much more time to grow and double their mass, including organelles, than dividing themselves. Thus, two gap-phases, comprised between the S-phase and the M-phase, complement the cell cycle: Gap phases 1 and 2 (G_1 and G_2, respectively). Interestingly, G_1, S and G_2 phases constitute the interphase that takes 90% of a cell cycle time. M-phase, in turn, is technically divided into stages: prophase, metaphase, anaphase, and telophase. Finally, the physical separation of the two daughter cells is called cytokinesis, and it is not strictly considered part of the M-phase (Figure 12).

Moreover, at key transitions, three major checkpoints monitor the successful completion of upstream events before proceeding to the next phase (Hartwell & Weinert, 1989; Walworth, 2000). The three checkpoints occur at the entry of the S-phase (G_1-S transition), the M-phase (G_2-M transition), and during mitosis at the anaphase onset. Therefore, when cells accumulate troubles in any of the phases, commonly during DNA replication or mitosis, the cell cycle can be arrested in a particular phase while the problems are fixed, or otherwise undergo apoptosis, when it is not possible to figure them out (Pietenpol & Stewart, 2002) (Figure 12).

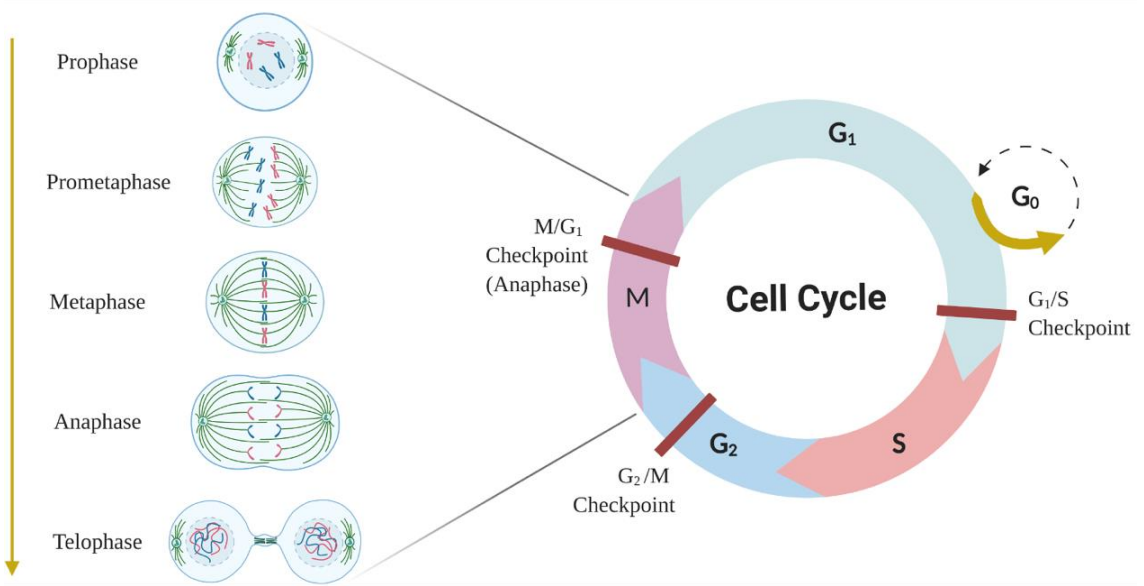

Figure 12 | Cell cycle phases. Cell cycle stages consisting of interphase, comprising G_1, S-phase and G_2; and Mitosis, which is composed of prophase, prometaphase, metaphase, anaphase, and telophase. Cytokinesis is not represented, and the three checkpoints are highlighted In red.

At the molecular level, the leading players of cell cycle regulation are CDKs (Cyclin-dependent Kinases) and their cofactors Cyclins (Cyc). The CDK's levels tend to be stable throughout the cell cycle, while cyclins expression is strongly regulated and limited to specific cell cycle phases and determines the presence of the functional complex CDK-Cyc. Hence, the regulation of cyclins expression ensures the proper cell cycle progression. Similarly, the transcriptional control of a set of proteins called CDK inhibitors (CKIs) negatively regulates the CDKs activity (Poon, 2016).

Although transcriptional control constitutes the first stage of regulation in the cell cycle progression, various posttranslational modifications, such as phosphorylation or ubiquitination, add several layers of complexity to the process (Dang et al., 2021; Fisher et al., 2012). For instance, the CDK-Cyc complex formation depends initially on cyclins expression; however, the complex activity ultimately relies on its phosphorylation state. The CDK-Cyc formation triggers a conformational change on the CDK, allowing a specific structure in the catalytic core called T-loop to move onto the protein surface. It is not until the CDK-Activating Kinase (CAK) phosphorylates specific residues on the T-loop that the complex becomes fully active (van den Heuvel, 2005).

On the other hand, ubiquitin-mediated proteolysis promotes the quick degradation of cyclins, CKIs and other essential regulatory elements, contributing to the rapid oscillation of the on-off switch-based system required for cell cycle regulation. Several E3 ubiquitin ligases, basically belonging to two superfamilies, the Skp1-Cullin-Fbox (SCF) and the Anaphase Promoting Complex (APC/C). are periodically expressed throughout the cell cycle and are in charge of protein-specific ubiquitination (Teixeira & Reed, 2013).

1.4.1. G_1-S transition

Control of cell proliferation generally occurs during the first gap phase (G_1), when cells mainly grow and get prepared to replicate their DNA. Entering in S-phase represents a non-return point called restriction point (R); cells that reach this step get committed to cell division and become refractory to any intracellular or extracellular signals. The G_1 to S transition is influenced by several intrinsic and extrinsic signals, ranging from growth factors to developmental cues, that represent the first cell cycle brake-point. Thus, when cellular and environmental conditions are optimal enough, cells move forward the cell cycle and get engaged to DNA replication initiation. (Pardee, 1989; Rubin et al., 2020; Stallaert et al., 2019).

Importantly, however, under non-suitable conditions, cells will not accomplish the cell cycle, reaching a quiescent state known as G_0. It can be reversible, allowing the cells to

eventually reenter the cell division cycle when the proliferative requirements get better; otherwise, it can be permanent, which happens in some differentiated cells that remain in a non-proliferative state despite being metabolically very active (Bertoli et al., 2013; Duronio & Xiong, 2013; Pardee, 1989).

The restriction point is fundamentally controlled by the Retinoblastoma (RB) pathway, named after the first tumor suppressor gene, identified in a human retinoblastoma tumor, the retinoblastoma protein (pRB) (Weinberg, 1995). In mammals, three different genes encode for this protein family (RB1, RBL1 or p107 and RBL2 or p130), whereas in *Drosophila*, only two proteins are present, the retinoblastoma family proteins 1 and 2 (RBF1 and RBF2). Retinoblastoma proteins directly interact with and repress the members of the E2F transcription factor family (Heuvel & Dyson, 2008). In *Drosophila*, it comprises two elements: a potent transcriptional activator (E2F1) and the transcriptional repressor (E2F2), which antagonistically regulate the transcription of many target genes involved in S-phase onset and DNA replication (Frolov et al., 2001). Importantly, E2F proteins require the cofactor PD (Protein Dimerization) which directly binds to DNA, to perform its transcription factor activity (Wu et al., 1995). In *Drosophila*, only one protein belongs to the PD family (dPD) and interacts with E2F1 and E2F2. Interestingly, it was demonstrated that E2F1 and E2F2 activity is modulated explicitly by RBF1 and RBF2, respectively (Stevaux et al., 2002, 2005).

During the early G_1 phase of a mitotic cell cycle, RBF1 is present in a dephosphorylated active form, able to bind and sequester E2F1. Upon mitogenic signals, the cyclin D (Cyc D) transcription is enhanced, which binds and activates its partners, CDK4 and CDK6 (CDK4/6). In mammals, three different isoforms of CycD are found (CycD1, D2 and D3), which form complex with both CDK4 and CDK6, whereas in flies, a single gene encodes for CycD and no CDK6 has been identified yet, reducing the active complex to CDK4/CycD.

Several signal transduction cascades are activated upon mitogenic signals which ultimately induce the expression of CycD. The canonical Ras–Raf–MEK–ERK mitogen-activated protein kinase (MAPK) pathway is the best-characterized pathway upstream

CycD transcription (Morrison, 2012). However, other molecular mechanisms can stimulate this step like the NOTCH or the WNT pathways or extracellular matrix (ECM) proteins, such as integrins or cytokines (Bertoli et al., 2013; Duronio & Xiong, 2013; Rubin et al., 2020).

In late G_1, near the R point, the CDK4/CycD complex mono-phosphorylates RBF1, contributing to its dissociation from E2F1, and ultimately allowing the transcription of genes that will promote the transition from G_1 to S phase (Dyson, 1998; Harashima et al., 2013; Heuvel & Dyson, 2008). E2F1 is a master transcriptional regulator in the cell, essential for the G_1 to S transition, but also responsible for the expression of a wide range of genes involved in other cell cycle stages, and other cellular processes such as apoptosis or differentiation (Blais & Dynlacht, 2004; Bracken et al., 2004). Among the E2F-target genes, are the cyclins E and A (CycE and CycA), which in combination with CDK2, regulate the entering and progression throughout S-phase, respectively. Importantly, the CDK2/CycE complex promotes the RBF1 hyperphosphorylation, generating a positive feedback loop that completely bypasses the R point and culminates in S-phase entry.

Additionally, two more positive feedback loops arise from the E2F1 activation, ensuring that cells can not go back to G1, after reaching the R point. Firstly, E2F1 enhances its own expression. Furthermore, E2F1 regulates the expression of SKP2, an SCF-E3 ubiquitin ligase responsible for the CDK2-inhibitor DACAPO (DAP) degradation, which reinforces the CDK2/CycE and CDK2/CycA complexes activity (Duia et al., 2013; D. G. Johnson et al., 1994; Yung et al., 2007). Figure 13 illustrates the G_1 to S transition and the R point.

Intriguingly, different models have been postulated about the contribution of each complex (CDK4-CycD and CDK2-CycE) to the E2F1 release and activation. Although, CDK4/CycD was initially characterized as the main responsible for the RBF1 phosphorylation, it has been also linked with cellular growth in *Drosophila* (Datar et al., 2000). Interestingly, a recent study places CDK4/6-CycD at the crossroad between cell proliferation and cellular growth, coordinating both processes, and points to CDK2/CycE

as the main regulator of the RBF1 phosphorylation (Yiqin Ma & Edgar, 2021). In any case, what is the exact contribution of each complex to the E2F1-mediated transcriptional cascade at the S-phase onset is still under debate (Grant & Cook, 2017; Rubin et al., 2020).

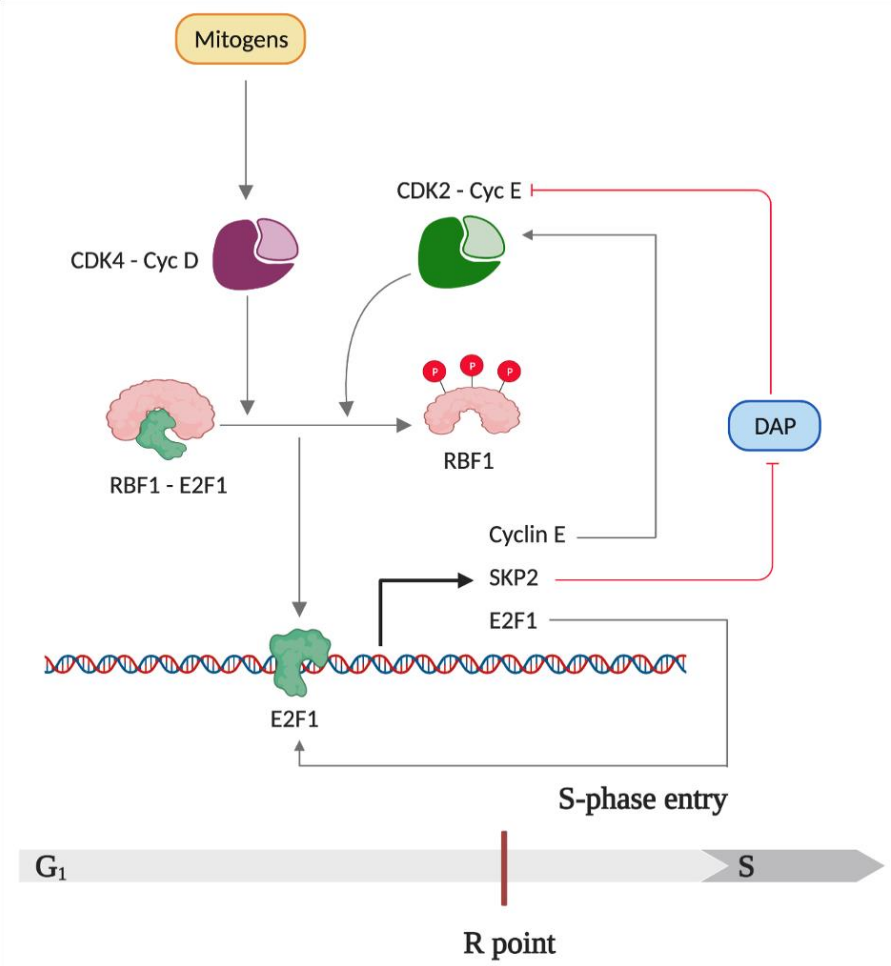

Figure 13 | Restriction point. Cyclin D expression depends mainly on mitogenic signals. CDK4/CycD promotes E2F1 release and transcriptional activity which triggers three different positive feedback loops that pushes the cell towards S-phase through the transcription of CycE, SKP2 and its own gene. Grey arrows represent activation and red arrows represent inhibition. The R-point is represented in red.

1.4.2. DNA replication (S-phase)

The S-phase onset is characterized by the simultaneous firing of multiple origins of replication along the chromosomes. Interestingly, in yeast and lower organisms like

bacteria or archaea, a particular sequencing pattern defines the location of the origins of replication, whereas in higher eukaryotes, including flies, the replication origin topology depends more on the chromatin accessibility and epigenetic mechanisms rather than a particular sequence (Leonard & Mechali, 2013; Remus et al., 2004).

Initiation of DNA replication is tightly controlled in order to maintain genomic integrity. In eukaryotes, the pre-replication complex (PreRC) assembly constitutes the first essential step for ensuring a successful DNA replication. The PreRC formation occurs during the late mitosis and early G_1 phase, when the Origin Recognition Complex (ORC) binds to the chromosomes and defines the replication origins topology. The ORC complex comprises six elements (ORC1-6) in a ring-shaped structure that arranges around the DNA helix in AT-rich regions (F. Comoglio et al., 2015). The ORC complex also interacts with and activates the cell division cycling 6 (CDC6) (X. Feng et al., 2021) . The origin licensing process is concluded when the Double-Parked (DUP), the *Drosophila* homolog of the mammalian CDT1, loads the helicases consisting of the MCM2-7 complex (minichromosome maintenance 2-7 complex) onto the replication origin (Hua & Orr-Weaver, 2017; Parker et al., 2017). Importantly, the helicase loading is accompanied by the release of ORCs and CDC6 from the origin of replication (Tsakraklides & Bell, 2010).

Remarkably, the peak of expression of some E2F1-target genes like CHIF (DBF4 in mammals) or the cyclins E and A at the S-phase onset is crucial for the replication fork firing. Thus, the S-phase kinases CDK2, activated by both CycE and CycA, and DDK (CDC7 in complex with CHIF) phosphorylate the MCM2-7 complex enhancing the union of CDC45 and Go-Ichi-Ni-San (GINS) to the complex (I. Ilves et al., 2010). Together, the CDC45/MCM2–7/GINS (CMG) complex forms the functional replicative helicase, and the PreRC becomes the pre-initiation complex (Pre-IC) (Georgescua et al., 2017). The Figure 13 illustrates the origin licensing and firing.

It is fundamental for a successful cell cycle progression and progeny integrity that each replication origin only fires once per S-phase, otherwise it could lead to re-replication, replicative stress, or DNA damage. Thus, the levels of the proteins orchestrating

replication origin licensing and firing is strongly regulated. For instance, DUP, which has been demonstrated to cause re-replication and replicative stress upon overexpression is strictly controlled by different mechanisms that synergistically contribute to its degradation at the entry of S-phase (Marguerite T. et al, 2004). Firstly, DUP is phosphorylated by the CDK2 (coupled to cyclins E and A), which promote its degradation. Moreover, the E2F target gene, SKP2, highly expressed at this stage, is a component of the Skp1-Cullin-F-box (SCF) ubiquitin ligase family, responsible for its degradation. Finally, Geminin, another E2F1 target gene with raising levels during S-phase, is a direct inhibitor of DUP. Altogether, those pathways ensure the decrement of DUP activity at the S-phase onset, and avoid the origin re-licensing or re-replication (Kenichi, Yoshida & Inoue, 2004; Pozo & Cook, 2017; H. Zhang, 2021).

Importantly, each origin sustains two CMGs that will simultaneously unwind the DNA in opposite directions upon origin firing, generating two bidirectional replication forks. During DNA replication elongation, the DNA leader strand is synthesized continuously by the DNA polymerase ε, while the lagger strand is replicated by the DNA polymerase δ, discontinuously, in a Okazaki fragment-dependent manner (Marygold et al., 2020; S.A. Lujan et al., 2016). Moreover, an essential element of DNA replication is the PCNA, a ring-shaped structure composed of three identical subunits that act as a sliding clamp, tethering the replicative DNA strand with the corresponding DNA polymerase. Besides, PCNA has been link to several DNA replication-related processes, including collaborating with the ubiquitin-mediated proteolysis of cell cycle regulatory proteins or being involved in the DNA damage checkpoint activation. Markedly, topoisomerases are responsible for releasing the stress generated on the ssDNA caused by the helicases unwinding during DNA replication, while the replication protein A (RPA) directly stabilizes the ssDNA (Jónsson & Hübscher, 1997; Moldovan et al., 2007) (Figure 14).

The DNA replication elongation continues until two replication forks, coming from neighbor origins, get extremally close, which leads to the formation of supercoiled structures at the replication forks boundaries. Then, the exonuclease Fen1 removes the RNA primers from the Okazaki fragments, and the DNA ligase I seals the gaps left between them, resulting in the ligated DNA sister chromatids. Finally, the replication

machinery needs to be completely released from the DNA. Although the molecular mechanism underlying the replication fork disassembly is unknown, it seems to be promoted by the ubiquitin-mediated degradation of the CMG components. Indeed, in yeast, it is known that DIA2, a component of the SCF ubiquitin ligase superfamily, stimulates the degradation of MCM7, while in flies, the mechanism is not fully clear (Dewar & Walter, 2017; Gambus, 2017; Recolin et al., 2014).

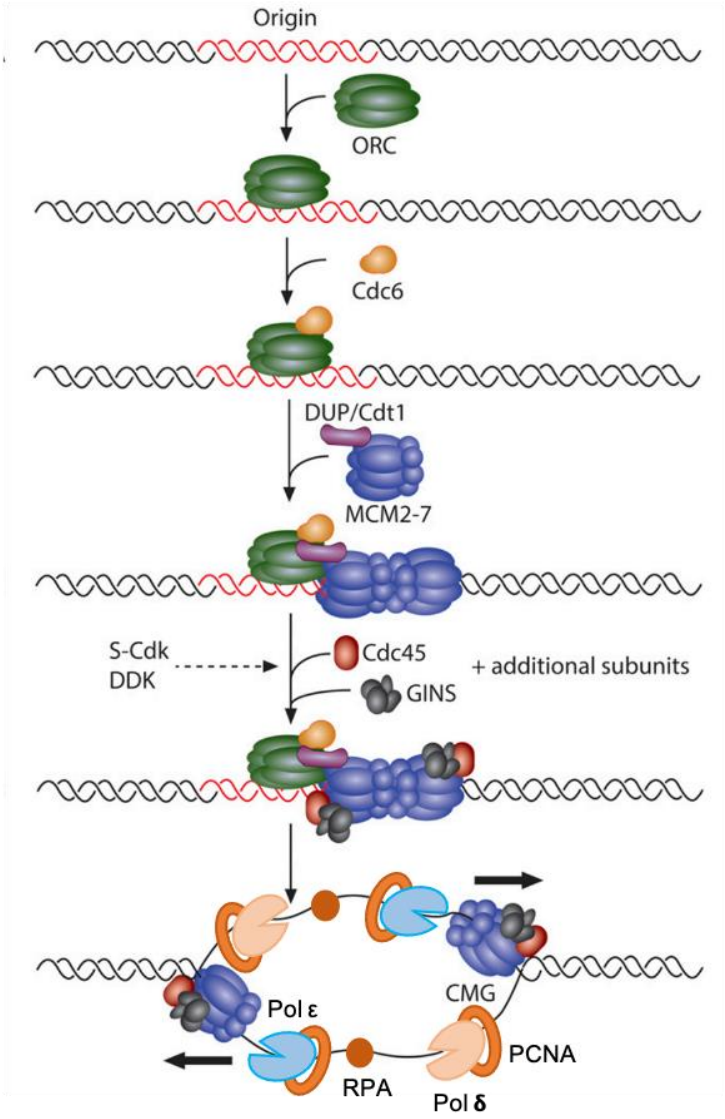

Figure 14 | DNA replication. The figure illustrates the replication origin licensing and firing. First, ORC recognizes the origin of replication together with CDC6. Then the MCM2-7 complex is loaded by DUP, forming the PreRC during the late mitosis and early G_1. At the S-phase onset the CDK2 (together with CycE and CycA) and the DDK (Chif-CDC7) phosphorylate the MCM2-7, promoting the union of CDC45 and GINS. It conforms the CMG and works as the functional helicase, which unwinds the DNA strands both directions upon origin firing. The DNA polymerase

ε (blue) synthetases the leading strand, while the DNA polymerase δ (yellow) replicates the lagging strand. PCNA is represented as an orange ring and RPA as brown sphere. Adapted from (Hua & Orr-Weaver, 2017).

Notably, most of the elements involved in DNA replication, such as PCNA, DNA polymerases, ORCs, MCMs and some enzymes involved in nucleotide metabolism, among others, result from the E2F1-mediated transcriptional cascade. However, since the origin licensing takes place in late mitosis and early G_1, it is thought that the PreRC complex member are used in the next cell cycle origin licensing (Herr et al., 2012).

1.4.3. G_2/M transition and DNA damage checkpoint

During the G_2 phase, the cell gets prepared for cellular division within mitosis, which accomplishes the inactivation of the S-phase proteins and the activation of the mitotic kinases. Throughout the G_2 phase, the cyclin B (CycB) levels increase and promote the CDK1 nuclear internalization. Once the complex is formed, it is phosphorylated at the tyrosine 15 (Tyr15) by the kinase WEE1, becoming inactive. The CDK1/CycB, also known as mitosis promoting factor (MPF), remains inactive until the phosphatase STRING (STG, homolog to the mammalian CDC25) removes the inhibitory phosphate at Tyr15.

Importantly, the MPF promotes the activation of STG and inactivation of WEE1, maintaining a positive feedback loop of self-activation that culminates in the mitosis entry. Although the mechanism that initially triggers the CDK1/CycB activation is not fully understood, it is thought that STG is primarily activated by the Aurora A-BORA-POLO kinase (PLK1 in mammals) axis (E. S. Johnson & Kornbluth, 2012; Poon, 2016). Nonetheless, a recent study in mammals suggests that the CDK2/CycA2 complex is exported to the cytosol at the end of S-phase and synergistically contributes to the STG activation together with PLK1 (Cascales et al., 2021; Gheghiani et al., 2017).

Guaranteeing the quality of the genetic information transfer is essential to ensure a progeny viability. Thus, when DNA replication leads to replicative stress and DNA

damage, cells activate the G_2/M checkpoint, which prevents entering mitosis until the S-phase derived troubles have been solved. Basically, two kinases orchestrate the DNA damage checkpoint, the Ataxia Telangiectasia Rad3-related kinase (ATR) and the Ataxia Telangiectasia Mutated kinase (ATM). In mammals, ATR is activated upon general replicative stress and activates downstream the CHK1 and CHK2, while ATM has been described to be specifically involved in the double strand breaks (DSB)-related DNA damage. In contrast, mei-41, the *Drosophila* homolog of ATR has been suggested to mediate the DNA damage response in flies, through the downstream activation of Grapes (CHK1 in mammals). Conversely, the TEFU-LOK (the *Drosophila* homologs of ATM and CHK2, respectively) axis has been demonstrated to be dispensable for DNA damage response and it was suggested to be more related to telomer processing (de Vries et al., 2005).

Upon DNA damage, mei-41 is activated and recruited to the growing single stranded DNA, where downstream it phosphorylates GRP (Grapes). Claspin and mus101 (TOPBP1 in mammals), are known as "checkpoint mediators" and contribute to the mei-41-dependent GRP activation (S, Liu et al., 2006). Afterwards, GRP impacts the cell cycle on two stages: firstly, it induces MDM2 degradation, promoting p53 activation and triggering Dacapo (DAP) transcription. DAP is a CKI responsible for CDK2 inhibition, which ultimately impairs the G_1-S transition in the next cell cycle. Moreover, GRP promotes a G_2 arrest of the cell cycle by downstream simultaneously activation of the WEE1 kinase and inhibition of the STG phosphatase, which ultimately impacts on the MPF activity and impairs mitosis entry (Recolin et al., 2014) (Figure 15).

Interestingly, it has been reported an intra-S-phase DNA damage checkpoint, which is activated immediately when the DNA damage is detected and affects the current DNA replication. The molecular mechanism is very similar to the explained above, with mei-41 and GRP as leading players, but it seems to happen earlier in the cell cycle (Iyer & Rhind, 2017).

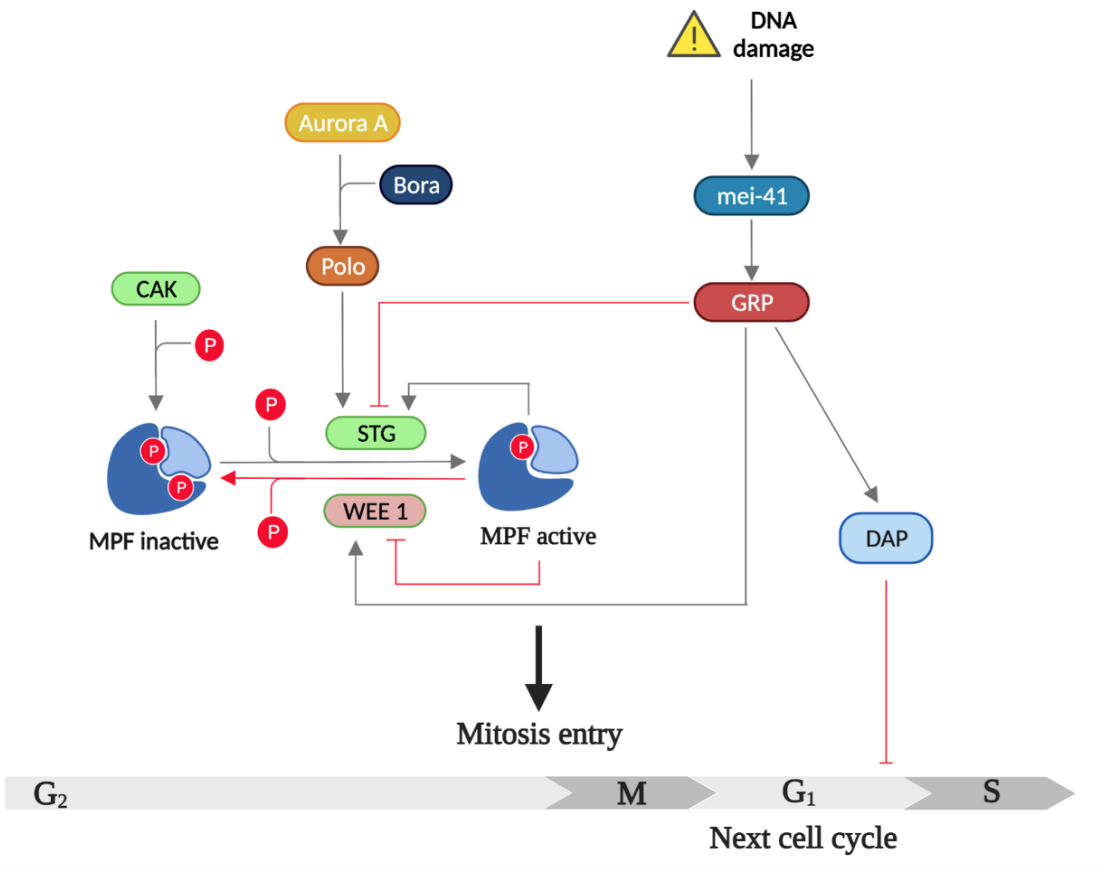

Figure 15 | G_2-M checkpoint. The figure illustrates the molecular mechanism underlying the G_2-M transition. The CDK activating Kinase (CAK) and STG activate the MPF (CDK1/CycB), while WEE1 inhibits the kinase, impairing the mitosis entry. STG is upstream activated by the Aurora A-BORA-POLO axis. The MPF generates a positive feedback loop that simultaneously activates STG and inhibits WEE1. Upon DNA damage, mei-41 activates GRP which suppresses STG, arresting cells in G_2 and preventing them to enter mitosis. Moreover, GRP inhibits the S-phase entry of the next cell cycle through triggering the DACAPO (DAP) transcription.

1.4.4. Mitosis and M-G_1 transition

Mitosis is a complex stage of the cell cycle, divided in five different stages: prophase (sister chromatids are separated), prometaphase (the nuclear envelop is disassembled and the microtubules attach to the centromeres), metaphase (chromatids align at the middle of the cell forming the mitotic spindle), anaphase (sister chromatids are separated and pulled apart in cell opposite poles by microtubules), and telophase

(microtubules disappear and cell division begins). Finally, the cytosol and organelles will be split into two daughter cells during cytokinesis. At the molecular level, upon mitosis entry the CDK1/CycB complex activates the kinase Greatwall (GTW) which enhances a positive feedback loop to maintain a high activity of the CDK1/CycB until the beginning of anaphase. On the one hand, through the phosphorylation and activation of STG, it promotes the inactivation of TWINS (TWN), a regulatory subunit of the protein phosphatase 2A (PP2A), responsible for the dephosphorylation of the CDK1/CycB substrates (Poon, 2016).

Remarkably, cells ensure the proper chromosome segregation through the anaphase checkpoint which prevents the sister chromatids separation until the conditions are optimal for cell division. During metaphase, the sister chromatids are joined by a ring of cohesin, and a complex called Chromosome passenger complex (CPC) is responsible for the spindle assembly and the microtubule-kinetochore interaction. Moreover, the CPC phosphorylates cohesin at the centrosome and promote its degradation by PD55 and WAPL. However, a small portion of cohesin still remains attached to the kinetochore, since it is protected by DMT (SGO1 in mammals). DMT interacts with the phosphatase PP2A which maintains dephosphorylated DMT itself and the kinetochore cohesine, preventing it from degradation. During the metaphase to anaphase transition, the tension on the mitotic spindle pushes away DMT, triggering the cohesin phosphorylation by the CPC at the kinetochore promoting its degradation, which culminates with the telophase, with the and chromosome segregation on opposite poles of the cell.

Moreover, during anaphase, FZY (CDH1 in mammals), a subunit of the anaphase promoting factor APC/C E3 ubiquitin ligase, is expressed. FZY is responsible for depredating CycB, consequently inactivating the MPF complex at the end of mitosis. Interestingly, FZY also ubiquitinates Securine, an inhibitor of Separase. The Securin proteolysis also contributes to chromatids separation during anaphase. Finally, it also degrades geminin and SKP2, both involved in the inactivation of DUP, which at the late mitosis starts with the origin licensing again. Furthermore, the CycB was inhibiting another APC/C component, FZR (CDH1 in mammals), which becomes active at the beginning of G_1 phase and, in turn, degrades FZY. During early G_1 FZR promote the

degradation of SKP2, an SCF E3 ubiquitin ligase element in charge of degrading DUP and also DACAPO (DAP), a CDK2 inhibitor. Additionally, it also degrades the DUP inhibitor, Geminin, and the transcriptionally activator of CycD, ETS2. Altogether the ubiquitin-mediated proteolysis system ensures the proper cell cycle progression and timing (Teixeira & Reed, 2013; W. Wei et al., 2004; Yatskevich et al., 2021).

In balance, cell cycle progression is a central process in cellular biology, tightly regulated, which relies in a wide range of molecular pathways and mechanism that guarantee the integrity of genomic information transferring through generations and ultimately the cellular and organism viability. Interestingly, a recent review suggests that the normal cell cycle progression requires three brakes, rather than checkpoints, to ensure the progeny viability. The G_1-S brake prevents the cell from entering the cell cycle until it has grown enough and receives mitogenic signals; the G_2-M brake, allows to invest time in figuring out any replicative stress appeared during S phase before entering mitosis; and the intra-M brake ensures the proper chromosome segregation and guarantees the proper genetic information transferring through generations (Lemmens & Lindqvist, 2017).

1.5. SLIMP

SLIMP (Seryl-tRNA Synthetase-Like Insect Mitochondrial Protein) is an ARS-like protein resulting from a gene duplication at the base of metazoans. It was identified during the generation of a mitochondrial human disease fly model as a previously uncharacterized paralog of the *Drosophila* mitochondrial seryl-tRNA synthetase (SerRS2). Thus, SLIMP represents a new type of fast-evolving aaRS-like protein, which have acquired novel cellular functions despite a relatively modest divergence from its paralog SerRS2 in terms of structure (Guitart, et al., 2010). Interestingly, during an initial characterization of SLIMP, it was found universally distributed in insects, although recent phylogenetic analysis pointed that it might also be present in some species of echinoderms, molluscs, and hemichordates (De Potter, 2020) (Figure 16).

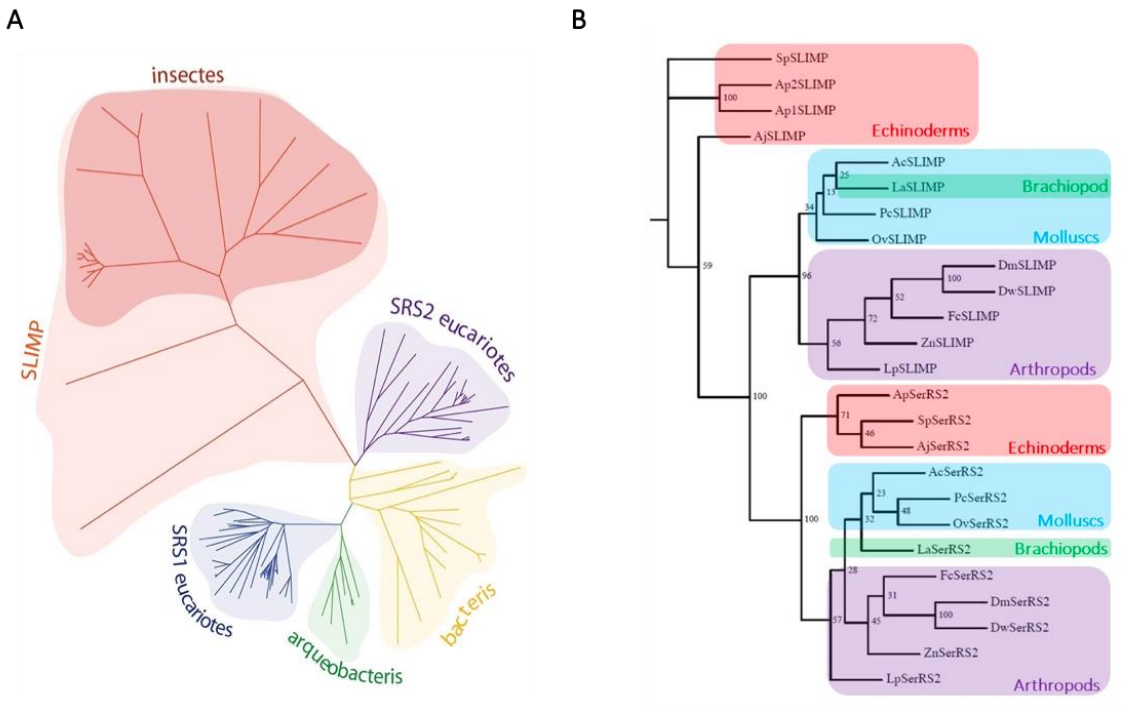

Figure 16 | Phylogenetic analysis of SLIMP and SerRS2 in different invertebrate species. (A) First phylogenetic analysis performed during an initial characterization. The distance tree shows that all the SLIMP proteins cluster together and share the same ancestor than the mitochondrial SerRS2. Moreover, it indicates that SLIMP clade evolved faster than SerRS2 and SerRS1. (B) Recently performed phylogenetic analysis including more species. The distance tree shows that

SLIMP sequence is present in echinoderms, molluscs and a specie of Brachiopod (hemichordate) beyond arthropods. Adapted from (De Potter, 2020; Guitart, et al., 2010).

Seryl-tRNA synthetases (SerRS), responsible for the tRNA serylation in the cell, belong to the class IIa of aminoacyl-tRNA synthetases. The crystal structure of SerRS has been elucidated for various organisms: *Escherichia coli* (Cusack et al., 1990), mitochondrial SerRS of *Bos taurus* (Chimnaronk et al., 2005), and *Homo sapiens* (Xu et al., 2013), among others. Interestingly, a highly conserved structure was unveiled comprising a C-terminal catalytic domain, according to the typical aaRS class II catalytic domain structure, and an N-terminal tRNA-binding domain folded into a long coiled-coil structure.

Accordingly, SLIMP maintains a similar SerRS structure, consisting of an N-terminal coiled-coil domain (CC) and a C-terminal globular domain (GD). However, an *in-silico* analysis of the three-dimensional model of SLIMP compared to the *B. taurus* mitochondrial SerRS2 (BtSRS2) indicated that six of the eleven amino acids of the catalytic core responsible for the seryl-adenylate recognition are not conserved in SLIMP (Figure 17). Hence, SLIMP lost the aminoacylation activity since the mutated residues are physically incompatible with the interactions established between serine, ATP and SerRS. In contrast, these positions are perfectly conserved in the canonical SerRS2 in *Drosophila*.

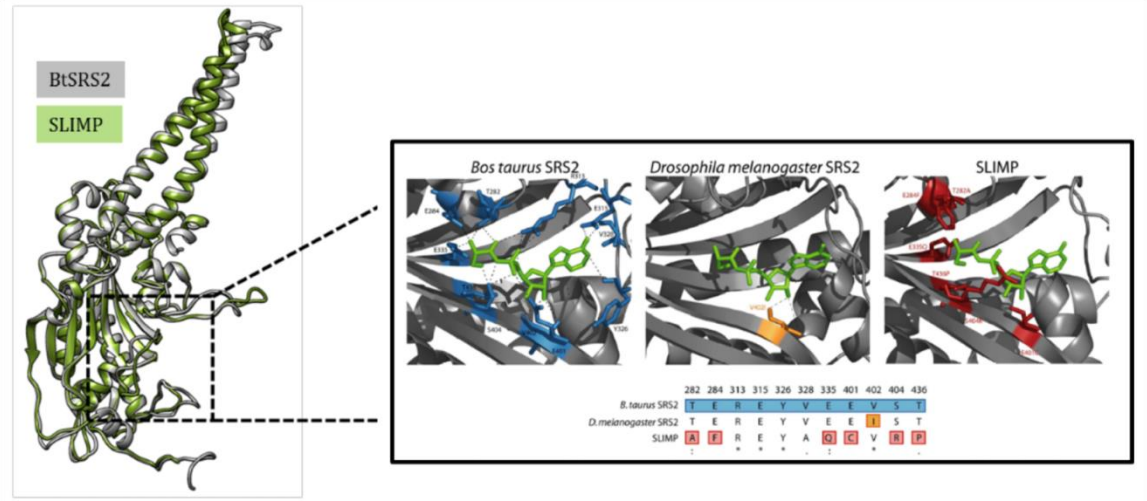

Figure 17 | SLIMP globular domain structural analysis. The model of the *D. melanogaster* SLIMP (in green) and the *B. Taurus* SRS2 (in grey) are represented in the left panel. A zoom in of the

catalytic core of both structures plus the *D. melanogaster* SerRS2 are represented in the right panel. The seryl-adenylate is marked in green, the residues contacting with the intermediate are painted in blue, while the non-conserved residues that would disrupt the interaction between SerRS and the substrate are shown in red (SLIMP) and yellow (DmSerRS2). Adapted from (Guitart, et al., 2010).

Interestingly, it is well known that the coiled-coil N-terminal domain is involved in the cognate tRNA recognition and binding. The SLIMP coiled-coil domain is structurally conserved, indicating that probably the ability to bind the $tRNA^{Ser}$ is preserved. Conversely, *in-silico* assays, performed in our group, revealed that the SerRS2 coiled-coil domain is fully or partially lost in species where SLIMP is present, including *Drosophila melanogaster* (De Potter, 2020).

Moreover, SLIMP is an essential protein; the SLIMP depletion in *Drosophila* dramatically reduces the lifespan of the organism. Specifically, in glia cells, SLIMP knock-down produces brain vacuoles, and, in wing imaginal discs, it causes significant morphological defects. Intriguingly, the SLIMP and SerRS2 reduction have a similar impact on *D. melanogaster* at systemic and tissue-specific levels (Guitart et al., 2013; Guitart, et al., 2010).

SLIMP is a mitochondrial protein encoded in the nucleus which is translocated into the organelle matrix post-translationally through the TIM/TOM translocase system. Accordingly, SLIMP sequence has been suggested to possess a hydrophobic mitochondrial signal peptide (MSP) at the N-terminal part of the protein (Guitart, et al., 2010).

Importantly, SLIMP has mainly two interactors in the mitochondria, its paralog SerRS2 and LON protease. These interactions have been extensively demonstrated through pull-down assays coupled with mass spectrometry analysis and confirmed by immunoprecipitation assays (Figure 18A). Moreover, a BioID assay was recently performed in our group, which further demonstrate those two interactions. Interestingly, the biotin-based analysis suggested other potential interactors, including

mitochondrial, cytosolic, and even nuclear proteins (Figure 18B). Additionally, SLIMP has been described to interact unspecifically with mitochondrial transcripts, including tRNAs and mRNAs, but not with mtDNA or cytosolic tRNAs (Picchioni, et al., 2019).

A

PROTEIN NAME	#PSM IN SLIMP-TAP	#PSM IN WT
HSP60	334	297
SERRS2	76	0
SLIMP	53	3
TCP-1	20	10
EF1G(A)	12	0
NMD3	7	0
OPA1	7	0
TIM44	6	0
MRSPS22	4	0
DREF	3	0
GLORUND	3	0
LON	2	0
MITOFILLIN	2	0
CG7791	2	0
BURGUNDY	2	0

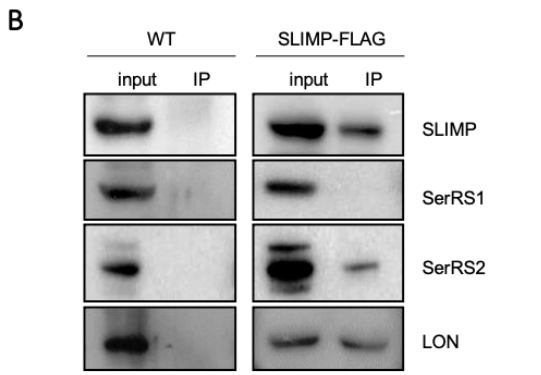

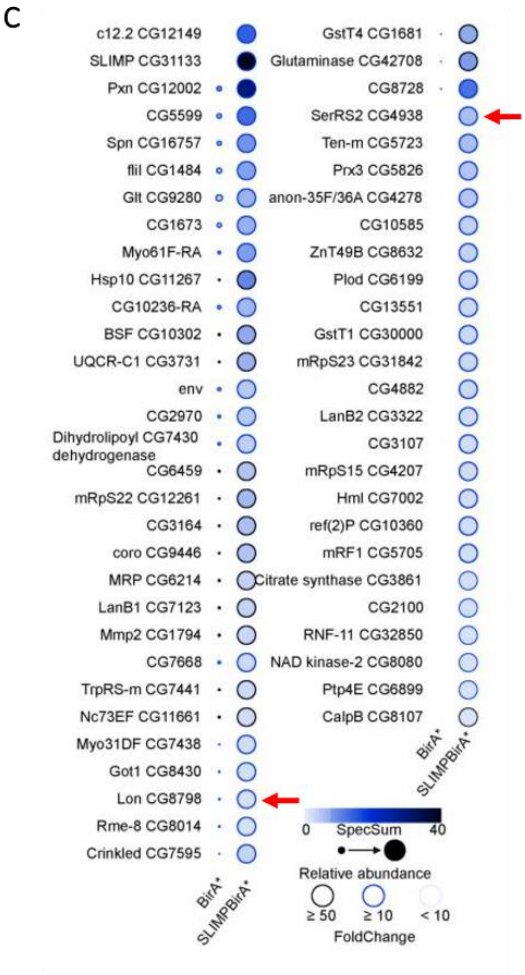

Figure 18 | SLIMP interactome. (A) SLIMP interactors obtained by a pull-down coupled to mass spectrometry analysis. (B) SLIMP immunoprecipitation assay showing SerRS2 and LON as SLIMP interactors. (C) Putative SLIMP interactors obtained from a BioID assay. The bigger and more intense the dot is, the more significant the potential interaction becomes. SerRS2 and LON are highlighted with a red arrow in A and C panels. Adapted from (Picchioni, et al., 2019).

Furthermore, SLIMP and SerRS2 protein levels are interdependent. Multi Angle Light Scattering (MALS) analysis showed that both proteins form an αβ-heterodimeric structure in the mitochondrial matrix which stabilizes each other. The SLIMP-SerRS2 dimer was demonstrated to function as the seryl-tRNA synthetase in the mitochondria since any of the proteins expressed individually is not capable of charging the $tRNA^{Ser}$.

During the first characterization of both proteins, it was observed that the depletion of SLIMP or SerRS2 seriously compromises mitochondrial integrity, which looked more prominent and electrodense with notable fewer cristae (Guitart et al., 2013; Guitart, et al., 2010). Furthermore, recent in vivo and in vitro assays, showed a dramatic decrease in the aminoacylation rate upon SLIMP or SerRS2 depletion, which significantly reduces the global mitochondrial translation and ultimately impacts mitochondrial respiration, oxygen consumption and ATP production (Picchioni, et al., 2019) (Figure 19).

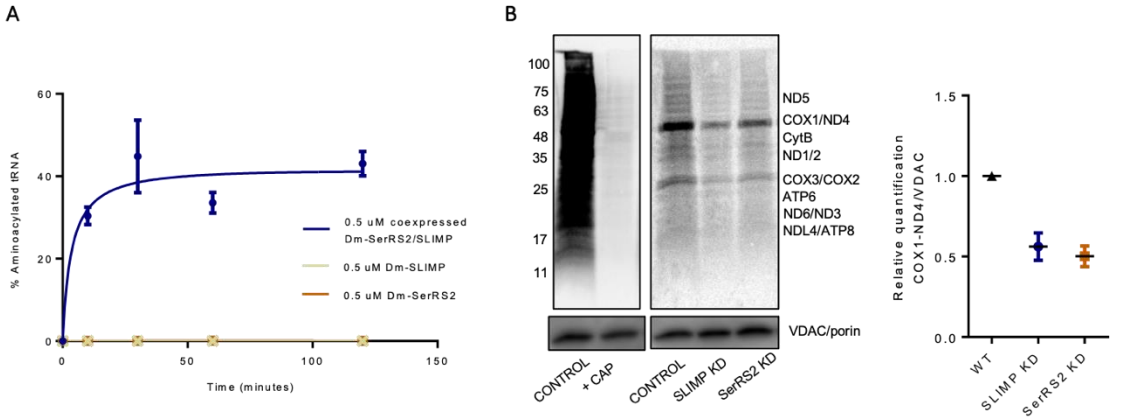

Figure 19 | SLIMP and SerRS2 heterodimer is fundamental for mitochondrial translation. (A) In vitro aminoacylation assay showing that nor SLIMP or SerRS2 alone are sufficient for $tRNA^{Ser}$ aminoacylation, while the co-expression of both proteins is enough for reach normal levels of aminoacylation. (B) Pulse-chase assay showing the mitochondrial global translation rate of SLIMP-depleted (SLIMP-KD) cells, SerRS2-depleted (SerRS2-KD) cells and control cells. The corresponding quantification is shown in the right panel. Adapted from (Picchioni, et al., 2019).

Interestingly, considering these data together and the structural analysis mentioned before, it seems likely that SLIMP and SerRS2 evolved together. Probably, when the gene duplication occurred, both genes were identical and worked as a homodimer, just like rest of the class IIa aaRS. However, having two copies of the same gene would open the possibility of accumulating mutations in one of them which eventually would affect the catalytic core. As a result, only one of the two subunits of the heterodimer would be able to aminoacylate (SerRS2), and consequently only the other one would be in charge of tRNA recognition through the coiled coil (SLIMP). Finally, the unutilized coiled-coil

wound end up disappearing, which corresponds to the scenario found in most of the species where both proteins co-exist.

On the other hand, SLIMP interacts with the substrate-binding domain of the LON protease, one of the leading mitochondrial proteases. Their interaction is nucleic acid-independent, and their protein levels are independent, meaning that SLIMP is not a substrate of LON. Several mitochondrial processes have been linked to LON protease, including unfolded or damaged proteins degradation, chaperon activity or mtDNA maintenance (Pinti et al., 2016). As mentioned in the introduction, the mitochondrial transcription factor A (TFAM) is well known to be a target of LON, involved in mtDNA stabilization and replication initiation. We recently demonstrated that SLIMP regulates TFAM levels in a LON-dependent manner (Figure 20A and 20B). Moreover, a luminescence-dependent assay with a peptide designed as a LON target which emits luminescence upon cleavage, allowed us to determine that this effect is specific for TFAM (Figure 20C). Hence, upon SLIMP depletion, an increase in TFAM levels and mtDNA copy number is observed (Picchioni, et al., 2019) (Figure 20).

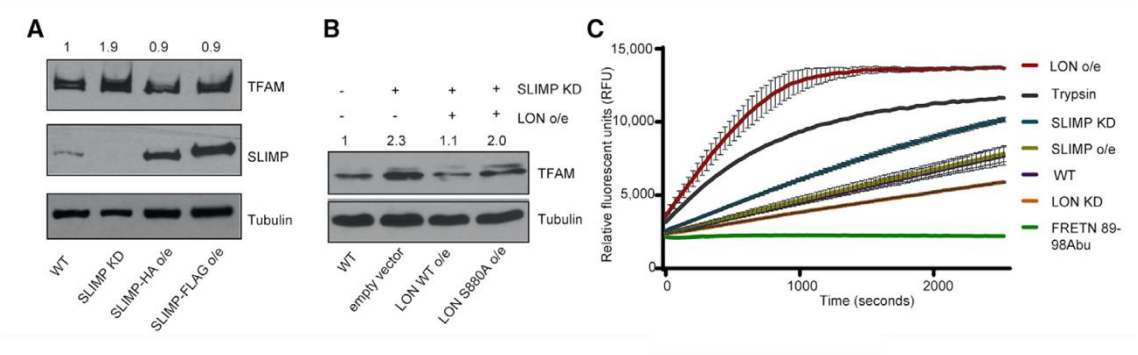

Figure 20 | SLIMP modulates TFAM levels in a LON-dependent manner. (A) Western blot analysis showing the increase in TFAM levels upon SLIMP depletion. (B) Immunoblot analyses of TFAM levels upon SLIMP knockdown and with or without LON overexpression (LON WT or the mutated form LON S880A). The band quantification is normalized to S2 WT cells. (C) LON protease activity assay using FRETN 89–98Abu and monitoring the relative fluorescence during time (s). The means of three independent experiments ± SDs are shown. Adapted from (Picchioni, Antolin-fontes, et al., 2019).

In conclusion, SLIMP plays a crucial role in mitochondrial homeostasis, simultaneously modulating both the mitochondrial translation and mtDNA replication (Figure 21).

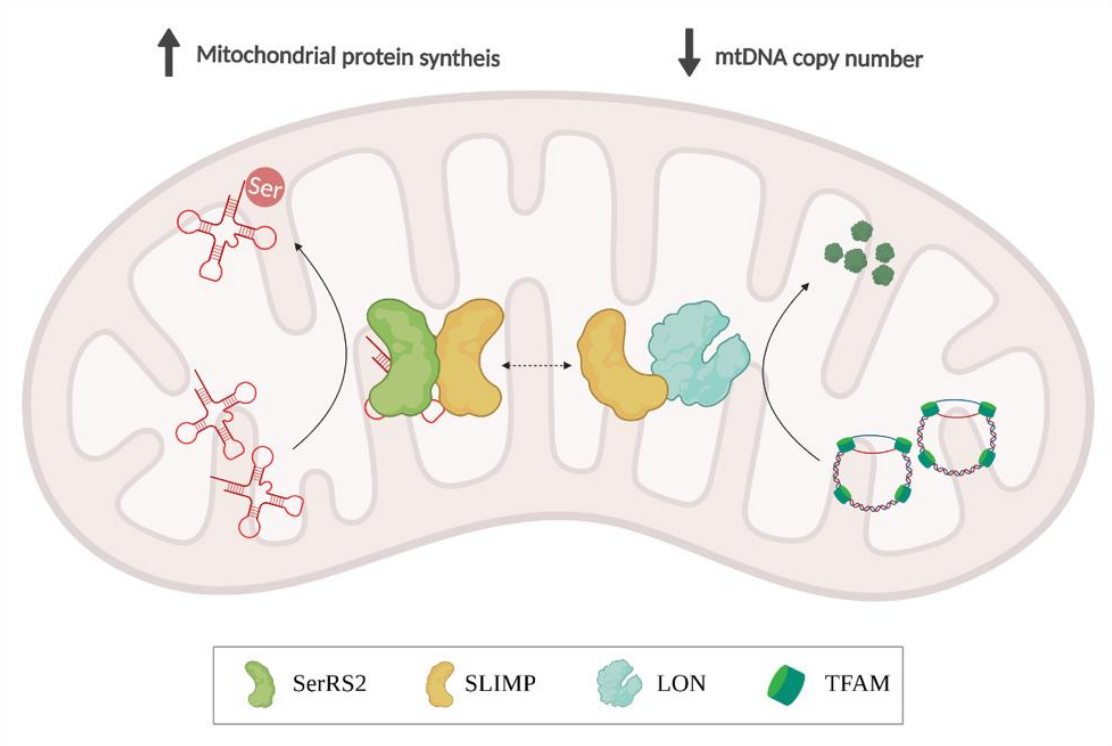

Figure 21 | Mitochondrial function of SLIMP. The figure summarizes the mitochondrial function of SLIMP, simultaneously modulating the mitochondrial translation and mtDNA replication.

Moreover, upon SLIMP or SerRS2 depletion, a growth impairment is observed in *Drosophila* cultured cells, more severe in the SLIMP knock-down scenario. Moreover, it was observed that SLIMP-depleted cells get temporally arrested in G_2. This accumulation is specific for SLIMP since it does not occur by decreasing levels of its primary mitochondrial interactors (SerRS2 or LON). Interestingly, it also was demonstrated that although the mitosis rate is lower upon SLIMP knock-down, cells can eventually enter mitosis, meaning that they show a delay but not a permanent arrest in G_2. Interestingly, this phenotype can be rescued by overexpressing the SLIMP full length and a truncated version of the protein lacking the mitochondrial signal peptide (ΔN-SLIMP). Altogether, these results suggest a mitochondrial-independent role of SLIMP related to the cell cycle (Figure 22) (Antolin-Fontes, 2019).

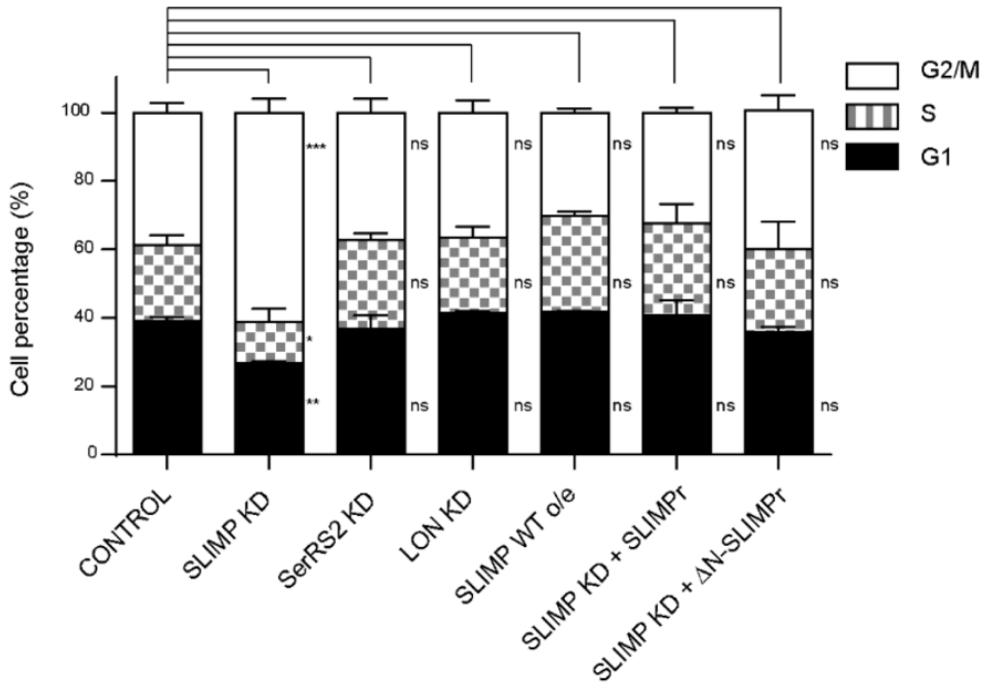

Figure 22 | SLIMP causes a G2 delay in cell cycle. Graphical representation of the cell cycle profile of SLIMP depleted cells (SLIMP-KD), SerRS2 depleted cells (SerRS2-KD), LON depleted cells (LON-KD), SLIMP-KD cells overexpressing a RNAi-resistance form of SLIMP (SLIMP-KD + SLIMPr) and SLIMP-depleted cells overexpressing a truncated form of RNAi-resistance SLIMP lacking the MSP (SLIMP-KD + ΔN-SLIMPr) (Antolin-Fontes, 2019).

Furthermore, two independent genomic screens performed in Drosophila pointed to SLIMP as a fundamental factor for cell cycle progression. On the one hand, SLIMP was identified as a clue element for cell cycle progression with a highly periodic expression profile throughout the cell cycle in both imaginal wing disc and S2 cells (Liang et al., 2014). Interestingly, in this study, the authors also appreciate the G_2 accumulation phenotype in SLIMP-depleted cells. On the other hand, SLIMP was identified as a potential suppressor of the E2F1 pathway in *Drosophila* (Ambrus et al., 2009). As mentioned previously, the E2F transcription factor family essentially transcribes several genes involved in the G_1-S transition and DNA replication onset. Accordingly, it is well known that a decrease in E2F1 activity generates an arrest in G_1 and an impairment for entering in S-phase. Intriguingly, in this study, they demonstrated that SLIMP depletion in E2F1 mutant flies partially compensates for the G_1-S transition impairment caused by

the lack of E2F1, apparently in an E2F1-independent molecular mechanism (Ambrus et al., 2009).

Remarkably, a recently performed microarray assay unveiled a significant transcriptional upregulation of a set of E2F-target genes in SLIMP-depleted cells. The overexpressed transcripts are essentially involved in the PreRC formation, and replication origin licensing and firing, including MCMs, ORCs and CDC6. Moreover, a gene ontology analysis revealed an upregulation of the G_2/M checkpoint pathway, including genes such as WEE1, mei-41 or GRP, among others (Figure 23). It is remarkable that ORC2 and CDC6 were also shown to be upregulated at the protein level in SLIMP-KD cells. Importantly, this data agrees with and reinforces the idea of SLIMP having an antagonistic effect on E2F1 in G_1 to S transition (Antolin-Fontes, 2019).

	Gene	Fc	*pvalue*
E2F targets	Mcm2	1.632236	0.001049
	Mcm7	1.337468	0.005019
	Mcm5	1.450156	0.005224
	Wee1	1.381788	0.005703
	Spc25	1.247871	0.007302
	Cdk1	1.253367	0.010014
	Zw10	1.253518	0.011968
	Slbp	1.223056	0.016191
	Mcm6	1.278536	0.016278
	Orc2	1.431965	0.020072
	Mlh1	1.394759	0.020299
	Mcm3	1.221756	0.024944
	Orc6	1.260618	0.033033
	Pms2	1.168902	0.043739
	Cdk4	1.161705	0.046205
G2/M checkpoint	Mcm2	1.632236	0.001049
	Cdc6	1.969177	0.001863
	Ndc80	1.299852	0.005211
	Mcm5	1.450156	0.005224

	Gene	Fc	*pvalue*
G2/M checkpoint	Orc5	1.389678	0.009987
	Cdk1	1.253367	0.010014
	Nek2	1.365188	0.01136
	Mcm6	1.278536	0.016278
	Mcm3	1.221756	0.024944
	Incenp	1.258085	0.030338
	Orc6	1.260618	0.033033
	Bub3	1.180506	0.039573
	Cdc7	1.170344	0.043571
	Cdk4	1.161705	0.046205
Myc targets	Mcm2	1.632236	0.001049
	Set	1.328365	0.001978
	Cdk2	1.408006	0.004965
	Mcm7	1.337468	0.005019
	Mcm5	1.450156	0.005224
	Mcm6	1.278536	0.016278
	Orc2	1.431965	0.020072
	Bub3	1.180506	0.039573
	Uba2	1.17849	0.043598
	Cdk4	1.161705	0.046205

Figure 23 | Microarray analysis of SLIMP-KD cells. Top upregulated genes in the significant upregulated categories E2F targets, G_2/M checkpoint and Myc targets. Gene name, fold change and p value for each gene is indicated. Adapted from (Antolin-Fontes, 2019). Microarray data is fully available at Gene Expression Omnibus with the number GSE104516.

Collectively these data suggested that SLIMP could have a role blocking somehow the transition from G_1 to S phase and the DNA replication onset causing, in its absence, an aberrant S-phase that could explain the consequent G_2 accumulation phenotype observed. Therefore, based on this hypothesis, a couple of preliminary experiments aiming to check for DNA damage or aberrant DNA replication were performed in the group.

Firstly, it is known that replication forks movement strongly relies on the deoxyribonucleotides (dNTPs) availability, and it has been proposed that the problem caused by the lack of free nucleotides can be eventually solved by adding more dNTPs to the media (Kunz et al., 1994; Pai & Kearsey, 2017; Siddiqui et al., 2013). Notably, the G_2 accumulation phenotype of SLIMP depleted cells can not be restored by incubating the cells with nucleosides, and unexpectedly, the arrest becomes even more pronounced instead (Figure 24A).

Finally, it is broadly known that double-strand brakes-related DNA damage leads to the phosphorylation of histone H2 A variant (H2Av) (Talbert & Henikoff, 2010). In a preliminary approach trying to check if SLIMP-depleted cells carried with DNA damage, we checked for the levels of phosphorylated H2Av via western blot analysis. However, no changes in H2Av phosphorylation were observed even after irradiating the cells in presence and absence of SLIMP (Figure 24B) (Antolin-Fontes, 2019).

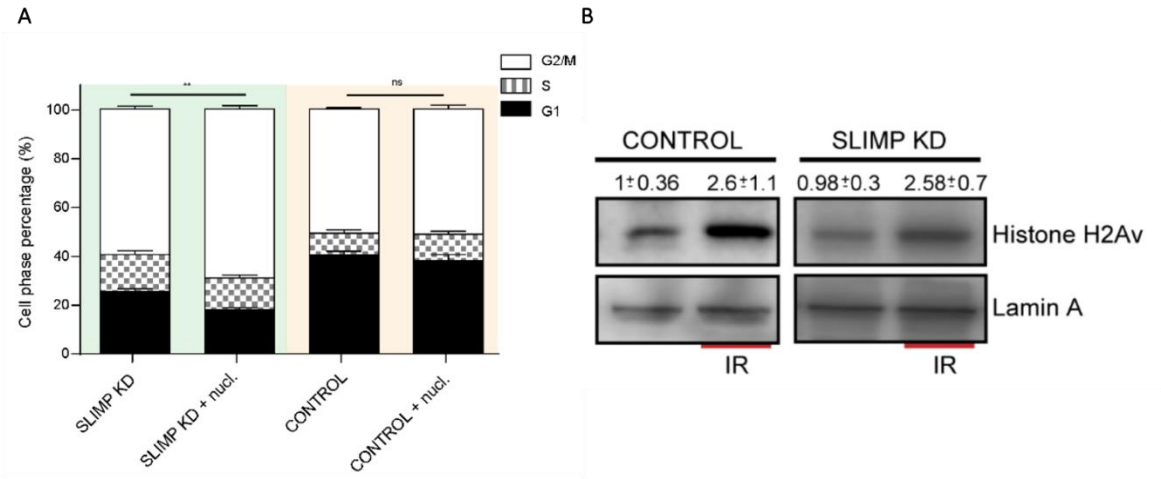

Figure 24 | Checking for DNA damage in SLIMP-KD cells. (A) Cell cycle profile of SLIMP-KD and Control cells incubated with nucleosides. (B) Western blot analysis of H2Av phosphorylated levels in SLIMP-KD and control cells after irradiating them (IR) and non-irradiating them. The quantification is normalized to non-irradiated cells. Lamin A is used as loading control. Adapted from (Antolin-Fontes, 2019)

OBJECTIVES

2. OBJECTIVES

The aim of this thesis is to deeper explore the cell cycle function of SLIMP using *Drosophila melanogaster* S2 cells as experimental model. More specifically, we focused on the following goals:

- Experimentally characterize the SLIMP mitochondrial signal peptide (MSP).
- Determine the subcellular distribution of SLIMP beyond the mitochondria.
- Further characterize the role of SLIMP in the cell cycle progression.
- Analyze the impact of the SLIMP heterologous expression in budding yeast, on both the mitochondrial homeostasis and the cell cycle progression.

MATERIALS AND METHODS

3. MATERIALS AND METHODS

3.1. EXPERIMENTAL MODEL

Although most of the experiments presented in this work were done in *Drosophila* cultured cells, a set of assays were performed using *S. cerevisiae* as a model organism.

3.1.1. *D. melanogaster* S2 cells: maintenance and transfection

Drosophila melanogaster Schneider 2 cells (S2 cells) (ATCC CRL-1963) were maintained at 25ºC in Schneider's *Drosophila* medium (Gibco) supplemented with 10% fetal bovine serum (FBS) and 50 µg/ml penicillin and streptomycin (Gibco). Cells were visualized using an Ellipse TD2-FL microscope and the NIS-elements BR software (Nikon) was utilized for imaging acquisition. Moreover, cells were dyed with Trypan Blue solution 0.4% (Thermofisher) and counted using the Countess Automated Cell Counter (Invitrogen) for cell counting. Finally, we used the TransIT-Insect Transfection Reagent (MirusBio #6100) following the manufacturer protocol instructions for cellular transfection.

Cells were frozen in 1 mL vials containing around 10^7 cells in FBS with 10% DMSO. Cells were stored for 24 hours at -80ºC and afterwards transferred into liquid nitrogen. Conversely, vials were directly taken from liquid nitrogen for the thawing process and brought to room temperature as quickly as possible. Cells were then plated in complete fresh media, which was changed after six hours.

Furthermore, cellular transfection coupled with antibiotics selection was used for stable cell line generation. Specifically, 200 µg/ml of hygromycin B (Gibco) for cell lines transfected with pMK33-Hygro-derived plasmids and 2.5 µg/ml of puromycin (InvitroGen) for cell lines transfected with pMT-Puro-derived plasmids were added to

the media. Cells were maintained under these conditions until the global viability reached 85%. This process can take from three to six weeks, depending on the cell line and the construct. Finally, the stable cell lines were maintained in complete media, with and without antibiotics, periodically. Table 1 shows all the cell lines used in this thesis.

The constructs employed for the stable cell lines generation basically derive from two backbones: pMK33-Hygromycin (Flybase: FBmc0003027) and pMT-Puromycin (Addgene #17923). Both contain a *Drosophila* metalloprotein inducible promoter upstream of the corresponding insert, meaning that the cells do not express the insert constitutively, but only upon promoter induction. Thus, cells were induced with 600µM $CuSO_4$ for three days for protein overexpression and eight days for RNAi-dependent knock-down generation. The media was changed, and fresh $CuSO_4$ was added every two days. Table 2 lists all the constructs used in this work.

3.1.2. *S. cerevisiae*: maintenance and transfection

W303-1A ADGEV bar1D budding yeast strain was cultured in YPD complete media (1% yeast extract, 2% peptone, 2% dextrose) at 37ºC in shaking conditions. Yeast growth was measured using a spectrophotometer to calculate the Optic Density (OD) at 600nm wavelength**.**

For yeast transformation, cultured cells were diluted at OD_{600} = 0.2 and grown for 3.5 hours until they reached the optimal OD_{600} of 0,8. Cells were then centrifuged at 3000rpm for 3 minutes and washed with sterilized water. Afterwards, cells were resuspended in 500µl of AcLi solution (TE 1x, AcLi 100mM in Mili-Q water) to make them competent. Following, 100µl of competent cells were mixed with the transformation solution containing 10µl of single-strand DNA (boiled for 10 minutes before), 600µl of PEG solution (PEG 50%, TE 1x, AcLi 100mM) and 100ng of the transforming plasmid. The mixture was vortex vigorously and incubated for 45 minutes at 30ºC. Then, we added 70µl of DMSO to the mixture and incubated the sample for 15 minutes at 42ºC. Finally, cells were centrifuged at 3000rpm for 1 minute and plated in agar plates with the selection marker. In our case, the plasmid used in all the experiments is the pYES2

(ThermoFisher V285-20) and contains a uracil-coding gene (URA3), so we used YPD media lacking uracil (URA-media) as a selection system. It is specified in each experiment the usage of YPD or URA-media, although transformed cells were usually grown in selective media.

Moreover, the pYES2 bears a GAL4 inducible promoter. However, instead of inducing the insert expression with galactose, we used 100nM β-estradiol. The ADGEV system (Figure 25), previously incorporated into the strain, allows inducing the GAL4 promoter with β-estradiol and growing the cells with glucose as the principal carbon source.

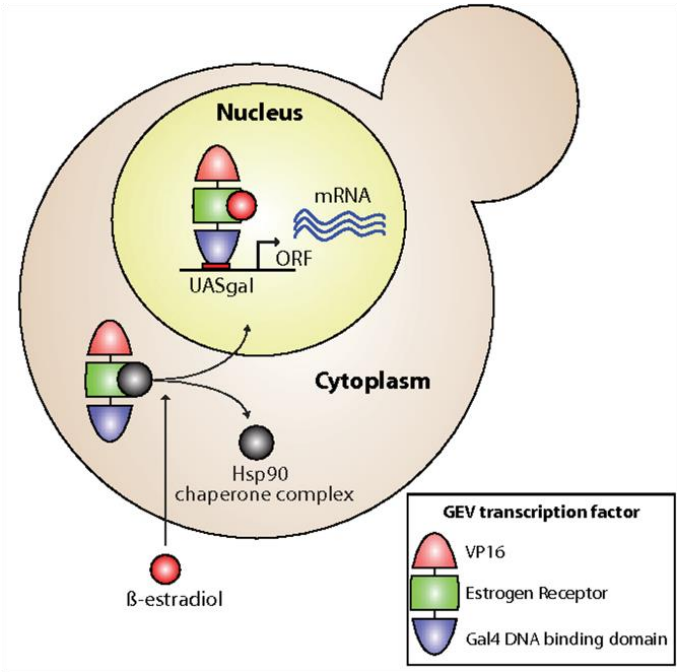

Figure 25 | Schematic representation of the ADGEV system in budding yeast. The GEV transcription factor only can join the GAL4 promoter in presence of β-estradiol. Upon adding this molecule to the culture media, the system is induced, and the plasmid (pYES2-GAL4) is expressed.

3.2. GENOMIC DNA EXTRACTION

For genomic DNA extraction, 1mL of confluent S2 cells was collected and resuspended in 200ul of lysis buffer (100mM Tris-HCl pH=8,5, 5mM EDTA pH=8, 0,2% (w/v) SDS, 100ug/ml Proteinase-K). The mixture was shaken at 400rpm and 55ºC for at least one

hour until it was homogenized entirely. After that, the lysate was centrifuged at maximum speed for 5 minutes, and the supernatant comprising the DNA fraction was transferred into an Eppendorf tube containing 500ul of ice-cold isopropanol. The tube was incubated for 20 minutes at -20ªC to promote the DNA precipitation. Then the sample was 4ºC-centrifuged at maximum speed for 15 minutes, and the supernatant was discarded. The pellet containing the gDNA was then washed with ice-cold ethanol 70% and dried. Finally, the gDNA was resuspended in nuclease-free water. Nucleic acid concentration of 1µl of the sample was quantified with Nanodrop ND-1000 Spectrophotometer (Thermo Scientific) at 260nm.

3.3. CLONING AND CONSTRUCTS GENERATION

All the constructs used in the present work are listed in Table 2. Firstly, the insert sequence is amplified by PCR, using the Phusion DNA Polymerase (ThermoFisher) following the manufacturer instructions for all the expression vectors generated. Next, PCR products were purified through DNA electrophoresis (one hour at 120 V) in a 1% agarose gel stained with StainG, responsible for marking the DNA. The GeneRuler ladder mix from ThermoFisher (#11803983) was used as a molecular weight marker. Bands were visualized with a UV-light spectrophotometer. Finally, DNA purification from agarose cut bands was performed with NucleoSpin Gel and PCR clean-up kit (Macherey-Nagel Thermofisher #740609250) following the manufacturer's instructions.

Plasmid and insert digestions were performed with New England Biolabs restriction enzymes and following the suggested protocol. Table 2 collect the restriction sites used per each construct. The ligation reaction was performed overnight at 16ªC using the T4 DNA ligase (Fermentas) with a 3:1 (insert:vector) proportion. A negative control checking for vector self-ligation was performed in parallel in each experiment.

DH5-alpha *E. coli* competent cells were directly transformed with the ligation product using the heat-shock method for plasmid amplification. Firstly, 100µl of competent cells

were mixed with 100ng of DNA and shaken at 300rpm and 42ºC for 45 seconds. The mixture was then placed on ice for 5 minutes, supplemented with 500µl of rich media SOC (ThemoFisher #15544034), vigorously vortexed and incubated for 1 hour at 37ºC and shaking (300rpm). Finally, 200µl of the mixture was plated in LB-agar plates containing the corresponding antibiotic selection.

After 37ºC overnight incubation, a single colony was picked and grew in 5mL LB-Broth-Antibiotic 1x, shaking at 37ºC for around 16h for miniprep preparation. Cells were then centrifuged at 4000G for 10 minutes, the supernatant was discarded, and the plasmid was purified from the cell pellet. For that, the Miniprep Kit (NZYTech) was employed following the manufacturer's instructions. A similar procedure was performed for maxiprep preparation using the Link HiPure Plasmid Filter Maxiprep Kit (Invitrogen) with a final culture volume of 250mL, according to the manufacturer's instructions.

All plasmids were sequenced to confirm the correct inserted sequences in the proper orientation and ensure no additional mutations have been introduced to the plasmid during DNA manipulation. Sequencing reactions were performed by an external provider (GATC Biotech). All the oligonucleotide sequences used in this thesis for expression constructs generation are collected in Table 3.

3.4. RNA EXTRACTION, REVERSE TRANSCRIPTION AND RT-PCR.

Total RNA was extracted from cultured cells with TRIzol (Invitrogen). 500 ng of total RNA was retrotranscribed into cDNA using random primers (Reverse Transcription System, Promega-A3500) to perform quantitative real-time polymerase chain reactions (RT-qPCR) through Power SYBR Green and a StepOnePlus Real-time PCR System (Applied Biosystems) following manufacturer's instructions. Standard curves were calculated for both primer pairs to ensure a high-efficiency level. Fold expression changes were calculated using the 2-ΔΔCT method, where ΔΔCT is the sample ΔCT [CT average for target gene - CT average for the reference gene (RPL32)] - the control ΔCT [CT average

for target gene - CT average for the reference gene (RPL32)]. The sequences of the oligonucleotides used in this thesis for qPCR are collected in Table 4.

3.5. PICO-PROFILING

RNA was isolated using magnetic beads from 6000 cells. cDNA synthesis, library preparation and amplification were performed as described by (Gonzalez-Roca et al., 2010). The cDNA generated by reverse transcription from each sample is added to an amplification mix, and the cDNA:mix is divided into three equivalent parts for PCR amplification. In addition, a sample without RNA, sample "0", has been included in the amplification experiment. Amplification was performed for 21 cycles. Subsequently, cDNA was purified on PureLink Quick PCR Purification Kit (Invitrogen) and eluted in 40 ul. cDNA concentration was determined using the Nanodrop 1000 spectrophotometer. This protocol was performed by the Genomic Facility at the IRB Barcelona.

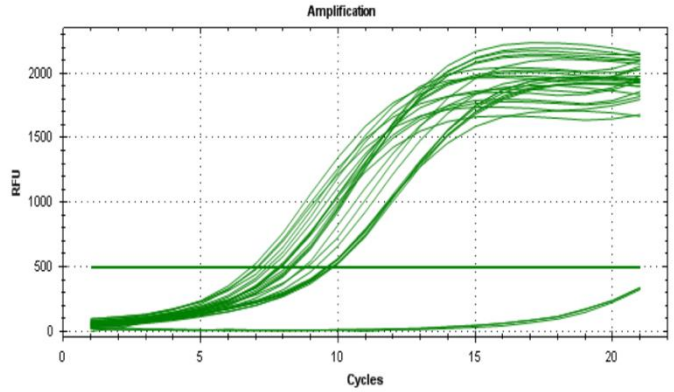

Threshold setting: 491.23	C(t) mean
1590 2020	9.18
1591 2020	9.76
1592 2020	8.40
1593 2020	9.57
1594 2020	7.75
1595 2020	7.40
1596 2020	8.22
1597 2020	7.82
1598 2020	7.00
Zero Control	N/A

Figure 26 | Pico-profiling. cDNA amplification (left panel) and quantification (right panel) of the nine samples analyzed. Three biological replicates of sorted cells in G1, S, and G2 phase were processed for RNA extraction and DNA amplification. A sample without RNA (sample cero) was used as negative control.

3.6. PROTEIN EXTRACTION AND QUANTIFICATION

For protein extraction, 1ml of confluent S2 cultured cells were collected and resuspended in 200µl RIPA lysis buffer**.** Then, the lysates were incubated on ice for 30

minutes and centrifuge at 16000g for the same time. Finally, the supernatant containing soluble proteins was transferred into a new tube. Finally, samples were diluted in protein loading buffer (PLB) 6x, boiled for 5 minutes at 95ºC and stored at -20ºC.

Furthermore, protein extraction for phosphorylated CDK1 analysis was performed with a modified RIPA buffer supplemented with 1mM Na_3VO_4, 5 mM $Na_4P_2O_7$, and 50mM NaF.

For protein quantification, Pierce BCA Protein Assay Kit (ThermoFisher) was used according to the manufacturer's instructions. The samples' absorbance was measured at 570nm with a spectrophotometer, and the amount of protein was inferred using a BSA standard curve.

In yeast, protein extraction was performed by taking the samples and directly resuspending them in PLB 6x. Finally, the samples were sonicated twice at 30% for 0.5 seconds and stored at -20ºC.

3.7. CELLULAR FRACTIONATION

Three different cellular fractionation protocols were performed in this work:

3.7.1. Mitochondrial fraction isolation

Around 10^7 cells were collected by centrifuging them at 500g for 3 minutes and resuspended with 1ml of IBcells buffer (225mM Mannitol, 75mM Sucrose, 0.1mM EGTA, 30mM Tris-HCl pH=7.4 (KOH) + Protease inhibitor). Cells were homogenized with a tight pestle (25 strokes), and the lysate was transferred to a new tube and centrifuged at 300g for 5 minutes at 4ºC. The pellet containing the nuclear fraction and non-lysate cells was discarded, while the supernatant comprising the cytosolic and organelle fraction was centrifuged at 6000g for 10 minutes at 4ºC. Afterwards, the supernatant bears the

cytosolic fraction and the pellet the mitochondrial fraction. The resulting mitochondrial pellet was finally washed three times with ice-cold Wash Buffer (225mM Mannitol, 75mM Sucrose, 10mM KCl, 10mM Tris-HCl, 5mM KH2PO4 pH 7.2 + Protease inhibitor) and resuspended with MRB lysis buffer (250mM Mannitol, 5mM HEPES, 0.5mM EGTA pH= 7.4 (KOH) + Protease inhibitor). The protocol was adapted from (Villa-Cuesta & Rand, 2015).

3.7.2. Nuclear fraction isolation

The nuclear fraction isolation was performed using the NE-PER kit (Thermofisher). The protocol was based on the manufacturer's instructions, but a few variations were included to set up conditions for *Drosophila* S2 cells. First, the volume ratio was applied for 20µl package volume, corresponding to $20 \cdot 10^6$ cells. Moreover, two additional washes with ice-cold PBS 1x were incorporated before the nuclear fraction lysis step to purify the nuclear fraction as much as possible. Finally, the nuclear fraction was obtained by resuspending the nuclear pellet in RIPA lysis buffer.

3.7.3. Mitochondrial and nuclear fraction isolation

The goal of this protocol is the obtention of three fractions enriched in cytosol, mitochondria and nucleus. First, around $5 \cdot 10^6$ cells were collected, washed and resuspended in 300µl of IBcells Buffer. After homogenizing the cells using a tight pestle (25 strokes), the lysate was centrifuged at 300g for 5 min. Next, the supernatant containing the cytosolic fraction and the mitochondrial fraction was centrifuged for 10 min at 6000g at 4ºC, resulting in a supernatant (cytosolic-enriched fraction), and a mitochondrial pellet, which was washed with PBS 1X and lysate with 100µl of RIPA lysis buffer. On the other hand, the enriched nuclear fraction was obtained by applying the NE-PER kit adapted protocol explained above to the pellet obtained in the first centrifugation. The volume ratio, in this case, corresponding to a package volume of 10µl.

Importantly, in parallel with the three cellular fractionation protocols, the same number of cells was collected and directly lysate with RIPA Buffer to use a whole-cell protein extract as control.

3.8. IMMUNOBLOTING

For western blot analysis, 30ug of protein lysates was loaded in an acrylamide gel (the gel percentage is indicated in each experiment). Firstly, gels were run at 110V in Tris-Glycine running buffer for the electrophoresis separation. Proteins were then transferred to a PDV membrane (Immobilon-P, Millipore) in Transfer buffer (Tris-Glycine 1X, ethanol 2X, SDS 0,01%) at 250mA for 105 minutes. Then, the membrane was incubated in blocking solution (TBS 1x, 0,001% Tween 20, 5% milk) for one hour at room temperature. Finally, the membrane was incubated with the corresponding primary antibody diluted in fresh blocking solution overnight at 4ºC. After that, the membrane was three times washed with TBS-t (TBS 1X, 0,001% Tween 20) and incubated with the secondary antibody diluted at 1:10000 in blocking solution for one hour at room temperature. Finally, after three washes with TBS-t solution, the membrane was developed through chemiluminescence using the ECL system (GE Healthcare ECL Amersham, Thermofisher #12316992). After incubating the membrane with the corresponding reagents for 1 minute in the dark, it was visualized using the Odyssey Infrared Imaging System (Li-Cor; Lincoln, NE)**.** All the antibodies used in this thesis are collected in Table 6.

3.9. PULL-DOWN AND PROTEIN PURIFICATION

Cells overexpressing SLIMP-FLAG were collected and lysed. After protein extraction, SLIMP was purified using anti-FLAGM2- conjugated magnetic Dynabeads (Invitrogen) according to the manufacturer's protocol with some minor modifications. Firstly, 20 packed gel beads per sample were washed and equilibrated twice in TBS buffer (50 mM

Tris-HCL, 150 mM NaCl, pH 7.4) before incubating the sample overnight at 4ºC in a rotating wheel. Beads attached to SLIMP-FLAG were then washed with TBS buffer, and the rest of the lysate was discarded. Finally, two different kinds of elution were performed as indicated in each experiment. On one hand, we eluted by adding Protein Loading Buffer (PLB – 100mM Tris-HCl pH 6.8, 4% SDS, 0.1% bromophenol blue, 20% glycerol) and boiling the sample at 60ºC for 5 min. In this case, the elution was analyzed by SDS-PAGE and western blot. Alternatively, we eluded SLIMP-FLAG by adding 20ul of glycine solution (pH 2.8) and incubating for 15 minutes in a rotating wheel at room temperature. After the elution, the sample was directly sent to the mass spectrometry facility for digestion (explained in the next section).

3.10. MITOCHONDRIAL SIGNAL PEPTIDE CHARACTERIZATION

The mitochondrial signal peptide identification by mass spectrometry samples was obtained from polyacrylamide gel-cut bands and glycine-mediated liquid elution.

On one hand, protein bands were reduced with DTT 10mM for 30 min at 56ºC and alkylated for 30 min in the dark with 55 mM iodoacetamide (IAM). Then, samples were digested directly in polyacrylamide gel using two different enzymes for the three biological replicates. We used trypsin (0.1 µg/µL) in 50mM NH_4HCO_3 at 37ºC, which cleaves after lysine (K); and arginine (R), and Glu-C (0.1 µg/µL) in 50mM NH_4HCO_3 at 25ºC overnight, which cleaves after glutamic acid (E) and aspartic acid (D). Digestions were stopped by adding formic acid. On the other hand, samples obtained by liquid elution were directly processed in the same experimental conditions detailed above.

Peptides were extracted with 100% acetonitrile (ACN) and ultimately evaporated. Next, the bands were reconstituted in 15 µL 1% formic acid aqueous solution with 3% ACN for MS analysis. Next, samples were loaded into strong cation exchange columns, and peptides were eluted in 5% NH_4OH, 30% MeOH. Finally, samples were evaporated to

dryness and reconstituted in 15 µL of 1% formic acid and 3% ACN for mass spectrometry analysis.

LC-MS coupling was performed with the Advion Triversa Nanomate (Advion BioSciences, Ithaca, NY, USA) as the nanoelectrospray ionization (nanoESI) source performing nanoelectrospray through chip technology. The Nanomate was attached to an Orbitrap Fusion LumosTM Tribrid mass spectrometer and operated at a spray voltage of 1.6 kV and delivery pressure of 0.5 psi in positive mode. A database search was performed with Proteome Discoverer software 2.1 (Thermofisher) using Sequest HT search engine and contaminants database and protein SLIMP manually introduced. The search was run against a targeted and decoy database to determine the false discovery rate (FDR). Search parameters included no enzyme, allowing for two missed cleavage sites, carbamidomethyl in cysteine as a static modification, methionine oxidation and acetylation in N-terminal as dynamic modifications. Peptide mass tolerance was ten ppm, and the MS/MS tolerance was 0.6 D. Peptides with a q-value lower than 0.1 and a FDR < 1% were considered as positive identifications with a high confidence level. Finally, the Percolator FDR node was used to estimate the number of falsely identified proteins among all the identified proteins.

This analysis was performed by the Mass Spectrometry Facility at the IRB Barcelona.

3.11. IMMUNOFLUORESCENCE

S2 Drosophila cells are in suspension, and consequently, the immunostaining assays require the previous treatment of coverslips with Concanavalin A. Coverslips (18 mm) were incubated for half an hour with 50 ul of Concanavalin A (0.5 mg/ml SigmaAldrich) in a 12-well plate. On the other hand, cells were collected and incubated for 15 minutes at 25ºC with 100nM of Mitotracker Red (Invitrogen-M7512) added directly to the media. Next, cells were washed twice with PBS 1X, resuspended with fresh media and plated over the treated coverslips. After an hour, cells were adequately attached to the

coverslip, and the media was aspirated. After two PBS 1X washes, cells were fixed by incubating them with 300µl of paraformaldehyde 4% for 15 min. Afterwards, paraformaldehyde solution was removed, cells were washed twice with PBS 1X, and cells were permeabilized by treating them with 500µl of permeabilization buffer (PBS, 0.3% Triton 100X, 0.2% BSA) for 20 minutes at room temperature.

Afterwards, we incubated the coverslips with the primary antibody, diluted 1:500 in permeabilization buffer, and overnight at 4 º C in shaking conditions. Cells were then washed with the permeabilization buffer three times and incubated with the secondary fluorophore-conjugated antibody at 1:400 for an hour at room temperature. Afterwards, cells were washed twice with the permeabilization buffer and then twice with PBS 1X. The cellular nuclei were then stained with DAPI (1:1000, five minutes in the dark). Finally, after two more PBS 1X washes, coverslips were mounted with 5µl of Mowiol (MercK). Slides were left overnight in the dark at room temperature to dry them thoroughly and stored at 4ºC. Images were acquired with Leica TCS SP5 MP confocal laser-scanning microscope and processed using ImageJ/Fiji software.

3.12. IN VIVO CELL IMAGING

S2 cells overexpressing SLIMP-GFP or GFP were collected and incubated for 15 minutes at 25ºC with 100nM Mitotracker red (Invitrogen-M7512) added directly to the media. Then cells were washed twice with PBS 1X and plated with fresh media in a six-well plate at 10^6 cells/ml. Cells were then visualized in the Leica TCS SP5 MP confocal laser-scanning microscope and processed with the ImageJ/Fiji software.

For budding yeast in vivo cell imaging, cells were collected and incubated with 100nM Mitotracker Red (Invitrogen-M7512) for 15 minutes at room temperature. Cells were then washed and visualized with Leica TCS SP5 MP confocal laser-scanning microscope. Images were analyzed and processed with the ImageJ/Fiji software.

3.13. CELLULAR SYNCHRONIZATION

The cellular synchronization applied in this work was always in the G1 phase. For S2 cells synchronization, $5 \cdot 10^5$ cells/ml were grown overnight in fresh media. Then, cells were incubated for 24 hours with 1.5mM hydroxyurea (HU) (SigmaAldrich), an inhibitor of the ribonuclease-reductase enzyme that prevents the cells from entering the S-phase. Cells then were washed twice carefully with fresh media and finally plated in the same flask. Time points were collected every hour or two hours, specified in each experiment, and samples were fixed for cell cycle analysis and stored at -20ºC.

Yeast cells synchronized by adding alpha factor. Cells were grown in solution and incubated for 3 hours with 5µg/ml of alpha-factor. Finally, cells were washed three times with PBS 1X and cultured again with complete (YPD) media in solution. Time points were collected as indicated in the experiment.

3.14. CDK4 INHIBITION ASSAY

Palbociclib is an antitumoral drug acting as a CDK4 inhibitor which was used to mimic the E2F1 mutant. First, S2 cells were plated at 10^6 cells/ml and incubated with Palbociclib (the concentration and time of incubation are indicated in each experiment). Afterwards, cells were collected, fixed for cell cycle analysis and stored at -20ºC. FACs results were statistically analyzed with R-Studio software through a linear regression model.

3.15. CELL CYCLE ANALYSIS

For cell cycle analysis by flow cytometry, S2 cells were collected and fixed with ethanol 70% and frozen at -20ºC overnight. Afterwards, ethanol was removed by centrifuging cells at 800xg for 3 minutes, and cells were washed twice with PBS 1X. Then, cells were resuspended in 250µl of propidium iodide (PI) solution containing 40 µg/ml RNase A (Sigma) and 1 µg/ml PI (Sigma). Cells were incubated at 37ºC for 30 minutes and finally analyzed by FACS**.** Flow cytometry experiments were carried out using an Epics Cyan ADP flow cytometer (Beckman Coulter, Inc, US). The instrument was set up with the standard configuration. Excitation of the sample was done at 488nm. FSC, SSC and red (613/20 nm) fluorescence for PI were recorded. PI fluorescence was projected on a monoparametrical histogram. Aggregates were excluded by gating single cells by their area vs their peak fluorescence signal. Time was used as a control of the stability of the instrument. Histograms were analyzed using Multicycle Software (Phoenix).

For S2 cell sorting in G_1 and G_2, cells were collected and diluted to 10^6 cells/ml. Cells were then incubated with 1µl of Vybrant DyeCycle Violet Stain (Thermofisher #V35003) for 30 minutes at 25ºC. Sorting cell cycle populations was performed by flow cytometry using a FacsAria Fusion sorter (Beckton Dickinson, San Jose, California). Scatter parameters were obtained from a blue (488nm) laser; red (582/15) fluorescence from propidium iodide was used to exclude dead cells, and cell cycle from live cells stained with Vybrant DyeCycle Violet Stain was obtained using a violet (405nm) laser for excitation and collecting the blue emission (450/50nm). Single cells were gated according to the fluorescence area-peak signal.

For budding yeast cell cycle analysis, cells were collected and fixed with 1ml of 70% ethanol overnight at -20ºC. Afterwards, cells were centrifuged at 3000g for 5 minutes, and ethanol was removed. Cells were then resuspended in 1 ml of 50nM sodium citrate + 0.1mg/ml of RNAse and incubated for four hours at 30ºC. Afterwards, 500ul of cells were transferred into a FACs tube with 1ml of 50mM $C_6H_5Na_3O_7$ (Sodium citrate) +

1µg/ml PI (Sigma). All samples were sonicated twice at 30% for 0.5 seconds**.** Finally, cells were analyzed by the GALLIOS 3L 10C de Beckman Coulter equipment.

3.16. GENOME EDITING THROUGH CRISPR/Cas9 SYSTEM

The guides were designed using the Benchling online tool considering the on-target and off-target scores given by the software. For the CRISPR/Cas9 Guides plasmid cloning, two oligonucleotides containing the guides complementary sequence were ordered flanked by the overhang ends resulting from the BspQ1 digestion. Then, they were hybridized by complementarity and inserted into the BspQ1-digested vector, as explained above. Finally, a sequencing-based screening allowed us to select the properly cloned plasmid.

Regarding the Donor Plasmid (DP), the cloning was performed in three steps:

1. The 5'HA was ligated with the GFP.
2. The 3'HA was ligated with the previous fragment.
3. The long insert of around 2.8 Kb was inserted into the vector.

Cells were co-transfected at 1:3 (Guides:DP) ratio, and GFP-positive cell sorting was performed by flow cytometry using a FacsAria Fusion sorter (Beckton Dickinson, San Jose, California). Scatter parameters were obtained from red (582/15) fluorescence laser from propidium iodide was used to exclude dead cells, and live cells stained with GFP were obtained using a blue (488nm) laser for excitation and collecting the green emission (530/30nm). Single cells were gated according to the fluorescence area-peak signal and single clones were sorted into 96 well plates.

Growing clones were visualized using an epifluorescence microscope. Positive clones were grown and screened by Taq Polymerase-mediated PCR. The sequences of the oligonucleotides used for the CRISPR/Cas9 cell line generation are listed in Table 5.

3.17. BIOINFORMATIC TOOLS AND STATISTICAL ANALYSIS

Statistical analyses were performed using GraphPad Prism software version 6.0 (GraphPad Software). Data is shown as the mean ± standard deviation (SD). Two-tailed t-test was performed when comparing two groups with normal distribution. ANOVA test was used when comparing more than two groups, followed by a Dunnett multiple comparison. Chi-Square test was performed when comparing categorical data among populations. Finally, a linear regression model was generate using R-studio software and used to analyze interaction significance in a multi-variable analysis.

Finally, all the non-referenced schemes presented in this thesis were elaborated using the BioRender online tool.

TABLES

TABLE 1: CELL LINES

Name	Description	Resístanse
S2 WT	S2 Drosophila cells Wild Type	-
CTL	S2 WT + empty pMK33-Hy vector	Hygromycin
SLIMP-KD	S2 WT + SLIMP RNAi cloned in pMK33	Hygromycin
SerRS2-KD	S2 WT + SerRS2 RNAi cloned in pMK33	Hygromycin
SLIMP-Flag	S2 WT + SLIMP-Flag tag in pMk33 vector	Hygromycin
CTL + pMT empty	48 cells + empty pMT-Puro vector	Hygromycin + Puromycin
SLIMP-KD + pMT empty	45 cells + empty pMT-Puro vector	Hygromycin + Puromycin
SLIMP-KD + full length SLIMP	45 cells + SLIMP full length different codon usage (DCU) in pMT-Puro vector	Hygromycin + Puromycin
SLIMP-KD + ΔN-SLIMP	45 cells + DN-SLIMP DCU in pMT-puro vector	Hygromycin + Puromycin
SLIMP-KD + CC-Flag	45 cells + DN-Coiled coil domain of SLIMP DCU in pMT-Puro vector	Hygromycin + Puromycin
SLIMP-KD + Flag-CC	45 cells + DN-Coiled coil domain of SLIMP DCU in pMT-Puro vector	Hygromycin + Puromycin
SLIMP-KD + GD-Flag	45 cells + DN-Globular domain of SLIMP DCU in pMT-Puro vector	Hygromycin + Puromycin
SLIMP-KD + Flag-GD	45 cells + DN-Globular domain of SLIMP DCU in pMT-Puro vector	Hygromycin + Puromycin

TABLE 2: PLASMIDS GENERATED IN THIS THESIS

Plasmid	Insert description	Backbone (Vector)	Restriction sites	Expression system
pAPP_01	SLIMP CC domain (Different codon usage)-Flag	pMT-Puro (Addgene #17923)	PmeI, XhoI	*Drosophila* S2 cells
pAPP_02	Flag-SLIMP CC domain (Different codon usage)	pMT-Puro (Addgene #17923)	PmeI, XhoI	*Drosophila* S2 cells
pAPP_03	SLIMP GD (Different codon usage)-Flag	pMT-Puro (Addgene #17923)	PmeI, XhoI	*Drosophila* S2 cells
pAPP_04	Flag-SLIMP GD (Different codon usage)	pMT-Puro (Addgene #17923)	PmeI, XhoI	*Drosophila* S2 cells
pAPP_05	CRISPR Donor plasmid (DP)	pAc5.1/V5-HisA (Thermofisher #V411020)	KpnI, BamHI, EcoRV, SacI	*Drosophila* S2 cells
pAPP_06	CRISPR Guides plasmid	pAC_sgRNA_Cas9 (Addgene #49330)	BspQI	*Drosophila* S2 cells
pAPP_07	SLIMP-EGFP	pMK33-Hy	SpeI, XhoI	*Drosophila* S2 cells
pAPP_08	SLIMP-Flag	pYES2-URA (Thermofisher #V825–20)	BamHI, XbaI	*S. Cerevisiae*
pAPP_09	ΔN-SLIMP-Flag	pYES2-URA (Thermofisher #V825–20)	BamHI, XbaI	*S. Cerevisiae*
pAPP_10	SerRS2-Flag	pYES2-URA (Thermofisher #V825–20)	BamHI, XbaI	*S. Cerevisiae*

TABLE 3: OLIGONUCLEOTIDES FOR PROTEIN EXPRESSION CONSTRUCTS.

Oligo code	Purpose	Forward (FW) oligo sequence (5’ – 3’)	Reverse (RV) oligo sequence (5’ – 3’)
oAAF_133; oAPP_21	pAPP_01 cloning	ATCGCTCGAGATGGACTACAAAGACGATGAC GACAAGATCTCCGCGCTGTACAT	CGATGTTTAAACTTTATTCCTCCCCTCCAACAG
oAPP_22; oAPP_23	pAPP_02 cloning	ATCGCTCGAGATGCCCAACCTTCTGCATG	CGATGTTTAAACTTCACTTGTCGTCATCGTCTTTGTA GTCGGTAAACAGATCTTTGAATTG
oAPP_24; oAPP_25	pAPP_03 cloning	ATCGCTCGAGATGGACTACAAAGACGATGAC GACAAGCCCAACCTTCTGCATG	CGATGTTTAAACTTCAGGTAAACAGATCTTTGA
oAPP_26; oAPP_27	pAPP_04 cloning	ACATGTGGATCCTTATCAATGGTGAGCAAG	TGATCAGATATCTCTTCACTTGTACAGCTC
oAPP_01; oAAF_135	pAPP_07 cloning	ATCGCTCGAGATGATCTCCGCGCTGTA	CGATGTTTAAACTTTACTTGTCGTCATCGTCTTTGTA GTCTTCCTCCCCTCCAACAG
oAPP_32; oAPP_37	pAPP_08 cloning	AGTCGGGATCCAACACAATGCTCTTGAGCCT GCGAAG	GACTTCTAGATTACTTGTCGTCATCGTCTTTGTAGT CCGTGAAAAGGTCCTT
oAPP_34; oAPP_37	pAPP_09 cloning	AGTCGGGATCCAACACAATGATCTCCGCGCT GTA	GACTTCTAGATTACTTGTCGTCATCGTCTTTGTAGT CCGTGAAAAGGTCCTT
oAPP_42; oAPP_43	pAPP_10 cloning	AGTCGGGATCCAACACAATGAAATTGCCGAC GAAT	GACTTCTAGATTACTTGTCGTCATCGTCTTTGTAGT CGGCCTTGATGAATTT

TABLE 4: OLIGONUCLEOTIDES FOR RT-PCR.

OLIGO NAME	Amplified gene	Forward (FW) oligo sequence (5' – 3')	Reverse (RV) oligo sequence (5' – 3')
oAPP_46; oAPP_47	SLIMP	GAGTATCCGGGCAGTCATCG	GCTGATACGTCCCACACACA
oAPP_102; oAPP_103	Cyclin B	CGAGCACCATACGATGTCCA	GCAATCTCCGATGGCCTGTA
oAPP_104; oAPP_105	Cyclin E	GCCCAATCGCTATCCTTCCA	CTGCTGAGGTTCCTGGTAGC
oAPP_52; oAPP_53	RPL32	AAGCGGCGACGCACTCTGTT	GCCCAGCATACAGGCCCAAG

TABLE 5: OLIGONUCLEOTIDES FOR THE CRISPR/Cas9 SYSTEM GENERATION.

Oligo code	Purpose	Forward (FW) oligo sequence (5' – 3')	Reverse (RV) oligo sequence (5' – 3')
oAPP_38; oAPP_11	5'HA into pAPP_05	GTCGATGGTACCGACTCTCTATCCCATAGAGGA	ACCGGATCCTCCACCCGTGAAAAG
oAPP_15; oAPP_39	GFP into pAPP_05	GGTGGAGGATCCGGTGTGAGCAAG	CGGAGTGATATCTCACTTGTACAGCTCGTCCA
oAPP_40; oAPP_41	3'HA into pAPP_05	CGACATGATATCAAAACGATCGGTGTTTAGTT	CGGAGTGAGCTCCCAATTACACCGCTTCAGTG
oAPP_44; oAPP_45	pAPP_05 sequencing	TGCATTCGATAATAAAAATAATGTTGAGC	AACAAACAACAAGAAACTAAACACCG
oAPP_19; oAPP_20	pAPP_06 (sgRNA guides)	TTCGCTTTTCACGTAAAAAACGAT	AACATCGTTTTTTACGTGAAAAGC

TABLE 6: ANTIBODIES.

Antibody name	Biogenic origin	Dilution	Source
α -SLIMP	Rabbit	IF – 1:400 / WB -1:1000	Home-made in Ribas' Lab
α -SRS2	Chicken	WB – 1:1000	Home-made in Ribas' Lab
α -LON	Rabbit	WB – 1:2000	L. Kaguni's Lab (Michigan S. University)
α -SerRS1	Chicken	WB – 1:1000	Innovagen
α -VDAC	Mouse	WB – 1:1000	Abcam (Cat. #14734)
α -GARS	Rabbit	WB – 1:1000	Abcam (Cat. #42905)
α -Lamin A	Mouse	WB – 1:3000	DSHB (Cat. #ADL67.10)
α -NDUFS3	Mouse	WB – 1:1000	Mitoscience (Cat. #MS112)
α -FLAG tag	Mouse	WB – 1:2000	Sigma-Aldrich (Cat. #F3165)
α -CDK1-P (Y15)	Rabbit	WB – 1:1000	Cell signaling (Cat. #9111T)
Alexa Fluor 488 α -Rabbit	Rabbit	IF – 1:500	Invitrogen (Cat. #A11008)
α-Rabbit HRP	Rabbit	WB – 1:10000	Amersham (Cat. #NA934)
α-Mouse HRP	Mouse	WB – 1:10000	Amersham (Cat. #NA931)
α-Chicken HRP	Chicken	WB – 1:10000	MERK (Cat. #AP194P)

RESULTS

4. RESULTS

4.1. CHAPTER I: SLIMP SUBCELLULAR LOCATION

The recently described Seryl-tRNA synthetase-Like Insect Mitochondrial Protein (SLIMP) was initially characterized as a mitochondrial localized protein (Guitart, et al., 2010). SLIMP is an essential protein involved in mitochondrial homeostasis. As explained in the introduction (see section 1.5), we recently reported that SLIMP plays a vital role in co-regulating mitochondrial protein synthesis and mtDNA copy number through its interactions with SerRS2 and LON, respectively (Picchioni, et al., 2019). However, other experiments indicate that SLIMP plays a role in cell cycle regulation, carried out potentially from outside the organelle. For this reason, in the present chapter, we aim to determine the SLIMP subcellular distribution beyond the mitochondria, using as a model system *D. melanogaster* embryonic S2 cells.

4.1.1. SLIMP Mitochondrial Signal Peptide

As mentioned before, previous studies in our group demonstrated that SLIMP is encoded in the nucleus and driven into the organelle through a N-terminal mitochondrial signal peptide (MSP) (Guitart, et al., 2010).

During an initial characterization of SLIMP, we tried to predict the mitochondrial-targeted sequence using various bioinformatic approaches; nevertheless, the outputs obtained differ a bit between them (Antolin-Fontes, 2019). To experimentally determine the SLIMP MSP exact sequence, we coupled enzymatic digestion and mass spectrometry analysis. We firstly overexpressed SLIMP fused to a C-terminal FLAG tag in S2 cells, and we performed a cellular fractionation assay that enabled us to enrich a fraction in mitochondria. Then, a SLIMP immunoprecipitation of the mitochondrial-enriched fraction allowed us to purify enough amount of SLIMP for enzymatic digestion. In

parallel, two different strategies were used for the immunoprecipitation elution. On one hand, the protein was eluted with Protein Loading Buffer (PLB) and directly run into an SDS-PAGE gel (Figure 27A). The SLIMP corresponding band (around 48 KD) was cut and processed by enzymatic digestion. On the other hand, the sample was eluted with Glycine pH=2.8 (Figure 27B) and directly digested in the liquid phase.

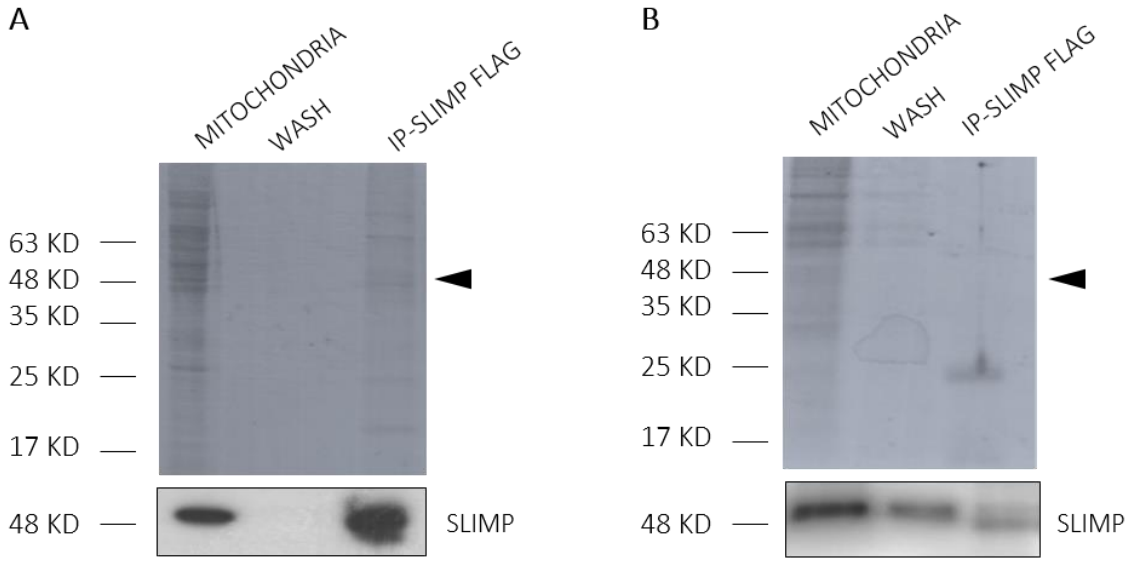

Figure 27 | SLIMP-FLAG purification. (A) SLIMP- FLAG eluted with PLB (upper panel). (B) SLIMP-FLAG eluted with Glycine pH=2.8 (upper panel). Immunoblot analysis for SLIMP detection is also shown in both cases (lower panels). A black arrowhead indicates the band size corresponding to SLIMP-FLAG (around 48 KD). The mitochondrial enriched fraction and the elution wash were loaded into the gel as controls. The IP was performed using a FLAG-tag antibody fused to magnetic beads (anti-FLAGM2- conjugated magnetic Dynabeads) as explained section 3.9. SLIMP-FLAG was detected using a homemade polyclonal SLIMP antibody. A black arrowhead indicates the size corresponding to the SLIMP band in the SDS-PAGE gel.

Figure 27 reveals that SLIMP, present in the mitochondrial enriched fraction, was properly eluted with both strategies. Although we obtained enough material in both cases to proceed with the experiment, notice that PLB seems to be more efficient than glycine for SLIMP elution. Purified SLIMP was digested with Trypsin, which cuts after arginine (R) and lysine (K) and Glu-C that cuts after aspartic acid (D) and glutamic acid (E). Finally, the peptides obtained from enzymatic digestions were mapped to the SLIMP sequence, as shown in Figure 28. Since none of the enzymes used could have cut after

an asparagine, we concluded that the cut before the I-22 must correspond to the MSP's biological cleavage. Thus, we defined the SLIMP mitochondrial signal peptide as the first 21 amino acids of the protein sequence, corresponding to **M L S L R S V L K H C L S A K K T C S R N** (Figure 28).

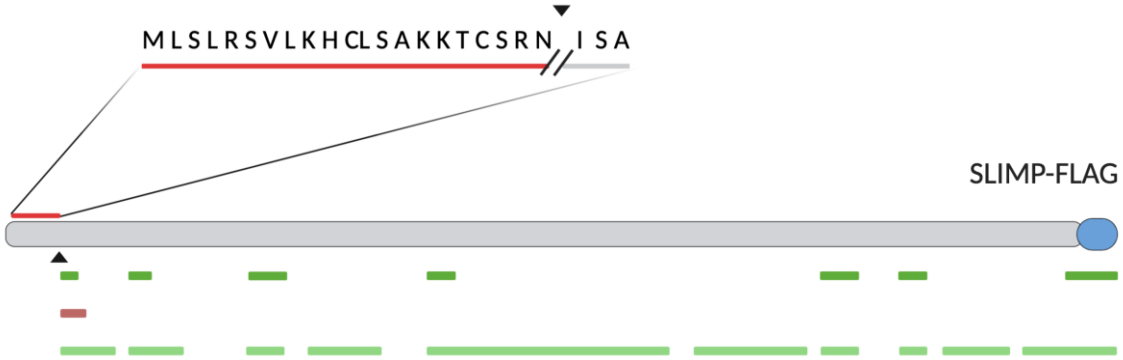

Figure 28 | SLIMP Mitochondrial Signal Peptide. Schematic representation of SLIMP-FLAG sequence (in grey). Peptides obtained from enzymatic digestion are represented in different colours below the protein sequence: Peptides obtained from the glycine-eluted sample after trypsin digestion (in dark green); peptides obtained from the glycine-eluted sample after Glu-C digestion (in brown); peptides obtained from SDS-PAGE purified band PLB-eluded after trypsin digestion (in light green). A black arrowhead points to the MSP biological cut position. The 21 amino acids corresponding to the mitochondrial-targeting sequence are zoomed in and highlighted in red.

In order to further verify that the sequence just described above actually corresponds to the MSP of SLIMP, we overexpressed the protein with and without those 21 N-terminal amino acids in S2 cells. We next checked for subcellular localization of SLIMP by performing immunofluorescence assays (Figure 29).

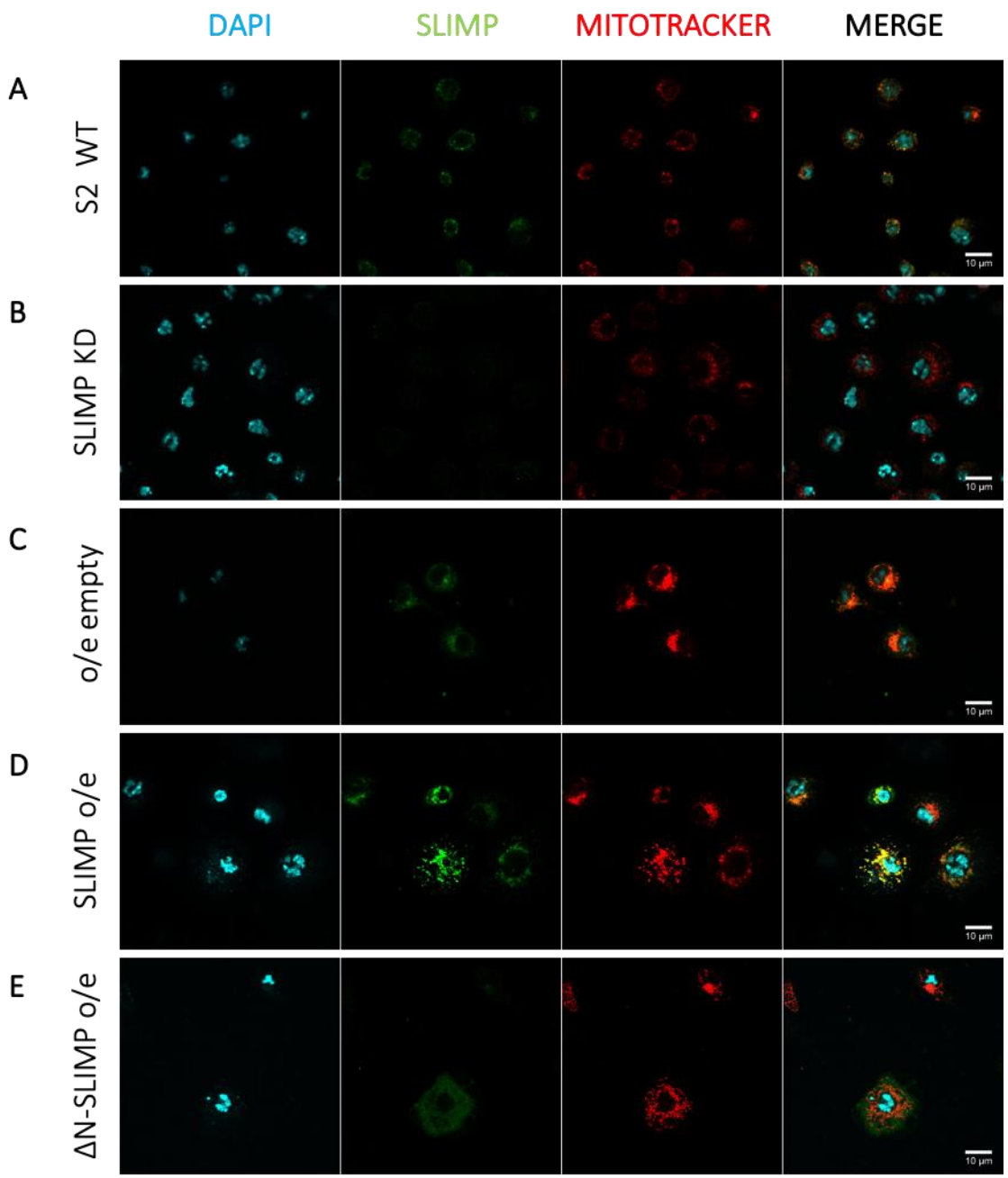

Figure 29 | SLIMP immunostaining. Representative images from immunofluorescence assays of (A) S2 wild type cells, (B) SLIMP depleted cells, (C) S2 stable cell line overexpressing empty pMK33-Hy vector, (D) S2 stable cell line overexpressing SLIMP, (E) S2 stable cell line overexpressing a truncated form of SLIMP without the first 21 aa. For SLIMP detection (in green), we used a homemade polyclonal primary antibody together with an Alexa Fluor 488 secondary antibody. For mitochondrial staining (in red), we used Mitotracker Red, and DAPI staining was used to dye the nucleus (in blue). The last column corresponds to the merge of the three channels. In A, C and D, SLIMP co-localises with mitochondria (yellow), while in E, SLIMP is

visualized mainly in the cytosol. SLIMP depleted cells (B) were used as a control for SLIMP antibody specificity.

As observed in Figure 29A and 29C, endogenous SLIMP is primarily localized at the mitochondrial compartment. Interestingly, the immunodetection of SLIMP in S2 cells overexpressing the full-length form of the protein shows a clear co-localization of SLIMP with the organelle (Figure 29D). Nevertheless, after overexpressing the truncated form of SLIMP lacking the MSP, SLIMP appears spread all over the cell, manly at the cytosolic compartment (Figure 29E). This result allowed us to confirm that the sequence, previously defined as the SLIMP MSP, corresponded to the mitochondrial-targeting sequence of SLIMP and demonstrate that it is essential and sufficient for leading the protein into the organelle. Since when it is removed, SLIMP can not reach its canonical mitochondrial location.

4.1.2. SLIMP subcellular distribution

As mention before, although SLIMP localizes essentially at the mitochondria, it has been suggested that SLIMP carries out a cell cycle-related function from outside the organelle. SLIMP-depleted cells show a G_2 delay in the cell cycle profile that may be rescued by overexpressing SLIMP without the MSP. To deeply explore the possibility of an extra-mitochondrial population of SLIMP co-existing within the cell, we optimized and performed a variety of cellular fractionation protocols.

On one hand, we developed a cellular fractionation assay in S2 cells, consisting of the isolation of mitochondrial enriched fraction from the cytosolic fraction (see section 3.7.1). This experiment allowed us to confirm with a different technique the mitochondrial localization of endogenous SLIMP (Figure 30). This result is in concordance with what we observed in Figure 29A and published data (Guitart, et al., 2010). Moreover, a light band of SLIMP in the cytosolic fraction preliminary points to the possibility of a tiny extra-mitochondrial population of SLIMP. With the following experiments, we further explore that possibility.

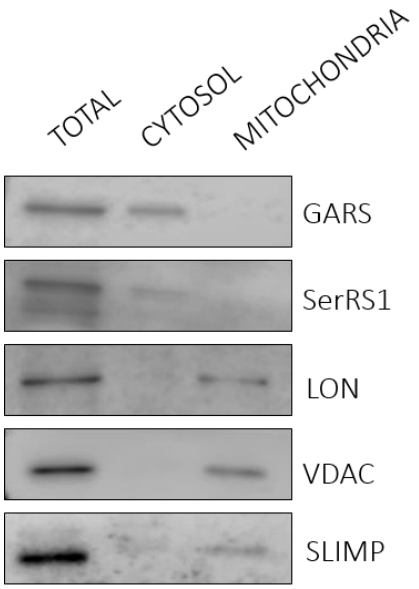

Figure 30 | Mitochondrial enrichment in S2 cells. Western blot analysis of a cellular fractionation assay. S2 wild type cells were fractionated to enrich a fraction in mitochondria and separated from the cytosol. SLIMP was detected with a homemade polyclonal antibody and is observed mainly at the mitochondrial enriched fraction. VDAC, LON (mitochondrial markers), GARS and SerRS1 (cytosolic markers) were used as controls for the cellular fractionation assay. The first lane of the gel corresponds to a whole-cell lysate used as a control for protein detection. This western blot is representative of the three biological replicates performed.

On the other hand, since the cell cycle regulatory proteins tend to reside in the nucleus, we initially, focused on that compartment. Proteins that are nuclear imported, require a Nuclear Localization Signal (NLS), which lead them into the nuclear compartment. Thus, a bioinformatic NLS prediction tool allowed us to primary approach whether SLIMP sequence comprises a nuclear localization signal. Interestingly, NLS-Mapper (Kosugi et al., 2009a) predicted a 31 aa-length NLS peptide starting at position 28 after the MSP cleavage site, coinciding with the coiled-coil domain, with an score of 4.1 (Figure 31). Remarkably, NLS-Mapper predicts that proteins holding a NLS with an score around four localize at both nuclear and cytosolic compartments (Kosugi et al., 2009b). Intriguingly, this outcome was only obtained by analyzing the SLIMP sequence without the MSP, but not the full-length sequence, suggesting that probably, when both targeting sequences are present and available, the MSP eclipses the NLS.

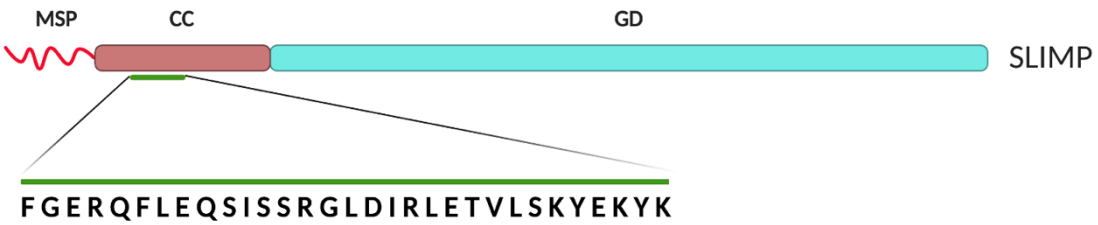

Figure 31 | SLIMP NLS peptide prediction. NLS-Mapper prediction of a potential NLS sequence within the SLIMP coiled-coil sequence with an score of 4,1. The MPS appears in red, the coiled-coil domain (CC) in purple and the globular domain (GD) in blue. The predicted NLS peptide is zoomed in and highlighted in green.

According with the previous *in silico* result we decided to experimentally verify the potential nuclear localization of SLIMP. Thus, we focused on a cellular fractionation protocol for the nuclear compartment-enrichment (see section 3.7.2). Cellular fractionation protocols depend on cell membrane composition, size, and cell adherence, among other factors, so they vary a lot between different cell lines. For this reason, we firstly optimized the NE-PER TM KIT cell fractionation protocol for *D. melanogaster* S2 cells.

The cell fractionation assay was performed following the manufacturer's instructions, considering $2 \cdot 10^7$ cells a packed cell volume equal to 10µl for S2 cells. Markedly, aiming to purify as much as possible the nuclear fraction, two PBS 1X washes before the nuclear lysis were incorporated to the primary protocol, which significantly increased the purity of the nuclear-enriched fraction. The two resulting fractions (Cytosolic + organelle fraction and nuclear fraction) and a whole-cell lysate, used as control, were analyzed by western blot (Figure 32).

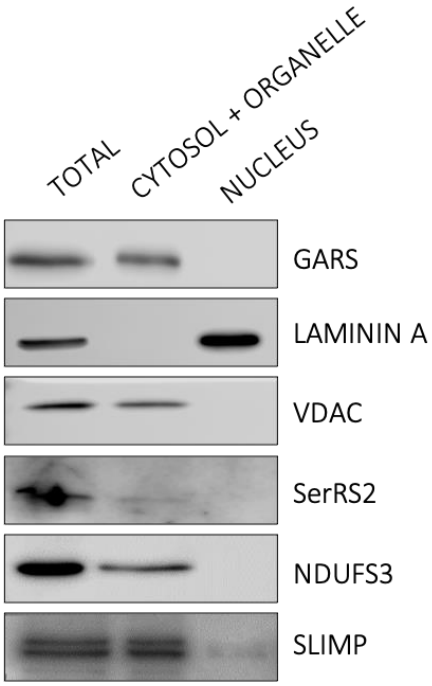

Figure 32 | Nuclear enrichment in S2 cells. Western blot analysis of cellular fractionation assay. S2 wild type cells were fractionated to separate the nuclear-enriched fraction (Nucleus) from the rest of the cell (Cytosol + organelle). The assay was performed using an adaptation of the commercial NE-PER KIT (ThermoFisher) manufacturer's protocol, by adding two extra washes to the nucleus-enriched pellet. GARS (Cytosolic marker), Laminin A (Nuclear marker), SerRS2, VDAC and NDUFS3 (Mitochondrial markers) were used as controls of the cell fractionation assay. The first lane corresponds to a whole-cell lysate used as a control for protein detection. Although SLIMP is observed mainly in the "cytosol + organelle" fraction, a little band is also observed in the nuclear-enriched fraction. This western blot is representative of the three biological replicates performed for this assay.

Based on the compartment markers, we can affirm that cells were properly fractionated in Figure 32. Moreover, this result suggests that a small portion of SLIMP localizes at the nuclear compartment while most of the protein remains at the cytosolic + organelle fraction. This is in concordance with previous results showing that SLIMP is majorly at the mitochondrial compartment.

Furthermore, we wondered whether SLIMP could also localize at the cytosol since it was already suggested in Figures 30 and 31. In this direction, we developed a protocol to

separate the three cellular compartments: cytosolic, mitochondrial, and nuclear fractions (Figure 33).

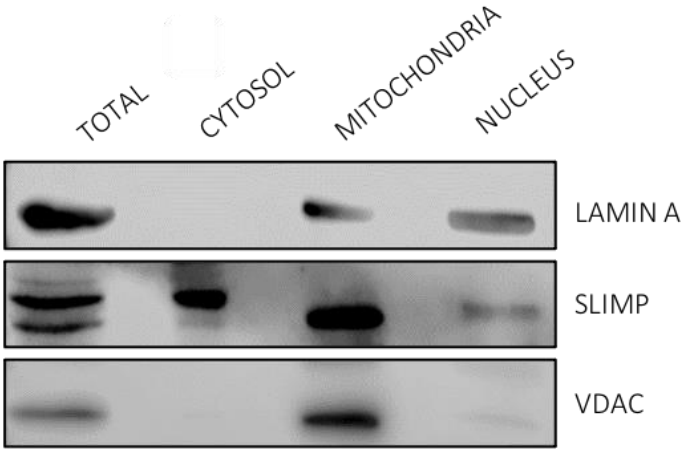

Figure 33 | Cytosol enrichment in S2 cells. Western blot analysis of cell fractionation assay. S2 cells were fractionated using a homemade protocol (see section 3.7.3) to separate the cytosolic fraction (Cytosol) from the mitochondrial (Mitochondria) and the nuclear fractions (Nucleus). Lamin A (Nuclear marker) and VDAC (Mitochondrial marker) were detected with commercial antibodies and used as controls for the cell fractionation assay. The first lane of the gel corresponds to a whole-cell lysate used as a control for protein detection. SLIMP is detected in all cellular compartments with the highest proportion at the mitochondria. This western blot is representative of the three biological replicates done for this assay.

As shown in Figure 33, when the three cellular compartments are separated, SLIMP is found predominantly at the mitochondrial compartment, which is consistent with previous experiments. Interestingly, it is remarkable that this result also points to a small population of SLIMP residing in the cytosol, a fraction reasonably well isolated. Conversely, some cross-contamination between mitochondrial and nuclear compartment is appreciated; thus, we can not wholly trust the SLIMP band appearing in the nuclear fraction using this protocol.

Altogether, these results show that endogenous SLIMP is essentially present in mitochondria. Moreover, they point to the existence of an extra-mitochondrial population of SLIMP co-existing in other cellular compartments. Two different experiments showed that SLIMP could be present in the nucleus (Figure 32) and cytosol

(Figure 33), which was already predicted *in silico* (Figure 31). However, it is crucial to keep in mind that cellular fractionation assays allow us to observe enrichments and not purifications of cellular compartments. Hence, more experiments in this direction need to be performed to confirm the subcellular distribution of SLIMP beyond the mitochondria.

In that sense, we decided to address this issue with a more sophisticated approach based on genome editing: the generation of a cell line expressing endogenously SLIMP fussed to a C-terminal GFP tag using the CRISPR/Cas9 system.

4.1.3. SLIMP-GFP S2 CRISPR/Cas9 cell line generation.

Clustered regularly interspaced short palindromic repeat (CRISPR)/CRISPR-associated nuclease 9 (Cas9), was discovered as part of bacteria and archaea adaptive immune system and has recently emerged as a powerful tool for genome editing. CRISPR/Cas9 tool consists in introducing a single guide RNA (sgRNA) complementary to the genome locus aimed to be modified, together with the Cas9 endonuclease. Both molecules form a complex, so the resulting base pairing between the sgRNA and the endogenous DNA strand will guide the endonuclease to that particular locus. Finally, it will promote the Cas9-mediated double-strand DNA cleavage. The Cas9 endonuclease always cuts few nucleotides upstream of the Protospacer Adjacent Motif (PAM). This sequence can vary among species, for the *Streptococcus pyogenes* system used in the present work, it corresponds to the triplet NGG. As soon as the DNA is cleaved, it can be repaired through two different mechanisms. On one side, non-homologous-end joining repair (NHJR) which randomly adds nucleotides to fill in the gap. Alternatively, homologous-directed repair (HDR) allows the addition of a specific genomic sequence at that particular cleaved locus, filling the gap through homologous recombination (Doudna & Charpentier, 2014; Y Ma et al., 2014; Wang et al., 2016).

The HDR mechanism is mainly applied to generate gene insertions (knock-ins). Importantly, in this case it is required to provide the foreign DNA sequence flanked by

two homologous arms, which need to be complementary to the DNA cleavage site surrounding genomic regions. Hence, after the DNA cut, homologous recombination (HR) will promote the exogenous sequence's insertion into the genome. Since our goal was to create a *Drosophila melanogaster* S2 transgenic cell line expressing SLIMP fused to a GFP tag at the C-terminal end, we worked in this last scenario which is represented below in Figure 34.

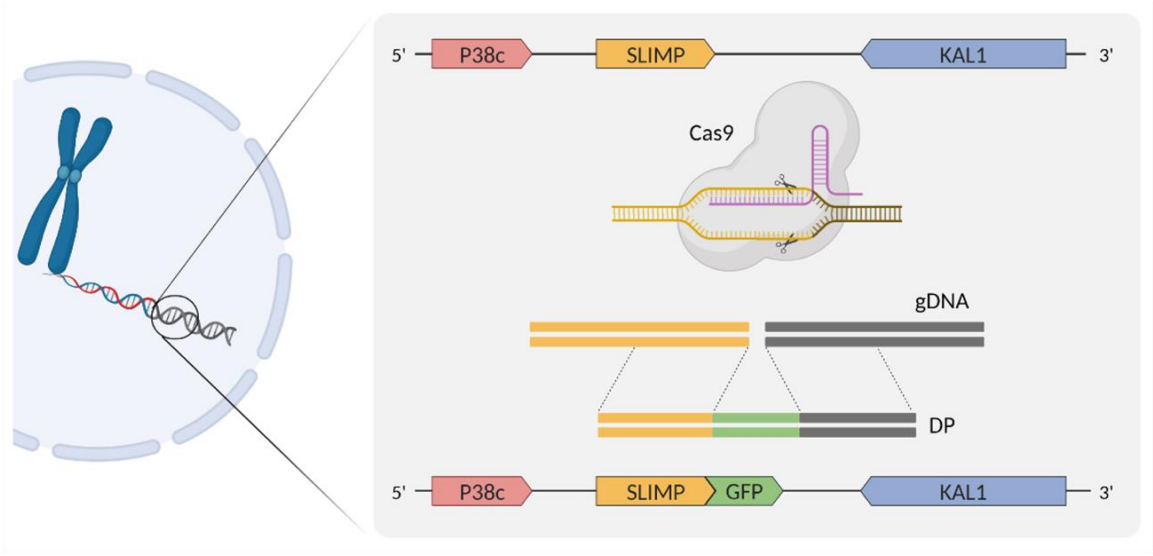

Figure 34 | CRISPR/Cas9 system for the SLIMP-GFP knock-in generation. Endogenous DNA strand containing SLIMP gene is represented in 5'→3' sense. SLIMP is represented in orange and flanked by p38c (pink) and Kal1 (blue). The sgRNA, represented in purple, hybridize to the SLIMP 3'-end, promoting Cas9-mediated double-strand DNA cleavage. Finally, homologous recombination allows the GFP (green) incorporation through the HDR mechanism.

Tagging endogenous SLIMP with a C-terminal GFP could be an extremely powerful tool. It would allow us to explore deeper the subcellular distribution of SLIMP, in addition to analyze the SLIMP expression pattern under different cellular conditions. Furthermore, we could use this tool for pulling down endogenous SLIMP and further study its interactome, inside and outside the organelle, among other applications. However, even though CRISPR/Cas9 looks elementary and straightforward, it often turns out to be truly low efficient, and it requires a meticulous design.

Firstly, we overexpressed the SLIMP-GFP fusion protein in S2 wild type cells to check for its viability in vivo. Live confocal microscopy imaging allowed us to guarantee that SLIMP-GFP is expressed and behaves, at least in terms of localization, like the endogenous SLIMP (Figure 35B). In contrast, when GFP is expressed alone, the green fluorescence is observed all over the cell (Figure 35A). Thereby, we concluded that the GFP tag fused to SLIMP does not impair the SLIMP expression or mitochondrial import.

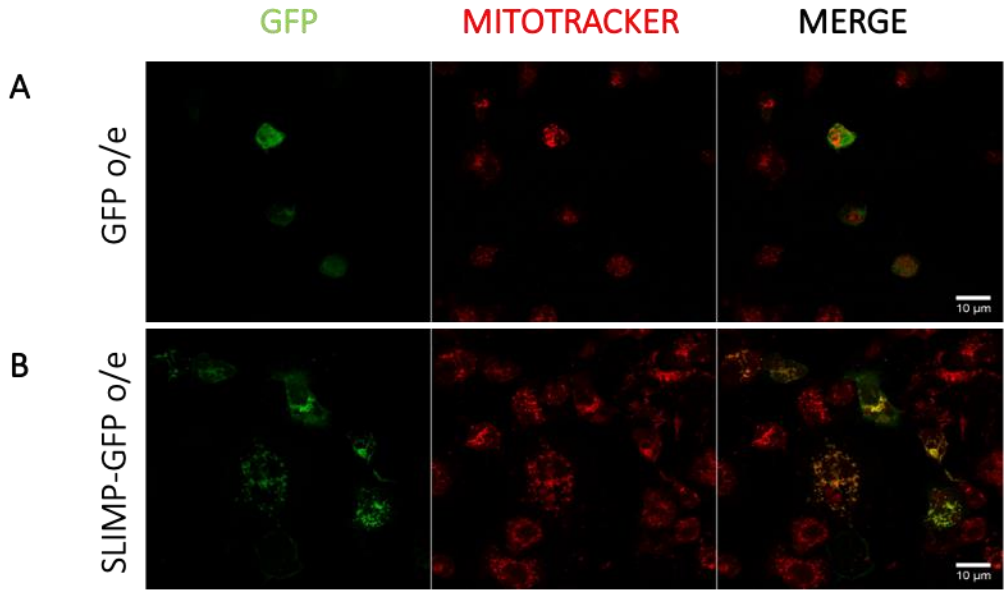

Figure 35 | SLIMP-GFP overexpression in S2 cells. Representative images of (A) S2 wild type cells overexpressing GFP and (B) S2 wild type cells overexpressing SLIMP fussed to a C-terminal GFP tag. GFP is observed in green (first lane), mitochondria stained with Mitotracker are shown in red (middle lane), and the last column shows the merge of both channels. SLIMP-GFP co-localizes with mitochondrial (in yellow). Overexpression of GFP alone was used as control.

As previously described, a knock-in generation requires essentially two plasmids: the sgRNA-Cas9 plasmid and the donor plasmid (DP), containing the foreign DNA sequence intended to be inserted, flanked by two homology arms that will allow the HR process.

It has been shown that the sgRNA sequence is vital for both targeting specificity and cleavage efficiency (Hsu et al., 2013; Jinek et al., 2013). A proper guide design is fundamental to avoid off-targets, which occur when the sgRNA hybridize similar sequences elsewhere in the genome leading to an off-target cleavage, potentially

resulting in unintended knockout effects (Hsu et al., 2013). Many bioinformatic tools have been developed in recent years to design sgRNA with the higher efficiency and specificity. They predict the better oligonucleotide sequence based on the on-target and the off-target scores. These scores are calculated considering numerous features like, for instance, the sequence length (proper sgRNA is known to be around 18 to 20 nucleotides), CG% content, structure, or mismatches ratio. Moreover, it is fundamental the existence of a PAM sequence downstream of the intended cleavage site.

For the sgRNA design, we used Benchling online software (Pellegrini, 2016), which gave us three different sequences as potential RNA single guides (Figure 36 and Table 7).

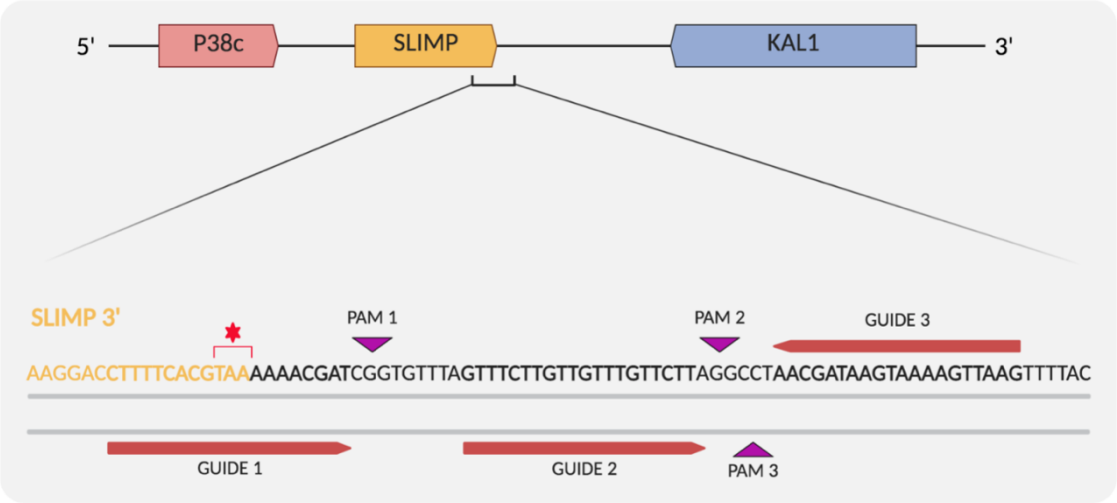

Figure 36 | Schematic representation of CRISPR/Cas9 sgRNA design. SLIMP is represented in orange. In the lower part, the 3'-end of SLIMP with the adjacent nucleotide sequence is zoomed in. The three suggested guides are represented in pink and corresponding PAMs sequences in purple. SLIMP stop codon is marked with a red asterisk.

As shown in Table 7, the sequence that fulfils most of the features required is Guide 1, with the highest on- and off-target scores. Moreover, it overlaps both sites of the cleavage site, precisely cutting the endogenous genome and not the DP. Thus, the oligonucleotide sequence corresponding to the Guide 1 and its complementary were inserted into the pAC_sgRNA_Cas9 vector as reported in (Bassett et al., 2013). See section 3.16.

TABLE 7 | Putative sgRNA guides for SLIMP-GFP CRISPR/Cas9 cell line generation.

Guide	Sequence (5' - 3')	Length	PAM	On target score	Off target score
1	CTTTTCACGTAAAAAACGAT	20	CGG	64.6	48.7
2	GTTTCTTGTTGTTTGTTCTT	20	AGG	35.4	39.2
3	CTTAACTTTTACTTATCGTT	20	AGG	44.3	49.0

On the other hand, two homology arms of 1 KB length were inserted into the donor plasmid, flanking the GFP gene without ATG^{MET} first codon. Upstream of the GFP, we added a linker sequence (GGGSG) which provides flexibility and stability to the SLIMP-GFP fusion protein. A stop codon was also inserted downstream of GFP. Moreover, we used a relatively small backbone as donor plasmid to make the co-transfection more efficient (see table 2 and section 3.16).

Finally, S2 wild type cells were co-transfected with both constructs at optimized ratio (1 sgRNA-Cas9: 3 DP), grown for three days after transfection and analysed by FACS. Since any fluorescent marker is present in the plasmids for transfection selection control, only the cells that have incorporated the GFP tag will emit green fluorescence. The GFP positive cells were sorted into single clones and grown in 96-well plates (Figure 37A). Moreover, cells co-transfected under the same conditions with sgRNA-Cas9 plasmid plus empty-DP were used as a negative control (Figure 37B).

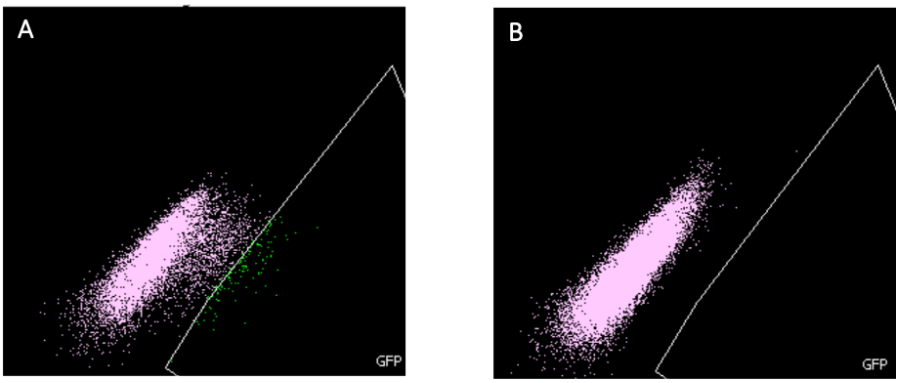

Figure 37 | GFP-positive cell sorting. Graphical representation of (A) CRISPR: cells co-transfected with sgRNA-Cas9 plasmid and DP, and (B) CTL-: cells co-transfected with empty-DP and sgRNA-Cas9 plasmid. Cells under the GFP window represent the positive clones, found only

in the CRISPR sample (A). Cells on the left of the GFP window are negative clones with intrinsic autofluorescence.

We sorted 288 cells, considered positive clones, in three 96-well plates (around 1.3% of total sorted cells), and only 16 of them were able to grow and expand from one single cell. Furthermore, only 6 of those clones looked green under an epifluorescence microscope (Figure 38).

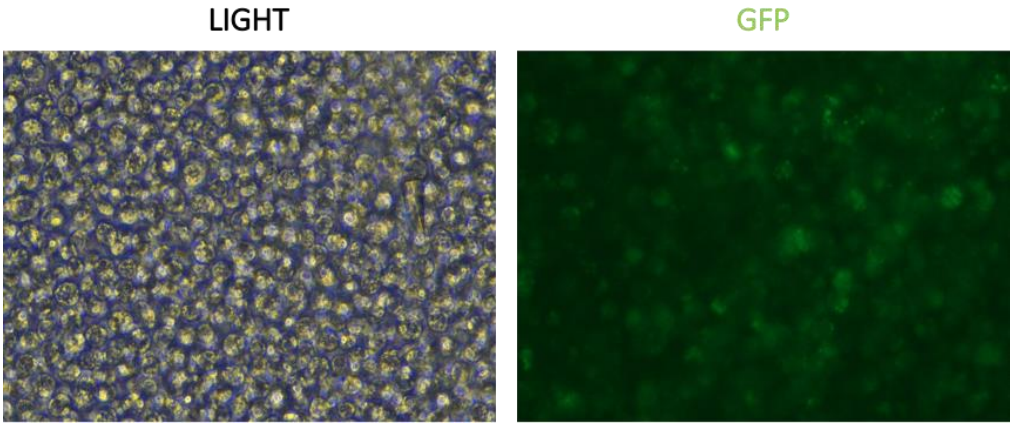

Figure 38 | GFP positive clone. Representative image of cells coming from a single GFP-positive clone after three weeks of growing. The images were taken with light (left panel) and green fluorescence microscopy (right panel). Some of the cells show a stronger green signal, although the pattern is difficult to determine.

Surprisingly, after a couple of months growing cells lost the green fluorescence. We wondered whether it could be due to a decrease in SLIMP expression, so the GFP incorporation was checked at DNA level by PCR. For checking the presence of the GFP incorporation we used a primer pair flanking the SLIMP region in the genome. Thus, in positive clones, the band size should be approximately of 2.2 KB, while in negative clones, the band size would be around 1.5 kb (Figure 39A). Finally, PCR products were run into an agarose gel and results are shown in Figure 39B.

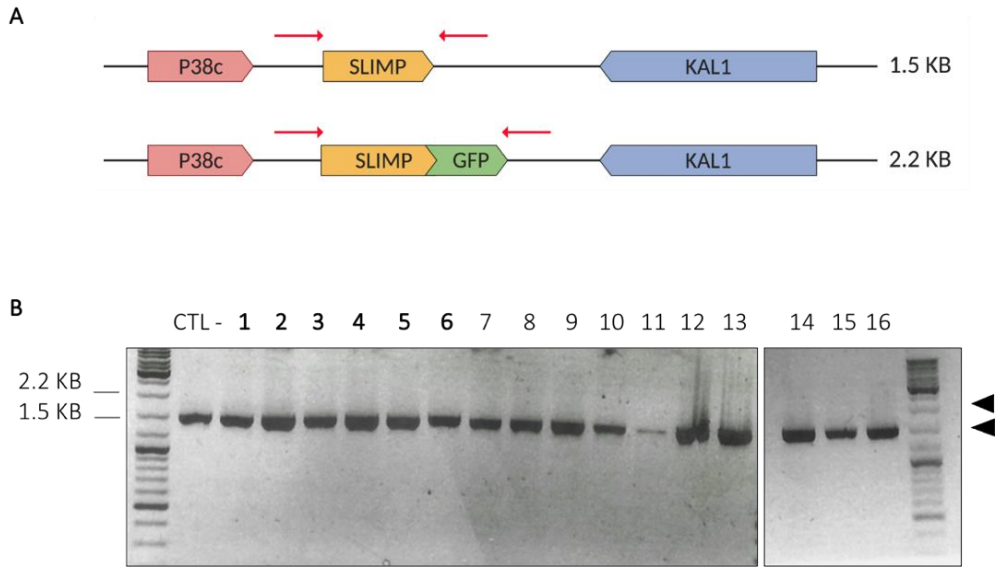

Figure 39 | Endogenous SLIMP amplification in CRISPR/Cas9 colonies. (A) Schematic representing the band size according to the amplification length of the SLIMP region without (top) and with (bottom) fused GFP. (B) Agarose gel showing the PCR products of the SLIMP gene amplification for the 16 putative positive clones. The six colonies that showed green fluorescence at the beginning of the experiment are highlighted in bold. Genomic DNA from S2 wild type cells was used as a negative control.

Figure 39B reveals that all colonies were negatives. Moreover, we collected cells from clones 1, 4 and 5 and re-analyzed them by FACS using the same settings as previously (Figure 37A). Importantly, those clones come from a single cell that appeared on the GFP-positive window (Figure 37A). Furthermore, they showed green fluorescent after some passages (Figure 38). Unfortunately, as shown in Figure 40, none of them comprised green cells, in fact, they looked exactly like the negative control.

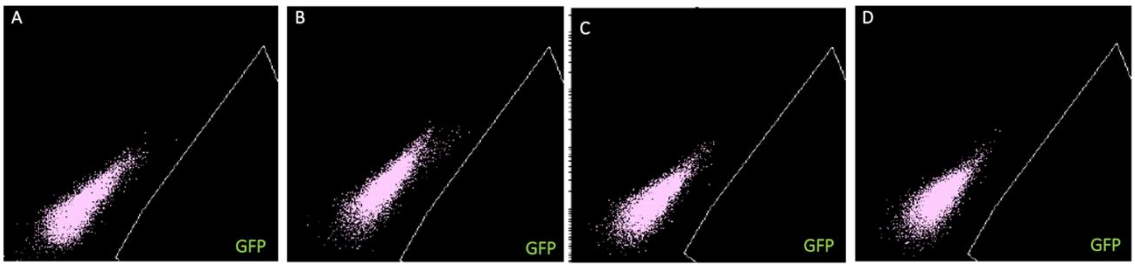

Figure 40 | GFP-positive cell sorting of CRISPR/Cas9 colonies. (A) S2 WT cells, (B) Clone 1, (C) Clone 4 and (D) Clone 5. Cells on the left of the GFP window present intrinsic autofluorescence

of this cell line, while cells under the GFP window would be considered GFP-positive clones. All the three clones showed the same pattern as the negative control (S2 wild type cells).

Altogether these results, suggest that although some of the clones had green fluorescence after transfection (Figures 37 and 38), some passages later, the entire population of cells had lost it (Figure 40). Moreover, it does not seem to be due to a decrease in SLIMP expression, since at the DNA level, none of the clones shows the GFP gene incorporation either (Figure 39). The CRISPR/Cas9 knock-in was probably achieved, but it seems that cells somehow managed to lose the modified alleles over time and cell divisions. Maybe another genome editing tool would be more suitable for this cellular model. This issue will be further discussed in the discussion (see section 5.1).

In this chapter, we experimentally defined the SLIMP MSP sequence and demonstrated that it is essential and sufficient to drive SLIMP into the mitochondria. Unfortunately, we could not tag the endogenous SLIMP with a GFP tag, which would allow us to explore changes in the protein expression and distribution under different cellular conditions. In contrast, the cellular fractionation assays raised the possibility of an extra-mitochondrial population of SLIMP present in the cytosol and the nucleus. More experiments must be performed in this direction to address this question and decipher the subcellular localization of SLIMP beyond the mitochondria.

4.2. CHAPTER II: SLIMP AND THE CELL CYCLE

As mentioned before, SLIMP plays an essential role in cell cycle regulation; however, the molecular mechanism underlying this function remains still unknown. Previous studies in our group showed that upon SLIMP depletion, cells get temporally accumulated in the G_2 phase of the cell cycle. Interestingly, this effect is specific for SLIMP, considering that it does not occur upon the downregulation of SerRS2 or LON, their main mitochondrial interactors (Figure 22). Furthermore, the SLIMP depletion promotes an upregulation of specific genes involved in S-phase onset and DNA replication initiation (Figure 23). Nevertheless, the molecular mechanism linking SLIMP with the cell cycle regulation still needs to be revealed. In this chapter, we address this issue from different angles.

4.2.1. SLIMP levels through the cell cycle

In organisms ranging from yeast to humans, the regulation of periodicity at transcriptional and translational level ensures that proteins required for cell cycle regulation are produced at the appropriate phase (Bonke et al., 2013).

Firstly, to check if SLIMP was periodically expressed through the cell cycle, we analysed SLIMP mRNA levels in different cell cycle phases (G_0/G_1, S and G_2/M) by coupling cellular synchronization and qPCR. S2 wild type cells were synchronized in the late G_1 phase with hydroxyurea (HU), a deoxyribonucleotide reductase inhibitor. After the treatment, cells were collected at different time points: at time zero, around 60% of the cells were synchronized in G_1, four hours later, the cell culture was enriched in S-phase and after eleven hours in G_2/M (Figures 41A and 41B). RNA extraction and qPCR analysis were performed to study differences in SLIMP mRNA levels between the cell cycle phases (Figure 41C).

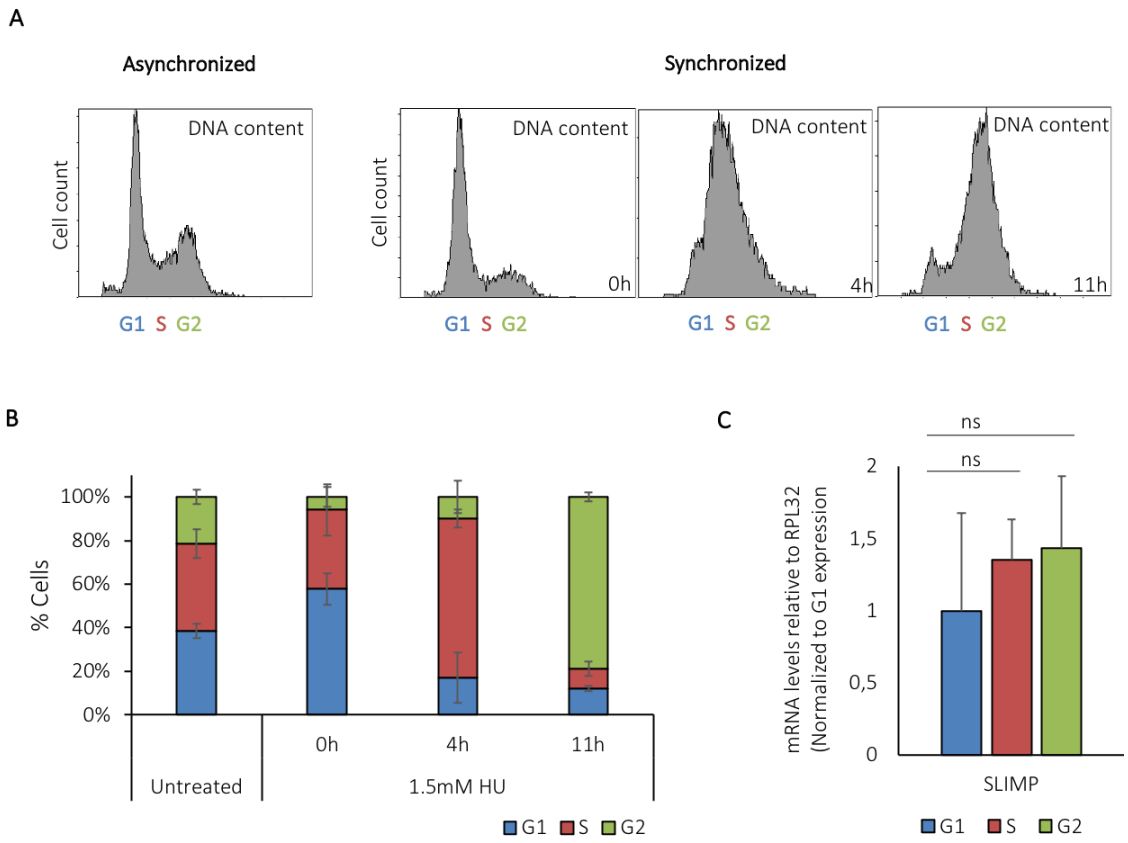

Figure 41 | SLIMP mRNA levels through the cell cycle, using synchronized S2 cells. (A) Schematic representation of cell cycle profiles of non-synchronized cells (left panel) and synchronized cells at 0, 4 and 11 hours after 24 hours of 1.5mM HU treatment (right panel). (B) Graphical representation of the quantified percentages of cells in each cell cycle phase. (C) SLIMP mRNA levels in cellular population enriched in G_1 (blue), S (red) and G_2 (green). RPL32 (house-keeping gene) was used as a control to normalize SLIMP values. S and G_2 are normalized to G_1. Three biological replicates were performed. Statistical analysis was done by applying an unpaired t-test with GraphPad software (* p<0,05; ** p< 0,01; *** p<0,001).

Although Figure 41C suggests a tendency of increasing levels of SLIMP through the cell cycle with a peak of expression in the G_2 phase, the observed differences are not statistically significant. The high variability between samples could come from the intrinsic heterogeneity of synchronized cell populations.

Therefore, we coupled cell sorting to pico-profiling RNA extraction to decipher whether SLIMP mRNA levels fluctuate between the different cell cycle phases. S2 wild type cells were sorted in vivo, and 6000 cells were collected per cell cycle phase (Figure 42A).

Afterwards, we performed a pico-profiling assay, consisting of RNA extraction from a very low number of cells coupled retro-transcription and strongly cDNA amplification (see section 3.5 and Figure 26). Finally, we performed qPCR assays to analyze SLIMP mRNA levels through the cell cycle. Moreover, mRNA levels of Cyclin E (G_0/G_1 phase marker) and Cyclin B (G_2/M phase marker) were quantified as controls (Siu et al. 2012; Whitfield et al. 1990) (Figure 42B).

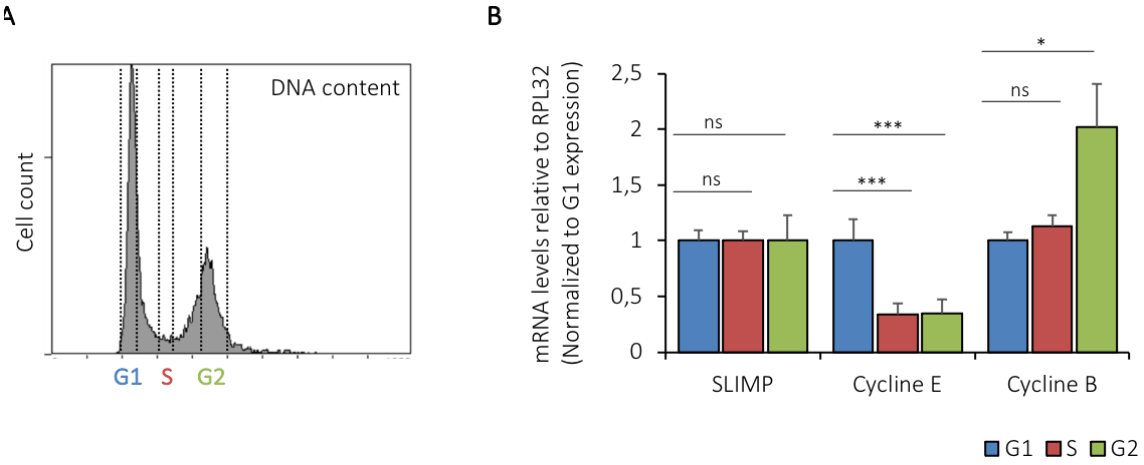

Figure 42 | SLIMP mRNA levels through the cell cycle from sorted S2 cells. (A) Schema representing a regular cell cycle profile of S2 wild type cells, indicating the sorting windows to collect cells in G_1, S and G_2 phases. (B) Representation of qPCR results for SLIMP, cyclin E and cyclin B levels in different cell cycle phases. Cyclins E was used as control of G_1 phase, were its expression peaks, and cyclin B was used as control of G_2 phase. All the values are a normalized to RLP32, used as control, and the S phase and G_2 phase values are normalized to G_1, per each gene. No significant differences in SLIMP mRNA levels are observed between the cell cycle phases. Three biological replicates were performed. Statistical analysis was done by applying unpaired t-test with GraphPad software (* p<0,05; ** p< 0,01; *** p<0,001).

As observed in Figure 42B, although we can conclude from the cyclins E and B levels that cells were sorted correctly, SLIMP expression does not change through the cell cycle.

4.2.2. SLIMP structure in cell cycle regulation

Previous experiments in the lab suggested that the overexpression of a different codon usage version of SLIMP, resistant to the RNAi (SLIMP DCU), could rescue the G_2

accumulation phenotype in SLIMP-KD cells. Interestingly, it can also be recovered by overexpressing a truncated form of SLIMP lacking the MSP (ΔN-SLIMP DCU) (Figures 22 and 43). These data suggested that the cell cycle-related role of SLIMP would be carried out from outside the organelle; however, the molecular mechanism or the interactors involved in this function remain unknown.

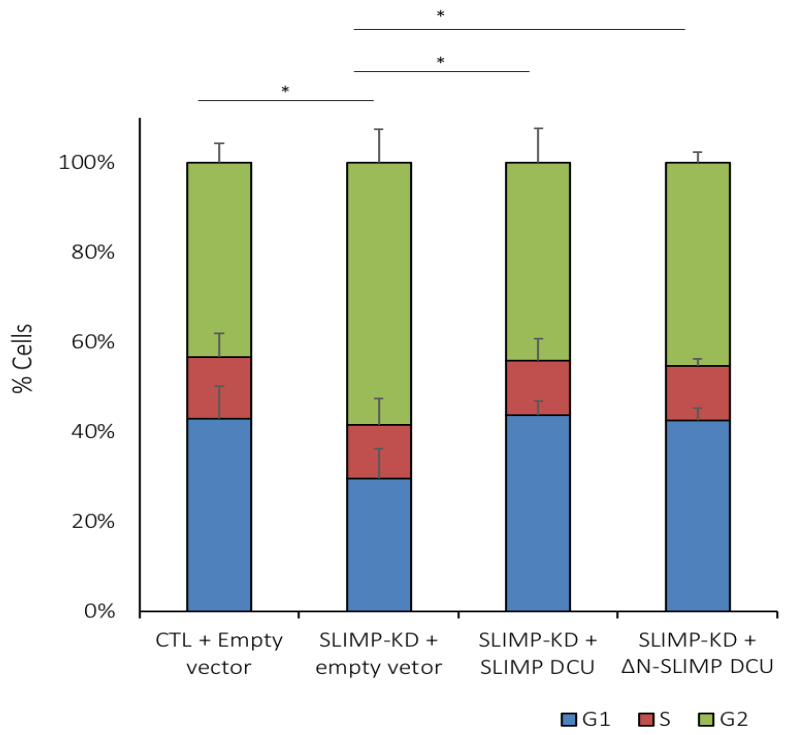

Figure 43 | SLIMP overexpression rescues G2 accumulation phenotype in SLIMP-KD cells. Graphic representing the cell cycle profile of (from left to right) control cells (CTL), SLIMP depleted cells (SLIMP-KD), SLIMP-KD cells overexpressing SLIMP full length with different codon usage (SLIMP DCU) and SLIMP DCU without MSP (ΔN-SLIMP DCU). All of them are stable cell lines induced for 8 days with 600μM $CuSO_4$. The cell cycle profile is restored by overexpressing both forms of SLIMP. CTL cells express pMK33-Hygromycin and pMT-Puromycin empty vectors. Three biological replicates were performed. $\%G_2$ was statistically analyzed by applying an unpaired t-test with GraphPad software (* p<0,5; ** p< 0,01; *** p<0,001).

As mentioned in the introduction (see section 1.5), SLIMP shows a typical aaRS structure, consisting of a large globular domain with the catalytic core (not very conserved, and inactive in SLIMP) and an N-terminal coiled-coil domain (Figure 44A). Aiming to elucidate new information about the molecular pathway underlying SLIMP function, we wondered whether a particular domain of SLIMP would be responsible for its cell cycle

related function. Thus, we tested if the overexpression of the two SLIMP domains separately would be enough to recover the G_2 accumulation phenotype in SLIMP depleted cells. A different codon usage version of the coiled-coil (CC) and globular domain (GD) were cloned with a FLAG tag on both sides of the peptide and expressed in SLIMP-KD cells (Figure 44B).

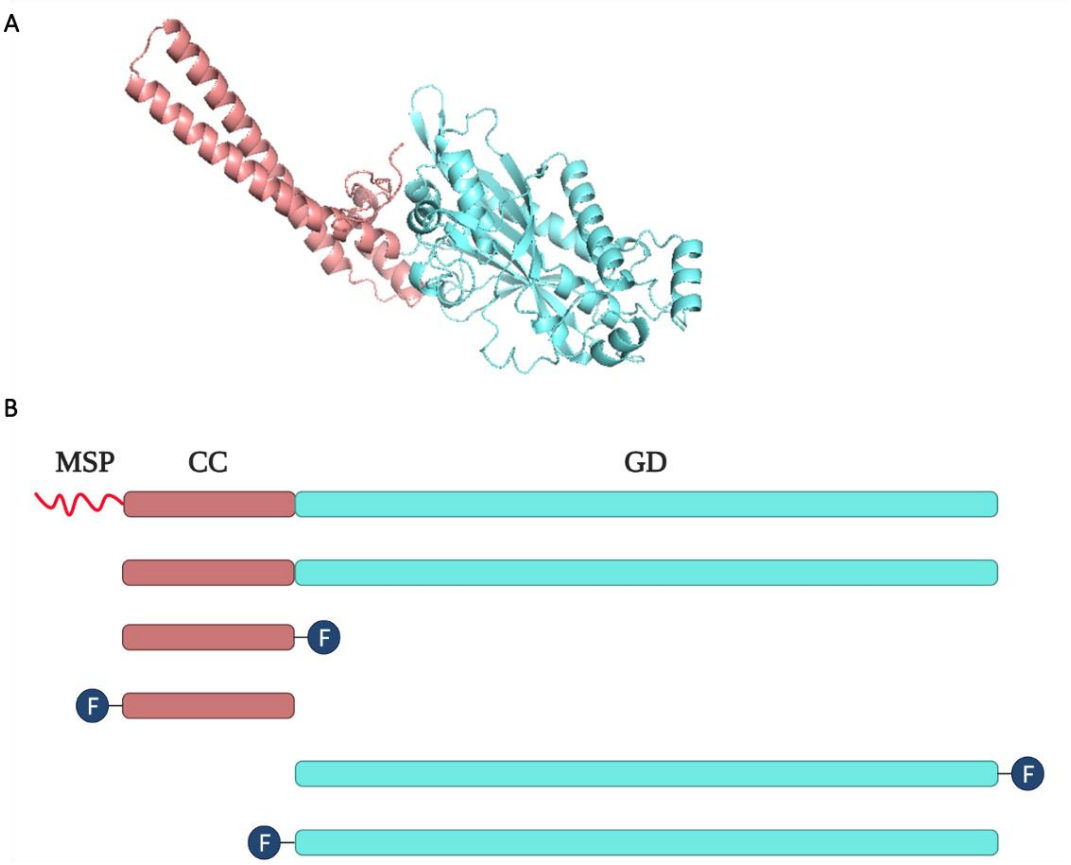

Figure 44 | SLIMP structure. Both panels show the SLIMP structure with the GD (in light blue) and the CC at the N-terminus (in purple). (A) 3D structure of the ΔN-SLIMP, generated with Adobe Pymol from a PDB file of SLIMP sequence. (B) Schema representing SLIMP structure linearly and the different constructs used in the recovery experiment shown below (Figure 46). The FLAG tag is represented in dark blue, and the MSP in red.

We cloned the different constructs indicated in Figure 44B in the pMT-Puro vector (see Table 2) and transfected SLIMP-KD stable cell line with each of them for the recovery experiment. We generated stable cell lines containing both plasmids (pMK33-Hy-SLIMP RNAi and pMT-Puro-SLIMP domain), by antibiotic selection. Cells were induced with $CuSO_4$ for eight days since both constructs hold a metalloprotein inducible promoter.

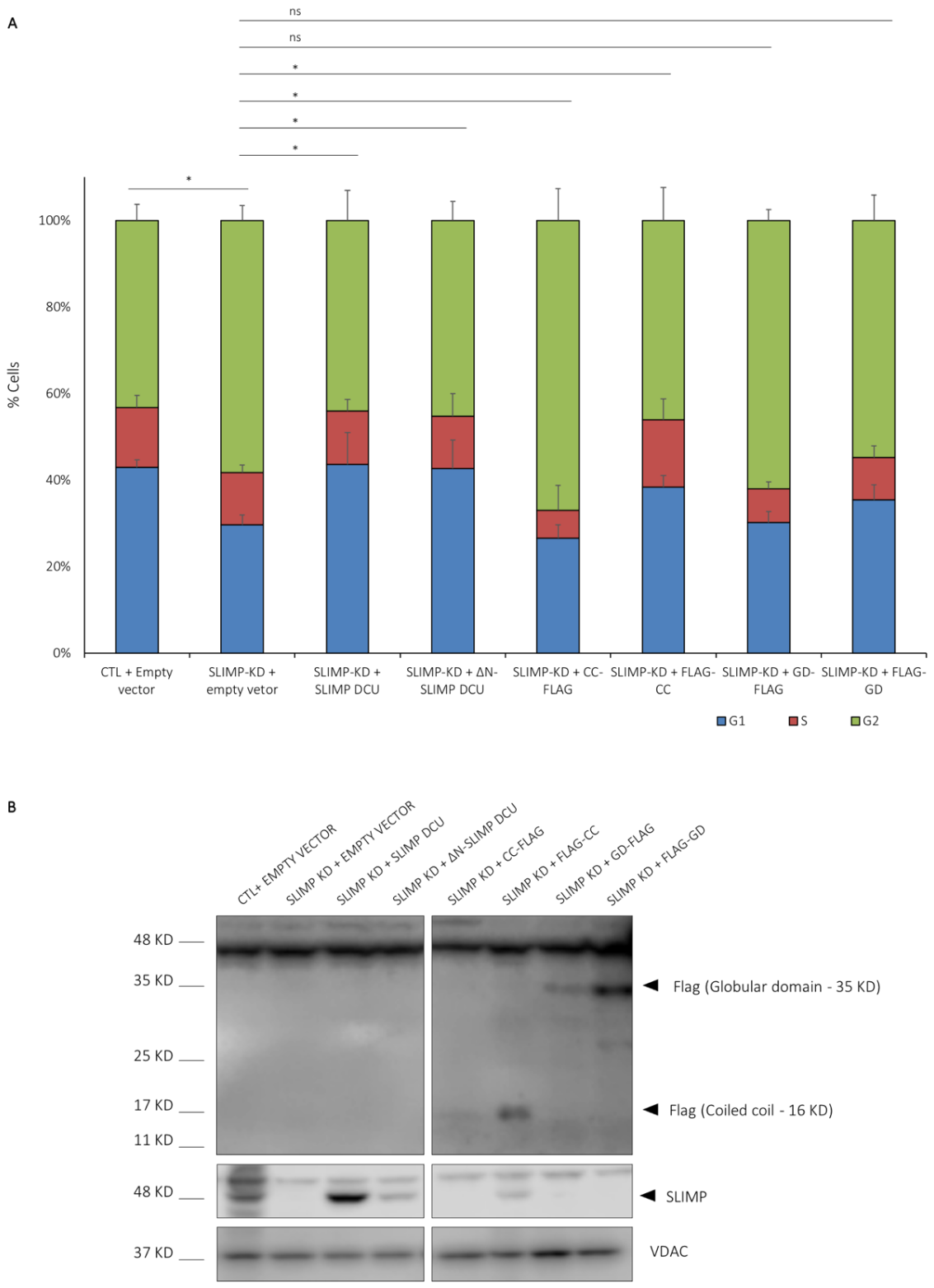

Figure 45 | SLIMP domains overexpression in SLIMP-depleted cells. (A) Cell cycle and (B) western blot analysis of SLIMP depleted cells overexpressing SLIMP DCU, ΔN-SLIMP DCU, CC-FLAG, FLAG-CC, GD-FLAG and FLAG-CD. After $CuSO_4$ (600μM) induction, cells were collected, (A) fixed, and dyed with PI for cell cycle FACS analysis, and (B) processed for protein extraction and western blot. CTL cells were expressing the pMK33-Hy and the pMT-Puro empty vectors. Four

biological replicates were performed. $\%G_2$ was statistically analyzed by applying an unpaired t-test with GraphPad software (* p<0,05; ** p< 0,01; *** p<0,001).

There results show that both SLIMP domains are expressed correctly in SLIMP-depleted cells, although the expression is higher with the N-terminal FLAG tag in both cases (Figure 45B). Moreover, SLIMP full length seems to be more efficiently expressed than SLIMP lacking the MSP, probably due to a lower stability of the truncated protein. Interestingly, only the FLAG-CC expression rescues the G_2 accumulation phenotype (Figure 45A). Conversely, either GD-FLAG, FLAG-GD or CC-FLAG are not able to rescue the SLIMP-depleted cells G_2 accumulation phenotype. Of note, a very thin band corresponding to SLIMP full-length molecular weight is observed when overexpressing the FLAG-CC. This result suggests that the coiled-coil domain could somehow stabilize the SLIMP mRNA or protein, preventing them from degradation. This issue will be discussed deeper in the discussion (see section 5.2).

4.2.3. SLIMP role in the G_1 - S transition

As mentioned in the introduction, a couple of papers in the literature linked SLIMP with the cell cycle. Importantly, it was proposed that SLIMP could play an antagonistic role to E2F1 through a complementary molecular pathway during the G_1-S transition (Ambrus et al., 2009).

E2F is a transcription factor family involved in the transcriptional regulation of genes that promote the transition from G_1 to S-phase (Figure 46A). While several E2F genes are found in mammals, only two components have been described in *Drosophila* so far: E2F1, which activates transcription and E2F2, playing the repressive role.

It is well known that mutations in the E2F1 gene result in a G_1 arrest in flies (Figure 46B). The main goal of Ambrus and colleagues was to find suppressor genes of the E2F1 pathway, so they elaborate a mosaic genetic screening based on random mutations in E2F1 mutant flies. Interestingly, one of the mutated genes found which could partially

rescue the E2F1-dependent G_1 arrest, was SLIMP. They observed that, when SLIMP is mutated in an E2F1-lacking cell context, cells could progress from G_1 to S phase, suggesting that SLIMP depletion somehow overcomes the E2F1 mutation effect (Figure 46C) (Ambrus et al., 2009).

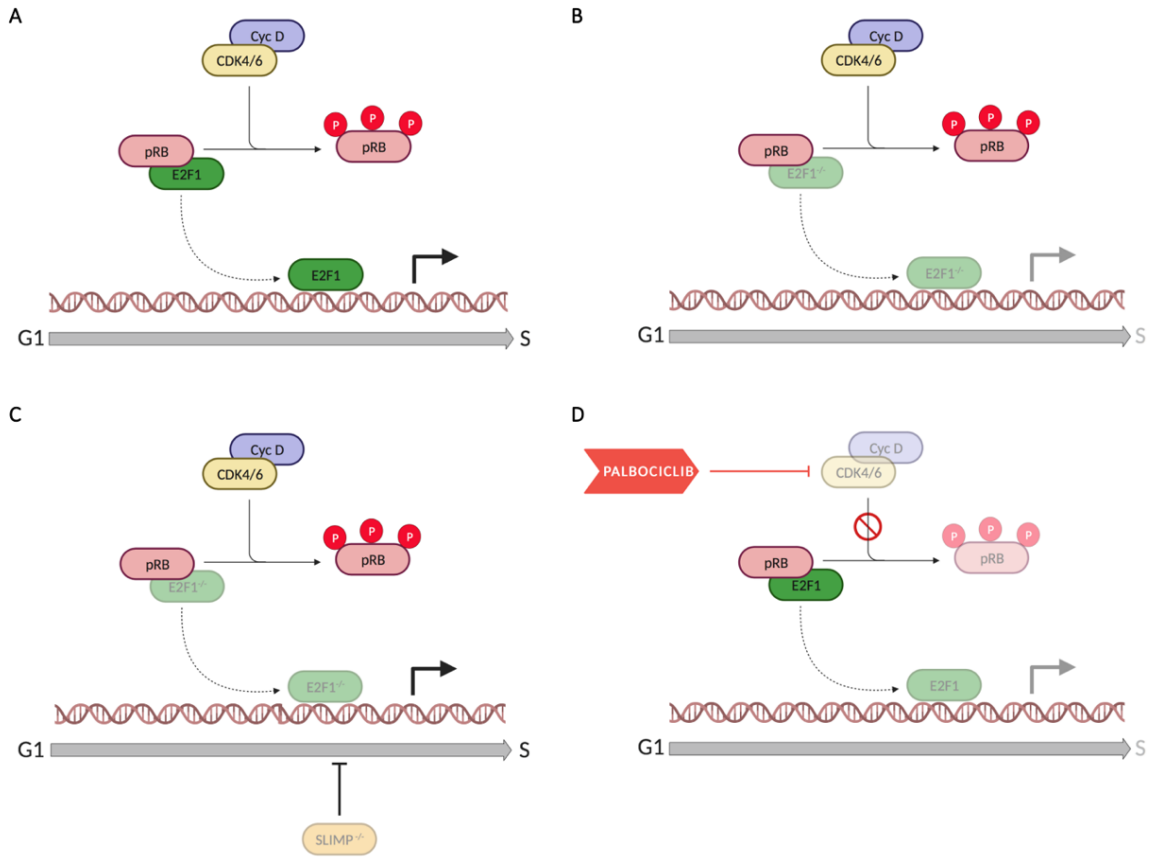

Figure 46 | E2F1 pathway. (A) In physiological conditions, E2F1 activate the transcription cascade that will promote the transition from G_1 to S phase once the CKD4-CycD complex has phosphorylated pRB. (B) When E2F1 is mutated, cells get arrested in G_1 since the transcription cascade that allows the S-phase onset is inactive. (C) When SLIMP is mutated together with E2F1, cells previously arrested in G_1 can somehow overcome the problem and enter S-phase. (D) Palbociclib inhibits CDK4 kinase, upstream of pRB which is not phosphorylated, and consequently E2F1 is not released, so as a result, cells get arrested in G_1.

The authors performed this study using as experimental model the *D. melanogaster* eye imaginal disk Second Mitotic Wave (SMW), and the G_1 - S transition was measured by BrdU incorporation. However, the global cell cycle profile of the E2F1 + SLIMP double

mutant was not analyzed. Hence, we designed an experiment to check the effect of inhibiting the E2F1 activity in the presence and absence of SLIMP in S2 cells.

To mimic the effect of E2F1 mutant in our cells, we used Palbociclib, a commercial antitumoral drug that inhibits CDK4/6 kinases. Therefore, under Palbociclib treatment, CDK4 will not phosphorylate retinoblastoma protein (RBF1 in *Drosophila*), consequently, E2F1 will not be released, and the transcription cascade that promotes the S-phase onset will not be activated. As a result, cells should get arrested in G_1 (Figure 46D).

First, since Palbociclib was never used in *D. melanogaster* before, we started setting up the conditions for S2 cells, performing a testing assay with different Palbociclib concentrations and incubation times (Figure 47). We concluded that the most outstanding G_1 arrest was achieved under 10μM Palbociclib treatment for 24 hours. Therefore, we used these experimental conditions to perform the following assays.

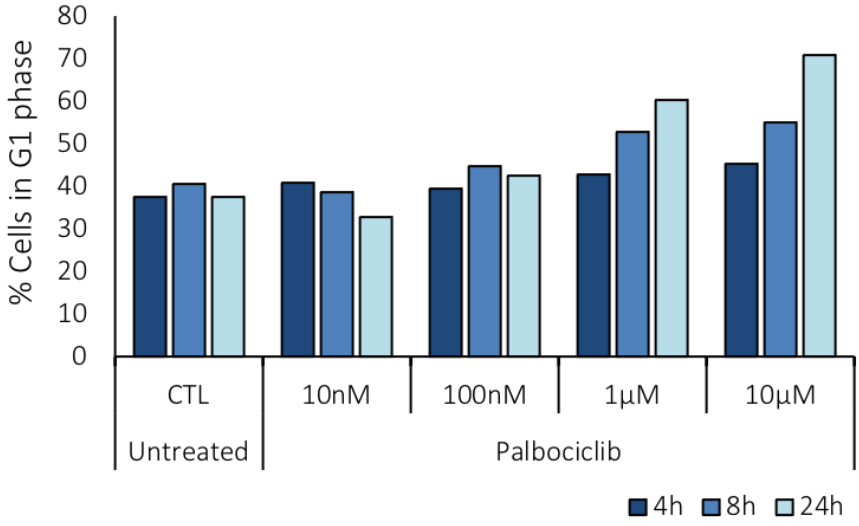

Figure 47 | Palbociclib treatment test. Graphical representation of the percentage of cells in G_1 at different experimental conditions. S2 wild type cells were treated with increasing Palbociclib concentrations (10μM, 100μM, 1mM and 10mM) during 4, 8 and 24 hours. Cells were fixed, dyed with propidium iodide and analyzed by FACS. Non-treated S2 cells were used as control (CTL).

Afterwards, a combination of Palbociclib treatment and SLIMP depletion induction allowed us to explore the putative interaction between both proteins, E2F1 and SLIMP, during the G_1 - S transition. In that sense, what we were expecting to happen was that cell with lower SLIMP levels (SLIMP-KD) would be less accumulated in G_1 upon Palbociclib treatment than control cells.

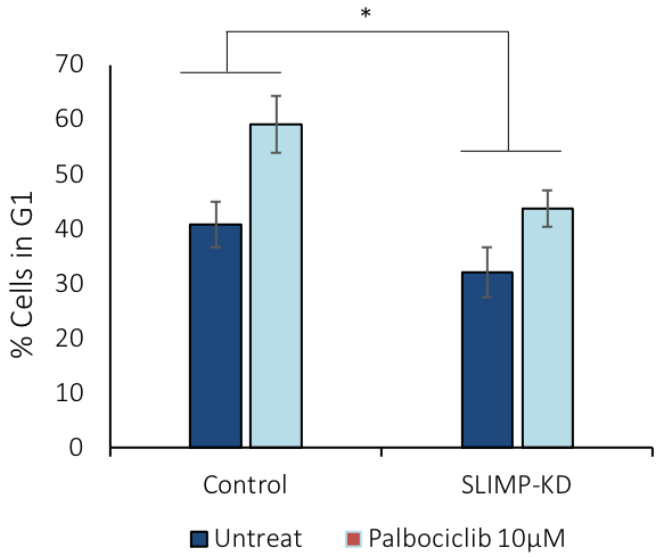

Figure 48 | SLIMP-KD and CTL cells upon Palbociclib treatment. Graphic representing the percentage of cells in G_1 of CTL and SLIMP-KD cells upon Palbociclib treatment. Cells were induced for eight days with 600µM $CuSO_4$ and treated with Palbociclib (10µM for 24h). Finally, cells were collected and analyzed by FACS. The increase of cells arrested in G_1 upon Palbociclib treatment is significantly higher in CTL cells than in SLIMP-depleted cells. CTL cells expressed pMK33-Hy empty vector. Four biological replicates were performed for this assay. The statistical analysis comparing the increase in the Palbociclib-derived G_1 accumulation between the two cell lines was performed through a linear regression model build with the R-Studio software. (* p<0,5; ** p< 0,01; *** p<0,001).

The increase of cells arrested in G_1 due to the Palbociclib treatment in SLIMP-depleted cells is significantly lower than in control cells (Figure 48). Hence, this result is in concordance with published data (Ambrus et al., 2009), and it confirms that, at least in our experimental model, SLIMP depletion impairs the Palbociclib treatment effect. Consequently, it strongly suggests that SLIMP is somehow blocking the transition from G_1 to S phase in the cell cycle progression in a complementary pathway to E2F1.

In this direction, cellular synchronization coupled with FACS analysis allowed us to analyse specifically the G_1 to S transition stage, in SLIMP-depleted cells. Both cell lines (SLIMP-KD and CTL) were induced (600μM CuSO4 for eight days) and synchronized with hydroxyurea (1.5mM for 24 hours). Finally, cells collected at different time points and analyzed by FACS.

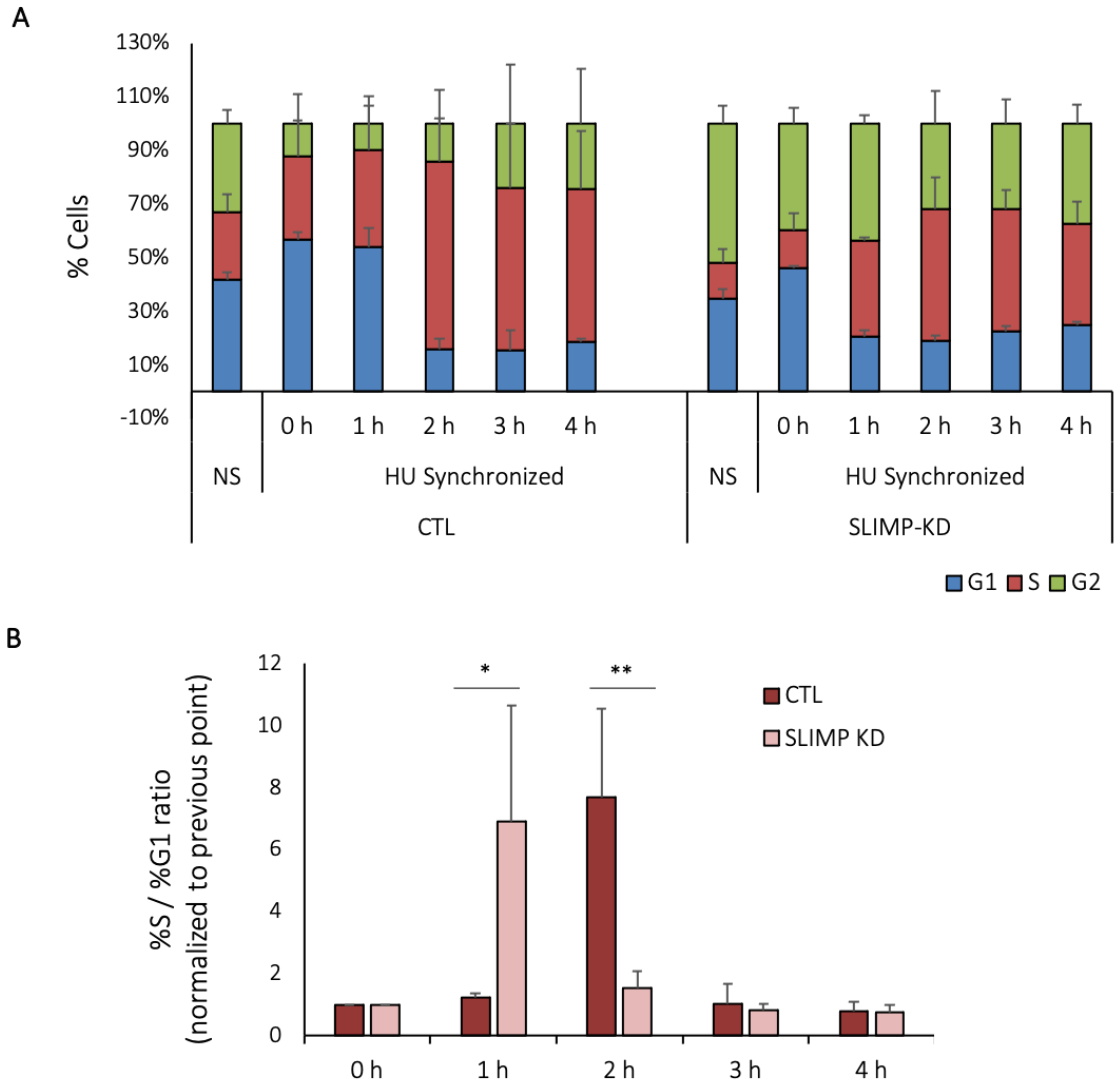

Figure 49 | Cellular synchronization in SLIMP-KD and CTL cells. (A) Cell cycle profile of CTL and SLIMP-KD cells at different time points. Non-synchronized (NS) cells were used as control. (B) Graphic representing the ratio of cells that moved from G_1 to S phase at each time point regarding to the previous one. Three biological replicates were performed from this assay. Statistical analysis was done by applying two-way ANOVA with GraphPad software (* p<0,05; ** p< 0,01; *** p<0,001).

As observed in Figure 49A, the G_1 - S transition in SLIMP-depleted cells occurs around one hour before than in control cells. Intriguingly, the synchronization is less efficient in SLIMP-KD cells than in CTL cells since the depletion of SLIMP always carries an intrinsic G_2 accumulation phenotype. To focus on the S-phase onset and visualize the differences between both cell lines better, we calculated the ratio of cells moving from G_1 to S phase at each point compared to the previous one. It allowed us to conclude that while in CTL cells, the G_1-S transition occurs mainly after 2 hours of treatment, SLIMP-KD cells have already entered in S-phase at 1 hour after the HU treatment (Figure 49B).

4.2.4. SLIMP depletion impacts on G_2 - M transition

As mentioned in the introduction (see section 1.4), the cell cycle is one of the most crucial and tightly regulated processes in the cell. Several mechanisms and pathways cooperate to ensure the genetic and physical integrity of the cellular progeny. For this reason, three checkpoints during the cell cycle avoid an aberrant progression: the restriction point (also called G_1/S checkpoint), G_2/M checkpoint and intrinsic M-checkpoint.

The Cyclin-Dependent Kinase 1 (CDK1), the *D. melanogaster* CDC-2 homolog, plays a vital role in orchestrating the G_2/M checkpoint. Together with its partner Cyclin B forms the Mitotic Promoting Factor (MPF), which triggers the mitotic entry when the cell is ready to divide. The complex remains inactive until the Cyclin-dependent Activating Kinase (CAK) activates it by phosphorylation. Simultaneously, the kinase WEE1 adds a repressive phosphate at the position tyrosine 15 (Tyr15), inactivating the MPF again. When the cell has fulfilled the requirements in terms of synthesis and energy, for entering in M-phase, the phosphatase CDC25 (STG in *Drosophila*) removes the Tyr15-phosphate, the CDK1/CycB complex becomes active, and cells undergo mitosis (Figure 50).

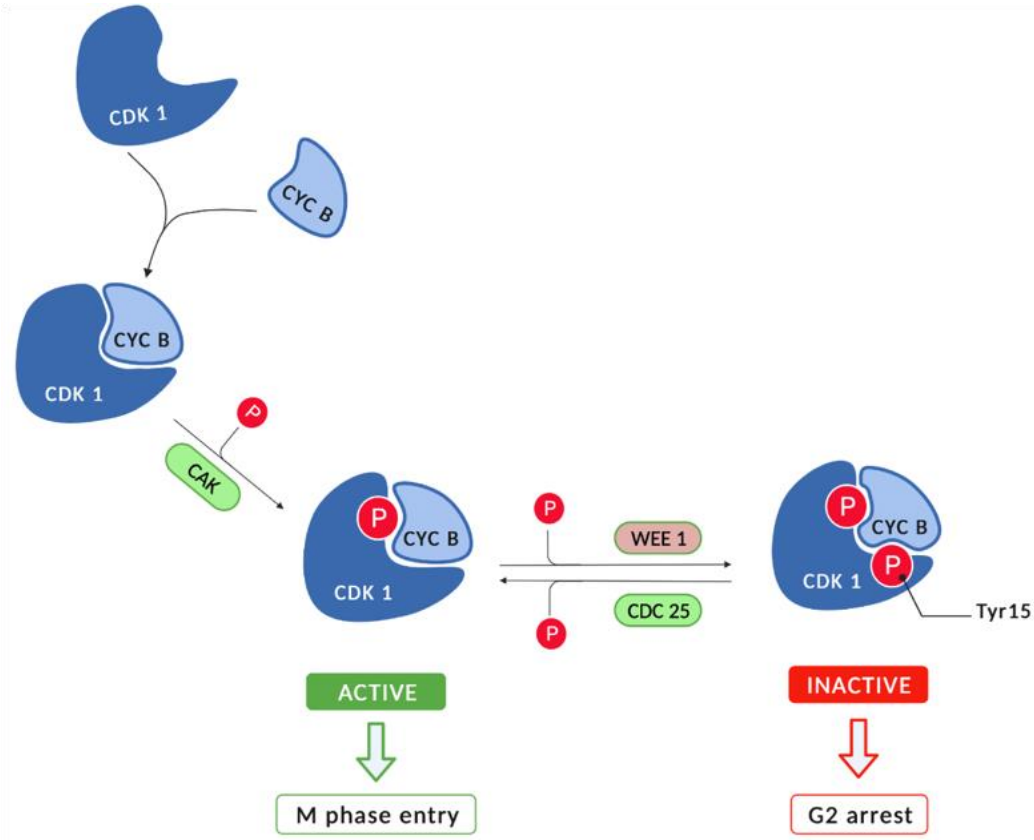

Figure 50 | CDK1 in the G_2 – M transition. CDK1 remains double phosphorylated and inactive until the phosphatase CDC25 takes out the Tyr-15 phosphate. When it occurs, CDK1 becomes active and, along with Cyclin B, promotes entering mitosis.

Interestingly, a microarray analysis previously performed in our group suggested an up-regulation of the WEE1 mRNA levels in SLIMP-depleted cells compared to the control cells. Besides, it was previously reported (Liang et al., 2014) and further demonstrated in this work and previous studies from our group that the SLIMP-KD cells show a G_2 delay phenotype. Altogether it suggests an up-regulation of the G_2/M checkpoint in SLIMP-depleted cells. Considering CDK1-Tyr15-P as a marker of the G_2/M checkpoint, we approached this question by measuring the levels of CDK1 phosphorylated at tyrosine 15 in both SLIMP-KD and CTL cell lines.

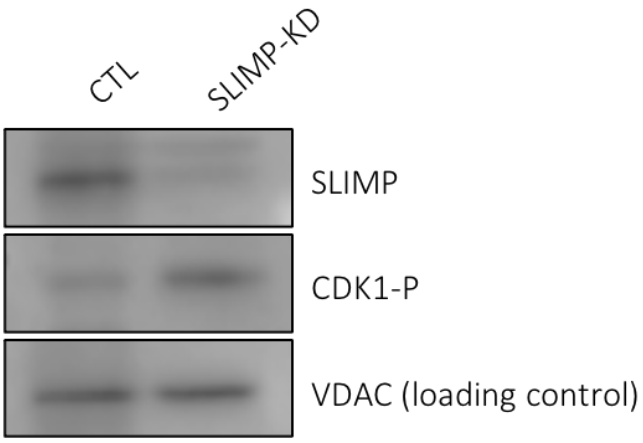

Figure 51 | CKD1-Tyr15-P levels in SLIMP-KD and CTL cells. Western blot analysis of protein extracts from SLIMP-KD and CTL cells. Cells were induced for eight days with 600μM $CuSO_4$ and lysate with a modified RIPA buffer for phosphorylated proteins (see section 3.6). CDK1-Tyr15-P was detected with a commercial antibody and SLIMP was detected with a homemade polyclonal antibody, and VDAC was used as the loading control. CDK1-Tyr15-P levels are increased in SLIMP-depleted cells. The CTL cells express the pMK33-Hy empty vector.

As we expected, SLIMP depleted cells showed higher levels of CDK1 phosphorylated at tyrosine 15 than control cells (Figure 51). This result confirms that the G_2 accumulation phenotype observed in SLIMP-KD cells is driven presumably by some problems during DNA replication caused by the SLIMP depletion, which eventually results in a G_2 delay and prevents the mitotic entry.

4.2.5. SLIMP subcellular distribution through the cell cycle

Interestingly, it has been reported that some proteins change their subcellular location under certain conditions, allowing them to perform different functions within the cell (Didiasova et al. 2019; Manning et al. 2018). Hence, after exploring the SLIMP implication in regulating the cell cycle progression and the impact on the different cell cycle phases, we wondered whether SLIMP could be changing its subcellular distribution throughout the cell cycle. To approach it, we performed cell fractionation assays of cellular populations specifically enriched in each cell cycle phase. Firstly, we sorted *in*

vivo S2 cells and collected them in G_0/G_1 (G_1) and G_2/M (G_2) phases and followed by performing cellular fractionation assays for nuclear enrichment (see section 3.7.1) of both cellular populations. Figure 52 shows two different replicates of this assay. In Figure 52A, a tiny band corresponding to SLIMP molecular weight is observed in the nuclear-enriched fraction of the G_1 phase. Unfortunately, this result was not consistent with the other biological replicates performed (Figure 52B), where SLIMP appears exclusively in the cytosolic + organelle fraction, presumably at the mitochondrial compartment, in both cell cycle phases.

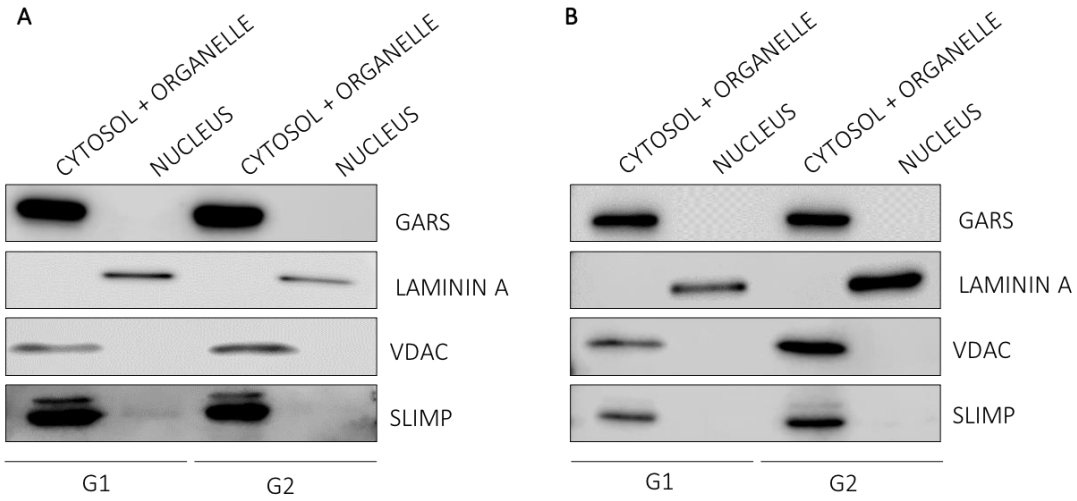

Figure 52 | Cellular fractionation of S2 cells in G_1 and G_2 phases. Western blot analysis of cellular fractionation assay. S2 wild type cells were sorted and collected in G_1 and G_2 phases. Each cell population was separated into the nucleus-enriched fraction (Nucleus) and the rest of the cell (Cytosol + organelle). (A) and (B) correspond to two different biological replicates of the same assay. SLIMP was detected mainly in the "cytosol + organelle" fraction, but also in the G_1 nucleus-enriched fraction, only in replicate A. GARS (Cytosolic marker), Lamin A (Nuclear marker) and VDAC (Mitochondrial markers) were used as controls of the cellular fractionation. These western blots are representatives of the four biological replicates performed for this assay.

Although results in Figure 52 open the possibility of a small population of SLIMP playing a role in the nucleus, specifically during G_1, the reproducibility was not ideal, so we could not extract a clear conclusion from them.

Furthermore, we analysed the subcellular distribution of SLIMP, particularly in S-phase. Since it is not that easy to obtain enough sorted cells in S-phase for cellular fractionation assays, we enriched a population of cells in S-phase by cellular synchronization. An asynchronous pull of cells was also fractionated in parallel as control. In this experiment, we performed the two cell fractionation protocols explained in sections 3.7.1 and 3.7.2 (Figure 53).

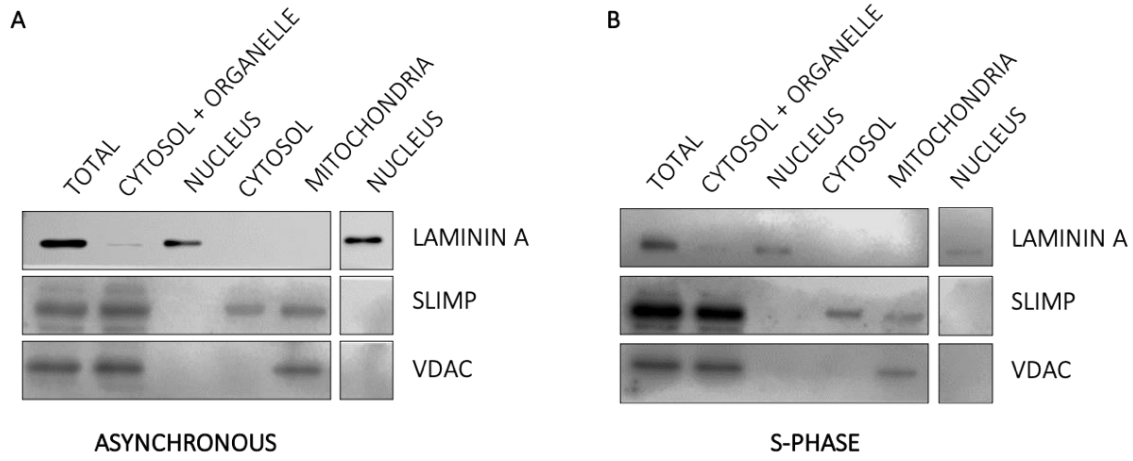

Figure 53 | Cell fractionation of S2 cells in S-phase. Western blot analysis of cellular fractionation assay of (A) asynchronous S2 cell population, and (B) S2 cells synchronized in S-phase (around 70%). For each cell population, two different cell fractionation protocols were performed. The first one separates the nucleus-enriched fraction (Nucleus) from the rest of the cell (Cytosol + organelle), while the second separates all cellular compartments (Cytosol, Mitochondria, and Nucleus). SLIMP appeared in both cases in the cytosolic and mitochondrial-enriched fractions. GARS (Cytosolic marker), Lamin A (Nuclear marker) and VDAC (Mitochondrial markers) were used as controls of cell fractionation. The first lane of both gels corresponds to a whole-cell lysate used as a control for protein detection.

Figure 53 shows the subcellular distribution of SLIMP in S-phase (Fig 53B) compared to non-synchronized cells (Figure 53A). The results present a similar SLIMP expression pattern; however, remarkably, the amount of SLIMP in the mitochondrial compartment in asynchronous cells is higher than the cytosolic SLIMP, while in cells synchronized in S-phase, it looks the other way around. The difference is subtill but still appreciable.

Altogether these results, confirmed the existence of an extra-mitochondrial population of SLIMP present at least in the cytosol, which apparently is lightly increased in S-phase However, unfortunately, we could not determine whether the population of nuclear SLIMP, already suggested in Figures 31 and 32, was specific for the G_1 phase or appeared under specific cellular conditions.

This chapter determined that SLIMP mRNA levels do not change through the cell cycle. Moreover, we observed that the overexpression of the coiled-coil domain of SLIMP is sufficient for the G_2 arrest recovery in SLIMP-KD cells. On the other hand, it has been proposed that SLIMP plays an antagonistic role to E2F1, blocking the G_1-S transition in physiological conditions. In the same direction, we observed that upon SLIMP depletion, cells enter earlier in S-phase. Additionally, we demonstrated that the CDK1-Tyr15-P levels get increased upon SLIMP depletion. Finally, although the changes in the distribution of SLIMP throughout the cell cycle are not fully understood, the results suggested an increase in the cytosolic SLIMP during S-phase. More experiments need to be done in this direction to clarify the subcellular distribution of the extra-mitochondrial SLIMP during the cell cycle.

WORKING MODEL

Based on the results shown in sections 4.1 and 4.2, together with previous studies from our group and published data, we elaborated our hypothesis: SLIMP would be involved in preventing the G_1-S transition in a complementary pathway than E2F1. Upon SLIMP depletion, this blockage would be impaired, and consequently, cells would enter earlier in S-phase, generating DNA synthesis problems that would need to be solved before cell division. Therefore, the cells would activate the G_2/M checkpoint in response to replicative stress and potential DNA damage, by phosphorylating CDK1, a scenario that would result in a G_2 temporal arrest. Moreover, SLIMP would be carrying out this role from outside the mitochondria, where it plays a crucial role by simultaneously regulating mtDNA copy number and mitochondrial protein synthesis. The working model is represented in Figure 54.

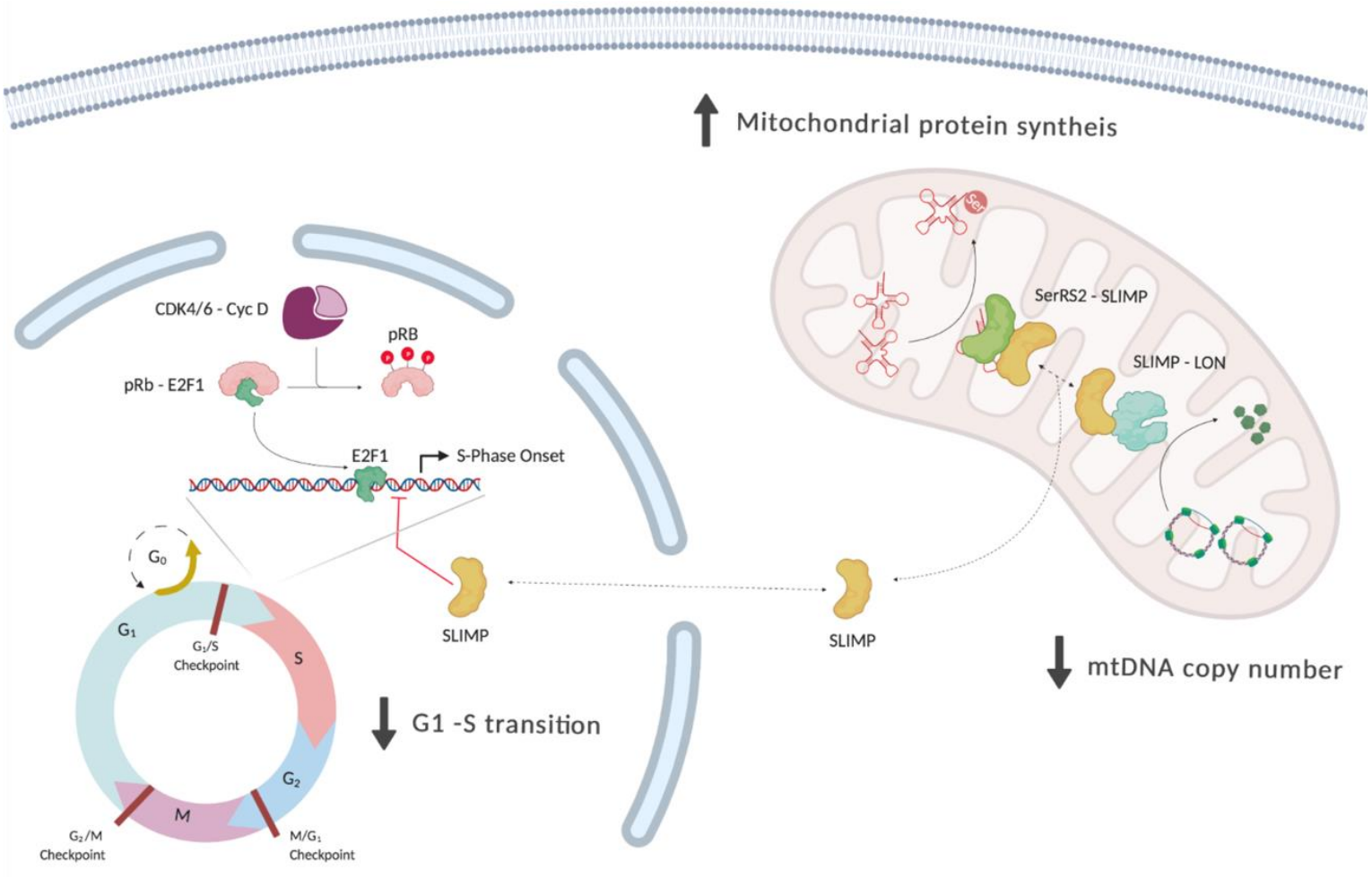

Figure 54 | Working model. Schematic representation summarizing the SLIMP cell cycle function based on the results shown in Chapters 1 and 2 together with already reported data.

4.3. CHAPTER III: SLIMP IN BUDDING YEAST

In collaboration with David Canadell

SLIMP was described as a previously uncharacterized paralog of the mitochondrial seryl-tRNA synthetase (SerRS2) (Guitart, et al., 2010). As mentioned in the introduction, SLIMP appeared from gene duplication in the base of metazoan, and it is present in arthropods, molluscs, echinoderms, and some hemichordates species (Figure 16). Nevertheless, no structural homolog of SLIMP has been found in vertebrates so far. Although SLIMP is not evolutionary conserved, we guess that its molecular function, involved in both mitochondrial homeostasis and cell cycle regulation, could have been acquired by other proteins and still be conserved through evolution.

During an initial characterization of SLIMP, a heterologous expression of SLIMP in human cells was performed In our group. Intriguingly, the cell cycle was not affected by the presence of SLIMP, but the mitochondrial morphology looked completely aberrant. Aiming to understand those phenotypes better and clarify some aspects of the SLIMP molecular function we decided to move to a more simply organism, the budding yeast (Antolin-Fontes, 2019; Picchioni, 2014).

Saccharomyces cerevisiae, also known as budding yeast, has been extendedly used as a model organism to study eukaryotic cell biology and functional genomics (Botstein & Fink, 2011). Budding yeast is considered an efficient system easy to work with from the technical point of view which is well characterized at the molecular and genomic level. For this reason, it soon became the ideal scenario for the study of numerous cellular processes, including cell division (Bähler, 2005; Wittenberg & La Valle, 2003), and mitochondrial homeostasis (Barros et al., 2010). Nonetheless, as expected, SLIMP is not present in *S. cerevisiae* since it appeared later in evolution. In fact, budding yeast has only two genes encoding for seryl-tRNA synthetases: SES1 (cytosolic) and DIA4 (mitochondrial) (Palecek et al., 2000; Weygand-Durasevic et al., 1987).

Considering that and aiming to elucidate some aspects of the putative interactors or molecular pathways related to the SLIMP function, we decided to express SLIMP in *S. cerevisiae* and analyze the impact on cell cycle progression and mitochondrial homeostasis in this organism.

First, we checked for the expression and toxicity of SLIMP in *S. cerevisiae*. SLIMP and ΔN-SLIMP were cloned into a yeast expression vector (pYES2) containing GAL4 inducible promoter and *URA3* (uracil encoding gene) as a selection marker. Constructs were transformed into the W303-1A ADGEV BAR*1*Δ strain in media lacking uracil (URA media). As previously mentioned, this strain has the GEV system incorporated so the GAL4 promoter can be induced with β-estradiol (see section 3.1.2). Cells were grown in URA media, induced with 100nM β-estradiol and collected at different time points (Figure 55).

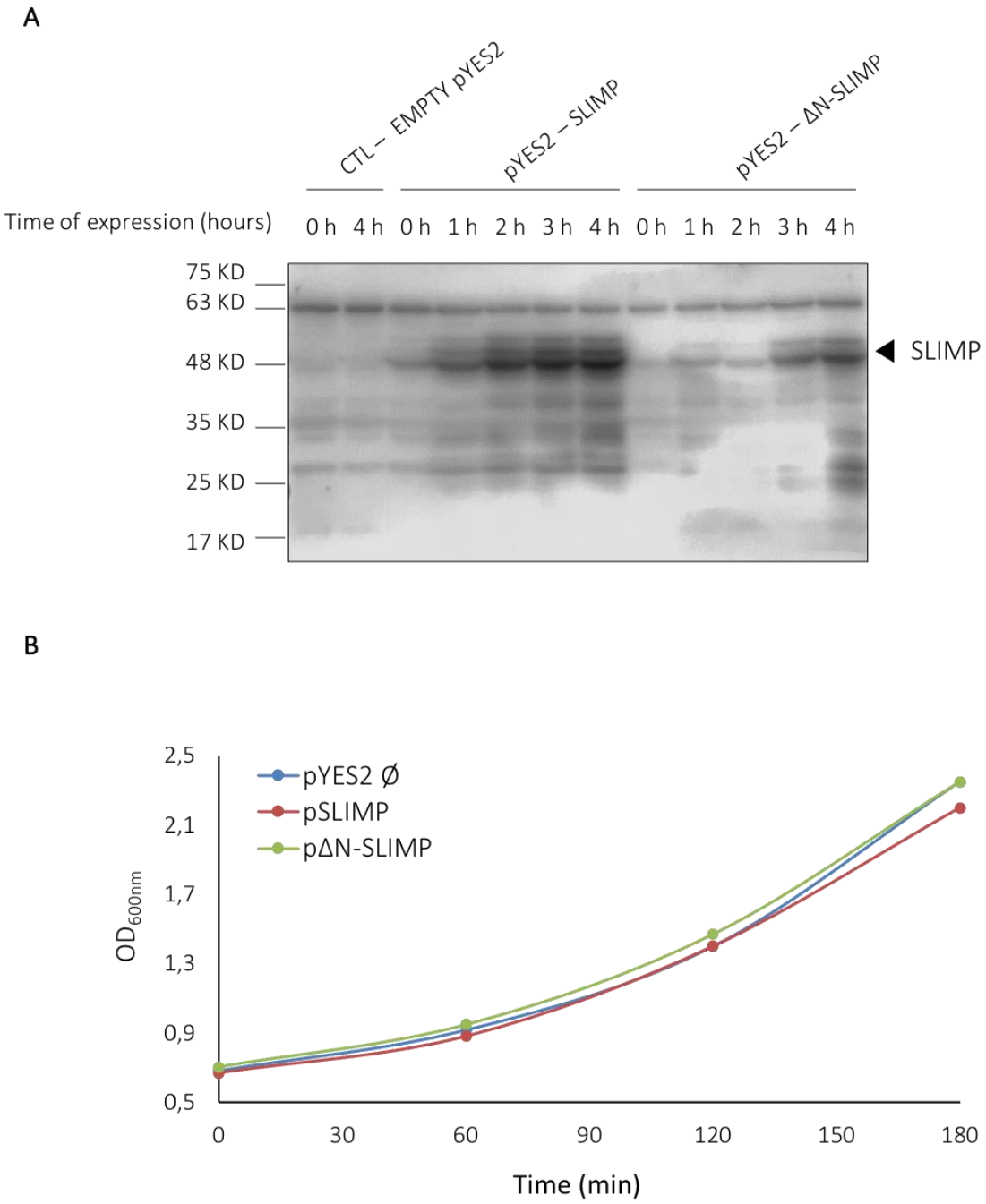

Figure 55 | Overexpression of SLIMP and ΔN-SLIMP in budding yeast. (A) Western blot analysis of protein extracts from budding yeast cells overexpressing SLIMP and ΔN-SLIMP after β-estradiol induction for one, two, three or four hours. SLIMP was detected using a homemade polyclonal primary antibody. (B) Growth curve of S. cerevisiae cells overexpressing SLIMP and ΔN-SLIMP after β-estradiol induction at the same time points. Cells overexpressing the pYES2 empty vector were used as the negative control. The growth curves were obtained by measuring the OD of the samples at 600nm wavelength.

An immunoblot assay allowed us to confirm that both forms of SLIMP can be expressed in budding yeast, although it can be observed a higher and faster expression of the full-length SLIMP than the ΔN-SLIMP, probably due to the lower stability of the truncated protein (Figure 55A). Moreover, we elaborate a growth curve with the same samples, and Figure 28B shows that there is no toxic effect or growth impairment upon SLIMP or ΔN-SLIMP heterologous expression in yeast cells, at least after three hours of expression (Figure 55B).

However, we wondered whether the long-term overexpression of SLIMP could impact on the yeast growth rate. To check that, we elaborated a growth curve of yeast cells overexpressing both forms of SLIMP for 24 hours. We performed this experiment under three induction conditions: non-induced cells, cells induced with β-estradiol and cells induced with galactose, the GAL4 promoter cognate inductor.

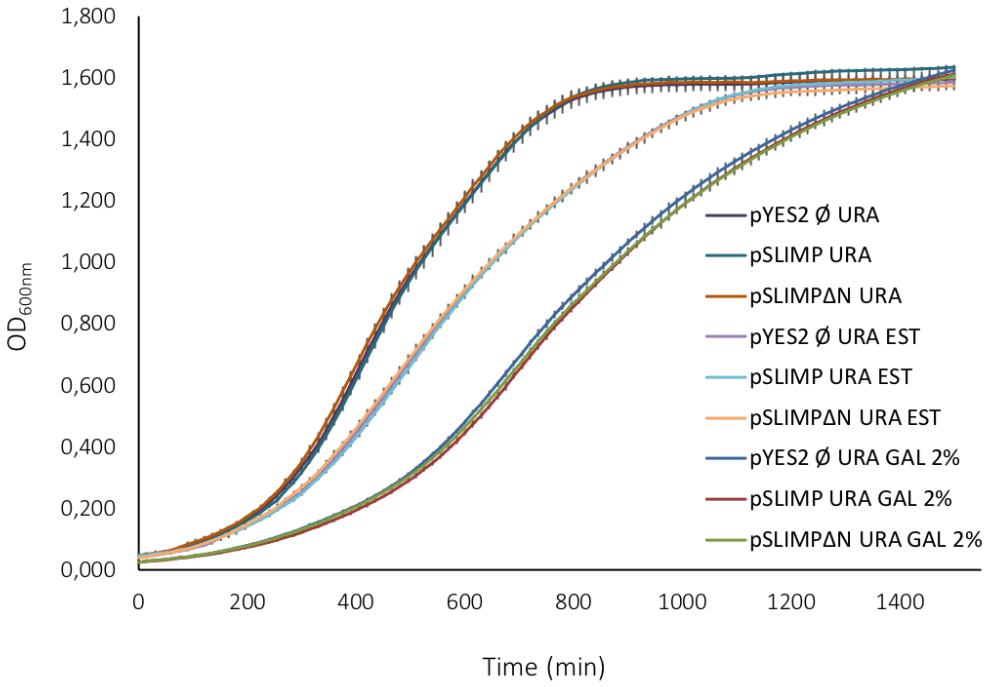

Figure 56 | Long-term expression of SLIMP and ΔN-SLIMP in *S. cerevisiae*. Graphical representation of growth curves of W303-1A ADGEV BAR1D expressing SLIMP, ΔN-SLIMP and empty pYES2 vector (negative control) for 24 hours. Cells were grown in URA media, URA plus 100nM β-estradiol and URA (without glucose) plus 2% galactose. The growth curves were obtained by measuring the OD of the samples at 600nm wavelength. The variations observed are due to the growing media and equivalent for the three strains. This experiment was performed in triplicates.

As shown in Figure 56, cells overexpressing SLIMP or ΔN-SLIMP for a more extended period do not show a growth impairment compared to control cells (empty pYES2). Moreover, it reveals that cells grow faster induced with β-estradiol than with galactose, confirming that cellular growth is more efficient with glucose as main carbon source. . Non-induced cells show the fastest growth rate, and the three strains grow exactly equal for each culture condition (Figure 56).

After verifying the model system, we checked how the presence of SLIMP may impact on the cell cycle progression and mitochondrial homeostasis in this organism.

4.3.1. SLIMP and the cell cycle in budding yeast

As previously mentioned, the SLIMP homolog in yeast has not been reported so far. However, we wondered whether its presence could somehow alter the yeast cell cycle progression since SLIMP has an essential function related to cell cycle regulation in *D. melanogaster*. Our working model suggests that the SLIMP cell cycle role is carried out from outside the mitochondria (Figure 54). Thus, we analyzed the cell cycle pattern upon expressing both the SLIMP full-length and the truncated form of SLIMP lacking the MSP (ΔN-SLIMP) (Figure 57).

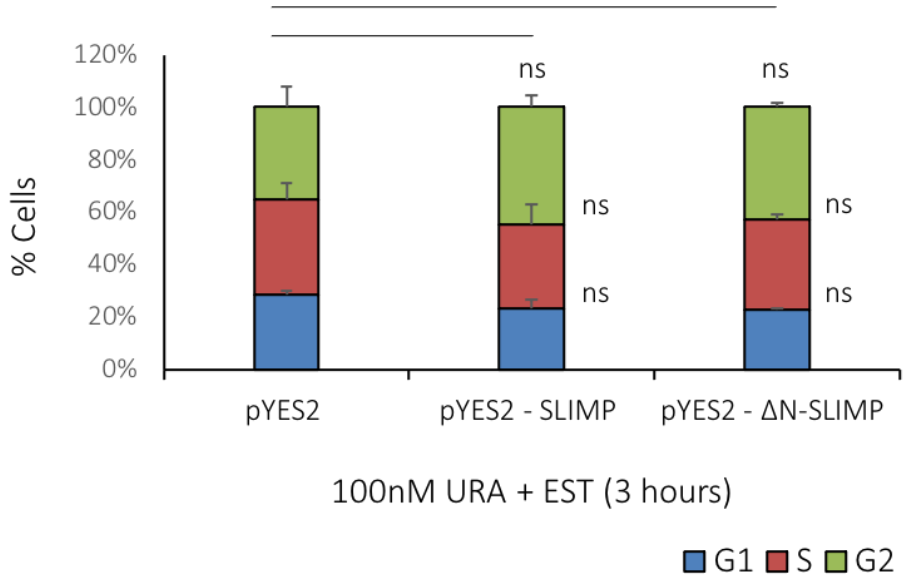

Figure 57 | Cell cycle profile of B. yeast overexpressing SLIMP and ΔN-SLIMP. Graphical representation of the cell cycle profile of yeast cells overexpressing SLIMP, ΔN-SLIMP and pYES2 empty vector. Cells were grown in URA media and induced for three hours with 100nM β-estradiol. Afterwards, cells were collected, fixed, dyed with propidium iodide, and finally analyzed by FACS. Cells show an identical cell cycle pattern with no significant differences in the absence and presence of SLIMP. Three biological replicates were performed. Statistical analysis was done by applying unpaired t-test with GraphPad software (* p<0,05; ** p< 0,01; *** p<0,001).

Based on Figure 57, SLIMP overexpression inside or outside the mitochondria does not seem to alter the cell cycle progression of *S. cerevisiae*. Nevertheless, to further explore this possibility and especially analyze the G_1-S transition, where SLIMP may play a role in *Drosophila*, we synchronized the cells in G_1, and followed them throughout the cell cycle.

For the cellular synchronization experiment, it is essential to understand the *S. cerevisiae* life cycle. Cells can live as haploid or diploid organisms, and in turn, haploid cells can have two mate types, allele "a" or "α" (alpha). Usually, haploid cells keep cycling and dividing through mitosis, but two haploid cells from opposite alleles can eventually mate generating a diploid organism. For mating, α-cells segregate a pheromone called α-factor that is recognized by a-cells and vice versa, a-cells secrete a-factor recognized by α-cells. As soon as this phenomenon occurs, cells remain arrested in the G_1 phase until

they find each other and mate. At this point, the cell cycle is resumed, and the new diploid cell enters in S-phase. Diploid cells can then keep cycling and dividing by mitosis or enter to a sporulation state and undergo meiosis, resulting in four new haploid spores (Figure 58).

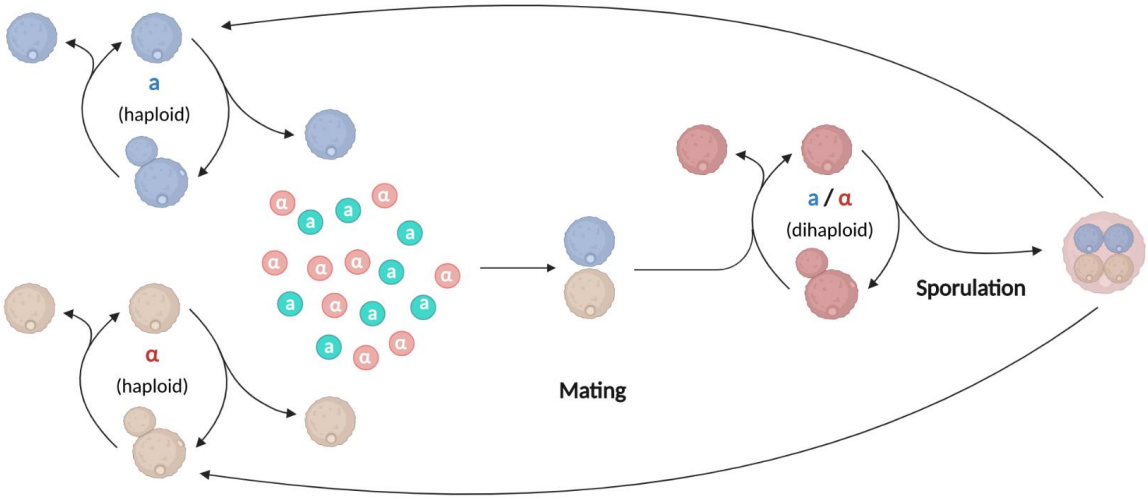

Figure 58 | Life cycle of *S. cerevisiae*. Schematic representation of *S. cerevisiae* life cycle.

Based on this information and considering that the strain W303 is haploid "a", cells were synchronized by incubating them with α-factor. Cells transformed with SLIMP and ΔN-SLIMP were grown and induced overnight with 100nM β-estradiol in URA media and afterwards incubated with 5µg/ml α-factor in complete media (YPD). After three hours, the pheromone was removed, and cells were grown in YPD media plus 100nM β-estradiol to guarantee the SLIMP overexpression. To follow the cell cycle progression of synchronized cells in the presence and absence of SLIMP, cells were collected at several time points and analyzed by FACS (Figure 59A).

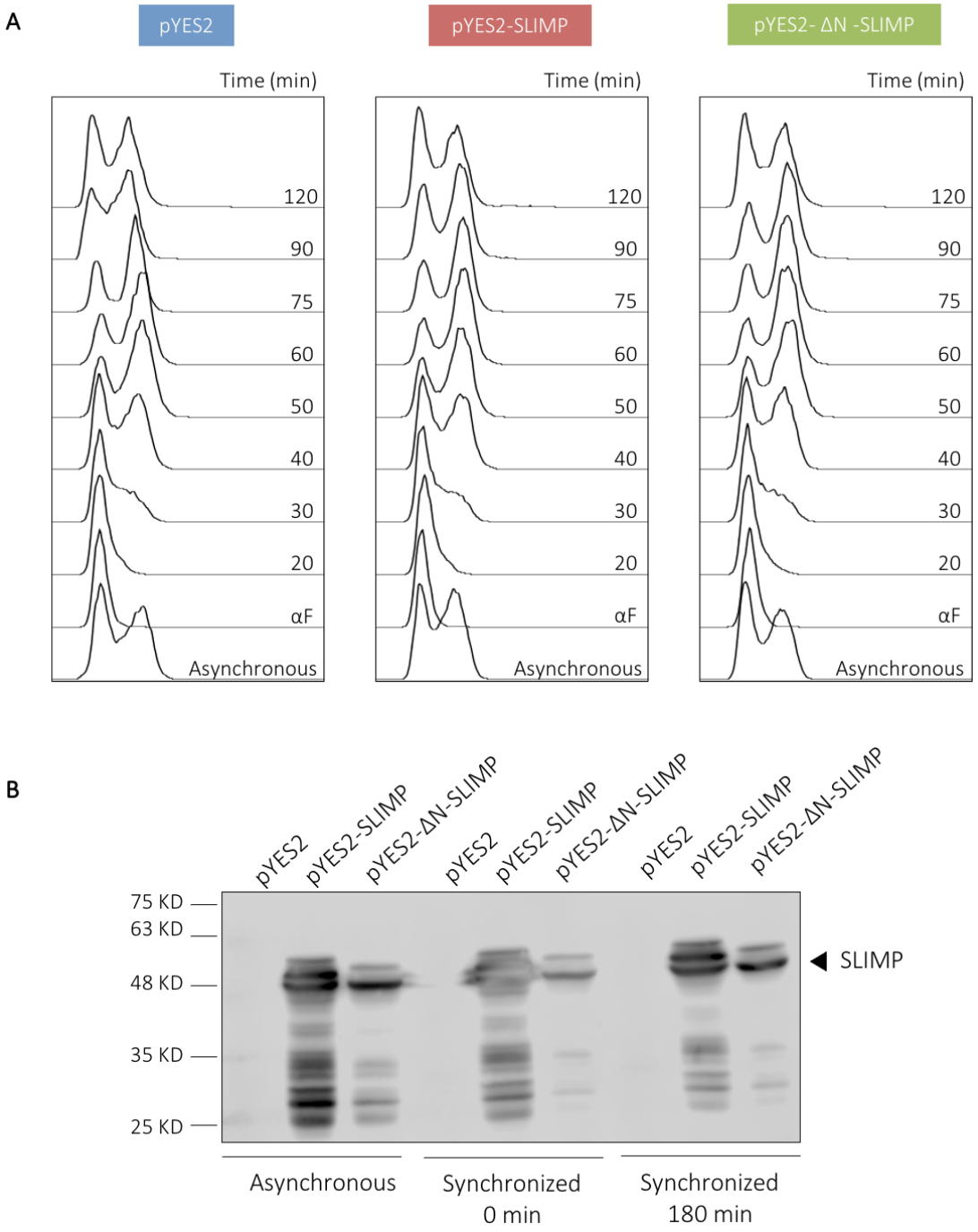

Figure 59 | Budding yeast cell cycle progression upon SLIMP overexpression. (A) Graphical representation of the cell cycle profile of synchronized cells overexpressing SLIMP (red) and ΔN-SLIMP (green) at different time points. Cells expressing the empty vector pYES2 (blue) were used as a negative control. (B) Western blot analysis detecting SLIMP overexpression of asynchronous cells and synchronized cells at the beginning (zero minutes) and end (180 minutes) of the experiments. An arrowhead highlights the SLIMP corresponding band (around 48KD).

Figure 59A shows that even in synchronized cells, the presence of SLIMP or ΔN-SLIMP does not make any difference in the cell cycle progression pattern compared to control cells (expressing empty vector). Moreover, immunoblot assay allowed us to ensure that both SLIMP and ΔN-SLIMP were correctly expressed during the whole experiment (Figure 59B).

Altogether these results suggest that, in *S. cerevisiae*, the cell cycle progression, including the G_1-S transition, is not affected by the presence of SLIMP, despite being essential for the cell cycle regulation in *D. melanogaster*.

4.3.2. SLIMP and mitochondrial environment in budding yeast

On the other hand, we wondered whether the overexpression of SLIMP in budding yeast could have any effect on mitochondrial homeostasis. Firstly, we analyzed the mitochondrial morphology under SLIMP presence in yeast. To approach this issue using confocal microscopy live imaging (Figure 60).

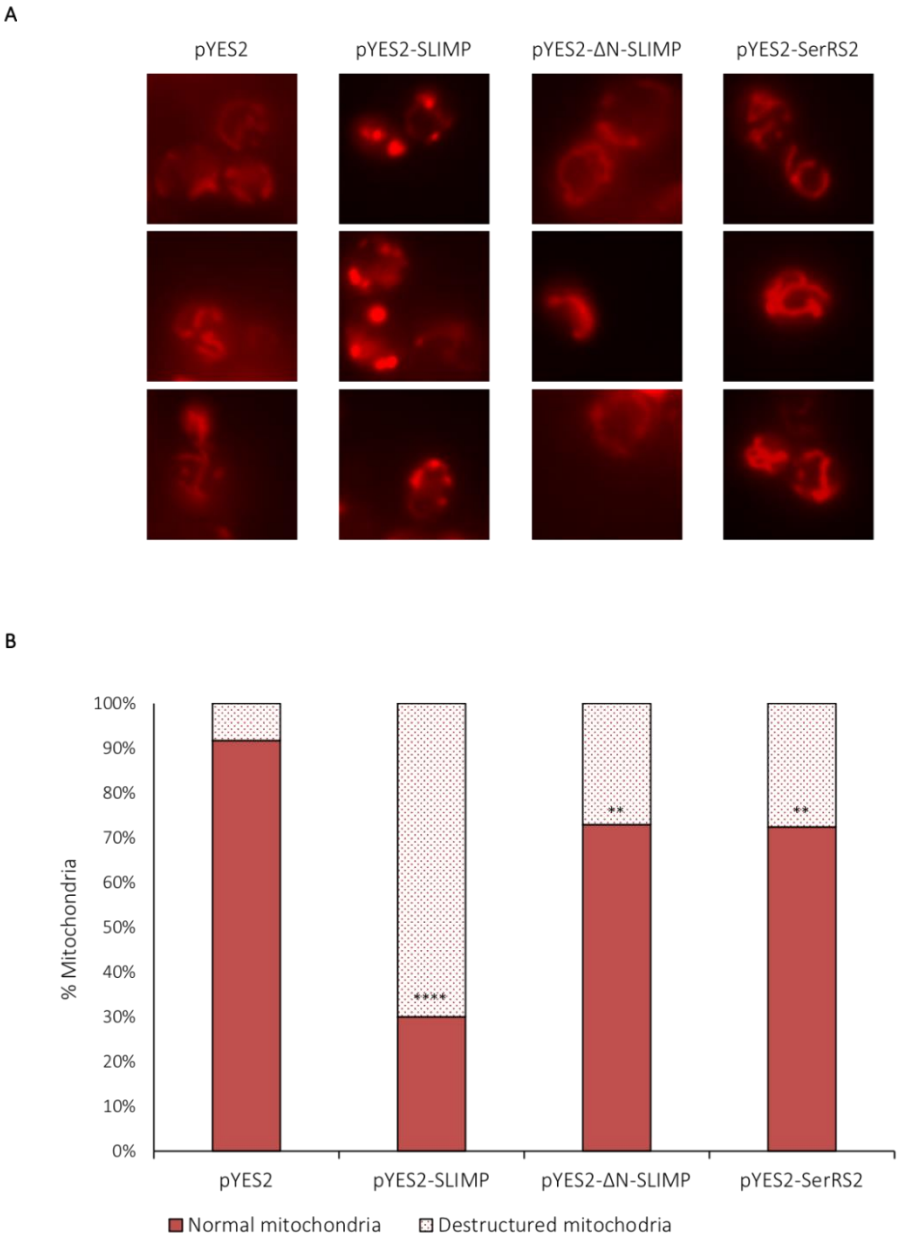

Figure 60 | Mitochondrial morphology analysis of yeast cells expressing SLIMP. (A) Fluorescent microscopy live imaging of budding yeast cells overexpressing SLIMP, ΔN-SLIMP and SerRS2. Cells were grown and induced overnight in URA media and afterwards incubated with 100nM of Mitotracker Red. Cells were visualized under confocal microscopy using red fluorescent channel. (B) Graphical representation showing the quantification of regular (red closed) and morphologically aberrant (stripped) mitochondria per strain. Cells expressing the empty vector were used as a negative control. Around fifty images were taken and around 300 mitochondria were analyzed per condition. Statistical analysis is referred to control cells and was performed by applying the Chi-Square test with GraphPad software (* p<0,05; ** p< 0,01; *** p<0,001; **** p<0,0001).

Interestingly, Figure 60 shows a remarkable deleterious effect on mitochondrial morphology upon SLIMP overexpression. This impact is specific for the full-length form of SLIMP since when the truncated form of SLIMP (unable to reach the organelle) or its paralog SerRS2 (SLIMP paralog in flies) are expressed, the aberrant:regular mitochondria ratio is significantly higher than in control cells but much less dramatic than upon SLIMP full-length overexpression (Figure 60B). Probably this mild effect on mitochondrial morphology observed under the ΔN-SLIMP or SerRS2 overexpression is simply due to the presence of an exogenous protein that disturbs in some manner the cellular homeostasis. In any case, the effect on mitochondrial morphology is much more notorious under SLIMP full-length overexpression.

Afterwards we wondered whether, in addition to compromising the mitochondrial morphology, the SLIMP presence in *S. cerevisiae* could lead to a mitochondrial dysfunction. In that direction, we tested the growth ratio of the strains overexpressing SLIMP, ΔN-SLIMP and SerRS2 in plates with glycerol or ethanol as carbon source. Thus, as both are non-fermentable carbon sources, we would detect a growth impairment only in case of mitochondrial dysfunction. Moreover, the *DIA4* (SerRS2 homolog in yeast) mutant (Dia4Δ) was used as a positive control since it was reported to not survive in non-fermentable carbon sources (Merz and Westermann et al. 2009; Rokov-Plavec et al. 2002). Finally, cells were grown in URA media agar plates and induces with 500nM β-estradiol (Figure 61).

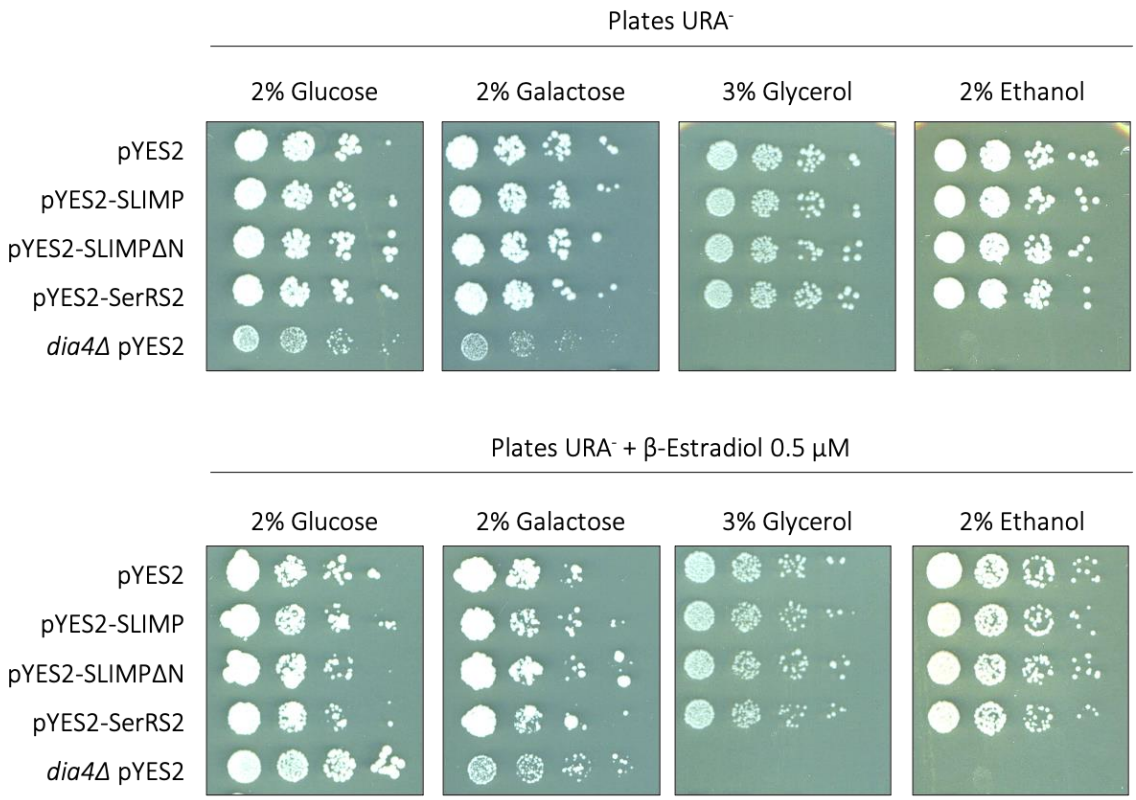

Figure 61 | Cells growing in non-fermentable carbon sources-media plates. Cells were grown in URA media plates containing different carbon sources: glucose and galactose, as positive controls, and ethanol and glycerol, as non-fermentable carbon sources. Non-induced cells are shown in the upper panel. Cells induced with 500nM β-estradiol are shown in the lower panel. The Dia4Δ mutant cells were used as a positive control and cells overexpressing the empty vector (pYES2) as a negative control. Cells were grown for three days and different dilutions per condition were performed to visualize better the growth capacity.

Figure 61 suggests that cells expressing SLIMP, ΔN-SLIMP or SerRS2, show the same growth ratio as non-induced cells for all the carbon sources, meaning that mitochondria might be functional in all the strains. Conversely, as expected, the Dia4Δ strain shows an evident growth impairment in non-fermentable carbon sources (glycerol and ethanol), which goes in concordance with published data.

From these results, we can conclude that although SLIMP expression in *S. cerevisiae* cells causes an alteration in mitochondrial morphology, the organelle seems to be still

functional, since cells can grow normally in non-fermentable carbon sources, such as glycerol or ethanol.

In summary, in this third chapter, the results shown suggest that the expression of SLIMP or ΔN-SLIMP in budding yeast do not modify the cell cycle progression. In contrast, however, the full-length form of SLIMP dramatically compromises the mitochondrial structure and morphology, although the organelle still seems to be functional or, at least, able to obtain ATP from ethanol and glycerol through the respiratory chain. Some of the possible molecular explanations underlying this phenomenon will be further discussed in the next section (see section 5.3).

DISCUSSION

5. DISCUSSION

Collectively, the work described in this thesis contributed to the further characterization of SLIMP, an aaRS-like protein involved in regulating mitochondria homeostasis and cell cycle progression, in *Drosophila melanogaster*.

As mentioned in the introduction, aaRS are considered evolutionary hotspots, prone to accumulate mutations and acquire new cellular functionalities. Accordingly, many recent studies reported a wide range of non-canonical functions associated with aaRS and aaRS-like proteins, which presumably originated from an aaRS-gene duplication and evolved as completely new proteins (Levi et al., 2020; Paul & Schimmel, 2013).

SLIMP was identified as a previously uncharacterized paralog of the mitochondrial seryl-tRNA synthetase (SerRS2) in *D. melanogaster*. SLIMP originated from a gene duplication at the base of metazoans, and it constitutes an essential protein universally distributed in insects, molluscs and echinoderms (De Potter, 2020; Guitart, et al., 2010). Furthermore, we recently demonstrated that SLIMP plays a crucial role in mitochondrial homeostasis by simultaneously coordinating global protein synthesis and mtDNA copy number within the organelle, through its interactions with SerRS2 and LON, respectively (Picchioni, et al., 2019).

Additionally, we recently observed that the SLIMP depletion in *Drosophila* cultured cells leads to a G_2 accumulation phenotype coupled to a transcriptional upregulation of a core set of genes involved in the preRC formation and S-phase onset (Antolin-Fontes, 2019).

In this regard, in the following sections, we will discuss how the results obtained in this thesis complement and expand the knowledge about the cell cycle function of SLIMP.

5.1. SLIMP SUBCELLULAR DISTRIBUTION

Interestingly, according to the established mitochondrial function of SLIMP, it might localize at the mitochondrial matrix, near the nucleoid, together with the rest of the transcriptional and translational machinery. In this regard, during an early characterization of SLIMP, it was assumed that its mitochondrial localization would rely on an N-terminal hydrophobic residue-enriched mitochondrial-targeting sequence, similarly to other mitochondrial matrix-residing proteins (Schmidt et al., 2010). Therefore, several bioinformatic analyses were performed to define the sequence of the SLIMP mitochondrial signal peptide (MSP) *in silico*, although unfortunately, no consensus sequence was obtained (Antolin-Fontes, 2019).

Here, we experimentally characterized the mitochondrial-targeting sequence of SLIMP using pull-down assays coupled to enzymatic digestion and mass spectrometry analysis (Figure 28). Moreover, we demonstrated that the SLIMP MSP, consisting of the first 21 amino acids of the protein sequence, is essential and sufficient to drive the protein into the mitochondria (Figure 29). Significantly, as observed in Figure 29D, we showed through immunofluorescence assays that, when SLIMP is overexpressed in S2 cells with the N-terminal MSP, it is localized mainly in the mitochondria. In contrast, SLIMP is observed mostly in the cytosol when a truncated version of the protein lacking the mitochondrial-targeting sequence is overexpressed in S2 cells (Figure 29E). Additionally, cellular fractionation assays for the mitochondrial enrichment performed in S2 WT cells further confirmed the prominent mitochondrial localization of SLIMP (Figure 30).

On the other hand, we demonstrated that SLIMP is predicted to bear a potential NLS peptide within the coiled-coil region of the protein sequence, starting at position 28 after the MSP natural cleavage (Figure 31). Notably, the score obtained using the NLS-Mapper online server was 4.1, which is reported to correspond to a medium-weak signal, usually held by proteins that localize at both the nuclear and the cytosolic compartments (Kosugi, et al., 2009).

Interestingly, although the NLS-Mapper tool was built using budding yeast as a model system, it has been reported to be reliable for other species since nuclear-targeting sequences are known to be highly conserved through evolution (Kosugi, et al., 2009). In fact, in a recently published study about the developmental control of transgelins (highly conserved actin-binding proteins), the authors used NLS-Mapper for NLS-predicting in *Drosophila*. They estimated that transgelins would localize at nuclear and cytosolic compartments based on a NLS-Mapper score above 4, similar to SLIMP's. Significantly, they experimentally confirmed this data and demonstrate that those proteins reside at both compartments, validating the NLS-Mapper *in silico* predictions in *D. melanogaster* (Vakaloglou et al., 2021).

Accordingly, we also experimentally confirmed the previous bioinformatics findings through cell fractionation assays. Hence, we assessed that although SLIMP predominantly localizes at the mitochondrial compartment, a small portion of the protein co-exists in the nuclear and cytosolic fractions (Figures 32 and 33, respectively). Importantly, these results are in concordance with a previous BioID-based interactome study performed in our group, where few potential nuclear and cytoplasmatic partners were suggested for SLIMP, although most of them were mitochondrial (Antolin-Fontes, 2019; Picchioni, et al., 2019).

Interestingly, the potential NLS predicted for SLIMP was only detected when analyzing the SLIMP sequence lacking the MSP, but not the full-length form of the protein. Therefore, the extra-mitochondrial population of SLIMP may require the MSP to be inaccessible or previously cleaved to reach other cellular compartments. In this regard, few potential situations have been described for dual-localized proteins that could apply to the case of SLIMP. On one hand, SLIMP could have more than one protein isoform (with and without the MSP), resulting from an alternative transcription start site (TSS), a second translation initiation codon, or a splicing process. Interestingly, all those situations have been described for dual-localized aaRS in different species (Mireau et al., 1996; Nishimura et al., 2019; Waldron et al., 2017). In that sense, since SLIMP sequence bears a single exon and only one conserved AUG codon upstream of the potential NLS peptide, the most likely possibility for another SLIMP isoform lacking the

MSP is the presence of an alternative TSS. However, non-AUG initiation codons have been recently proposed as alternative translation start sites for some dual-localized ARS, mainly in yeast. Although the non-AUG initiation codons reported to date tend to be upstream of the AUG-conventional codon and responsible for the longer isoform translation, an alternative SLIMP isoform translated from a downstream non-AUG initiation codon should not be discarded and is interesting to be explored. (Kearse & Wilusz, 2017; Monteuuis et al., 2019).

Otherwise, if only one isoform of SLIMP was present in the cell, protein interactions or post-translational modifications could eventually impair the availability of the MSP, promoting an extra-mitochondrial population in other compartments (see section 1.3.3) In this regard, a pull-down assay specific for the extra-mitochondrial SLIMP would shed light on its potential partners or post-translational modifications outside the organelle. Moreover, it would be interesting to unveil how is SLIMP imported into the mitochondria, since this scenario would require a post-translationally import of SLIMP, and the co-translational import has not been discarded so far.

Interestingly, despite the well-established post-translational mitochondrial protein import, recent studies revealed nuclear-encoded mRNAs of mitochondrial proteins at the vicinity of the organelle supporting the co-translational import (Avendaño-Monsalve et al., 2020; Garin et al., 2020; Golani-Armon & Arava, 2016; Lashkevich & Dmitriev, 2021). In that sense, the mRNA subcellular distribution has been demonstrated to contribute to a more accurate spatio-temporal translation control. Moreover, it has been proposed that two elements contribute to the mRNA localization at the mitochondrial surface for the co-translational import. On one hand, the 3'-UTR non-translational region seems to interact with the Puf3 RNA-binding protein (Saint-Georges et al., 2008). On the other hand, the nascent MSP has been suggested to interact with NAC (Nascent Associating Complex) and be recognized by the TIM/TOM translocase complex Tom20 subunit at the mitochondrial surface (Eliyahu et al., 2010). Thus, the mitochondrial targeting sequence still constitutes an essential element for both mitochondrial protein import, post-translationally and co-translationally. Interestingly, a newly published high-throughput analysis in yeast reported a massive diversity in the

mitochondrial proximity-localizing mRNA molecules. Notably, most of the mRNAs for mitochondrial aaRS were detected in the study, including DIA4 (the yeast homolog of SerRS2) (Williams et al., 2014). Therefore, although the post-translational is the best-known MPS-dependent mitochondrial import mechanism, this data raises the possibility of a co-translational import of SLIMP into the organelle.

Finally, SLIMP could be first imported into the mitochondria and afterwards exported from the organelle. Recently, it has been described that some mitochondrial proteins or protein fragments can be eventually retro-translocated from the organelle into the cytosol, through vesicles, for example (Fessler et al., 2020; X. Guo et al., 2020; Sugiura et al., 2014).

Intriguingly, we can detect the extra-mitochondrial population of SLIMP by cell fractionation followed by western blot analysis, but not through immunofluorescence techniques (Figures 29A and 29C), not even upon SLIMP overexpression (Figure 29D). This has been described to happen when a protein is predominantly present in a particular compartment, and a tiny portion co-exists outside (Regev-Rudzki & Pines, 2007). Thus, most likely we are not visualizing the extra-mitochondrial SLIMP population because the mitochondrial population of the protein is eclipsing the fluorescence signal outside the organelle.

Furthermore, it has also been suggested that proteins present in both the nucleus and the cytosol may be shuttling between them. Indeed, we observe significant differences in the extra-mitochondrial SLIMP distribution between experiments or even biological replicates. For instance, in the cell fractionation assays performed with cells in different cell cycle phases (see Section 4.2.5) we observed a small portion of SLIMP in the nuclear fraction in the G_1 phase, but only in one of the replicates (Figure 52). Conversely, in the cell fractionation assay of cells in S-phase versus control cells, SLIMP does not appear in the nuclear-enriched fraction, and the proportion of cytoplasmatic SLIMP is more prominent than in previous experiments, showing a slight increase in the S-phase (Figure 53).

Several possibilities can explain the high variability observed within cell fractionation experiments regarding the extra-mitochondrial SLIMP distribution. For instance, it was proposed that the shuttling rate between cytosol and nucleus can vary a lot depending on the cell culture confluence and proliferative state of the cells (Radyuk et al., 2009). In this regard, the experimental conditions (I. e., number of cells, % of confluence) of a cell fractionation assay performed directly from the cell culture (Figures 32 and 33), after cell sorting (Figure 52) and coupled to cellular synchronization (Figure 53) are pretty different. Thus, perhaps this may be influencing our results.

Alternatively, SLIMP could vary its subcellular distribution under certain cellular conditions, such as oxidative stress, hypoxia, or extracellular stimuli among others (see section 1.3.4). Surely, it may be some variables that we are not considering, which could explain the variability observed in the extra-mitochondrial SLIMP subcellular distribution. However, under which conditions SLIMP is present at those compartments and which mechanisms underlies the shuttling remains unknown. More experiments in this direction would be necessary to explore it deeper.

In this regard, we started building a transgenic S2 cell line, expressing the endogenous SLIMP fused to a GFP tag, using the CRISPR/Cas9 knock-in system. Abundant papers have applied the CRISPR/Cas9 technology to many organisms and cell lines, including bacteria, yeast, plants, flies, and humans. Remarkably, some studies have been reported to apply it to *Drosophila* cultured cells, such as S2 cells, despite being a considerable low efficient model system (Bassett et al., 2015; Kamiyama et al., 2016; Wissel et al., 2016). Unfortunately, although the experiment was designed carefully and considering most of the common troubleshooting issues reported, we could not successfully generate a new transgenic S2 cell line expressing SLIMP-GFP.

We initially proved that tagging SLIMP with a GFP at the C-terminus would not affect its natural subcellular distribution (Figure 35). This step was essential since it is broadly known that GFP or other fluorescent tags can interfere with the endogenous protein localization or functionality when are fused to them. Then, the cloning strategy was elaborated based on Basset et al., and the guides were designed using the online server

Benchling (Figure 36 and Table 7). Interestingly, around 1,3% of the transfected cells incorporated the green-fluorescent tag (Figure 37), and a few grew and showed temporally green fluorescence (Figure 38). However, after some passages, none of the clones could maintain the GFP tag inserted in their genome (Figures 39 and 40).

It is possible that genome editing was achieved, but cells lost the GFP incorporation. In this regard, two issues can be addressed to increase the chance of success in future experiments. Firstly, try to elucidate how the cells managed to remove the insert from their genome; and secondly, improve as much as possible the efficiency of the process from the beginning.

Accordingly, it was proposed that non-tumoral cells bearing wild type p53 are more prone to activate the DNA repair pathway in response to genome editing, either excision or insertion, which would allow them to revert the genome edition (Haapaniemi et al., 2018; Ihry et al., 2018). Alternatively, considering that S2 cells are tetraploid, the positive clones are likely to be heterozygous for the GFP insertion. Thus, another possibility would be that cells that initially were positive clones would undergo homologous recombination between two heterozygous alleles, enabling the cell to remove the GFP insertion from their genome (Luhur et al., 2019).

On the other hand, although the problem seemed to be more related to the impossibility of maintaining the GFP insert through time rather than the CRISPR/Cas9 tool itself, the process showed abysmal efficiency. Intriguingly, optimizing specific steps of the process could significantly improve it and potentially allow us to obtain a long-term positive clone. In this regard, it has been reported that the previous downregulation of the ligase4 (lig4) gene, involved in Non-Homologous End Joining (NHEJ) DNA repair, is particularly useful when the goal is a knock-in generation, since this significantly increases the homologous recombination rate (Bottcher et al., 2014; Brand & Winter, 2019). Moreover, the transfection efficiency of S2 cells is relatively low, so decreasing the homology arms-length could be a way to improve it. In this regard, recently published studies proposed some alternative CRISPR-derived methods, such as the Drop-in or CRISPaint, which rely on shorter homology arms, around 100nt, and

incorporate PCR-derived methods to facilitate the donor plasmid cloning process (Bosch et al., 2020; Kanca et al., 2019). Additionally, considering the difficulty of S2 cells for proliferating from a single cell clone, a recent study proposes a technique to overcome this problem: sorting a pool of cells instead of single clones (Franz et al., 2017). Finally, as a more drastic solution, we could move to the Kc *Drosophila* cell line which is diploid and theoretically would be less prone to recombine and lose the tag.

5.2. CELL CYCLE FUNCTION OF SLIMP

Interestingly, two studies pointed to SLIMP as a key regulator of cell cycle progression in *D. melanogaster* (Ambrus et al., 2009; Liang et al., 2014). On one hand, Liang et al. described a core set of genes differentially expressed during the cell cycle through a cell cycle-associated transcriptomic microarray analysis in *Drosophila* wing disc and S2 cultured cells. Markedly, only 150 genes were suggested to be expressed with a certain periodicity through the cell cycle on both cellular models. Intriguingly, one of them was SLIMP (CG31133), which was described to present a peak of expression in G_2. Moreover, the authors generated knockdowns and mutants for all the differentially expressed genes. Interestingly, they observed that SLIMP depletion resulted in an accumulation of cells in the G_2/M phase.

Notably, the latter results about the impact of SLIMP knockdown on the cell cycle are in concordance with our data since the G_2 accumulation phenotype upon SLIMP depletion was firstly demonstrated in vivo (Guitart, et al., 2010) and more recently in S2 cultured cells (in vitro) (Antolin-Fontes, 2019). In contrast, we analyzed the mRNA levels of SLIMP in G_1/G_0, S and G_2/M sorted cells by qPCR, and no differences were observed between cell populations (Figure 42B). Thus, we did not detect any periodicity associated with SLIMP expression through the cell cycle in S2 cells. In agreement with this data, no differences in SLIMP transcript levels were observed either in the microarray analysis previously performed in our group (Antolin-Fontes, 2019).

On the other hand, as previously explained, Ambrus et al. performed a sizeable genetic screen to identify new E2F1 suppressor genes in *Drosophila melanogaster*. First, the authors generated an E2F1 mutant fly associated with a well-established G_1 arrest phenotype. Afterwards, they randomly mutated the E2F1-mutant fly genome and analyzed which mutations could revert the G_1 accumulation phenotype. The read-through of their experiments was based on BrdU incorporation in the second mitotic wave (SMW) of the *Drosophila* eye imaginal disc. Interestingly, they observed that the E2F1 and SLIMP double mutant showed more BrdU incorporation than the E2F1 single

mutant, meaning that SLIMP depletion could help overcome the E2F1-mutant phenotype stimulating the progression through the cell cycle from G_1 to S phase.

In concordance with Ambrus et al. results, we demonstrate here that the simultaneous depletion of SLIMP and E2F1 activity through chemical inhibition of CDK4 (upstream regulator of E2F1), produced a similar effect in S2 cells (Figure 46). To do so, we used Palbociclib (also known as PD-0332991), a commercial antitumoral drug utilized to treat pRB-positive tumors, which specifically inhibits CDK4 and CDK6 kinases abrogating the pRB (RBF1 in flies) phosphorylation and consequently the downstream G_1 to S transition (Ingham & Schwartz, 2017). Palbociclib has been reported to generate a cell cycle arrest in G_1 at lower doses and induce cellular senescence at higher concentrations in mammalian cells (Llanos et al., 2019). However, much less is known about the impact of Palbociclib in *Drosophila* cultured cells. Therefore, we carefully characterized the optimal concentration and treatment duration for inducing a reversible G_1 arrest in S2 cells. Thus, we established that the best experimental conditions for our model system were 10μM treatment for 24 hours (Figure 47). Afterwards, we used the drug to mimic the E2F1-mutant effect in SLIMP-depleted and control cultured S2 cells.

Interestingly, we observed the same dynamic in S2 cells as that reported by the mentioned study *in vivo*. Thus, upon Palbociclib-mediated E2F1 indirect inhibition, the accumulation of cells in G_1 was significantly lower in SLIMP depleted cells than in control cells (Figure 48). This result points to a synergistic effect of the SLIMP depletion and E2F1 pathway boosting the G_1 - S transition, meaning that probably SLIMP is somehow blocking the cell cycle progression near the R-point. Moreover, we demonstrated by hydroxyurea-mediated cellular synchronization that SLIMP depleted cells enter in S-phase earlier or faster than wild type cells (Figure 49). Importantly, these results agree with formerly published data and reinforce the idea of SLIMP as a potential E2F1-suppressor gene that would negatively modulate the cell cycle progression at the G_1/S transition in an E2F1-complementary pathway.

In concordance with this hypothesis, the previous transcriptomic analysis performed in our group showed a remarkable upregulation of genes involved in the S-phase onset

upon SLIMP knockdown. Distinctly, after a gene ontology analysis, three major categories resulted upregulated in cells knocked down for SLIMP: E2F1-target genes, MYC-target genes, and the G_2/M checkpoint (Figure 23). Intriguingly, it is well-known that when cells enter in S-phase, a bunch of overlapping inhibitory mechanisms downregulate the replication licensing factors. Indeed, it has been reported that non-controlled expression of some proteins involved in origin licensing and firing tend to lead to replicative stress.

For instance, overexpression of Double Parked (DUP), involved in origin licensing, has been reported to be sufficient to induce re-replication-mediated replicative stress (Kroeger et al., 2013; Thomer et al., 2004). Indeed, DUP and its inhibitor Geminin are E2F1-target genes that tend to be increased in replicative stress scenarios (Kenichi, Yoshida & Inoue, 2004; May et al., 2005). Similarly, the S-phase cyclin, Cyc E, involved in the R-point bypass and DNA replication initiation, is roughly known to cause premature S-phase entry upon overexpression, carrying a replication stress phenotype (Jones et al., 2012; Resnitzky et al., 1994).

Additionally, MCMs transcript levels are also increased under SLIMP knockdown. Although, it has been suggested that the replication rate depend more on the loading efficiency rather than the protein levels (Crevel et al., 2011; Dukaj & Rhind, 2021), it was demonstrated in humans that the simultaneous upregulation of CDT1 (DUP human homolog), CDC6 and ORC1 strongly reinforce the MCM loading and origin licensing, leading to a re-replication-mediated replicative stress situation (Sugimoto et al., 2009).

Accordingly, this data absolutely fits with the scenario observed upon SLIMP depletion, where a significant increase in transcript levels for licensing and firing factors, such as DUP, Cyc E, MCMs, Geminin, ORCs and CDC6, is detected coupled to a G_2 accumulation phenotype (Figures 22 and 23).

Interestingly, Resnitzsky et al. demonstrate that CycE overexpression-derived replicative stress results from conflicts between DNA replication and transcription, and it can be eventually compensated by treating the cells with Cordycepin, a transcription inhibitor.

However, the authors also observed that the replicative stress phenotype was associated with a reduction in the dNTP availability and an increase In the H2Av-phosphorylated, contrary to our previous findings (Figure 24). Therefore, more experiments are needed to elucidate whether the SLIMP depletion generates replication-transcription conflicts derived from the Cyc E upregulation.

Moreover, it is well-established that replicative stress associated to a shorter G_1 or earlier S-phase onset tend to trigger the G_2/M checkpoint activation with a later entering into mitosis. Thus, the potential troubles generated during DNA replication would be solved during G_2, or otherwise the cell would undergo apoptosis. Notably, the G_2/M checkpoint was one of the most robustly upregulated categories in the microarray gene ontology analysis for SLIMP-KD cells. In fact, proteins like GRP, MEI-41 or DAP, which constitute crucial elements of the DNA damage response (DDR)-activating pathway, are modestly upregulated in SLIMP depleted cells (see section 1.4.3 and Figure 15).

Furthermore, as mentioned in the introduction, upon DDR-dependent G_2/M checkpoint activation, the mitotic promoting factor subunit CDK1 remains phosphorylated and inactive until the cell is ready to undergo mitosis. Accordingly, WEE1 kinase, responsible for the inhibitory phosphorylation of CDK1, is significantly upregulated in SLIMP-depleted cells. While, STRING, involved in the M-phase entry through CDK1 dephosphorylation, is slightly downregulated in the SLIMP-KD context. Remarkably, we here experimentally ratified that the levels of the CDK1-Tyr15-P inactive form increase upon SLIMP depletion (Figure 51).

Finally, it has been reported that downregulation of the APC/C family members CDC20 or CDH1 (mammalian homologs of FZY and FZR, respectively) usually leads to a G_1 shortness and prematurely S-phase entering (Grant & Cook, 2017; Sigl et al., 2009). Interestingly, although both FZY and FZR show a slightly downregulation in our transcriptomic analysis, it is not statistically significant. In this regard, it would be interesting to re-check the mRNA levels of these proteins and others mentioned in this section by qPCR as a more sensitive technique. Moreover, analyze the protein levels by western blot would be very informative to verify our hypothesis since it is known that

ubiquitin-mediated proteolysis is crucial for modulating the cell cycle regulatory elements levels.

Thus, these results altogether highlight the hypothesis that SLIMP might repress the transition from G_1 to S phase in a pathway independent from E2F1. Consequently, it may potentially generate troubles during DNA replication, which will ultimately trigger the DDR and G_2/M checkpoint activation, leading to the G_2 accumulation phenotype (Figure 54).

Unfortunately, the molecular mechanism underling the SLIMP regulatory function on the G_1/S transition remains unknown. In this regard, few hypotheses can be speculate based on all the data obtained in our group and others. On one hand, DREAM (DP, RB-like, E2F And MuvB) is a potent transcriptional repressor complex which, in collaboration with RBF2/E2F2, downregulates the E2F1-derived transcriptional cascade at the G_1/S and G_2/M transition (Fischer & Müller, 2017; Sadasivam & Decaprio, 2013). Interestingly, it is known that the depletion of E2F2 leads to an upregulation of the E2F1-target genes. Moreover, the double mutant E2F1 and E2F2 has been demonstrated to partially compensates for the E2F1 mutant-derived G_1 arrest in flies (Frolov et al., 2001). Accordingly, one possibility would be that SLIMP was somehow collaborating with the E2F2/DREAM-mediated E2F-target genes repression. Thus, upon SLIMP depletion the E2F1-transcriptional cascade would be less repressed and lead to an upregulation of E2F1-target genes. In this direction, it has been reported in mammals that under E2F6 depletion, a repressor member of the E2F transcription factor family and a DREAM complex component, generates a faster S phase coupled to a G_2 accumulation phenotype, non-linked to H2Av phosphorylation. This phenotype is very similar to the scenario observed upon SLIMP depletion in *Drosophila*. However, the authors did not observe a prematurely S-phase entry but an increased replication speed, instead (Pennycook et al., 2020). Thus, SLIMP and E2F6 depletion phenotypes partially correlate, still raising the possibility that SLIMP could directly or indirectly contribute to the DREAM-mediated repression of the E2F1 transcriptional cascade-dependent G_1 to S transition. Nonetheless, more experiments would need to be performed to approach this hypothesis.

On the other hand, a very recent paper pointed to CABUT (CBT) as a new transcription factor involved in cell cycle progression in *Drosophila melanogaster* (P. Zhang et al., 2021). CBT is a Krüppel-like factor (KLF) responsible for the transcription of a core set of E2F1-target genes. Interestingly, the authors propose that CBT acts parallelly and synergistically to E2F1 in a tissue-specific manner. Moreover, they showed that CBT overexpression generates an upregulation of E2F1-target genes coupled to early S-phase onset, triggering an anomalous DNA replication scenario, that results in a G_2 accumulation phenotype. Distinctly, the CBT overexpression-derived phenotype strongly resembles the scenario observed upon SLIMP depletion. Hence, it raises the possibility that SLIMP could be involved in the same regulatory axis as CBT, probably somehow repressing its activity upstream of the pathway.

Finally, the cell cycle is a tightly regulated process that relies on several mechanisms to guarantee its proper progression. Thus, some redundant pathways influence the cell cycle progression, predominantly modulating the critical step of G_1/S transition. Notably, the transcriptional regulation of certain E2F1-target genes has been reported to overlap with various transcription factors, such as MYC, DREF or the HIPPO-Yorkie pathway (Dominguez-Sola & Gautier, 2014; Nicolay et al., 2011; Santoni-Rugiu et al., 2000; Sawado et al., 1998). Interestingly, DREF was detected in the first pull-down-mediated SLIMP interactome study performed in our group (Figure 18A). DREF (DNA replication-related element binding factor), initially described in *Drosophila*, is a master transcriptional regulator especially crucial in developmental control, which specifically binds to the DRE sequence at gene promoters (Matsukage et al., 2007; Tue et al., 2017). Although the putative SLIMP-DREF interaction was not detected in the BioID interactome analysis performed later in our group (Figure 18C), it would be interesting to explore deeper this potential interaction. Since some of the most upregulated E2F1-target genes upon SLIMP depletion, such as ORC2 and ORC5, have been reported to hold DRE elements on their promoter sequences (Lefai et al., 2000; Okudaira et al., 2005).

On the other hand, we observed that upon SLIMP depletion, the overexpression of its coiled-coil domain alone was sufficient to recover the G_2 accumulation phenotype

typical from SLIMP-KD cells (Figure 45A). This observation raises the question of whether the coiled-coil domain represents a crucial element for the cell cycle-related role of SLIMP. Interestingly, the coiled-coil domain used in this experiment lacked the mitochondrial-targeting sequence, reinforcing the idea that the SLIMP cell cycle function is mitochondrial independent (Figure 44). This phenotype is only rescued when the CC domain is tagged with a FLAG tag at the N-terminus, while a C-terminal FLAG tagged SLIMP coiled-coil domain failed to rescue it and was poorly expressed (Figure 45B). Thus, these results suggest that the coiled-coil structure might be critical for the domain stability and may be disrupted by the addition of a FLAG tag at the C-terminus. Both constructs with the globular domain were properly expressed but failed to rescue the G2 delay phenotype (Figure 45).

As observed in Figure 45B, upon SLIMP depletion, the protein becomes undetectable by western blot analysis. Intriguingly, when SLIMP depleted cells are supplemented with the empty vector or any of the constructs excepting the FLAG-CC (CC-FLAG, GD-FLAG or FLAG-GD), no SLIMP is appreciated by immunoblotting. However, when SLIMP-KD are transfected with the FLAG-CC, able to rescue the G_2 accumulation phenotype, a tiny portion of SLIMP is detected. Interestingly, this band is much lighter than the endogenous protein, discarding the possibility of an inefficient knockdown. Nonetheless, this result raises the question of whether SLIMP could autoregulate its own mRNA translation. Interestingly, a couple of studies in budding yeast just demonstrated that most of aaRS bind to their own mRNAs very efficiently (Levi et al., 2020). Moreover, some of them such as HisRS, seem to self-regulate their protein levels through mRNA binding-dependent translation rate modulation. The mRNA has been suggested to acquire an anticodon-like structure which would compete with the cognate tRNA for the aaRS attachment. Thus, when tRNA levels are low, the aaRS will bind its own mRNA auto-inhibiting translation. In contrast, when tRNA levels increase, the synthetase will attach to its cognate tRNA, releasing its mRNA and stimulating its own translation. Hence, the equilibrium aaRS:tRNA will be maintained (Levi & Arava, 2019b).

Reported data to date supports the idea of an RNA-binding-mediated self-translation inhibition, rather than activation. However, little is known about it yet and given the fact

that coiled coils are typical nucleic acid binding domains, an enhancing effect on its own translation rate mediated by self-mRNA binding can not be discarded for SLIMP. Alternatively, another possibility could be that the SLIMP coiled coil competes with the RNAi for binding the mRNA molecule, leading to a lower effectivity of our silencing mechanism. It must be considered that 3 days of $CuSO_4$ induction is enough for a protein overexpression, but eight days of induction are required for an efficient RNAi-mediated knockdown. Thus, another potential explanation would be that the coiled-coil could stabilize a tiny portion of the protein before the RNAi would be fully effective, pointing to a putative dimerization of SLIMP outside the organelle.

5.3. SLIMP IN BUDDING YEAST

In this section, we will discuss the data shown in the third chapter of Results (section 4.3). Although it is less related to the molecular role of SLIMP in cell cycle regulation, it offers a more evolutionary perspective and opens new interesting research lines about the SLIMP structure and its mitochondrial function.

As mentioned in the introduction, SLIMP appeared from a gene duplication at the base of metazoan; hence, it is not present in yeast. However, aiming to elucidate some aspects of its potential interactors or molecular function, we overexpressed SLIMP in budding yeast and analyzed the impact on the mitochondrial homeostasis and cell cycle progression.

Firstly, we proved that SLIMP is correctly expressed in the budding yeast system and does not generate any cytotoxic effects (Figure 55), not even upon long-term overexpression (Figure 56). Then, we observed that either the presence of SLIMP full length or the truncated form of SLIMP lacking the MSP caused no effect on the cell cycle profile of an asynchronous cell culture (Figure 57). Moreover, although SLIMP plays a crucial role repressing the S-phase entry in flies, presumably from outside the mitochondria, no differences were observed upon expressing both forms of SLIMP (with and without the MSP) in G_1-synchronized cells (Figure 59).

In contrast, interestingly, we observed by confocal microscopy that cells overexpressing the SLIMP full length show a substantial increase in structurally aberrant mitochondria, compared to cells overexpressing the truncated form of SLIMP (unable to reach the organelle) or its paralog SerRS2, which are much similar to control cells (Figure 60). Notably, despite the impact on the mitochondrial network structure, cells overexpressing SLIMP present a regular respiration capacity, meaning that their mitochondria are probably morphologically deleterious but still functional (Figure 61).

As mentioned in the section 4.3, SLIMP was also overexpressed in HeLa cells previously in our group. Intriguingly, exactly the same impact detected in this thesis upon SLIMP overexpression in yeast was observed in human cells: a non-altered cell cycle profile (Antolin-Fontes, 2019), and a mitochondrial fragmentation phenotype (Picchioni, 2014). Nevertheless, the mitochondrial viability was not evaluated in human cells.

The fact that the SLIMP overexpression generates a similar effect on yeast and human cells, may suggest that SLIMP could impacts on a highly conserved pathway, generating the same phenotype on both species.

In this regard, a potential explanation for the SLIMP expression-associated mitochondrial fragmentation phenotype could be that the SLIMP presence somehow interferes with the mitochondrial fusion/fission equilibrium. OPA1, is an essential protein involved in the mitochondrial fusion process. However, upon stress conditions OPA1 is cleaved generating a shorter form unable to promote mitochondrial fusion. Consequently, this decrease in mitochondrial fusion immediately implicates an increase in mitochondrial fission (fragmentation) (Ishihara et al., 2006; T, Wai et al., 2015). In *Drosophila,* SLIMP interacts with the substrate-binding domain of LON protease. Thus, similarly to what happens in flies with the SLIMP-dependent TFAM degradation by LON, SLIMP could be artificially interacting with OMA1 (humans) or MGM1 (yeast) proteases and stimulating OPA1 degradation and ultimately resulting in an increase of mitochondrial fragmentation. Nevertheless, it has been described in different species that an increase in mitochondrial fission caused by a decrease in mitochondrial fusion, tend to impact on the cell cycle progression (Gupte, 2015), and our results do not present any cell cycle effect (Figure 59). Thus, more experiments will need to be done to approach this hypothesis.

Intriguingly, an OPA1-SLIMP interaction was suggested in the pull-down mediated SLIMP interactome analysis (Figure 18A). Moreover, although no increase in mitochondrial fission is observed in SLIMP-KD cells, some preliminary experiments pointed to an increase of the cleaved OPA1 shorter isoform levels upon SLIMP depletion in flies (Picchioni, 2014). Unfortunately, the interaction could not be fully validated. Moreover,

this data would suggest a similar effect upon SLIMP depletion in *Drosophila* and overexpression in other species, when a contrary outcome would be expected. Although the biological relevance of the SLIMP-OPA1 interaction in flies remains poorly understood, it would be interesting to explore it deeper considering the presented results. However, unfortunately, no experimental evidences support this speculation for the moment.

Conversely, the SLIMP-expression resulting phenotype in yeast could be due to a structural artifact. SLIMP would unspecifically interact with some mitochondrial elements, resulting in structurally aberrant mitochondria that are still functional. In any case, this phenotype would be an artefact resulting from the heterologous expression of SLIMP in yeast or human cells, and more experiments should be performed to elucidate the mechanism underlying the mitochondrial fragmentation.

In balance, the results presented in this thesis, together with the data previously obtained in our group, allowed us to build a model in which a mitochondrial SLIMP population is involved in the regulation of mitochondrial protein synthesis and mtDNA abundance, while an extra-mitochondrial population of SLIMP, probably shuttling between the nucleus and the cytosol, would be regulating the G_1 to S transition, in an E2F1 antagonistic pathway (Figure 54).

CONCLUSIONS

6. CONCLUSIONS

Considering the presented data, the following conclusions can be extracted.

- The SLIMP protein sequence bears a mitochondrial signal peptide at the N-terminus, consisting of the first 21 amino acids, which is responsible for importing SLIMP into the organelle.

- The SLIMP protein sequence is predicted to hold a nuclear localization signal downstream of the MSP, within the coiled coil domain.

- SLIMP localizes mainly in the mitochondria. However, a small portion of the protein co-exists outside the organelle, in the cytosolic and nuclear compartments.

- SLIMP mRNA levels do not change through the cell cycle.

- SLIMP depleted cells show a less prominent G_1 arrest upon E2F1 blockage resulting from Palbociclib treatment, than control cells.

- SLIMP depleted cells pass faster through the G_1-S transition and enter in S-phase earlier than control cells.

- The overexpression of the coiled-coil domain of SLIMP in SLIMP depleted cells is sufficient for rescuing the G_2 accumulation phenotype.

- SLIMP depleted cells show higher levels of CDK1 phosphorylated at position Y15 than control cells, probably due to a major activation of the G_2/M checkpoint.

- The heterologous expression of SLIMP in *S. cerevisiae* does not cause a toxic effect or a growth impairment.

- The heterologous expression of SLIMP in budding yeast does not alter the cell cycle progression of the organism.

- The heterologous expression of SLIMP full length, but not a truncated form of SLIMP lacking the MSP, in budding yeast, induces mitochondrial fragmentation. However, the respiration capacity is not reduced in these cells, suggesting that the structurally aberrant mitochondria are still functional.

REFERENCES

7. REFERENCES

Adrian Gabriel Torres and Lluı´s Ribas de Pouplana. (2016). Transfer RNA Modifications: From Biological Functions to Biomedical Applications. In *Modified Nucleic Acids in Biology and Medicine* (pp. 2–21).

Ahel, I., Korencic, D., Ibba, M., & Söll, D. (2003). Trans-editing of mischarged tRNAs. *Proceedings of the National Academy of Sciences of the United States of America*, *100*(26), 15422–15427. https://doi.org/10.1073/pnas.2136934100

Ahmed, A. U., & Fisher, P. R. (2009). Import Of Nuclear-Encoded Mitochondrial Proteins. A Cotranslational Perspective. In *International Review of Cell and Molecular Biology* (Vol. 273, Issue C, pp. 49–68). Academic Press. https://doi.org/10.1016/S1937-6448(08)01802-9

Akimoto, T., Pohnert, S. C., Li, P., Zhang, M., Gumbs, C., Rosenberg, P. B., Williams, R. S., & Yan, Z. (2005). Exercise stimulates Pgc-1α transcription in skeletal muscle through activation of the p38 MAPK pathway. *Journal of Biological Chemistry*, *280*(20), 19587–19593. https://doi.org/10.1074/jbc.M408862200

Ambrus, A. M., Rasheva, V. I., Nicolay, B. N., & Frolov, M. V. (2009). Mosaic genetic screen for suppressors of the de2f1 mutant phenotype in drosophila. *Genetics*, *183*(1), 79–92. https://doi.org/10.1534/genetics.109.104661

Antolin-Fontes, A. (2019). *Mitochondrial and cell cycle functions of SLIMP*. University of Barcelona (UB).

Arif, A., Jia, J., Moodt, R. A., DiCorleto, P. E., & Fox, P. L. (2011). Phosphorylation of glutamyl-prolyl tRNA synthetase by cyclin-dependent kinase 5 dictates transcriptselective translational control. *Proceedings of the National Academy of Sciences of the United States of America*, *108*(4), 1415–1420. https://doi.org/10.1073/pnas.1011275108

Avadhani, N. G., Sangar, M. C., Bansal, S., & Bajpai, P. (2011). Bimodal targeting of cytochrome P450s to endoplasmic reticulum and mitochondria: The concept of chimeric signals. In *FEBS Journal* (Vol. 278, Issue 22, pp. 4218–4229). FEBS J. https://doi.org/10.1111/j.1742-4658.2011.08356.x

Avendaño-Monsalve, M. C., Ponce-Rojas, J. C., & Funes, S. (2020). From cytosol to mitochondria: The beginning of a protein journey. *Biological Chemistry*, *401*(6–7), 645–661. https://doi.org/10.1515/hsz-2020-0110

B. Alberts, A. Johnson, J. Lewis, D. Morgan, M. Raff, K. Roberts, P. W. (2015). *Molecular Biology of The Cell 6th edition*.

Bähler, J. (2005). Cell-cycle control of gene expression in budding and fission yeast. In *Annual Review of Genetics* (Vol. 39, pp. 69–94). Annu Rev Genet. https://doi.org/10.1146/annurev.genet.39.110304.095808

Barros, M. H., da Cunha, F. M., Oliveira, G. A., Tahara, E. B., & Kowaltowski, A. J. (2010). Yeast as a model to study mitochondrial mechanisms in ageing. *Mechanisms of Ageing and Development*, *131*(7–8), 494–502. https://doi.org/10.1016/j.mad.2010.04.008

Bassett, A. R., Kong, L., & Liu, J. L. (2015). A Genome-Wide CRISPR Library for High-Throughput Genetic Screening in Drosophila Cells. *Journal of Genetics and Genomics*, *42*(6), 301–309. https://doi.org/10.1016/j.jgg.2015.03.011

Bassett, A. R., Tibbit, C., Ponting, C. P., & Liu, J. (2013). Mutagenesis and homologous recombination in Drosophila cell lines using CRISPR / Cas9. *Biology Open*, *3*, 42–49. https://doi.org/10.1242/bio.20137120

Berg, M. D., Giguere, D. J., Dron, J. S., Lant, J. T., Genereaux, J., Liao, C., Wang, J., Robinson, J. F., Gloor, G. B., Hegele, R. A., O'Donoghue, P., & Brandl, C. J. (2019). Targeted sequencing reveals expanded genetic diversity of human transfer RNAs. *RNA Biology*, *16*(11), 1574–1585. https://doi.org/10.1080/15476286.2019.1646079

Berthier, F., Renaud, M., Alziari, S., & Durand, R. (1986). RNA mapping on Drosophila mitochondrial DNA: precursors and template strands. In *Nucleic Acids Research* (Vol. 14).

Bertoli, C., Skotheim, J. M., & M de Bruin, R. A. (2013). Control of cell cycle transcription during G1 and S phases. *Nature Publishing Group*. https://doi.org/10.1038/nrm3629

Blais, A., & Dynlacht, B. D. (2004). Hitting their targets: an emerging picture of E2F and cell cycle control. *Current Opinion in Genetics & Development 2004, 14*, 527–532. https://doi.org/10.1016/j.gde.2004.07.003

Blaise, M., Becker, H. D., Lapointe, J., Cambillau, C., Giegé, R., & Kern, D. (2005). Glu-Q-tRNAAsp synthetase coded by the yadB gene, a new paralog of aminoacyl-tRNA synthetase that glutamylates tRNAAsp anticodon. *Biochimie*, *87*(9–10), 847–861. https://doi.org/10.1016/j.biochi.2005.03.007

Bogenhagen, D. F., Rousseau, D., & Burke, S. (2008). *The Layered Structure of Human Mitochondrial DNA Nucleoids*. https://doi.org/10.1074/jbc.M708444200

Bonke, M., Turunen, M., Sokolova, M., Vähärautio, A., Kivioja, T., Taipale, M., Björklund, M., & Taipale, J. (2013). Transcriptional networks controlling the cell cycle. *G3: Genes, Genomes, Genetics*, *3*(1), 75–90. https://doi.org/10.1534/g3.112.004283

Bosch, J., Knight, S., Kanca, O., Zirin, J., Yang-Zhou, D., Hu, Y., Rodiger, J., Amador, G., Bellen, H., Perrimon, H., & Mohr, S. (2020). Use of the CRISPR-Cas9 System in Drosophila Cultured Cells to Introduce Fluorescent Tags into Endogenous Genes. *Current Protocols in Molecular Biology*, *130*(1). https://doi.org/10.1002/CPMB.112

Botstein, D., & Fink, G. R. (2011). Yeast: An Experimental Organism for 21st Century Biology. *Genetics*, *189*(3), 695–704. https://doi.org/10.1534/genetics.111.130765

Bottcher, R., Hollmann, M., Merk, K., Nitschko, V., Obermaier, C., Philippou-massier, J., Wieland, I., Gaul, U., & Klaus, F. (2014). Efficient chromosomal gene modification with CRISPR / cas9 and PCR-based homologous recombination donors in cultured Drosophila cells. *Nucleic Acids Research*, *42*(11), 2–16. https://doi.org/10.1093/nar/gku289

Bracken, A. P., Ciro, M., Cocito, A., & Helin, K. (2004). E2F target genes: unraveling the biology. *Trends in Biochemical Sciences*, *29*, 409–417. https://doi.org/10.1016/j.tibs.2004.06.006

Brand, M., & Winter, G. (2019). Locus-Specific Knock-In of a Degradable Tag for Target Validation Studies. *Methods in Molecular Biology*, *1953*, 105–119. https://doi.org/10.1007/978-1-4939-9145-7_7

Campanacci, V., Dubois, D. Y., Becker, H. D., Kern, D., Spinelli, S., Valencia, C., Pagot, F., Salomoni, A., Grisel, S., Vincentelli, R., Bignon, C., Lapointe, J., Giegé, R., & Cambillau, C. (2004). The Escherichia coli YadB gene product reveals a novel aminoacyl-tRNA synthetase like activity. *Journal of Molecular Biology*, *337*(2), 273–283. https://doi.org/10.1016/j.jmb.2004.01.027

Cao, X., Li, C., Xiao, S., Tang, Y., Huang, J., Zhao, S., Li, X., Li, J., Zhang, R., & Yu, W. (2017). Acetylation promotes TyrRS nuclear translocation to prevent oxidative damage. *Proceedings of the National Academy of Sciences of the United States of America*, *114*(4), 687–692. https://doi.org/10.1073/pnas.1608488114

Caprara, M. G., Mohr, G., & Lambowitz, A. M. (1996). A tyrosyl-tRNA synthetase protein induces tertiary folding of the group I intron catalytic core. *Journal of Molecular Biology*, *257*(3), 512–531. https://doi.org/10.1006/jmbi.1996.0182

Carmi-Levy, I., Yannay-Cohen, N., Kay, G., Razin, E., & Nechushtan, H. (2008). Diadenosine Tetraphosphate Hydrolase Is Part of the Transcriptional Regulation Network in Immunologically Activated Mast Cells. *Molecular and Cellular Biology*, *28*(18), 5777–5784. https://doi.org/10.1128/mcb.00106-08

Carter, C. W. (2017). Coding of Class I and II Aminoacyl-tRNA Synthetases. In *Advances in Experimental Medicine and Biology* (Vol. 966, pp. 103–148). Springer New York LLC. https://doi.org/10.1007/5584_2017_93

Cascales, H. S., Burdova, K., Middleton, A., Kuzin, V., Müllers, E., Stoy, H., Baranello, L., Macurek, L., & Lindqvist, A. (2021). Cyclin A2 localises in the cytoplasm at the S/G2 transition to

activate PLK1. *Life Science Alliance*, *4*(3), 1–15. https://doi.org/10.26508/lsa.202000980
Chacinska, A., Koehler, C. M., Milenkovic, D., Lithgow, T., & Pfanner, N. (2009). Importing Mitochondrial Proteins: Machineries and Mechanisms. *Cell*, *138*(4), 628–644. https://doi.org/10.1016/j.cell.2009.08.005
Chan, D. C. (2012). Fusion and fission: Interlinked processes critical for mitochondrial health. *Annual Review of Genetics*, *46*, 265–287. https://doi.org/10.1146/annurev-genet-110410-132529
Chandel, N. S. (2015). Evolution of Mitochondria as Signaling Organelles. In *Cell Metabolism* (Vol. 22, Issue 2, pp. 204–206). Cell Press. https://doi.org/10.1016/j.cmet.2015.05.013
Chimnaronk, S., Gravers Jeppesen, M., Suzuki, T., Nyborg, J., & Watanabe, K. (2005). Dual-mode recognition of noncanonical tRNAs(Ser) by seryl-tRNA synthetase in mammalian mitochondria. *The EMBO Journal*, *24*(19), 3369–3379. https://doi.org/10.1038/SJ.EMBOJ.7600811
Chrzanowska-Lightowlers, Z. M. A., Pajak, A., & Lightowlers, R. N. (2011). Termination of protein synthesis in mammalian mitochondria. In *Journal of Biological Chemistry* (Vol. 286, Issue 40, pp. 34479–34485). J Biol Chem. https://doi.org/10.1074/jbc.R111.290585
Ciesielski, G. L., Oliveira, M. T., & Kaguni, L. S. (2016). Animal Mitochondrial DNA Replication. In *Enzymes* (Vol. 39, pp. 255–292). Academic Press. https://doi.org/10.1016/bs.enz.2016.03.006
Ciesielski, Grzegorz L, Oliveira, M. T., & Kaguni, L. S. (2016). Animal Mitochondrial DNA Replication. *Enzymes*, *39*, 255–292. https://doi.org/10.1016/bs.enz.2016.03.006
Crevel, I., Crevel, G., Gostan, T., de Renty, C., Coulon, V., & Cotterill, S. (2011). Decreased MCM2-6 in Drosophila S2 cells does not generate significant DNA damage or cause a marked increase in sensitivity to replication interference. *PloS One*, *6*(11). https://doi.org/10.1371/JOURNAL.PONE.0027101
Crick F. H. (1958). On protein synthesis. *Symposia of the Society for Experimental Biology*, *12*, 138–163. http://s3.amazonaws.com/academia.edu.documents/31353481/Symp_Soc_Exp_Biol_1958_Crick_on_protein_synthesis.pdf?AWSAccessKeyId=AKIAIWOWYYGZ2Y53UL3A&Expires=1493406505&Signature=Pj68wjQq8HUhOBMD3niX5IHiQpM%253D&response-content-disposition=inline%253B filena
Crick, F. H. C. (1963). On the genetic code. *Science*, *139*(3554), 461–464. https://doi.org/10.1126/science.139.3554.461
Cusack, S., Berthet-Colominas, C., Härtlein, M., Nassar, N., & Leberman, R. (1990). A second class of synthetase structure revealed by X-ray analysis of Escherichia coli seryl-tRNA synthetase at 2.5 Å. *Nature 1990 347:6290*, *347*(6290), 249–255. https://doi.org/10.1038/347249A0
Dang, F., Nie, • Li, & Wei, W. (2021). Ubiquitin signaling in cell cycle control and tumorigenesis. *Cell Death & Differentiation*, *28*, 427–438. https://doi.org/10.1038/s41418-020-00648-0
Dardel, F., Panvert, M., & Fayat, G. (1990). Transcription and regulation of expression of the Escherichia coli methionyl-tRNA synthetase gene. *MGG Molecular & General Genetics*, *223*(1), 121–133. https://doi.org/10.1007/BF00315804
Datar, S. A., Jacobs, H. W., Cruz, A. F. A. de la, Lehner, C. F., & Edgar, B. A. (2000). The Drosophila Cyclin D–Cdk4 complex promotes cellular growth. *The EMBO Journal*, *19*(17), 4543. https://doi.org/10.1093/EMBOJ/19.17.4543
Davidov, Y., & Jurkevitch, E. (2009). Predation between prokaryotes and the origin of eukaryotes. *BioEssays*, *31*(7), 748–757. https://doi.org/10.1002/bies.200900018
De Potter, B. (2020). *The evolution of SLIMP: a Seryl-tRNA synthethase 2 paralog in invertebrates*.
de Vries, H. I., Uyetake, L., Lemstra, W., Brunsting, J. F., Su, T. T., Kampinga, H. H., & Sibon, O. C. M. (2005). Grp/DChk1 is required for G2-M checkpoint activation in Drosophila S2 cells, whereas Dmnk/DChk2 is dispensable. *Journal of Cell Science*, *118*(9), 1833–1842.

https://doi.org/10.1242/jcs.02309
Deinert, K., Fasiolo, F., Hurt, E. C., & Simos, G. (2001). Arc1p Organizes the Yeast Aminoacyl-tRNA Synthetase Complex and Stabilizes Its Interaction with the Cognate tRNAs. *Journal of Biological Chemistry*, *276*(8), 6000–6008. https://doi.org/10.1074/jbc.M008682200
Dever, T. E., & Green, R. (2012). The elongation, termination, and recycling phases of translation in eukaryotes. *Cold Spring Harbor Perspectives in Biology*, *4*(7), 1–16. https://doi.org/10.1101/cshperspect.a013706
Dewar, J. M., & Walter, J. C. (2017). Mechanisms of DNA replication termination. *Nature Reviews Molecular Cell Biology 2017 18:8*, *18*(8), 507–516. https://doi.org/10.1038/nrm.2017.42
Didiasova, M., Schaefer, L., & Wygrecka, M. (2019). When place matters: Shuttling of enolase-1 across cellular compartments. In *Frontiers in Cell and Developmental Biology* (Vol. 7, Issue APR, p. 61). Frontiers Media S.A. https://doi.org/10.3389/fcell.2019.00061
Dominguez-Sola, D., & Gautier, J. (2014). MYC and the Control of DNA Replication. *Cold Spring Harbor Perspectives in Medicine*, *4*(6), a014423. https://doi.org/10.1101/CSHPERSPECT.A014423
Doudna, J. A., & Charpentier, E. (2014). The new frontier of genome engineering with CRISPR-Cas9. *Science*, *346*(6213). https://doi.org/10.1126/SCIENCE.1258096
Dubrovsky, E. B., Dubrovskaya, V. A., Levinger, L., Schiffer, S., & Marchfelder, A. (2004). Drosophila Rnase Z processes mitochondrial and nuclear pre-tRNA 3′ ends in vivo. *Nucleic Acids Research*, *32*(1), 255–262. https://doi.org/10.1093/nar/gkh182
Dudek, J., Rehling, P., & van der Laan, M. (2013). Mitochondrial protein import: Common principles and physiological networks. *Biochimica et Biophysica Acta - Molecular Cell Research*, *1833*(2), 274–285. https://doi.org/10.1016/j.bbamcr.2012.05.028
Duia, W., Weia, B., Hec, F., Lua, W., Lia, C., Lianga, X., Maa, J., & Jiaoa, R. (2013). The Drosophila F-box protein dSkp2 regulates cell proliferation by targeting Dacapo for degradation. *Molecular Biology of the Cell*, *24*(11), 1676–1687. https://doi.org/10.1091/MBC.E12-10-0772
Dukaj, L., & Rhind, N. (2021). The capacity of origins to load MCM establishes replication timing patterns. *PLOS Genetics*, *17*(3), e1009467. https://doi.org/10.1371/JOURNAL.PGEN.1009467
Duronio, R. J., & Xiong, Y. (2013). Signaling pathways that control cell proliferation. *Cold Spring Harbor Perspectives in Biology*, *5*(3). https://doi.org/10.1101/cshperspect.a008904
Dyson, N. (1998). The regulation of E2F by pRB-family proteins. *Genes & Development*, *12*(15), 2245–2262. https://doi.org/10.1101/GAD.12.15.2245
Echevarría, L., Clemente, P., Herńandez-Sierra, R., Gallardo, M. E., Ferńandez-Moreno, M. A., & Garesse, R. (2014). Glutamyl-tRNAGln amidotransferase is essential for mammalian mitochondrial translation in vivo. *Biochemical Journal*, *460*(1), 91–101. https://doi.org/10.1042/BJ20131107
Eliyahu, E., Pnueli, L., Melamed, D., Scherrer, T., Gerber, A., Pines, O., Rapaport, D., & Arava, Y. (2010). Tom20 mediates localization of mRNAs to mitochondria in a translation-dependent manner. *Molecular and Cellular Biology*, *30*(1), 284–294. https://doi.org/10.1128/MCB.00651-09
English, J., Mean Son, J., Dafne Cardamone, M., Lee, C., & Perissi, V. (2020). Decoding the rosetta stone of mitonuclear communication. *Pharmacological Research*, *161*, 1043–6618. https://doi.org/10.1016/j.phrs.2020.105161
Fan, L., Sanschagrin, P. C., Kaguni, L. S., & Kuhn, L. A. (1999). The accessory subunit of mtDNA polymerase shares structural homology with aminoacyl-tRNA synthetases: Implications for a dual role as a primer recognition factor and processivity clamp. *Proceedings of the National Academy of Sciences of the United States of America*, *96*(17), 9527–9532. https://doi.org/10.1073/pnas.96.17.9527
Faye, G., & Sor, F. (1977). Analysis of mitochondrial ribosomal proteins of Saccharomyces

cerevisiae by two dimensional polyacrylamide gel electrophoresis. *MGG Molecular & General Genetics*, *155*(1), 27–34. https://doi.org/10.1007/BF00268557

Federico Comoglio, Schlumpf, T., Schmid, V., Remo, R., Beisel, C., & Paro, R. (2015). High-resolution profiling of Drosophila replication start sites reveals a DNA shape and chromatin signature of metazoan origins. *Cell Reports*, *11*(5), 821–834. https://doi.org/10.1016/J.CELREP.2015.03.070

Fernandez-Marcos, P. J., & Auwerx, J. (2011). Regulation of PGC-1α, a nodal regulator of mitochondrial biogenesis. *American Journal of Clinical Nutrition*, *93*(4). https://doi.org/10.3945/ajcn.110.001917

Fessler, E., Eckl, E. M., Schmitt, S., Mancilla, I. A., Meyer-Bender, M. F., Hanf, M., Philippou-Massier, J., Krebs, S., Zischka, H., & Jae, L. T. (2020). A pathway coordinated by DELE1 relays mitochondrial stress to the cytosol. *Nature*, *579*(7799), 433–437. https://doi.org/10.1038/s41586-020-2076-4

Fetterman, J. L., & Ballinger, S. W. (2019). Mitochondrial genetics regulate nuclear gene expression through metabolites. In *Proceedings of the National Academy of Sciences of the United States of America* (Vol. 116, Issue 32, pp. 15763–15765). National Academy of Sciences. https://doi.org/10.1073/pnas.1909996116

Fischer, M., & Müller, G. A. (2017). Cell cycle transcription control : DREAM / MuvB and RB-E2F complexes. *Critical Reviews in Biochemistry and Molecular Biology*, *0*(0), 638–662. https://doi.org/10.1080/10409238.2017.1360836

Fisher, D., Krasinska, L., Coudreuse, D., & La Nová, B. (2012). Phosphorylation network dynamics in the control of cell cycle transitions. *Journal of Cell Science*, *125*, 4703–4711. https://doi.org/10.1242/jcs.106351

Franz, A., Brunner, E., & Basler, K. (2017). Generation of genome-modified *Drosophila* cell lines using SwAP. *Fly*, *11*(4), 1–9. https://doi.org/10.1080/19336934.2017.1372068

Frolov, M. V, Huen, D. S., Stevaux, O., Dimova, D., Balczarek-strang, K., Elsdon, M., & Dyson, N. J. (2001). *Functional antagonism between E2F family members*. 2146–2160. https://doi.org/10.1101/gad.903901.repressor

Frugier, M., & Giegé, R. (2003). Yeast aspartyl-tRNA synthetase binds specifically its own mRNA. *Journal of Molecular Biology*, *331*(2), 375–383. https://doi.org/10.1016/S0022-2836(03)00767-8

Galluzzi, L., Kepp, O., Trojel-Hansen, C., & Kroemer, G. (2012). Mitochondrial control of cellular life, stress, and death. In *Circulation Research* (Vol. 111, Issue 9, pp. 1198–1207). Circ Res. https://doi.org/10.1161/CIRCRESAHA.112.268946

Gambus, A. (2017). Termination of Eukaryotic Replication Forks. *Advances in Experimental Medicine and Biology*, *1042*, 163–187. https://doi.org/10.1007/978-981-10-6955-0_8

Garesse, R. (1988). Drosophila melanogaster mitochondrial DNA: Gene organization and evolutionary considerations. *Genetics*, *118*(4), 649–663. https://doi.org/10.1093/genetics/118.4.649

Garesse, Rafael, & Kaguni, L. S. (2005). A Drosophila model of mitochondrial DNA replication: Proteins, genes and regulation. In *IUBMB Life* (Vol. 57, Issue 8, pp. 555–561). IUBMB Life. https://doi.org/10.1080/15216540500215572

Garin, S., Levi, O., Cohen, B., Golani-Armon, A., & Arava, Y. (2020). Localization and RNA Binding of Mitochondrial Aminoacyl tRNA Synthetases. *Genes*, *11*(10), 1–20. https://doi.org/10.3390/GENES11101185

Gaur, R., Grasso, D., Datta, P. P., Krishna, P. D. V., Das, G., Spencer, A., Agrawal, R. K., Spremulli, L., & Varshney, U. (2008). A Single Mammalian Mitochondrial Translation Initiation Factor Functionally Replaces Two Bacterial Factors. *Molecular Cell*, *29*(2), 180–190. https://doi.org/10.1016/j.molcel.2007.11.021

Georgescua, R., Yuanc, Z., Lin Baic, 1, R. de L. A. S., Jingchuan Sunc, D. Z., Olga Yurievaa, b, H. L., Michael E. O'Donnella, b, 2, & ADepartment. (2017). Structure of eukaryotic CMG helicase at a replication fork and implications to replisome architecture and origin initiation.

Proceedings of the National Academy of Sciences of the United States of America, *114*(5), E697–E706. https://doi.org/10.1073/PNAS.1620500114

Geslain, R., & De Pouplana, L. R. (2004). Regulation of RNA function by aminoacylation and editing? *Trends in Genetics*, *20*(12), 604–610. https://doi.org/10.1016/j.tig.2004.09.012

Gheghiani, L., Loew, D., Lombard, B., Mansfeld, J., & Gavet, O. (2017). PLK1 Activation in Late G2 Sets Up Commitment to Mitosis. *Cell Reports*, *19*, 2060–2073. https://doi.org/10.1016/j.celrep.2017.05.031

Giegé, R., Sissler, M., & Florentz, C. (1998). Universal rules and idiosyncratic features in tRNA identity. In *Nucleic Acids Research* (Vol. 26, Issue 22, pp. 5017–5035). Oxford University Press. https://doi.org/10.1093/nar/26.22.5017

Golani-Armon, A., & Arava, Y. (2016). Localization of Nuclear-Encoded mRNAs to Mitochondria Outer Surface. *Biochemistry. Biokhimiia*, *81*(10), 1038–1043. https://doi.org/10.1134/S0006297916100023

Gold, V. A., Chroscicki, P., Bragoszewski, P., & Chacinska, A. (2017). Visualization of cytosolic ribosomes on the surface of mitochondria by electron cryo-tomography. *EMBO Reports*, *18*(10), 1786–1800. https://doi.org/10.15252/embr.201744261

Gonzalez-Roca, E., Garcia-Albéniz, X., Rodriguez-Mulero, S., Gomis, R. R., Kornacker, K., & Auer, H. (2010). Accurate Expression Profiling of Very Small Cell Populations. *PLOS ONE*, *5*(12), e14418. https://doi.org/10.1371/JOURNAL.PONE.0014418

Grant, G. D., & Cook, J. G. (2017). The Temporal Regulation of S Phase Proteins During G1. *Advances in Experimental Medicine and Biology*, *1042*, 335. https://doi.org/10.1007/978-981-10-6955-0_16

Gray, M. W. (2012). Mitochondrial evolution. *Cold Spring Harbor Perspectives in Biology*, *4*(9). https://doi.org/10.1101/cshperspect.a011403

Gray, M. W., Burger, G., & Lang, B. F. (1999). Mitochondrial evolution. In *Science* (Vol. 283, Issue 5407, pp. 1476–1481). Science. https://doi.org/10.1126/science.283.5407.1476

Guitart, T., Bernardo, T. L., Sagale, J., Stratmann, T., & Bernue, J. (2010). *New Aminoacyl-tRNA Synthetase-like Protein in Insecta with an Essential Mitochondrial Function * □*. *285*(49), 38157–38166. https://doi.org/10.1074/jbc.M110.167486

Guitart, T., Bernardo, T. L., Sagalés, J., Stratmann, T., Bernués, J., & De Pouplana, L. R. (2010). New aminoacyl-tRNA synthetase-like protein in insecta with an essential mitochondrial function. *Journal of Biological Chemistry*, *285*(49), 38157–38166. https://doi.org/10.1074/jbc.M110.167486

Guitart, T., Picchioni, D., & Pin, D. (2013). *Human mitochondrial disease-like symptoms caused by a reduced tRNA aminoacylation activity in flies*. *41*(13), 6595–6608. https://doi.org/10.1093/nar/gkt402

Guo, M., Schimmel, P., & Yang, X. L. (2010). Functional expansion of human tRNA synthetases achieved by structural inventions. In *FEBS Letters* (Vol. 584, Issue 2, pp. 434–442). NIH Public Access. https://doi.org/10.1016/j.febslet.2009.11.064

Guo, M., Yang, X. L., & Schimmel, P. (2010). New functions of aminoacyl-tRNA synthetases beyond translation. In *Nature Reviews Molecular Cell Biology* (Vol. 11, Issue 9, pp. 668–674). Nat Rev Mol Cell Biol. https://doi.org/10.1038/nrm2956

Guo, R. T., Chong, Y. E., Guo, M., & Yang, X. L. (2009). Crystal structures and biochemical analyses suggest a unique mechanism and role for human Glycyl-tRNA synthetase in Ap4A homeostasis. *Journal of Biological Chemistry*, *284*(42), 28968–28976. https://doi.org/10.1074/jbc.M109.030692

Guo, X., Aviles, G., Liu, Y., Tian, R., Unger, B. A., Lin, Y. H. T., Wiita, A. P., Xu, K., Correia, M. A., & Kampmann, M. (2020). Mitochondrial stress is relayed to the cytosol by an OMA1–DELE1–HRI pathway. *Nature*, *579*(7799), 427–432. https://doi.org/10.1038/s41586-020-2078-2

Gupte, T. M. (2015). Mitochondrial Fragmentation Due to Inhibition of Fusion Increases Cyclin B through Mitochondrial Superoxide Radicals. *PLOS ONE*, *10*(5), e0126829. https://doi.org/10.1371/JOURNAL.PONE.0126829

Haapaniemi, E., Botla, S., Persson, J., Schmierer, B., & Taipale, J. (2018). CRISPR–Cas9 genome editing induces a p53-mediated DNA damage response. *Nature Medicine*, *24*, 927–930. https://doi.org/10.1038/s41591-018-0049-z

Hällberg, B. M., & Larsson, N. G. (2014). Making proteins in the powerhouse. In *Cell Metabolism* (Vol. 20, Issue 2, pp. 226–240). Cell Press. https://doi.org/10.1016/j.cmet.2014.07.001

Han, J. M., Jeong, S. J., Park, M. C., Kim, G., Kwon, N. H., Kim, H. K., Ha, S. H., Ryu, S. H., & Kim, S. (2012). Leucyl-tRNA synthetase is an intracellular leucine sensor for the mTORC1-signaling pathway. *Cell*, *149*(2), 410–424. https://doi.org/10.1016/j.cell.2012.02.044

Harashima, H., Dissmeyer, N., & Schnittger, A. (2013). Cell cycle control across the eukaryotic kingdom. In *Trends in Cell Biology* (Vol. 23, Issue 7, pp. 345–356). Elsevier. https://doi.org/10.1016/j.tcb.2013.03.002

Hartmann, R. K., Gößringer, M., Späth, B., Fischer, S., & Marchfelder, A. (2009). The Making of tRNAs and More - RNase P and tRNase Z. In *Progress in Molecular Biology and Translational Science* (Vol. 85, Issue C, pp. 319–368). Prog Mol Biol Transl Sci. https://doi.org/10.1016/S0079-6603(08)00808-8

Hartwell, L. H., & Weinert, T. A. (1989). Checkpoints: Controls that ensure the order of cell cycle events. *Science*, *246*(4930), 629–634. https://doi.org/10.1126/science.2683079

Hellen, C. U. T. (2018). Translation termination and ribosome recycling in eukaryotes. *Cold Spring Harbor Perspectives in Biology*, *10*(10). https://doi.org/10.1101/cshperspect.a032656

Hernández, G., Altmann, M., & Lasko, P. (2010). Origins and evolution of the mechanisms regulating translation initiation in eukaryotes. In *Trends in Biochemical Sciences* (Vol. 35, Issue 2, pp. 63–73). Elsevier Current Trends. https://doi.org/10.1016/j.tibs.2009.10.009

Herr, A., Longworth, M., Ji, J. Y., Korenjak, M., Macalpine, D. M., & Dyson, N. J. (2012). Identification of E2F target genes that are rate limiting for dE2F1-dependent cell proliferation. *Developmental Dynamics*, *241*(11), 1695–1707. https://doi.org/10.1002/DVDY.23857

Heuvel, S. van den, & Dyson, N. J. (2008). Conserved functions of the pRB and E2F families. *Nature Reviews Molecular Cell Biology 2008 9:9*, *9*(9), 713–724. https://doi.org/10.1038/NRM2469

Holley, R. W., Apgar, J., Everett, G. A., Madison, J. T., Marquisee, M., Merrill, S. H., Penswick, J. R., & Zamir, A. (1965). Structure of a ribonucleic acid. *Science*, *147*(3664), 1462–1465. https://doi.org/10.1126/science.147.3664.1462

Hsu, P. D., Scott, D. A., Weinstein, J. A., Ran, F. A., Konermann, S., Agarwala, V., Li, Y., Fine, E. J., Wu, X., Shalem, O., Cradick, T. J., Marraffini, L. A., Bao, G., & Zhang, F. (2013). DNA targeting specificity of RNA-guided Cas9 nucleases. *Nature Biotechnology*, *31*(9), 827–833. https://doi.org/10.1038/nbt.2647

Hua, B. L., & Orr-Weaver, T. L. (2017). DNA Replication Control During Drosophila Development: Insights into the Onset of S Phase, Replication Initiation, and Fork Progression Insights into Regulation of DNA Replication from Localized Changes in DNA Copy Number 35. *Genetics*, *207*(September), 29–47. https://doi.org/10.1534/genetics.115.186627

Ibba, M., & Soll, D. (2000). Aminoacyl-tRNA synthesis. In *Annual Review of Biochemistry* (Vol. 69, pp. 617–650). Annu Rev Biochem. https://doi.org/10.1146/annurev.biochem.69.1.617

Ibba, Michael, & Francklyn, C. (2004). Turning tRNA upside down: When aminoacylation is not a prerequisite to protein synthesis. In *Proceedings of the National Academy of Sciences of the United States of America* (Vol. 101, Issue 20, pp. 7493–7494). National Academy of Sciences. https://doi.org/10.1073/pnas.0402276101

Ihry, R. J., Worringer, K. A., Salick, M. R., Frias, E., Ho, D., Theriault, K., Kommineni, S., Chen, J., Sondey, M., Ye, C., Randhawa, R., Kulkarni, T., Yang, Z., McAllister, G., Russ, C., Reece-Hoyes, J., Forrester, W., Hoffman, G. R., Dolmetsch, R., & Kaykas, A. (2018). p53 inhibits CRISPR–Cas9 engineering in human pluripotent stem cells. *Nature Medicine 2018 24:7*, *24*(7), 939–946. https://doi.org/10.1038/s41591-018-0050-6

Ingham, M., & Schwartz, G. K. (2017). Cell-Cycle Therapeutics Come of Age. *Https://Doi.Org/10.1200/JCO.2016.69.0032*, *35*(25), 2949–2959. https://doi.org/10.1200/JCO.2016.69.0032

Ishihara, N., Fujita, Y., Oka, T., & Mihara, K. (2006). Regulation of mitochondrial morphology through proteolytic cleavage of OPA1. *The EMBO Journal*, *25*(13), 2966. https://doi.org/10.1038/SJ.EMBOJ.7601184

Ivar Ilves, Petojevic, T., Pesavento, J. J., & Botchan, M. R. (2010). Activation of the MCM2-7 helicase by association with Cdc45 and GINS proteins. *Molecular Cell*, *37*(2), 247–258. https://doi.org/10.1016/J.MOLCEL.2009.12.030

Iyer, D. R., & Rhind, N. (2017). The Intra-S Checkpoint Responses to DNA Damage. *Genes 2017, Vol. 8, Page 74*, *8*(2), 74. https://doi.org/10.3390/GENES8020074

Jackson, R. J., Hellen, C. U. T., & Pestova, T. V. (2010). The mechanism of eukaryotic translation initiation and principles of its regulation. In *Nature Reviews Molecular Cell Biology* (Vol. 11, Issue 2, pp. 113–127). Nature Publishing Group. https://doi.org/10.1038/nrm2838

Jackson, R. J., Hellen, C. U. T., & Pestova, T. V. (2012). Termination and post-termination events in eukaryotic translation. In *Advances in Protein Chemistry and Structural Biology* (Vol. 86, pp. 45–93). Academic Press Inc. https://doi.org/10.1016/B978-0-12-386497-0.00002-5

Jin, M. (2019). Unique roles of tryptophanyl-tRNA synthetase in immune control and its therapeutic implications. *Experimental & Molecular Medicine*, *51*, 1. https://doi.org/10.1038/s12276-018-0196-9

Jinek, M., East, A., Cheng, A., Lin, S., Ma, E., & Doudna, J. (2013). RNA-programmed genome editing in human cells. *ELife*, *2013*(2). https://doi.org/10.7554/ELIFE.00471

Jõers, P., & Jacobs, H. T. (2013). Analysis of Replication Intermediates Indicates That Drosophila melanogaster Mitochondrial DNA Replicates by a Strand-Coupled Theta Mechanism. *PLoS ONE*, *8*(1). https://doi.org/10.1371/journal.pone.0053249

Jõers, P., Lewis, S. C., Fukuoh, A., Parhiala, M., Ellilä, S., Holt, I. J., & Jacobs, H. T. (2013). Mitochondrial Transcription Terminator Family Members mTTF and mTerf5 Have Opposing Roles in Coordination of mtDNA Synthesis. *PLoS Genetics*, *9*(9). https://doi.org/10.1371/journal.pgen.1003800

Johanson, K., Hoang, T., Sheth, M., & Hyman, L. E. (2003). GRS1, a yeast tRNA synthetase with a role in mRNA 3′ end formation. *Journal of Biological Chemistry*, *278*(38), 35923–35930. https://doi.org/10.1074/jbc.M304978200

Johnson, D. G., Kiyoshi Ohtani, & Nevins, J. R. (1994). Autoregulatory control of E2F1 expression in response to positive and negative regulators of cell cycle progression. *Genes & Development*, *8*(13), 1514–1525. https://doi.org/10.1101/GAD.8.13.1514

Johnson, E. S., & Kornbluth, S. (2012). Phosphatases Driving Mitosis: Pushing the Gas and Lifting the Brakes. *Progress in Molecular Biology and Translational Science*, *106*, 327–341. https://doi.org/10.1016/B978-0-12-396456-4.00008-0

Jones, R. M., Mortusewicz, O., Afzal, I., Lorvellec, M., García, P., Helleday, T., & Petermann, E. (2012). Increased replication initiation and conflicts with transcription underlie Cyclin E-induced replication stress. *Oncogene 2013 32:32*, *32*(32), 3744–3753. https://doi.org/10.1038/onc.2012.387

Jónsson, Z., & Hübscher, U. (1997). Proliferating cell nuclear antigen: more than a clamp for DNA polymerases. *BioEssays : News and Reviews in Molecular, Cellular and Developmental Biology*, *19*(11), 967–975. https://doi.org/10.1002/BIES.950191106

Jukes, T. H., & Osawa, S. (1993). Evolutionary changes in the genetic code. In *Comparative Biochemistry and Physiology -- Part B: Biochemistry and* (Vol. 106, Issue 3, pp. 489–494). Comp Biochem Physiol B. https://doi.org/10.1016/0305-0491(93)90122-L

Kaelin, W. G., & McKnight, S. L. (2013). Influence of metabolism on epigenetics and disease. In *Cell* (Vol. 153, Issue 1, pp. 56–69). Elsevier B.V. https://doi.org/10.1016/j.cell.2013.03.004

Kalderon, B., & Pines, O. (2014). Protein folding as a driving force for dual protein targeting in eukaryotes. In *Frontiers in Molecular Biosciences* (Vol. 1, Issue NOV). Frontiers Media S.A.

https://doi.org/10.3389/fmolb.2014.00023
Kamiyama, D., Sekine, S., Barsi-Rhyne, B., Hu, J., Chen, B., Gilbert, L. A., Ishikawa, H., Leonetti, M. D., Marshall, W. F., Weissman, J. S., & Huang, B. (2016). Versatile protein tagging in cells with split fluorescent protein. *Nature Communications*, *7*, 1–9. https://doi.org/10.1038/ncomms11046
Kanca, O., Zirin, J., Garcia-Marques, J., Knight, S., Yang-Zhou, D., Amador, G., Chung, H., Zuo, Z., Ma, L., He, Y., Lin, W., Fang, Y., Ge, M., Yamamoto, S., Schulze, K., Hu, Y., Spradling, A., Mohr, S., Perrimon, N., & Bellen, H. (2019). An efficient CRISPR-based strategy to insert small and large fragments of DNA using short homology arms. *ELife*, *8*, 1–22. https://doi.org/10.7554/ELIFE.51539
Karniely, S., & Pines, O. (2005). *Single translation–dual destination: mechanisms of dual protein targeting in eukaryotes*. *6*(5). https://doi.org/10.1038/sj.embor.7400394
Kearse, M., & Wilusz, J. (2017). Non-AUG translation: a new start for protein synthesis in eukaryotes. *Genes & Development*, *31*(17), 1717–1731. https://doi.org/10.1101/GAD.305250.117
Kenichi, Yoshida, & Inoue, I. (2004). Regulation of Geminin and Cdt1 expression by E2F transcription factors. *Oncogene*, *23*(21), 3802–3812. https://doi.org/10.1038/SJ.ONC.1207488
Kim, M. Y., Zhang, T., & Kraus, W. L. (2005). Poly(ADP-ribosyl)ation by PARP-1: "PAR-laying" NAD+ into a nuclear signal. In *Genes and Development* (Vol. 19, Issue 17, pp. 1951–1967). Cold Spring Harbor Laboratory Press. https://doi.org/10.1101/gad.1331805
Kim, S., Yoon, I., Son, J., Park, J., Kim, K., Lee, J.-H., Park, S.-Y., Kang, B. S., Han, J. M., Hwang, K. Y., & Kim, S. (2021). Leucine-sensing mechanism of leucyl-tRNA synthetase 1 for mTORC1 activation. *Cell Reports*, *35*(4), 109031. https://doi.org/10.1016/j.celrep.2021.109031
Ko, Y. G., Kang, Y. S., Kim, E. K., Park, S. G., & Kim, S. (2000). Nucleolar localization of human methionyl-tRNA synthetase and its role in ribosomal RNA synthesis. *Journal of Cell Biology*, *149*(3), 567–574. https://doi.org/10.1083/jcb.149.3.567
Ko, Y. G., Kim, E. K., Kim, T., Park, H., Park, H. S., Choi, E. J., & Kim, S. (2001). Glutamine-dependent Antiapoptotic Interaction of Human Glutaminyl-tRNA Synthetase with Apoptosis Signal-regulating Kinase 1. *Journal of Biological Chemistry*, *276*(8), 6030–6036. https://doi.org/10.1074/jbc.M006189200
Koch-Nolte, F., Fischer, S., Haag, F., & Ziegler, M. (2011). Compartmentation of NAD+-dependent signalling. In *FEBS Letters* (Vol. 585, Issue 11, pp. 1651–1656). No longer published by Elsevier. https://doi.org/10.1016/j.febslet.2011.03.045
Kosugi, S., Hasebe, M., Matsumura, N., Takashima, H., Miyamoto-Sato, E., Tomita, M., & Yanagawa, H. (2009). Six Classes of Nuclear Localization Signals Specific to Different Binding Grooves of Importin * □ S. *Journal of Biological Chemistry*, *284*(1), 478 –485. https://doi.org/10.1074/jbc.M807017200
Kosugi, S., Hasebe, M., Tomita, M., & Yanagawa, H. (2009). Systematic identification of cell cycle-dependent yeast nucleocytoplasmic shuttling proteins by prediction of composite motifs. *Proceedings of the National Academy of Sciences of the United States of America*, *106*(25), 10171–10176. https://doi.org/10.1073/PNAS.0900604106
Kroeger, P., Shoue, D., Mezzacappa, F., Gerlach, G., Wingert, R., & Schulz, R. (2013). Knockdown of SCF(Skp2) function causes double-parked accumulation in the nucleus and DNA re-replication in Drosophila plasmatocytes. *PloS One*, *8*(10). https://doi.org/10.1371/JOURNAL.PONE.0079019
Kunz, B. A., Kohalmi, S. E., Kunkel, T. A., Mathews, C. K., McIntosh, E. M., & Reidy, J. A. (1994). Deoxyribonucleoside triphosphate levels: A critical factor in the maintenance of genetic stability. *Mutation Research/Reviews in Genetic Toxicology*, *318*(1), 1–64. https://doi.org/10.1016/0165-1110(94)90006-X
Kyriacou, S. V., & Deutscher, M. P. (2008). An Important Role for the Multienzyme Aminoacyl-tRNA Synthetase Complex in Mammalian Translation and Cell Growth. *Molecular Cell*,

29(4), 419–427. https://doi.org/10.1016/j.molcel.2007.11.038
Lashkevich, K. A., & Dmitriev, S. E. (2021). mRNA Targeting, Transport and Local Translation in Eukaryotic Cells: From the Classical View to a Diversity of New Concepts. *Molecular Biology*. https://doi.org/10.1134/S0026893321030080
Lee, C., Zeng, J., Drew, B. G., Sallam, T., Martin-Montalvo, A., Wan, J., Kim, S. J., Mehta, H., Hevener, A. L., De Cabo, R., & Cohen, P. (2015). The mitochondrial-derived peptide MOTS-c promotes metabolic homeostasis and reduces obesity and insulin resistance. *Cell Metabolism*, *21*(3), 443–454. https://doi.org/10.1016/j.cmet.2015.02.009
Lee, Y.-N., & Razin, E. (2005). Nonconventional Involvement of LysRS in the Molecular Mechanism of USF2 Transcriptional Activity in FcεRI-Activated Mast Cells. *Molecular and Cellular Biology*, *25*(20), 8904–8912. https://doi.org/10.1128/mcb.25.20.8904-8912.2005
Lefai, E., Fernández-Moreno, M. A., Alahari, A., Kaguni, L. S., & Garesse, R. (2000). Differential Regulation of the Catalytic and Accessory Subunit Genes of Drosophila Mitochondrial DNA Polymerase *. *Journal of Biological Chemistry*, *275*(42), 33123–33133. https://doi.org/10.1074/JBC.M003024200
Lemmens, B., & Lindqvist, A. (2017). *DNA replication and mitotic entry: A brake model for cell cycle progression*. https://doi.org/10.1083/jcb.201909032
Leonard, A. C., & Mechali, M. (2013). DNA replication origins. *Cold Spring Harbor Perspectives in Medicine*, *3*(10), 2–17. https://doi.org/10.1101/cshperspect.a010116
Lesnik, C., Cohen, Y., Atir-Lande, A., Schuldiner, M., & Arava, Y. (2014). OM14 is a mitochondrial receptor for cytosolic ribosomes that supports co-translational import into mitochondria. *Nature Communications*, *5*(1), 1–11. https://doi.org/10.1038/ncomms6711
Lesnik, C., Golani-Armon, A., & Arava, Y. (2015). Localized translation near the mitochondrial outer membrane: An update. *RNA Biology*, *12*(8), 801–809. https://doi.org/10.1080/15476286.2015.1058686
Levi, O., & Arava, Y. (2019a). mRNA association by aminoacyl tRNA synthetase occurs at a putative anticodon mimic and autoregulates translation in response to tRNA levels. *PLoS Biology*, *17*(5), e3000274. https://doi.org/10.1371/journal.pbio.3000274
Levi, O., & Arava, Y. (2019b). mRNA association by aminoacyl tRNA synthetase occurs at a putative anticodon mimic and autoregulates translation in response to tRNA levels. *PLoS Biology*, *17*(5). https://doi.org/10.1371/journal.pbio.3000274
Levi, O., Garin, S., & Arava, Y. (2020). RNA mimicry in post-transcriptional regulation by aminoacyl tRNA synthetases. In *Wiley Interdisciplinary Reviews: RNA* (Vol. 11, Issue 2, p. e1564). Blackwell Publishing Ltd. https://doi.org/10.1002/wrna.1564
Liang, L., Haug, H., Seidel, C., & Gibson. (2014). Functional genomic analysis of the periodic transcriptome in the developing Drosophila wing. *Developmental Cell*, *29*(1), 112–127. https://doi.org/10.1016/J.DEVCEL.2014.02.018
Liesa, M., Palaci´n, M., Palaci´n, P., & Zorzano, A. (2009). *Mitochondrial Dynamics in Mammalian Health and Disease*. https://doi.org/10.1152/physrev.00030.2008.-The
Llanos, S., Megias, D., Blanco-Aparicio, C., Elena Hernández-Encinas, •, Rovira, M., Federico Pietrocola, •, & Serrano, • Manuel. (2019). Lysosomal trapping of palbociclib and its functional implications. *Oncogene*, *38*, 3886–3902. https://doi.org/10.1038/s41388-019-0695-8
Lu, J., Marygold, S. J., Gharib, W. H., & Suter, B. (2015). *The aminoacyl-tRNA synthetases of Drosophila melanogaster*. *June*, 53–61.
Luhur, A., Klueg, K. M., & Zelhof, A. C. (2019). Generating and working with Drosophila cell cultures: Current challenges and opportunities. *Wiley Interdisciplinary Reviews. Developmental Biology*, *8*(3), e339. https://doi.org/10.1002/WDEV.339
Ma, Y, Zhang, L., & Huang, X. (2014). Genome modification by CRISPR/Cas9. *The FEBS Journal*, *281*(23), 5186–5193. https://doi.org/10.1111/FEBS.13110
Ma, Yiqin, & Edgar, B. A. (2021). CDK4: Linking cell size to cell cycle control. *Developmental Cell*, *56*(12), 1695–1696. https://doi.org/10.1016/j.devcel.2021.06.001

Manning, S. A., Dent, L. G., Kondo, S., Zhao, Z. W., Plachta, N., & Harvey, K. F. (2018). Dynamic Fluctuations in Subcellular Localization of the Hippo Pathway Effector Yorkie In Vivo. *Current Biology*, *28*(10), 1651-1660.e4. https://doi.org/10.1016/j.cub.2018.04.018

Marguerite T. et al. (2004). Drosophila double-parked is sufficient to induce re-replication during development and is regulated by cyclin E/CDK2. *Development (Cambridge, England)*, *131*(19), 4807–4818. https://doi.org/10.1242/DEV.01348

Margulis, L. (1967). On the origin of mitosing cells. *Journal of Theoretical Biology*, *14*(3), 255–274. http://www.ncbi.nlm.nih.gov/pubmed/11541390

Martinis, S. A., Plateau, P., Cavarelli, J., & Florentz, C. (1999). Aminoacyl-tRNA synthetases: A family of expanding functions. *EMBO Journal*, *18*(17), 4591–4596. https://doi.org/10.1093/emboj/18.17.4591

Marygold, S. J., Attrill, H., Speretta, E., Warner, K., Magrane, M., Berloco, M., Cotterill, S., Mcvey, M., Rong, Y., & Yamaguchi, M. (2020). *The DNA polymerases of Drosophila melanogaster*. https://doi.org/10.1080/19336934.2019.1710076

Matsukage, A., Hirose, F., Yoo, M.-A., & Yamaguchi, M. (2007). The DRE/DREF transcriptional regulatory system: a master key for cell proliferation. *Biochimica et Biophysica Acta (BBA) - Bioenergetics*, 81–89. https://doi.org/10.1016/j.bbagrm.2007.11.011

Matsushima, Y., Adán, C., Garesse, R., & Kaguni, L. S. (2005). Drosophila mitochondrial transcription factor B1 modulates mitochondrial translation but not transcription or DNA copy number in Schneider cells. *Journal of Biological Chemistry*, *280*(17), 16815–16820. https://doi.org/10.1074/jbc.M500569200

Matsushima, Y., Garesse, R., & Kaguni, L. S. (2004). Drosophila mitochondrial transcription factor B2 regulates mitochondrial DNA copy number and transcription in Schneider cells. *Journal of Biological Chemistry*, *279*(26), 26900–26905. https://doi.org/10.1074/jbc.M401643200

Matsushima, Y., Goto, Y., & Kaguni, L. S. (2010). Mitochondrial Lon protease regulates mitochondrial DNA copy number and transcription by selective degradation of mitochondrial transcription factor A (TFAM). *PNAS*. https://doi.org/10.1073/pnas.1008924107/-/DCSupplemental.www.pnas.org/cgi/doi/10.1073/pnas.1008924107

May, N., Thomer, M., Murnen, K., & Calvi, B. (2005). Levels of the origin-binding protein Double parked and its inhibitor Geminin increase in response to replication stress. *Journal of Cell Science*, *118*(Pt 18), 4207–4217. https://doi.org/10.1242/JCS.02534

Mcbride, H. M. (2018). Mitochondria and endomembrane origins. In *Current Biology* (Vol. 28). https://doi.org/10.1016/j.cub.2018.03.052

McLelland, G. L., Soubannier, V., Chen, C. X., McBride, H. M., & Fon, E. A. (2014). Parkin and PINK1 function in a vesicular trafficking pathway regulating mitochondrial quality control. *EMBO Journal*, *33*(4), 282–295. https://doi.org/10.1002/embj.201385902

Merz, S., & Westermann, B. (2009). Genome-wide deletion mutant analysis reveals genes required for respiratory growth, mitochondrial genome maintenance and mitochondrial protein synthesis in Saccharomyces cerevisiae. *Genome Biology*, *10*(9), R95. https://doi.org/10.1186/gb-2009-10-9-r95

Mirande, M. (1991). Aminoacyl-tRNA synthetases and DNA replication Molecular mimicry between RNAII and tRNALys. *FEBS Letters*, *283*(1), 1–3. https://doi.org/10.1016/0014-5793(91)80539-F

Mireau, H., Lancelin, D., & Small, I. D. (1996). The same Arabidopsis gene encodes both cytosolic and mitochondrial alanyl-tRNA synthetases. *The Plant Cell*, *8*(6), 1027. https://doi.org/10.1105/TPC.8.6.1027

Miseta, A., Woodleys, C. L., Greenberg, J. R., & Slobin, L. I. (1991). Mammalian seryl-tRNA synthetase associates with mRNA in vivo and has homology to elongation factor 1 alpha. In *THE JOURNAL OF BIOLOGICAL CHEMISTRY* (Vol. 266, Issue 29). https://doi.org/10.1016/S0021-9258(18)54975-9

Moldovan, G.-L., Pfander, B., & Jentsch, S. (2007). PCNA, the Maestro of the Replication Fork. *Cell*, *129*, 665–679. https://doi.org/10.1016/j.cell.2007.05.003

Monaghan, R. M., & Whitmarsh, A. J. (2015). Mitochondrial Proteins Moonlighting in the Nucleus. *Trends in Biochemical Sciences*, *40*(12), 728–735. https://doi.org/10.1016/j.tibs.2015.10.003

Monteuuis, G., Miścicka, A., Świrski, M., Zenad, L., Niemitalo, O., Wrobel, L., Alam, J., Chacinska, A., Kastaniotis, A., & Kufel, J. (2019). Non-canonical translation initiation in yeast generates a cryptic pool of mitochondrial proteins. *Nucleic Acids Research*, *47*(11), 5777–5791. https://doi.org/10.1093/NAR/GKZ301

Morrison, D. K. (2012). MAP Kinase Pathways. *Cold Spring Harbor Perspectives in Biology*, *4*(11). https://doi.org/10.1101/CSHPERSPECT.A011254

Nagao, A., Suzuki, T., Katoh, T., Sakaguchi, Y., & Suzuki, T. (2009). Biogenesis of glutaminyl-mt tRNAGln in human mitochondria. *Proceedings of the National Academy of Sciences of the United States of America*, *106*(38), 16209–16214. https://doi.org/10.1073/pnas.0907602106

Nakatsu, T., Kato, H., & Oda, J. (1998). Crystal structure of asparagine synthetase reveals a close evolutionary relationship to class II aminoacyl-tRNA synthetase. *Nature Structural Biology*, *5*(1), 15–19. https://doi.org/10.1038/nsb0198-15

Nancy C Walworth. (2000). Cell-cycle checkpoint kinases. *Current Opinion in Cell Biology*, *12*, 697–704.

Nangle, L. A., Motta, C. M., & Schimmel, P. (2006). Global Effects of Mistranslation from an Editing Defect in Mammalian Cells. *Chemistry and Biology*, *13*(10), 1091–1100. https://doi.org/10.1016/j.chembiol.2006.08.011

Nargund, A. M., Fiorese, C. J., Pellegrino, M. W., Deng, P., & Haynes, C. M. (2015). Mitochondrial and nuclear accumulation of the transcription factor ATFS-1 promotes OXPHOS recovery during the UPRmt. *Molecular Cell*, *58*(1), 123–133. https://doi.org/10.1016/j.molcel.2015.02.008

Nargund, A. M., Pellegrino, M. W., Fiorese, C. J., Baker, B. M., & Haynes, C. M. (2012). Mitochondrial import efficiency of ATFS-1 regulates mitochondrial UPR activation. *Science*, *337*(6094), 587–590. https://doi.org/10.1126/science.1223560

Nicolay, B., Bayarmagnai, B., Islam, A., Lopez-Bigas, N., & Frolov, M. (2011). Cooperation between dE2F1 and Yki/Sd defines a distinct transcriptional program necessary to bypass cell cycle exit. *Genes & Development*, *25*(4), 323–335. https://doi.org/10.1101/GAD.1999211

Nishimura, A., Nasuno, R., Yoshikawa, Y., Jung, M., Ida, T., Matsunaga, T., Morita, M., Takagi, H., Motohashi, H., & Akaike, T. (2019). Mitochondrial cysteinyl-tRNA synthetase is expressed via alternative transcriptional initiation regulated by energy metabolism in yeast cells. *The Journal of Biological Chemistry*, *294*(37), 13781–13788. https://doi.org/10.1074/JBC.RA119.009203

Novoa, E. M., Vargas-Rodriguez, O., Lange, S., Goto, Y., Suga, H., Musier-Forsyth, K., & Ribas De Pouplana, L. (2015). *Ancestral AlaX Editing Enzymes for Control of Genetic Code Fidelity Are Not tRNA-specific **. https://doi.org/10.1074/jbc.M115.640060

Ojala, D., Montoya, J., & Attardi, G. (1981). TRNA punctuation model of RNA processing in human mitochondria. *Nature*, *290*(5806), 470–474. https://doi.org/10.1038/290470a0

Okudaira, K., Ohno, K., Yoshida, H., Asano, M., Hirose, F., & Yamaguchi, M. (2005). Transcriptional regulation of the Drosophila orc2 gene by the DREF pathway. *Biochimica et Biophysica Acta (BBA) - Gene Structure and Expression*, *1732*(1–3), 23–30. https://doi.org/10.1016/J.BBAEXP.2005.10.009

Owusu-ansah, E., Yavari, A., Mandal, S., & Banerjee, U. (2008). *Distinct mitochondrial retrograde signals control the G1-S cell cycle checkpoint*. *40*(3), 356–361. https://doi.org/10.1038/ng.2007.50

Pai, C.-C., & Kearsey, S. E. (2017). A Critical Balance: dNTPs and the Maintenance of Genome

Stability. *Genes*, *8*(2). https://doi.org/10.3390/GENES8020057
Palecek, S. P., Parikh, A. S., & Kron, S. J. (2000). Genetic analysis reveals that FLO11 upregulation and cell polarization independently regulate invasive growth in Saccharomyces cerevisiae. *Genetics*, *156*(3), 1005–1023. https://doi.org/10.1093/genetics/156.3.1005
Pang, Y. L. J., Poruri, K., & Martinis, S. A. (2014). tRNA synthetase: TRNA aminoacylation and beyond. *Wiley Interdisciplinary Reviews: RNA*, *5*(4), 461–480. https://doi.org/10.1002/wrna.1224
Pardee, A. B. (1989). G1 events and regulation of cell proliferation. *Science*, *246*(4930), 603–608. https://doi.org/10.1126/science.2683075
Park, B. J., Kang, J. W., Lee, S. W., Choi, S. J., Shin, Y. K., Ahn, Y. H., Choi, Y. H., Choi, D., Lee, K. S., & Kim, S. (2005). The haploinsufficient tumor suppressor p18 upregulates p53 via interactions with ATM/ATR. *Cell*, *120*(2), 209–221. https://doi.org/10.1016/j.cell.2004.11.054
Park, S.-C., Jia, B., Yang, J.-K., Van, D. Le, Shao, Y. G., Han, S. W., Jeon, Y.-J., Chung, C. H., & Cheong, G.-W. (2006). Oligomeric Structure of the ATP-dependent Protease La (Lon) of Escherichia coli. *Molecules and Cells*, *21*(1), 129–134. http://www.molcells.org/journal/view.html?spage=129&volume=21&number=1
Parker, M. W., Botchan, M. R., & Berger, J. M. (2017). Mechanisms and regulation of DNA replication initiation in eukaryotes. *Critical Reviews in Biochemistry and Molecular Biology*, *52*(2), 107–144. https://doi.org/10.1080/10409238.2016.1274717
Paul, M., & Schimmel, P. (2013). Essential nontranslational functions of tRNA synthetases. *Nature Chemical Biology*, *9*(3), 145–153. https://doi.org/10.1038/nchembio.1158
Pellegrini. R. (2016). Edit single bases with Benchling. https://blog.benchling.com/ Assessed 18 July 2016.
Pennycook, B. R., Vesela, E., Peripolli, S., Singh, T., Barr, A. R., Bertoli, C., & M de Bruin, R. A. (2020). E2F-dependent transcription determines replication capacity and S phase length. *Nature Communications*. https://doi.org/10.1038/s41467-020-17146-z
Picchioni, D. (2014). *Biological function of SLIMP, a mitochondrial seryl-tRNA synthetase paralog*.
Picchioni, D., Antolin-fontes, A., Camacho, N., Kaguni, L. S., Stracker, T. H., & Subunit, A. S. (2019). *Mitochondrial Protein Synthesis and mtDNA Levels Coordinated through an Aminoacyl-tRNA Synthetase Report Mitochondrial Protein Synthesis and mtDNA Levels Coordinated through an*. 40–47. https://doi.org/10.1016/j.celrep.2019.03.022
Picchioni, D., Antolin-Fontes, A., Camacho, N., Schmitz, C., Pons-Pons, A., Rodríguez-Escribà, M., Machallekidou, A., Güler, M. N., Siatra, P., Carretero-Junquera, M., Serrano, A., Hovde, S. L., Knobel, P. A., Novoa, E. M., Solà-Vilarrubias, M., Kaguni, L. S., Stracker, T. H., & Ribas de Pouplana, L. (2019). Mitochondrial Protein Synthesis and mtDNA Levels Coordinated through an Aminoacyl-tRNA Synthetase Subunit. *Cell Reports*, *27*(1), 40-47.e5. https://doi.org/10.1016/j.celrep.2019.03.022
Pietenpol, J. A., & Stewart, Z. A. (2002). *Cell cycle checkpoint signaling: Cell cycle arrest versus apoptosis*. www.elsevier.com/locate/toxicol
Pietromonaco, S. F., Denslow, N. D., & O'Brien, T. W. (1991). Proteins of mammalian mitochondrial ribosomes. *Biochimie*, *73*(6), 827–835. https://doi.org/10.1016/0300-9084(91)90062-6
Pinti, M., Gibellini, L., Nasi, M., De Biasi, S., Bortolotti, C. A., Iannone, A., & Cossarizza, A. (2016). Emerging role of Lon protease as a master regulator of mitochondrial functions. *Biochimica et Biophysica Acta - Bioenergetics*, *1857*(8), 1300–1306. https://doi.org/10.1016/j.bbabio.2016.03.025
Poon, R. Y. C. (2016). Cell cycle control: A system of interlinking oscillators. *Methods in Molecular Biology*, *1342*, 3–19. https://doi.org/10.1007/978-1-4939-2957-3_1
Popov, L. D. (2020). Mitochondrial biogenesis: An update. In *Journal of Cellular and Molecular Medicine* (Vol. 24, Issue 9, pp. 4892–4899). Blackwell Publishing Inc.

https://doi.org/10.1111/jcmm.15194
Pozo, P. N., & Cook, J. G. (2017). Regulation and Function of Cdt1; A Key Factor in Cell Proliferation and Genome Stability. *Genes*, *2*(8), 2–23. https://doi.org/10.3390/genes8010002
Putney, S. D., & Schimmel, P. (1981). An aminoacyl tRNA synthetase binds to a specific DNA sequence and regulates its gene transcription. *Nature*, *291*(5817), 632–635. https://doi.org/10.1038/291632a0
Quirós, P. M., Mottis, A., & Auwerx, J. (2016). Mitonuclear communication in homeostasis and stress. In *Nature Reviews Molecular Cell Biology* (Vol. 17, Issue 4, pp. 213–226). Nature Publishing Group. https://doi.org/10.1038/nrm.2016.23
Radyuk, S., Rebrin, I., Luchak, J., Michalak, K., Klichko, V., Sohal, R., & Orr, W. (2009). The catalytic subunit of Drosophila glutamate-cysteine ligase is a nucleocytoplasmic shuttling protein. *The Journal of Biological Chemistry*, *284*(4), 2266–2274. https://doi.org/10.1074/JBC.M805913200
Rebelo, A. P., Dillon, L. M., & Moraes, C. T. (2011). Mitochondrial DNA transcription regulation and nucleoid organization. In *Journal of Inherited Metabolic Disease* (Vol. 34, Issue 4, pp. 941–951). J Inherit Metab Dis. https://doi.org/10.1007/s10545-011-9330-8
Recolin, B., Laan, S. van der, Tsanov, N., & Maiorano, D. (2014). Molecular mechanisms of DNA replication checkpoint activation. *Genes*, *5*(1), 147–175. https://doi.org/10.3390/GENES5010147
Regev-Rudzki, N., & Pines, O. (2007). Eclipsed distribution: a phenomenon of dual targeting of protein and its significance. *BioEssays : News and Reviews in Molecular, Cellular and Developmental Biology*, *29*(8), 772–782. https://doi.org/10.1002/BIES.20609
Remus, D., Beall, E. L., & Botchan, M. R. (2004). DNA topology, not DNA sequence, is a critical determinant for Drosophila ORC–DNA binding. *The EMBO Journal*, *23*(4), 897. https://doi.org/10.1038/SJ.EMBOJ.7600077
Resnitzky, D., Gossen, M., Bujard, H., & Reed, S. (1994). Acceleration of the G1/S phase transition by expression of cyclins D1 and E with an inducible system. *Molecular and Cellular Biology*, *14*(3), 1669–1679. https://doi.org/10.1128/MCB.14.3.1669-1679.1994
Reynolds, J. C., Lai, R. W., Woodhead, J. S. T., Joly, J. H., Mitchell, C. J., Cameron-Smith, D., Lu, R., Cohen, P., Graham, N. A., Benayoun, B. A., Merry, T. L., & Lee, C. (2021). MOTS-c is an exercise-induced mitochondrial-encoded regulator of age-dependent physical decline and muscle homeostasis. *Nature Communications*, *12*(1), 1–11. https://doi.org/10.1038/s41467-020-20790-0
Rho, S. B., Lincecum, T. L., & Martinis, S. A. (2002). An inserted region of leucyl-tRNA synthetase plays a critical role in group I intron splicing. *EMBO Journal*, *21*(24), 6874–6881. https://doi.org/10.1093/emboj/cdf671
Ribas de Pouplana, L., & Schimmel, P. (2001). Two classes of tRNA synthetases suggested by sterically compatible dockings on tRNA acceptor stem. *Cell*, *104*(2), 191–193. https://doi.org/10.1016/S0092-8674(01)00204-5
Roberti, M., Bruni, F., Polosa, P. L., Gadaleta, M. N., & Cantatore, P. (2006). The Drosophila termination factor DmTTF regulates in vivo mitochondrial transcription. *Nucleic Acids Research*, *34*(7), 2109–2116. https://doi.org/10.1093/nar/gkl181
Rodnina, M. V, Beringer, M., & Wintermeyer, W. (2006). How ribosomes make peptide bonds. *Review TRENDS in Biochemical Sciences*, *Vol.32 No.*, 20–26. https://doi.org/10.1016/j.tibs.2006.11.007
Rokov-Plavec, J., Lesjak, S., Landeka, I., Mijakovic, I., & Weygand-Durasevic, I. (2002). Maize seryl-tRNA synthetase: Specificity of substrate recognition by the organellar enzyme. *Archives of Biochemistry and Biophysics*, *397*(1), 40–50. https://doi.org/10.1006/abbi.2001.2600
Rubin, S. M., Sage, J., & Skotheim, J. M. (2020). Integrating Old and New Paradigms of G1/S Control. *Molecular Cell*, *80*(2), 183–192. https://doi.org/10.1016/j.molcel.2020.08.020

Rubio-Cosials, A., Sidow, J. F., Jiménez-Menéndez, N., Fernández-Millán, P., Montoya, J., Jacobs, H. T., Coll, M., Bernadó, P., & Solà, M. (2011). Human mitochondrial transcription factor A induces a U-turn structure in the light strand promoter. *Nature Structural and Molecular Biology*, *18*(11), 1281–1289. https://doi.org/10.1038/nsmb.2160

S, LiuShizhou Liu, Bekker-Jensen, S., Niels Mailand, 1 Claudia Lukas, Bartek, J., & Lukas, J. (2006). Claspin operates downstream of TopBP1 to direct ATR signaling towards Chk1 activation. *Molecular and Cellular Biology*, *26*(16), 6056–6064. https://doi.org/10.1128/MCB.00492-06

Sadasivam, S., & Decaprio, J. A. (2013). The DREAM complex: master coordinator of cell cycle-dependent gene expression. *Nature Reviews*, *13*, 585–595.

Saint-Georges, Y., Garcia, M., Delaveau, T., Jourdren, L., Crom, S. Le, Lemoine, S., Tanty, V., Devaux, F., & Jacq, C. (2008). Yeast Mitochondrial Biogenesis: A Role for the PUF RNA-Binding Protein Puf3p in mRNA Localization. *PLOS ONE*, *3*(6), e2293. https://doi.org/10.1371/JOURNAL.PONE.0002293

Saito, S., Tamura, K., & Aotsuka, T. (2005). Replication origin of mitochondrial DNA in insects. *Genetics*, *171*(4), 1695–1705. https://doi.org/10.1534/genetics.105.046243

Sajish, M., Zhou, Q., Kishi, S., Valdez, D. M., Kapoor, M., Guo, M., Lee, S., Kim, S., Yang, X. L., & Schimmel, P. (2012). Trp-tRNA synthetase bridges DNA-PKcs to PARP-1 to link IFN-γ and p53 signaling. In *Nature Chemical Biology* (Vol. 8, Issue 6, pp. 547–554). Nature Publishing Group. https://doi.org/10.1038/nchembio.937

Sampath, P., Mazumder, B., Seshadri, V., Gerber, C. A., Chavatte, L., Kinter, M., Ting, S. M., Dignam, J. D., Kim, S., Driscoll, D. M., & Fox, P. L. (2004). Noncanonical function of glutamyl-prolyl-tRNA synthetase: Gene-specific silencing of translation. *Cell*, *119*(2), 195–208. https://doi.org/10.1016/j.cell.2004.09.030

Santoni-Rugiu, E., Falck, J., Mailand, N., Bartek, J., & Lukas, J. (2000). Involvement of Myc Activity in a G1/S-Promoting Mechanism Parallel to the pRb/E2F Pathway. *Molecular and Cellular Biology*, *20*(10), 3497. https://doi.org/10.1128/MCB.20.10.3497-3509.2000

Sass, E., Blachinsky, E., Karniely, S., & Pines, O. (2001). Mitochondrial and Cytosolic Isoforms of Yeast Fumarase Are Derivatives of a Single Translation Product and Have Identical Amino Termini. *Journal of Biological Chemistry*, *276*(49), 46111–46117. https://doi.org/10.1074/jbc.M106061200

Sass, E., Karniely, S., & Pines, O. (2003). Folding of Fumarase during Mitochondrial Import Determines its Dual Targeting in Yeast. *Journal of Biological Chemistry*, *278*(46), 45109–45116. https://doi.org/10.1074/jbc.M302344200

Sawado, T., Hirose, F., Takahashi, Y., Sasaki, T., Shinomiya, T., Sakaguchi, K., Matsukage, A., & Yamaguchi, M. (1998). The DNA replication-related element (DRE)/DRE-binding factor: System is a transcriptional regulator of the Drosophila E2F gene. *Journal of Biological Chemistry*, *273*(40), 26042–26051. https://doi.org/10.1074/jbc.273.40.26042

Schimmel, P., & Ribas De Pouplana, L. (2000). Footprints of aminoacyl-tRNA synthetases are everywhere. In *Trends in Biochemical Sciences* (Vol. 25, Issue 5, pp. 207–209). Elsevier Ltd. https://doi.org/10.1016/S0968-0004(00)01553-X

Schmidt, O., Pfanner, N., & Meisinger, C. (2010). Mitochondrial protein import: From proteomics to functional mechanisms. *Nature Reviews Molecular Cell Biology*, *11*(9), 655–667. https://doi.org/10.1038/nrm2959

Schuller, A. P., & Green, R. (2018). Roadblocks and resolutions in eukaryotic translation and protein control. *Nature Reviews Molecular Cell Biology*. https://doi.org/10.1038/s41580-018-0011-4

Scott A.Lujan, S.Williams, J., & A.Kunkel, T. (2016). DNA Polymerases Divide the Labor of Genome Replication. *Trends in Cell Biology*, *26*(9), 640–654. https://doi.org/10.1016/J.TCB.2016.04.012

Shaughnessy, D. T., McAllister, K., Worth, L., Haugen, A. C., Meyer, J. N., Domann, F. E., Van Houten, B., Mostoslavsky, R., Bultman, S. J., Baccarelli, A. A., Begley, T. J., Sobol, R. W.,

Hirschey, M. D., Ideker, T., Santos, J. H., Copeland, W. C., Tice, R. R., Balshaw, D. M., & Tyson, F. L. (2015). Mitochondria, energetics, epigenetics, and cellular responses to stress. In *Environmental Health Perspectives* (Vol. 122, Issue 12, pp. 1271–1278). Public Health Services, US Dept of Health and Human Services. https://doi.org/10.1289/ehp.1408418

Shiba, K. (2002). Intron positions delineate the evolutionary path of a pervasively appended peptide in five human aminoacyl-tRNA synthetases. *Journal of Molecular Evolution*, *55*(6), 727–733. https://doi.org/10.1007/s00239-002-2368-3

Siddiqui, K., On, K., & Diffley, J. (2013). Regulating DNA replication in eukarya. *Cold Spring Harbor Perspectives in Biology*, *5*(9). https://doi.org/10.1101/CSHPERSPECT.A012930

Sigl, R., Wandke, C., Rauch, V., Kirk, J., Hunt, T., & Geley, S. (2009). Loss of the mammalian APC/C activator FZR1 shortens G1 and lengthens S phase but has little effect on exit from mitosis. *Journal of Cell Science*, *122*(Pt 22), 4208–4217. https://doi.org/10.1242/JCS.054197

Sissler, M., Delorme, C., Bond, J., Ehrlich, S. D., Renault, P., & Francklyn, C. (1999). An aminoacyl-tRNA synthetase paralog with a catalytic role in histidine biosynthesis. *Proceedings of the National Academy of Sciences of the United States of America*, *96*(16), 8985–8990. https://doi.org/10.1073/pnas.96.16.8985

Siu, K. T., Rosner, M. R., & Minella, A. C. (2012). An integrated view of cyclin E function and regulation. In *Cell Cycle* (Vol. 11, Issue 1, pp. 57–64). Taylor and Francis Inc. https://doi.org/10.4161/cc.11.1.18775

Smirnova, E. V., Lakunina, V. A., Tarassov, I., Krasheninnikov, I. A., & Kamenski, P. A. (2012). Noncanonical functions of aminoacyl-tRNA synthetases. In *Biochemistry (Moscow)* (Vol. 77, Issue 1, pp. 15–25). Springer. https://doi.org/10.1134/S0006297912010026

Spencer, A. C., & Spremulli, L. L. (2004). Interaction of mitochondrial initiation factor 2 with mitochondrial fMet-tRNA. *Nucleic Acids Research*, *32*(18), 5464–5470. https://doi.org/10.1093/nar/gkh886

Springer, M., Graffe, M., Dondon, J., Grunberg-Manago, M., Romby, P., Ehresmann, B., Ehresmann, C., & Ebel, J. P. (1988). Translational control in E. coli: The case of threonyl-tRNA synthetase. *Bioscience Reports*, *8*(6), 619–632. https://doi.org/10.1007/BF01117341

Stahlberg, H., Kutejová, E., Suda, K., Wolpensinger, B., Lustig, A., Schatz, G., Engel, A., & Suzuki, C. K. (1999). Mitochondrial Lon of Saccharomyces cerevisiae is a ring-shaped protease with seven flexible subunits. *Proceedings of the National Academy of Sciences of the United States of America*, *96*(12), 6787–6790. https://doi.org/10.1073/pnas.96.12.6787

Stallaert, W., Kedziora, K. M., Chao, H. X., & Purvis, J. E. (2019). Bistable switches as integrators and actuators during cell cycle progression. *FEBS Letters*, *593*(20), 2805–2816. https://doi.org/10.1002/1873-3468.13628

Steitz, T. A. (2008). A structural understanding of the dynamic ribosome machine. In *Nature Reviews Molecular Cell Biology* (Vol. 9, Issue 3, pp. 242–253). Nature Publishing Group. https://doi.org/10.1038/nrm2352

Stevaux, O., Dimova, D., Frolov, M. V., Taylor-Harding, B., Morris, E., & Dyson, N. (2002). Distinct mechanisms of E2F regulation by Drosophila RBF1 and RBF2. *EMBO Journal*, *21*(18), 4927–4937. https://doi.org/10.1093/emboj/cdf501

Stevaux, O., Dimova, D. K., Ji, J., Moon, N. S., Frolov, V., Dyson, N. J., Stevaux, O., Dimova, D. K., Frolov, M. V, & Dyson, N. J. (2005). Retinoblastoma Family 2 is Required In Vivo for the Tissue-Specific Repression of dE2F2 target Genes. *Cell Cycle*, *4101*, 1272–1280. https://doi.org/10.4161/cc.4.9.1982

Strobel, G., Zollner, A., Angermayr, M., & Bandlow, W. (2002). Competition of spontaneous protein folding and mitochondrial import causes dual subcellular location of major adenylate kinase. *Molecular Biology of the Cell*, *13*(5), 1439–1448. https://doi.org/10.1091/mbc.01-08-0396

Sugimoto, N., Yoshida, K., Tatsumi, Y., Yugawa, T., Narisawa-Saito, M., Waga, S., Kiyono, T., & Fujita, M. (2009). Redundant and differential regulation of multiple licensing factors

ensures prevention of re-replication in normal human cells. *Journal of Cell Science*, *122*(Pt 8), 1184–1191. https://doi.org/10.1242/JCS.041889

Sugiura, A., McLelland, G., Fon, E. A., & McBride, H. M. (2014). A new pathway for mitochondrial quality control: mitochondrial-derived vesicles. *The EMBO Journal*, *33*(19), 2142–2156. https://doi.org/10.15252/embj.201488104

T, Wai, T., J, García-Prieto, J., MJ, Baker, M., C, Merkwirth, C., Benit, P., Rustin, P., Rupérez, F., Barbas, C., Ibañez, B., & Langer, T. (2015). Imbalanced OPA1 processing and mitochondrial fragmentation cause heart failure in mice. *Science*, *350*(6265). https://doi.org/10.1126/SCIENCE.AAD0116

Talbert, P., & Henikoff, S. (2010). Histone variants--ancient wrap artists of the epigenome. *Nature Reviews. Molecular Cell Biology*, *11*(4), 264–275. https://doi.org/10.1038/NRM2861

Teixeira, L. K., & Reed, S. I. (2013). Ubiquitin Ligases and Cell Cycle Control. *Http://Dx.Doi.Org.Sire.Ub.Edu/10.1146/Annurev-Biochem-060410-105307*, *82*, 387–414. https://doi.org/10.1146/ANNUREV-BIOCHEM-060410-105307

Thomer, M., May, N. R., Aggarwal, B. D., Kwok, G., & Calvi, B. R. (2004). Drosophila double-parked is sufficient to induce re-replication during development and is regulated by cyclin E/CDK2. *Development*, *131*(19), 4807–4818. https://doi.org/10.1242/DEV.01348

Torelli, N. Q., Ferreira-Júnior, J. R., Kowaltowski, A. J., & Da Cunha, F. M. (2015). RTG1- and RTG2-dependent retrograde signaling controls mitochondrial activity and stress resistance in Saccharomyces cerevisiae. *Free Radical Biology and Medicine*, *81*, 30–37. https://doi.org/10.1016/j.freeradbiomed.2014.12.025

Tsakraklides, V., & Bell, S. P. (2010). Dynamics of Pre-replicative Complex Assembly *. *The Journal of Biological Chemistry*, *285*(13), 9437–9443. https://doi.org/10.1074/jbc.M109.072504

Tue, N. T., Yoshioka, Y., Mizoguchi, M., Yoshida, H., Zurita, M., & Yamaguchi, M. (2017). DREF plays multiple roles during Drosophila development. *Biochimica et Biophysica Acta - Gene Regulatory Mechanisms*, *1860*(6), 705–712. https://doi.org/10.1016/j.bbagrm.2017.03.004

Tzima, E., & Schimmel, P. (2006). Inhibition of tumor angiogenesis by a natural fragment of a tRNA synthetase. In *Trends in Biochemical Sciences* (Vol. 31, Issue 1, pp. 7–10). Elsevier Ltd. https://doi.org/10.1016/j.tibs.2005.11.002

Vakaloglou, K., Mouratidou, M., Keramidioti, A., & Zervas, C. (2021). Differential Expression of Drosophila Transgelins Throughout Development. *Frontiers in Cell and Developmental Biology*, *9*. https://doi.org/10.3389/FCELL.2021.648568

van den Heuvel, S. (2005). Cell-cycle regulation. In *WormBook : the online review of C. elegans biology* (pp. 1–16). WormBook. https://doi.org/10.1895/wormbook.1.28.1

Villa-Cuesta, E., & Rand, D. M. (2015). Preparation of Mitochondrial Enriched Fractions for Metabolic Analysis in Drosophila. *JoVE (Journal of Visualized Experiments)*, *2015*(103), e53149. https://doi.org/10.3791/53149

Volkenstein, M. V. (1966). The genetic coding of protein structure. *BBA Section Nucleic Acids And Protein Synthesis*, *119*(2), 421–424. https://doi.org/10.1016/0005-2787(66)90204-8

Vongsamphanh, R., Fortier, P.-K., & Ramotar, D. (2001). Pir1p Mediates Translocation of the Yeast Apn1p Endonuclease into the Mitochondria To Maintain Genomic Stability. *Molecular and Cellular Biology*, *21*(5), 1647–1655. https://doi.org/10.1128/mcb.21.5.1647-1655.2001

Wakasugi, K., Slike, B. M., Hood, J., Otani, A., Ewalt, K. L., Friedlander, M., Cheresh, D. A., & Schimmel, P. (2002). A human aminoacyl-tRNA synthetase as a regulator of angiogenesis. *Proceedings of the National Academy of Sciences of the United States of America*, *99*(1), 173–177. https://doi.org/10.1073/pnas.012602099

Waldron, A., Cahan, S., Francklyn, C., & Ebert, A. (2017). A single Danio rerio hars gene encodes both cytoplasmic and mitochondrial histidyl-tRNA synthetases. *PloS One*, *12*(9).

https://doi.org/10.1371/JOURNAL.PONE.0185317
Wallin, I. (1927). *Symbionticism and the Origin of Species*.
Wang, H., La Russa, M., & Qi, L. (2016). CRISPR/Cas9 in Genome Editing and Beyond. *Annual Review of Biochemistry*, *85*, 227–264. https://doi.org/10.1146/ANNUREV-BIOCHEM-060815-014607
Wei, N., Shi, Y., Truong, L. N., Fisch, K. M., Xu, T., Gardiner, E., Fu, G., Hsu, Y. S. O., Kishi, S., Su, A. I., Wu, X., & Yang, X. L. (2014). Oxidative stress diverts trna synthetase to nucleus for protection against dna damage. *Molecular Cell*, *56*(2), 323–332. https://doi.org/10.1016/j.molcel.2014.09.006
Wei, W., Ayad, N. G., Wan, Y., Zhang, G. J., Kirschner, M. W., & Kaelin, W. G. (2004). Degradation of the SCF component Skp2 in cell-cycle phase G1 by the anaphase-promoting complex. *Nature*, *428*(6979), 194–198. https://doi.org/10.1038/nature02381
Weinberg, R. A. (1995). The retinoblastoma protein and cell cycle control. *Cell*, *81*(3), 323–330. https://doi.org/10.1016/0092-8674(95)90385-2
Wek, R. C., Jackson, B. M., & Hinnebusch, A. G. (1989). Juxtaposition of domains homologous to protein kinase and histidyl-tRNA synthetases in GCN2 protein suggests a mechanism for coupling GCN4 expression to amino acid availability. *Proceedings of the National Academy of Sciences of the United States of America*, *86*(12), 4579–4583. https://doi.org/10.1073/pnas.86.12.4579
Weygand-Durasevic, I., Johnson-Burke, D., & Söll, D. (1987). Cloning and characterization of the gene coding for cytoplasmic seryl-tRNA synthetase from Saccharomyces cerevisiae. *Nucleic Acids Research*, *15*(5), 1887–1904. https://doi.org/10.1093/nar/15.5.1887
Whitfield, W. G. F., Gonzalez, C., Maldonado-Codina, G., & Glover, D. M. (1990). The A-and B-type cyclins of Drosophila are accumulated and destroyed in temporally distinct events that define separable phases of the G2-M transition. In *The EMBO Journal* (Vol. 9, Issue 8).
Wiedemann, N., & Pfanner, N. (2017). Mitochondrial machineries for protein import and assembly. *Annual Review of Biochemistry*, *86*, 685–714. https://doi.org/10.1146/annurev-biochem-060815-014352
Williams, C. C., Jan, C. H., & Weissman, J. S. (2014). Targeting and plasticity of mitochondrial proteins revealed by proximity-specific ribosome profiling. *Science*, *346*(6210), 748–751. https://doi.org/10.1126/science.1257522
Wissel, S., Kieser, A., Yasugi, T., Duchek, P., Roitinger, E., Gokcezade, J., Steinmann, V., Gaul, U., Mechtler, K., Förstemann, K., Knoblich, J. A., & Neumüller, R. A. (2016). A Combination of CRISPR/Cas9 and Standardized RNAi as a Versatile Platform for the Characterization of Gene Function. *G3: Genes|Genomes|Genetics*, *6*(8), 2467–2478. https://doi.org/10.1534/g3.116.028571
Wittenberg, C., & La Valle, R. (2003). Cell-cycle-regulatory elements and the control of cell differentiation in the budding yeast. In *BioEssays* (Vol. 25, Issue 9, pp. 856–867). Bioessays. https://doi.org/10.1002/bies.10327
Woese, C. R. (1965). Order in the genetic code. *Proceedings of the National Academy of Sciences of the United States of America*, *54*(1), 71–75. https://doi.org/10.1073/pnas.54.1.71
Wu, C. L., Zukerberg, L. R., Ngwu, C., Harlow, E., & Lees, J. A. (1995). In vivo association of E2F and DP family proteins. *Molecular and Cellular Biology*, *15*(5), 2536–2546. https://doi.org/10.1128/mcb.15.5.2536
Xian Feng, Y, N., M, B., B, S., C, S., & H, L. (2021). The structure of ORC-Cdc6 on an origin DNA reveals the mechanism of ORC activation by the replication initiator Cdc6. *Nature Communications*, *12*(1), 3883. https://doi.org/10.1038/S41467-021-24199-1
Xu, X., Shi, Y., & Yang, X.-L. (2013). Crystal structure of human Seryl-tRNA synthetase and Ser-SA complex reveals a molecular lever specific to higher eukaryotes. *Structure (London, England : 1993)*, *21*(11), 2078–2086. https://doi.org/10.1016/J.STR.2013.08.021
Yao, P., Poruri, K., Martinis, S. A., & Fox, P. L. (2014). Non-catalytic regulation of gene expression by aminoacyl-tRNA synthetases. In *Topics in current chemistry* (Vol. 344, pp. 167–187). Top

Curr Chem. https://doi.org/10.1007/128_2013_422

Yatskevich, S., Kroonen, J. S., Alfieri, C., Tischer, T., Howes, A. C., Clijsters, L., Yang, J., Zhang, Z., Yan, K., Vertegaal, A. C. O., & Barford, D. (2021). Molecular mechanisms of APC/C release from spindle assembly checkpoint inhibition by APC/C SUMOylation. *Cell Reports*, *34*(13), 108929. https://doi.org/10.1016/j.celrep.2021.108929

Yogev, O., Yogev, O., Singer, E., Shaulian, E., Goldberg, M., Fox, T. D., & Pines, O. (2010). Fumarase: A mitochondrial metabolic enzyme and a cytosolic/nuclear component of the dna damage response. *PLoS Biology*, *8*(3), e1000328. https://doi.org/10.1371/journal.pbio.1000328

Yonghong Shi, Anke Dierckx, Paulina H. Wanrooij, Sjoerd Wanrooij, Nils-Göran Larsson, L. Marcus Wilhelmsson, M. F. and C. M. G. (2012). *Mammalian transcription factor A is a core component of the mitochondrial transcription machinery on JSTOR*. Proceedings of the National Academy of Sciences of the United States of America109. https://www.jstor.org/stable/41763379

Yung, Y., Walker, J. L., Roberts, J. M., & Assoian1, R. K. (2007). A Skp2 autoinduction loop and restriction point control. *The Journal of Cell Biology*, *178*(5), 741–747. https://doi.org/10.1083/JCB.200703034

Zhang, H. (2021). Regulation of DNA Replication Licensing and Re-Replication by Cdt1. *International Journal of Molecular Sciences*, *22*(10). https://doi.org/10.3390/IJMS22105195

Zhang, P., Katzaroff, A. J., Buttitta, L. A., Ma, Y., Jiang, H., Nickerson, D. W., Øvrebø, J. I., & Edgar, B. A. (2021). The Krüppel-like factor Cabut has cell cycle regulatory properties similar to E2F1. *Proceedings of the National Academy of Sciences of the United States of America*, *118*(7). https://doi.org/10.1073/pnas.2015675118

Zhou, X. L., Chen, Y., Zeng, Q. Y., Ruan, Z. R., Fang, P., & Wang, E. D. (2019). Newly acquired N-terminal extension targets threonyl-tRNA synthetase-like protein into the multiple tRNA synthetase complex. *Nucleic Acids Research*, *47*(16), 8662–8674. https://doi.org/10.1093/nar/gkz588